

**APPLICATION OF FRAGMENT-BASED METHODS
FOR THE DEVELOPMENT OF
PSEUDOMONAS AERUGINOSA
ANTI-VIRULENCE COMPOUNDS**

DISSERTATION

zur Erlangung des Grades

des Doktors der Naturwissenschaften

der Naturwissenschaftlich-Technischen Fakultät III

Chemie, Pharmazie, Bio- und Werkstoffwissenschaften

der Universität des Saarlandes

von

Michael Georg Zender

Saarbrücken

2016

Tag des Kolloquiums: 03.11.2016

Dekan: Prof. Dr. Guido Kickelbick

Berichterstatter: Prof. Dr. Rolf W. Hartmann

Prof. Dr. Rolf Müller

Vorsitz: Prof. Dr. Uli Kazmaier

Akad. Mitarbeiter: Dr. Martin Frotscher

Diese Arbeit wurde von August 2011 bis Dezember 2015 unter der Anleitung von Herrn Prof. Dr. Rolf W. Hartmann am Helmholtz Institute für Pharmazeutische Forschung Saarland (HIPS) sowie in der Fachrichtung 8.2 Pharmazeutische und Medizinische Chemie der Fakultät III der Universität des Saarlandes angefertigt.

“Success is stumbling from failure to failure with no loss of enthusiasm.”

Winston S. Churchill

Abstract

Pseudomonas aeruginosa is the cause of nosocomial infections and recurrent pneumonia in cystic fibrosis patients. Antibiotic treatment becomes increasingly difficult due to the spreading of multi-drug resistant strains and its ability to grow in a biofilm. The virulence of this pathogen is mainly controlled by quorum sensing (QS) systems. This process enables bacteria to coordinate the expression of virulence factors and biofilm formation as a function of cell density. For this purpose, *P. aeruginosa* utilize among others the *pqs* (Pseudomonas Quinolone Signal) system.

In this study anti-virulence agents were developed interfering with the *pqs* system. During a fragment-based drug discovery campaign antagonists of the Pseudomonas Quinolone Signal Receptor (PqsR) were synthesized. Based on hits identified in a surface plasmon resonance (SPR) screening, novel lead structures were generated. This development process involved selective synthetic modifications of the hit structures and structure-based design methods. Fragments were successfully merged with moieties of an alternative compound class. The optimized structures displayed potent reduction of virulence factors and signaling molecules in *P. aeruginosa*.

During another fragment screening the first synthetic PqsE ligands were identified. The binding mode of these fragments was elucidated. Furthermore, it was shown that the inhibition of the enzymatic activity did not translate into an effect on its virulence regulatory role.

Zusammenfassung

Pseudomonas aeruginosa ist ein Erreger nosokomialer Infektionen sowie von Pneumonien bei Patienten mit zystischer Fibrose. Die Antibiotikatherapie wird durch das vermehrte Auftreten von multiresistenten Stämmen und die Ausbildung von Biofilmen erschwert. Die Virulenz des Erregers wird hauptsächlich durch Quorum Sensing reguliert. Dies ermöglicht es dem Bakterium die Bildung von Virulenzfaktoren und Biofilmen in Abhängigkeit von der Zelldichte zu koordinieren. *P. aeruginosa* nutzt hierfür unter anderem das *pqs* (Pseudomonas Quinolone Signal) System.

In dieser Arbeit wurden Substanzen entwickelt, die in dieses System eingreifen. Zunächst wurden in einem Fragment-basiertem Ansatz PqsR Antagonisten synthetisiert. Ausgehend von Fragmenten, die einem Surface Plasmon Resonance (SPR) Screening gefunden wurden, konnten neue Leitstrukturen generiert werden. Dies gelang durch gezielte synthetische Modifikation der Ausgangsverbindungen und dem Einsatz Struktur-basierter Methoden. Weiterhin konnten Fragmente mit Motiven aus einer anderen Strukturklasse erfolgreich kombiniert werden. Die optimierten Strukturen zeigten eine potente Absenkung der Virulenz und der Produktion von Signalmolekülen in *P. aeruginosa*.

In einem weiteren Fragment Screening wurden die ersten synthetischen PqsE Liganden identifiziert und ihr Bindungsmodus aufgeklärt. Weiterhin konnte gezeigt werden, dass eine Inhibition der enzymatischen Funktion keinen Einfluss auf die Virulenz Regulation durch PqsE hat.

Contents

1	Introduction	10
1.1	Rational Drug Design	10
1.2	Fragment-based Drug Discovery	10
1.3	Biophysical Methods in Fragment-based Approaches	13
1.3.1	Surface Plasmon Resonance	13
1.3.2	Thermal Shift Assay	16
1.3.3	Isothermal Titration Calorimetry	16
1.4	Targeting the Virulence of <i>Pseudomonas aeruginosa</i>	19
1.4.1	The Opportunistic Pathogen <i>Pseudomonas aeruginosa</i>	19
1.4.2	The Quorum Sensing Networks of <i>Pseudomonas aeruginosa</i>	20
1.4.3	Interference with the <i>pqs</i> System as Antivirulence Strategy	24
1.4.4	The Transcriptional Regulator PqsR as Antivirulence Target	28
1.4.5	The Enigmatic Role of PqsE	29
2	Objectives	31
3	Results	32
3.1	Chapter A: Discovery and Biophysical Characterization of 2-Amino-oxadiazoles as Novel Antagonists of PqsR, an Important Regulator of <i>Pseudomonas aeruginosa</i> Virulence	32
3.2	Chapter B: Flexible-Fragment-Growing Boosts Potency of Quorum Sensing Inhibitors against <i>Pseudomonas aeruginosa</i> virulence.....	61
3.3	Chapter C: Effects of Next Generation PqsR-targeting Anti-infectives against Biofilm and Virulence of <i>Pseudomonas aeruginosa</i>	85
3.4	Chapter D: Dissecting the multiple roles of PqsE in <i>Pseudomonas aeruginosa</i> virulence by discovery of small tool compounds	105
4	Final Discussion	122
4.1	Development of PqsR Antagonists	123
4.2	Discovery of PqsE Ligands	129
4.3	Outlook	131
5	References	133
6	Abbreviations	142
7	Supplementary Material	143
7.1	Supplementary Material of Chapter A.....	143
7.2	Supplementary Material of Chapter B.....	157
7.3	Supplementary Material of Chapter C	172
7.4	Supplementary Material of Chapter D	176

Contents

8	Appendix	184
8.1	Curriculum Vitae	184
8.2	Publications	185
8.3	Oral Presentations	185
8.4	Poster Presentations	186
9	Acknowledgments	187

1 Introduction

1.1 Rational Drug Design

In the beginning of pharmaceutical research, the development of therapeutic drugs was mainly characterized by serendipity or the isolation of the active principles from biological samples and their subsequent chemical modification.(Drews, 2000; Klebe, 2009) The outcomes of these efforts still represent the groundwork of our present pharmaceutical portfolio. An impressive example of such an approach is the discovery of acetyl salicylic acid 1897 by the German chemist Felix Hoffmann.(Dreser, 1899) Another milestone of this era is the isolation of the antibiotic agent penicillin 1929 by Alexander Fleming.(Fleming, 1929) Paul Ehrlich's visionary concept of 'the magic bullet' laid the foundation for modern rational drug discovery approaches.(Strebhardt and Ullrich, 2008) He proclaimed that 'chemoreceptors' can be selectively targeted by chemically optimized therapeutic agents.(Ehrlich, 1909) From 1880 to the 1980, lead molecules were mainly developed without knowing the exact molecular mode of action mainly based on the 'trial and error' methodology.(Klebe, 2009) Over the last 30 years, after the rise of molecular biology, it was possible to gain novel insights into biochemical and pathophysiological processes on a molecular level.(Henderson et al., 1999) This provided researchers with the ability to identify suitable targets for the subsequent development of highly specific therapeutic agents.(Hopkins and Groom, 2002) Moreover, these new genetic techniques enabled cloning and expression of target proteins as well as the development of tailored *in vitro* assays to assess the potency of drug candidates. In course of this genetic revolution new disciplines joined the field. The implementation of computational methods, automatization and robotics as well as modern biophysical techniques to drug discovery approaches enabled to advance and to rationalize the development of novel lead compounds.(Henderson et al., 1999) These changes transformed drug discovery into a multidisciplinary endeavor.(Drews, 2000)

1.2 Fragment-based Drug Discovery

In 1894, Emil Fischer recognized that different glycosides were hydrolyzed by particular enzymes while others were not affected. From these observations he drew a pioneering conclusion: substrate and enzyme fit together like lock and key.(Fischer, 1894) For the first time, it was noticed that the complementary shape of a small molecule (substrate) and its molecular target (enzyme) leads to the formation of a ligand-receptor complex. Fischer's theory was extended by taking into account protein flexibility; the induced-fit model describes the complex formation as dynamic process where a small molecule induces a conformational change in the protein structure.(Koshland, 1958) These concepts have a sustained influence on modern drug discovery.

The discovery of a suitable ligand for a pharmaceutical target protein is a fundamental step in every drug development program. These ligands are also called hits or actives and generate a response above a defined threshold in a screening assay. (Proudfoot et al., 2011) A compound or compound class which met more predefined criteria such as target associated cellular activity, selectivity and metabolic stability is called a lead. (Proudfoot et al., 2011) Hit or lead molecules can originate from different strategies. Until nowadays, natural products have been a valuable source for biological active molecules, especially in the field of anti-infectives and anticancer therapeutics. (Harvey, 2008) In ligand-based approaches, the endogenous ligand of a given drug target has been used as framework for the design of active lead molecules. (Kubas and Stark, 2007) Additionally, known drugs and inhibitors were used as role models for the development of lead molecules in so called me-too approaches. (Wermuth, 2006) During the last decades large compound libraries were established in pharmaceutical companies and academic research institutes. Modern screening technologies allow screening for active molecules in a high-throughput format (HTS, high throughput screening) accounting for 10,000 to 100,000 compounds per day. (Inglese et al., 2007) HTS-derived lead compounds tend to have a higher molecular weight and lipophilicity than those discovered by other techniques. (Lipinski et al., 1997) These poor physicochemical properties are associated with insufficient pharmacokinetic properties (Lipinski et al., 1997; Leeson and Springthorpe, 2007) and increased risk for off-target toxicity issues (Price et al., 2009), overall leading to higher attrition rates during the drug development process. (Leeson and Springthorpe, 2007) Hence, Lipinski established 'the rule of five' as guideline for the successful development of orally bioavailable drugs. (Lipinski et al., 1997) Notably, natural products like antibiotics and cardiac glycosides form exceptions from these rules. (Lipinski et al., 1997)

Besides these more traditional approaches, fragment-based drug discovery (FBDD) evolved as a valuable alternative. (Murray and Rees, 2009) During such an approach significantly smaller libraries usually containing 500 to 2000 low molecular weight compounds were mostly screened by biophysical methods. Most of the fragment libraries are 'rule of three'-compliant which demands the following criteria: a molecular weight < 300 Da, only three or less H-bond donators and acceptors as well as $\text{clogP} \leq 3$. Additionally the number of rotatable bonds should be ≤ 3 and the polar surface area (PSA) ≤ 60 . (Congreve et al., 2003) These guidelines emphasize the need for sufficient physicochemical properties from early beginning in FBDD campaign. Hits identified by a fragment screening usually show low affinities (ranging from μM to mM) but in relation to their small molecular size, they form high quality interactions with their target protein. (Murray and Verdonk, 2002) This can also be embodied in the ligand efficiency (LE) of a particular hit compound. (Hopkins et al., 2004) This metric allows comparison between ligands of different sizes and shapes. LE refers to the average contribution of a single heavy atom (N) to the Gibbs free energy (ΔG) upon compound binding ($\text{LE} = \Delta G/\text{N}$). It has been reported that the

hit rates observed in fragment screenings are higher compared to a conventional HTS campaign.(Schuffenhauer et al., 2005) This observation is explained by simple theoretical ligand-receptor model which shows that less complex structures (fragments) are more likely to match the molecular requirements for binding to a receptor. The probability of a mismatch rises drastically with increasing complexity of the ligand.(Hann et al., 2001) The fragment-sized chemical space (< 12 heavy atoms) is calculated to consist of 145 million drug-like structures, whereas the Lipinski compliant lead-sized space (<25 heavy atoms) contains 10^{25} structures.(Fink et al., 2005) Therefore, a typical fragment-library (about 1000 entities) can cover the relevant chemical space more efficiently than a large HTS collection.(Fink et al., 2005; Leach et al., 2006)

A typical FBDD approach usually starts with a biophysical screening technique which can detect low affinity protein-ligand interactions and enables a sufficient throughput. For primary screening surface plasmon resonance (SPR) biosensors, thermal shift assays (TSA) and biomolecular nuclear magnetic resonance (NMR) methods are most widely used. Several methods are described in more detail below. The identified primary actives are further validated by another orthogonal technique to eliminate false-positives and screening artifacts. The hit validation phase ideally includes the elucidation of compound binding mode using x-ray crystallography (Figure 1) or protein NMR methods to facilitate the synthetic optimization.(Ciulli and Abell, 2007)

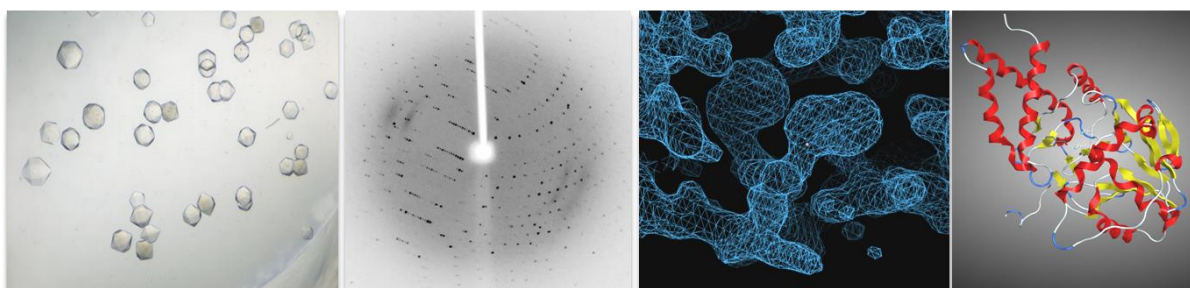


Figure 1: Structural biology workflow: protein crystals, diffraction pattern, electron density map, protein model (from left to right; with friendly permission by Florian Witzgall)

The optimization of a low affinity fragment hit into a highly active lead molecule is a challenging process. The determination of a protein-ligand complex structure enables the implementation of structure-based design methods into the drug discovery process leading to tremendously increased success rates.(Hajduk and Greer, 2007) During the optimization process potency is gained by enlargement of the initial hit compound. Different strategies were applied depending on the discovered hit compounds (Figure 2). If the screening affords two fragments which bind non-competitively into two adjacent regions of a binding pocket, the design of a suitable linker which connects both compounds was successfully employed to generate highly active leads (Fragment-linking; Figure 2A).(Hajduk et al., 1997) In most of the FBDD approaches, one

validated hit is nominated as starting point for fragment-growing (Figure 2B). Thereby, the fragment is enlarged iteratively by the use of gathered structural information and new areas within the binding pocket are occupied to enhance the potency (Fragment-growing; Figure 2B).(Shipe et al., 2015) In case the hit compounds occupy overlapping regions within the protein pocket, features of both compounds can be merged to advance compound development (Fragment-merging; Figure 2C).(Hudson et al., 2012) All these strategies are interconnected and can be combined depending on the situation and the specific requirements of a project.

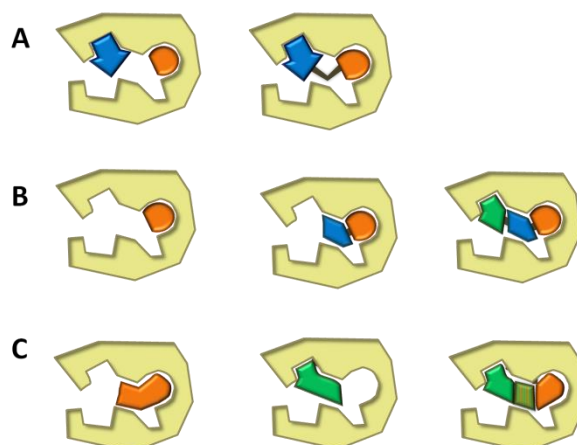


Figure 2: Schematic depiction of different fragment optimization strategies **A)** fragment-linking **B)** fragment-growing **C)** fragment-merging (adapted and modified Murray and Rees, 2009)

FBDD is the latest technology that was added to the arsenal of medicinal chemists. In 2011, the first fragment-derived drug got approval by the FDA.(Bollag et al., 2012) A recent analysis of clinical candidates proved that fragment-derived molecules show superior physicochemical properties.(Keserü and Makara, 2009)

1.3 Biophysical Methods in Fragment-based Approaches

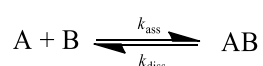
A fragment screening requires highly sensitive techniques to identify the expected weak interactions to a particular target protein. Usually, a combination of different biophysical methods is applied to detect and characterize fragment-protein interactions.(Holdgate et al., 2010; Silvestre et al., 2013) Surface plasmon resonance (SPR) screening, thermal shift assays (TSA, also known as differential scanning fluorimetry DSF) and isothermal titration calorimetry (ITC) have been mostly applied in the course of this thesis and will be outlined in more detail below. Notably, there are some other well established methods like biomolecular nuclear magnetic resonance (NMR) and mass spectroscopy (MS) available.(Holdgate et al., 2010)

1.3.1 Surface Plasmon Resonance

An SPR optical biosensor allows monitoring protein-ligand interactions in real time and subsequent evaluation of binding affinities and kinetics. In a usual setup, the target protein, also

called 'receptor', is attached to a gold surface and the analyte, e.g. a small molecule, flows in solution above the surface. In case of a complex formation between ligand and the immobilized protein, the refractive index of the medium close to gold surface is changed. This change is detected by use of polarized light, which is totally reflected at the interface of an optical prism and a gold surface (Figure 1A). Thereby, a surface plasmon wave (SPW) is generated at the outer boundary of the gold layer (biosensor surface). When the parameters of the incident light (wavelength, angle) and the propagation constants of the SPW fit together, resonance occurs leading to attenuation of total reflection at these specific parameters of the light beam. The propagation constants of the SPW are highly sensitive to the refractory index of the surrounding medium. Hence, a change in this medium can be monitored by tuning the angle or wavelength (depending on the instrument) of the incident light until resonance and attenuation of total reflection are achieved again. Therefore, a change in the refractory index, for example due to an interaction of a small molecule with a surface-attached protein directly correlates with the change in one of these characteristics which can be measured over time. (Homola, 2003; Cooper and Mayr, 2011)

A typical SPR experiment is outlined in Figure 1B. At time points before 0 buffer flows over the sensor surface and a baseline signal is monitored. At time point 0 to 60s, a small molecule is injected and interacts with the protein leading at first to an increasing response in the association phase (0 to 20s) and then to a plateau in the steady state phase (20 to 60s). After 60s buffer flows over the sensor surface and the molecule dissociates from the immobilized protein. (Cooper, 2002)



Equation 1: Simple 1:1 binding model with analyte A and immobilized protein B forming a complex AB. This process can be described by the association rate constant k_{ass} and dissociation rate constant k_{diss}

These processes can be described as a simple bimolecular interaction as illustrated in Equation 1. Mathematical analyses of the association and dissociation phase allow determination of the association rate constant (k_{ass}) and the dissociation rate constant (k_{diss}), respectively, which in turn enable to estimate the dissociation constant K_D of the biomolecular complex (Equation 2). (Cooper, 2002; Mol and Fischer, 2008)

$$K_D = \frac{1}{K_A} = \frac{k_{\text{diss}}}{k_{\text{ass}}}$$

Equation 2: Estimation of the dissociation constant K_D from association rate constant k_{ass} and dissociation rate constant k_{diss}

The amount of complex AB is proportional to the measured SPR response. Hence, the affinity can also be determined by plotting the measured response under steady-state conditions

against the compound concentration, respectively, and performing a non-linear regression analysis (Figure 3C). (Mol and Fischer, 2008; Cooper and Mayr, 2011)

Due to the low amount of protein and the high throughput of SPR biosensors, this technique is widely applied in various phases of a drug discovery process. (Cooper, 2002)

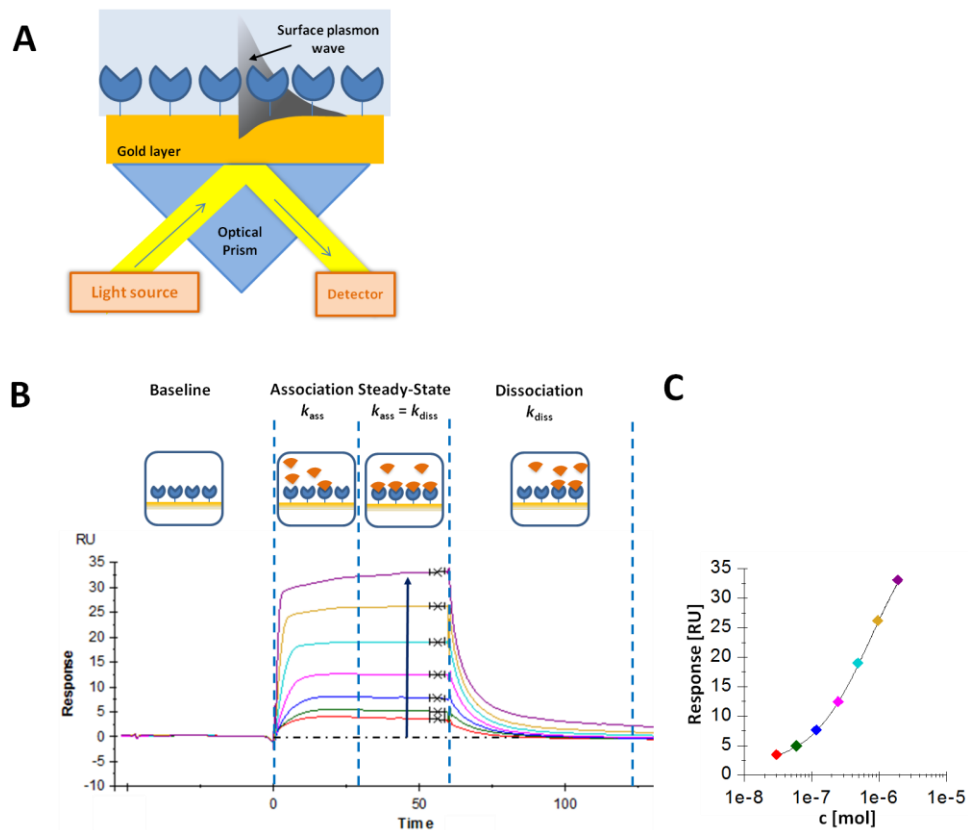


Figure 3: SPR binding experiment. A) Schematic representation of an SPR biosensor setup B) Overlay of SPR sensorgrams showing the particular phases of binding events as indicated and schematically depicted above. C) Derived dose-response plot for affinity estimation; SPR measured response at steady-state against the compound concentration, respectively. (adapted and modified from Cooper 2002 and Homola 2003)

1.3.2 Thermal Shift Assay

Thermal shift assays (TSA), also known as differential scanning fluorometry (DSF), is a technique which allows measuring the effect of a ligand on the thermal stability of a protein target. A protein is incubated with a putative ligand in the presence of an environment-sensitive fluorescent dye while applying a temperature ramp. For most proteins, the concentration of unfolded protein increases with rising temperatures. Hydrophobic regions of the protein structure are exposed to the surface during unfolding; the used dye displays an increase of fluorescence signal in such hydrophobic environments whereas its fluorescence is quenched in the polar aqueous buffer. Hence, the fluorescence signal correlates with the amount of unfolded protein. At the melting point, the concentrations of native and unfolded protein are equal. The fluorescence intensity is plotted over the applied temperature range and the inflection point of the resulting sigmoid curve represents the melting point (T_m) of the protein. (Niesen et al., 2007)

Ligands binding reversibly to the native state of a protein usually enhance the melting point compared to a ligand free control. This shift in the melting temperature ($\Delta T_m = T_{m(\text{ligand})} - T_{m(\text{control})}$) is proportional to the ligand concentration and affinity. (Matulis et al., 2005) Compounds which decrease the melting temperature are assumed to bind preferably to the unfolded protein. (Cimpmperman et al., 2008)

Compounds stabilizing the target protein are described to gain access for protein structure determination (Vedadi et al., 2006) what facilitates the application of structure-based methods in a follow-up drug discovery program. TSAs are applicable for a broad range of different proteins, require low amounts of protein and can be performed in high throughput format (Pantoliano et al., 2001; Lo et al., 2004) Hence, this technique is widely used as primary screening tool. (Ciulli and Abell, 2007)

1.3.3 Isothermal Titration Calorimetry

Isothermal titration calorimetry (ITC) provides detailed thermodynamic insights into the formation of macromolecular complexes. A typical setup for an ITC experiment is shown in Figure 2A. A binding partner (normally a small molecule) is added via successive injections into the sample cell containing the target protein. ITC measures the release (exothermic reaction) or the absorption (endothermic reaction) of heat associated with a biomolecular interaction. The rate of heat transfer to regain a thermal equilibrium between the sample cell and reference cell (containing water or buffer) is detected over time (Figure 2B). The association constant (K_A or ΔG), the enthalpic (ΔH) contribution and the stoichiometry N of the interaction can be estimated by fitting the integrated heats to an appropriate binding model as shown in Figure 2C. The entropic contribution (ΔS) is calculated from the Gibbs-Helmholtz equation. (Freyer and Lewis, 2008)

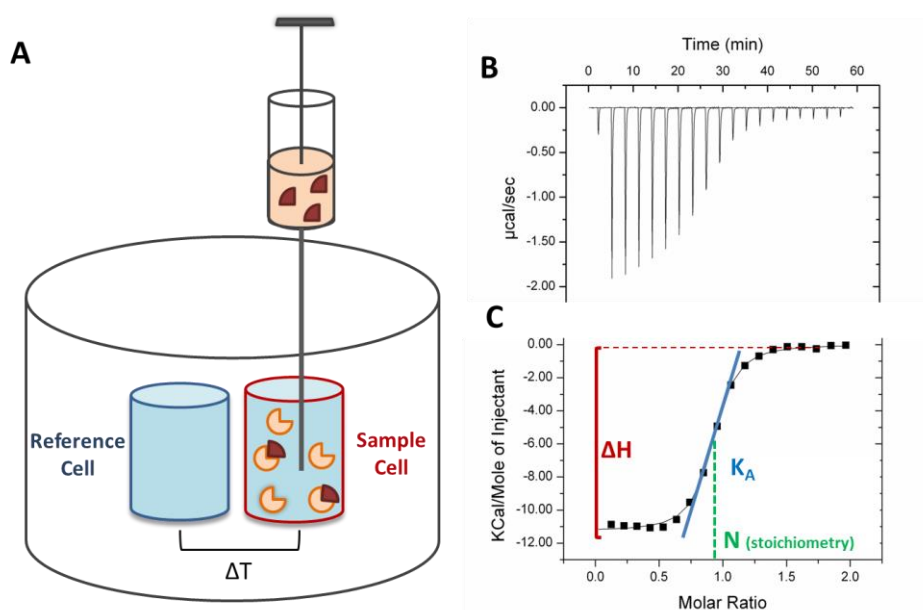


Figure 4: ITC experiment A) Schematic representation of an ITC experiment B) ITC raw data; differential heat for successive injections of a ligand to a binding partner C) Integrated heat of every injection against the molar ratio of the reaction. (adapted and modified from Malvern Instruments Ltd., 2015)

ITC is a powerful tool that allows differentiating between ΔH and ΔS as the main driving forces of a binding event. The enthalpic contribution (ΔH) is regarded as the sum of non-covalent interactions which were broken and formed upon formation of a protein-ligand complex. In detail, a ligand in solution is surrounded by a hydrate-shell. During the switch from the free to the bound state, the interactions between ligand and water molecules are detached. Subsequently, new interactions between protein and ligand are formed. Hence, for a beneficial enthalpic contribution these protein-ligand interactions have to overcompensate the energy spent for desolvation. Accordingly, polar moieties not forming beneficial interactions with the protein result in an enthalpic penalty. (Freire, 2004; Ladbury et al., 2010)

The entropic term consists of the favorable entropy associated with water that is displaced from the protein binding pocket upon ligand binding and the entropic penalty associated with the loss of conformational and translational freedom in the bound state. (Freire, 2004)

Given, that it is much easier to increase the affinity of hit compounds by the addition of space-filling hydrophobic moieties than by the introduction of polar groups forming directed interactions compounds tend to become more lipophilic during lead optimization. Therefore, Ladbury introduced the enthalpic efficiency (EE) metric which normalizes ΔH for the number of non-hydrogen atoms (N ; $EE = \Delta H/N$). This metric allows to rank hit compounds according to their strength of non-covalent interactions and it provides an alternative guidepost during lead optimization. (Ladbury et al., 2010)

ITC is a valuable tool during the drug discovery process, facilitating the investigation of multiple characteristics of a binding event in a single experiment. Despite the huge amount of protein and time-consuming measurements, ITC is considered as the 'gold standard' for the validation and characterization of identified hit compounds. (Ciulli and Abell, 2007)

1.4 Targeting the Virulence of *Pseudomonas aeruginosa*

1.4.1 The Opportunistic Pathogen *Pseudomonas aeruginosa*

Pseudomonas aeruginosa is a ubiquitous Gram-negative opportunistic pathogen. It is highly adaptable to different environmental conditions and able to infect a broad spectrum of host organisms ranging from plants, nematodes to humans (Silby et al., 2011). Most human infections are associated with an impaired immune response for example found in HIV (Franzetti et al., 1992) or are acquired in a hospital setting (Gaynes and Edwards, 2005). *P. aeruginosa* is able to grow on almost all human tissues thereby causing severe acute and chronic infections. Hence, the pathogen can be found prevalently in all kinds of nosocomial infection sites for example urinary tract (16%), surgical wounds (9%) and pneumonia (18%) (Gaynes and Edwards, 2005). Moreover, *P. aeruginosa* represents a serious threat for burned patients (Pruitt and McManus, 1984).

This opportunistic pathogen is the major cause of death for patients suffering from cystic fibrosis (CF). (Emerson et al., 2002) CF is caused by various genetic disorders leading to malfunction of the CFTR chloride channel expressed in the lung epithelium. (Riordan et al., 1989; Dean et al., 1990) The microenvironment within CF lungs enables *P. aeruginosa* to establish chronic infections. Several hypotheses are discussing the mechanism promoting bacterial colonization of CF lungs: reduced mucociliary clearance due to viscous airway surface liquid or impaired function of antibacterial peptides due to high salt concentrations in the liquid. (Davies, 2002)

The high genetic mutability of *P. aeruginosa* (Smith et al., 2006) as well as its ability to regulate gene expression in response to changing environmental conditions (Bragonzi et al., 2005) allow for rapid phenotypic adaption. These processes provide the bacterium with the ability to switch from a planctonic to a sessile biofilm lifestyle. Biofilms are bacterial communities embedded in hydrated extracellular matrix attached to a surface (Costerton et al., 1999). The composition of the matrix is highly variable depending on the present nutrients and conditions. Major structural components are polysaccharides, extracellular DNA (eDNA) and proteins. (Sutherland, 2001) Biofilm development is described as a multi-stage process: initially, free floating bacteria adhere to an inert or living surface; these bacteria proliferate and form microcolonies; from these colonies matured biofilms emerge. (Costerton et al., 1999) Chronic infections like pneumonia in the CF airways are associated with *P. aeruginosa* growing in a sessile biofilm mode. (Lam et al., 1980; Singh et al., 2000) This lifestyle leads to increased tolerance against host defense mechanisms and intensive antibiotic treatment. (Stewart and William Costerton, 2001) The biofilm forms a diffusion barrier slowing down the penetration of xenobiotics (Gordon et al., 1988) and antimicrobial peptides (Mulcahy et al., 2008) into lower compartments by capturing positively charged molecules on negatively charged matrix components or by enzymatic

degradation (Dibdin et al., 1996) of therapeutic agents. Furthermore, within a biofilm different microenvironments can be found. In such areas where nutrients and oxygen are limited, bacterial cells show low metabolic activity and slow growth rates leading to low antibiotic susceptibility. (Walters et al., 2003) Another reason for relapsing *P. aeruginosa* infections is the occurrence of persister cells. This small subpopulation of dormant cells possesses high tolerance to antibiotics and represents the basis for infection recurrence. (Lewis, 2010)

Another characteristic of *P. aeruginosa* is the expression and secretion of various virulence factors during the course of an infection. (Lyczak et al., 2000) Pili and flagella promote adhesion to the initial infection site as well as motility for the dissemination of the infection. (Sato et al., 1988) The adherence process is further supported by lectin A and B which bind to specific carbohydrates on the surface of host cells. (Chemani et al., 2009) The production of bacterial surfactants, especially rhamnolipids (RhlAB), increases the permeability of host epithelia thereby facilitating bacterial invasion. (Zulianello et al., 2006) Furthermore, the secretions of different cytotoxic extracellular products like, hydrogen cyanid (HCN) and the redoxactive blue pigment pyocyanin induce damage to host cells and impair the growth of competing pathogens. (Lau et al., 2004; Anderson et al., 2010) Additionally, the bacterium secretes various enzymes like elastase (LasB) degrading host proteins (Bejarano et al., 1989), phospholipases damaging cell membranes (Ostroff et al., 1990) and exotoxin A (Foley et al., 1995) impairing protein biosynthesis in eukaryotic cells. Overall, all these virulence determinates contribute to the establishment and maintenance of the infection process.

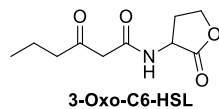
The release of virulence factors as well as the establishment and maturation of a biofilm are processes which would remain ineffective if they were carried out by single organisms. Hence, these activities need to be coordinated on a population-wide scale. Therefore, the regulation of such behaviors mostly involves bacterial cell-to-cell communication systems which are described in the following section. (Waters and Bassler, 2005)

1.4.2 The Quorum Sensing Networks of *Pseudomonas aeruginosa*

During the last decades our view on bacterial lifestyle changed drastically. Bacteria were previously regarded as unicellular planktonic organisms; nowadays it becomes more and more evident that bacterial colonies build organized communities. The synchronization of phenotypic actions on a colony-wide scale relies on the release and detection of small signaling molecules also known as autoinducers. The concentrations of these molecules increase as a function of cell density allowing the bacterium to sense its environment for the neighboring cells. If a critical concentration is reached gene expression is altered collectively. (Waters and Bassler, 2005) This bacterial cell-to-cell communication is called quorum sensing (QS) and was first discovered in the marine bacterium *Vibrio fischeri*. (Nealson and Hastings, 1979) In this bacterium the QS LuxR-LuxI regulatory circuitry controls characteristic bioluminescence and provides a prime

example for QS systems in other Gram-negative bacteria. In detail, the synthase LuxI generates an *N*-acyl-homoserine lactone (AHL) derivative as signaling molecule (Figure 5). (Eberhard et al., 1981; Engebrecht and Silverman, 1984) While the population density increases the signal accumulates in the medium. (Kaplan and Greenberg, 1985) When a certain threshold is reached, the molecule binds to transcriptional regulator LuxR, (Adar and Ulitzur, 1993) which in turn activates the expression of an operon encoding for luciferase enzymes responsible for bioluminescence and the AHL synthase LuxI. (Engebrecht and Silverman, 1984) The enhanced expression of the enzyme LuxI leads to increased biosynthesis of the autoinducer generating to a positive feedback loop.

Vibrio fischeri



Pseudomonas aeruginosa

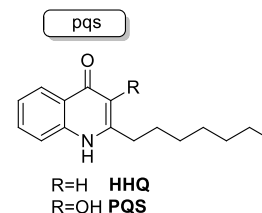
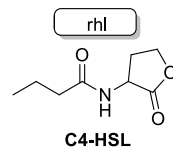
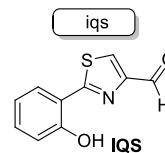
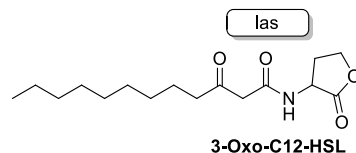


Figure 5: Quorum sensing autoinducer molecules found in *Vibrio fischeri* (upper part) and *P. aeruginosa* (lower part)

P. aeruginosa possesses four distinct QS systems (Figure 5 and 6). (Lee and Zhang, 2015) The *las* (Gambello and Iglewski, 1991; Passador et al., 1993) and the *rhl* (Ochsner et al., 1994; Ochsner and Reiser, 1995) systems use AHLs as autoinducers and belong to the LuxR-LuxI regulator family. The LuxI homologues LasI and RhII catalyze the synthesis of 3-oxo-C12-HSL (Pearson et al., 1994) and C4-HSL (Pearson et al., 1995), respectively (Figure 5). 3-oxo-C12-HSL activates the corresponding regulator LasR while C4-HSL acts as an agonist on RhIR. Transcriptomic analysis revealed that over 6% of the *P. aeruginosa* genome are regulated via these QS systems including genes required for basic metabolic pathways as well as for the expression for virulence determinates. (Schuster and Greenberg, 2006) Examples for key virulence factors controlled by the *las* and the *rhl* system are shown in Figure 6. These include the LasA protease, LasB elastase, ArpA alkaline protease, rhamnolipids, pyocyanin and hydrogen cyanid. (Lee and Zhang, 2015)

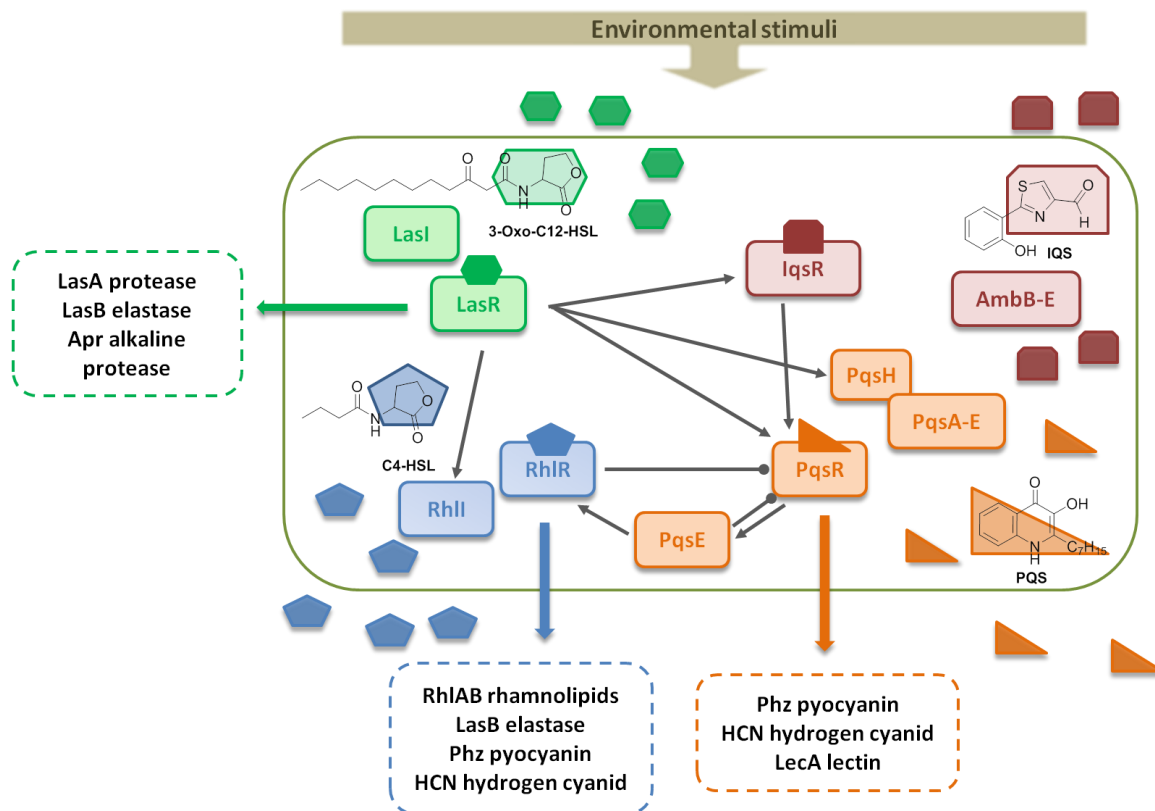


Figure 6: The interplay of the four quorum sensing networks and their contribution to *P. aeruginosa* virulence factor expression. (adapted and modified from Lee and Zhang, 2015)

In contrast to the widespread use of AHL derivatives by Gram-negative bacteria, *P. aeruginosa* uses two structurally unrelated scaffolds for QS cell-to-cell communication (Figure 5). The third QS network is called the Pseudomonas Quinolone Signal short *pqs* (Pesci et al., 1999) and employs the 4-hydroxy-2-alkylquinolones (HAQs) as messenger molecules. The HAQ signaling was found only in *Pseudomonas* and *Burkholderia* strains. (Diggle et al., 2006a) Over 50 HAQ congeners have been identified (Lepine et al., 2004) among them 2-heptyl-3-hydroxy-4-quinolone (PQS) and its precursor 2-heptyl-4-quinolone (HHQ) are the most prominent autoinducer molecules. HAQs were originally isolated from *P. aeruginosa* cultures and their structures were elucidated due to the antibacterial properties of some derivatives. (Hays et al., 1945; Cornforth and James, 1956) In 1999, Pesci and coworkers recognized the role of PQS as an intercellular signaling molecule. (Pesci et al., 1999)

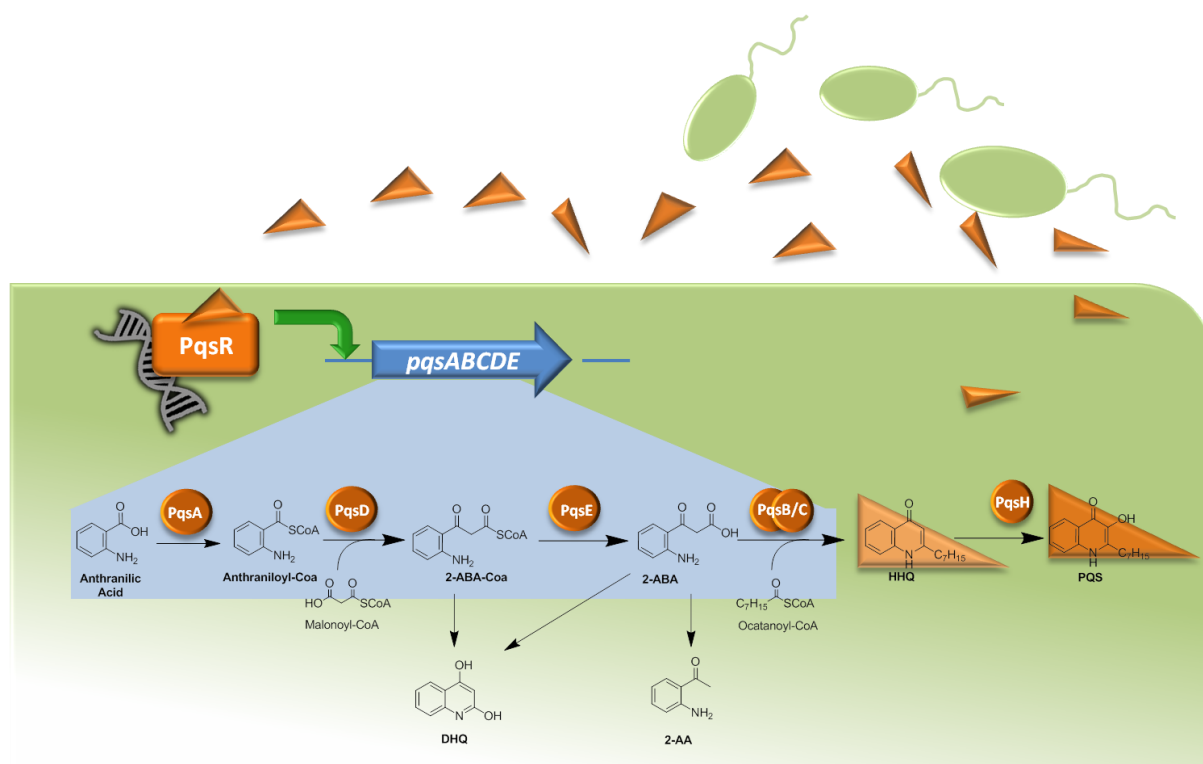


Figure 7: The *pqs* system and the biosynthesis of HHQ and PQS. (Drees and Fetzner, 2015)

The biosynthesis of HHQ and PQS is outlined in Figure 7 and involves the expression of the biosynthesis operon *pqsABCDE* and *pqsH*. (Gallagher et al., 2002) The coenzyme A ligase PqsA activates anthranilate to anthraniloyl-CoA. (Coleman et al., 2008) PqsD catalyses a Claisen-type condensation reaction using anthraniloyl-CoA and malonyl-CoA to yield 2-aminobenzoylacetate (2-ABA-CoA). (Zhang et al., 2008; Dulcey et al., 2013) The thioester of 2-ABA-CoA is cleaved by PqsE to obtain the free carboxylic acid 2-aminobenzoylacetate (2-ABA). (Drees and Fetzner, 2015) The heterodimer PqsBC directs the ring-closing reaction of 2-ABA and octanoyl-CoA to afford HHQ. (Dulcey et al., 2013) HHQ is hydroxylated in the 3-position by PqsH to form PQS. (Gallagher et al., 2002; Schertzer et al., 2010) Notably, this biosynthesis process furnishes two major degradation products: 2-ABA-CoA is highly instable and spontaneously decomposes to 2,4-dihydroxyquinoline (DHQ). (Zhang et al., 2008) Similarly, 2-ABA either undergoes spontaneous cyclization to form also DHQ or decarboxylates to 2-AA. (Dulcey et al., 2013; Drees and Fetzner, 2015) So far, a function of DHQ in QS signaling has not been reported. However, 2-AA is supposed to promote the switch to chronic infection phenotypes and the formation of persister cells. (Kesarwani et al., 2011; Que et al., 2013)

Both molecules, HHQ and PQS, bind to the *Pseudomonas* quinolone signal receptor (PqsR), also known as multiple virulence factor regulator (MvR). (Xiao et al., 2006) PqsR is a LysR-type transcriptional regulator (LTTR) which controls directly the expression of the *pqsABCDE* and *phnAB* operons. (Cao et al., 2001; Wade et al., 2005) The *phnAB* operon encodes for anthranilate synthase catalyzing the conversion of chorismate to anthranilate. (Gallagher et al., 2002) The interaction of PQS and HHQ with PqsR results in an enhanced expression of these

operons.(Wade et al., 2005; Xiao et al., 2006) Overall this leads to an autoinductive loop comparable to the ones found in AHL-based QS systems. The *pqs* system is essential for the full pathogenicity of *P. aeruginosa*.(Deziel et al., 2005) Accordingly, it takes part in the regulation of various virulence determinates such as pyocyanin, elastase and hydrogen cyanide.(Cao et al., 2001; Diggle et al., 2003; Deziel et al., 2005) The contribution of PqsE to these regulatory processes will be discussed in section 1.4.5. The *pqs* system clearly contributes to the establishment and maturation of biofilms by triggering the release of eDNA (Allesen-Holm et al., 2006) and the expression of lectins (Diggle et al., 2006b). Notably, the HHQ and PQS molecules possess immune suppressive properties.(Kim et al., 2010)

A recently discovered fourth QS circuitry is called *iqs* (Lee et al., 2013) and employs 2-(2-hydroxyphenyl)-thiazole-4-carbaldehyde also known as IQS (Figure 5) as signaling molecule. The biosynthetic gene cluster *ambBCDE* directs the biosynthesis of IQS. Though the transcriptional regulator has not been identified so far, *ambBCDE* knock-out studies clearly demonstrated the role of IQS in cell-to-cell communication.(Lee et al., 2013)

All four QS regulatory circuits are intertwined (Figure 6) and hierarchically organized, wherein the *las* system possesses a superordinate role. Activated LasR positively regulates the expression of *rhlR* (Latifi et al., 1996; Pesci et al., 1997) and *pqsR* (Wade et al., 2005) as well as *pqsH* (Gallagher et al., 2002). Furthermore, the autoinducer IQS is not detectable in *lasI* or *lasR* negative mutant strains when grown in rich medium.(Lee et al., 2013) Despite the central role of the LasR, loss-of-function mutations are frequently observed during the course of chronic infections.(Hoffman et al., 2009; Ciofu et al., 2010) It has been clearly shown that in a *lasR* mutant, the *pqs* and *rhl* systems are able overcome the *las* dependency and restore virulent phenotypes.(Diggle et al., 2003; Dekimpe and Déziel, 2009) The same phenomenon was observed for the *iqs* system. When encountering low phosphate levels IQS is produced in the absence of LasR. Under these conditions, *iqs* supersedes the position of the *las* system and drives the expression of the *rhl* and *pqs* systems.(Lee et al., 2013)

This complex regulatory network allows *P. aeruginosa* to collectively adapt to changing environmental conditions and represents the social intelligence of bacterial colonies.(Ben Jacob et al., 2004) The discovery of this bacterial cross talk opens the door for the development of anti-infectives with novel mode-of-action.

1.4.3 Interference with the *pqs* System as Antivirulence Strategy

Classical antibiotics target structures are essential for bacterial viability (bactericidal) or impair bacterial replication (bacteriostatic). The use of antibiotics provides organisms, which are resistant to this substance, with a growth advantage over bacteria which are susceptible.

Therefore antibiotics select for resistant mutants, thereby limiting their own efficacy and lifetime.(Walsh, 2003) Regardless of their underlying mechanisms or origin, bacteria developed resistance mechanisms against all established antibiotics.(Walsh, 2003; Alanis, 2005) “Resistance, then, has proven not to be a matter of if, but a matter of when.” Christopher Walsh

Most of the antibiotic classes, which are in use today, have been discovered between 1940 to 1960.(Fischbach and Walsh, 2009) These discoveries enabled the successful treatment of former life-threatening bacterial infections like pneumonia or tuberculosis and, hence, significantly contributed to an increase of life expectancy.(Centers for Disease Control and Prevention, 1999) After this golden age, most antibiotics introduced to the clinic represent synthetically modified derivatives of former identified scaffolds.(Fischbach and Walsh, 2009) This lack of innovation was accompanied by decreasing research efforts within the antibiotic field.(Projan, 2003) The popular belief that the “war against pestilence” (Spellberg and Taylor-Blake, 2013) is won was rapidly disproved by the spreading of resistant bacterial strains.(Alanis, 2005) Nowadays, highly resistant bacteria so called “superbugs” represent a serious and prevalent threat to public health while the development of novel treatment options stagnates.(Boucher et al., 2009) Alarmingly, the first plasmid-mediated resistance mechanism against the last resort antibiotic colistin emerged recently.(Liu et al., 2015)

The development of anti-virulence drugs which prevent the expression of highly virulent phenotypes without affecting bacterial viability possesses an attractive and innovative escape strategy from the antibiotic crisis.(Rasko and Sperandio, 2010) In contrast to conventional antibiotics, this strategy does not exert selective pressure on bacterial populations and, therefore, it is assumed to be less prone to rapid development and spreading of resistance.(Clatworthy et al., 2007) Notably, this claim is controversially discussed in the scientific community and has to be proven or falsified in future studies.(Allen et al., 2014)

In *P. aeruginosa* the expression of most virulence factors is tightly regulated by QS cell-to-cell communication.(Lee and Zhang, 2015) Hence, the interference with such superordinate regulatory processes provides a way to inhibit multiple virulence determinates with a single compound.(Rasko and Sperandio, 2010) Consequently, this strategy has been successfully applied and selected compounds interfering with QS regulated virulence in *P. aeruginosa* are shown in Figure 8.

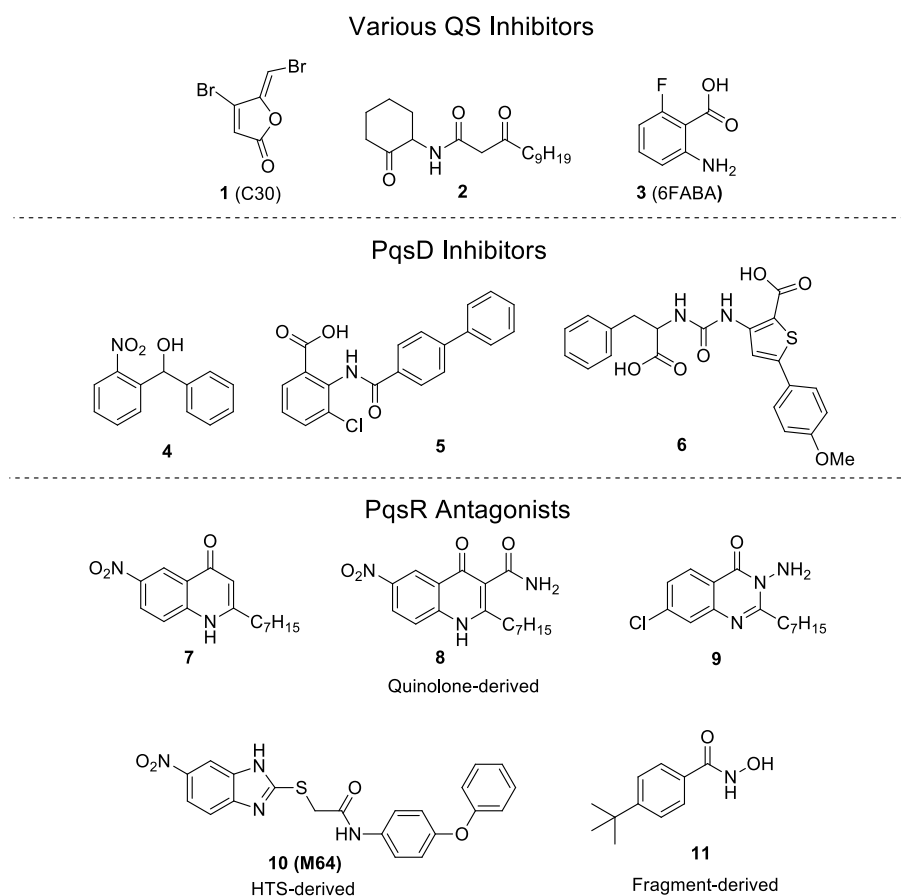


Figure 8: Selected QS inhibitors targeting *P. aeruginosa* virulence

The brominated furanon C30 (**1**) is a close synthetic analog of secondary metabolites isolated from the marine macroalga *Delisea pulchra*.(Nys et al., 1993; Manny et al., 1997) Compound **1** displayed potent inhibition of QS-regulated phenotypes by destabilizing LasR and *in vivo* efficacy in a mouse lung infection model.(Manefield et al., 2002; Hentzer et al., 2003) Various libraries of AHL analogs were synthesized.(Geske et al., 2005; Ishida et al., 2007; Amara et al., 2009) Compound **2** is one of the first analogs which showed antagonistic activity on LasR and RhIR resulting in reduction of pyocyanin, elastase and biofilm volume.(Smith et al., 2003)

A loss of *las* activity was frequently observed during chronic infections (Hoffman et al., 2009) which would render a *las*-targeting antivirulence therapy ineffective. Therefore, we and other groups focused on the development of compounds interfering with *pqs* system. Remarkably, the *pqs* system only occurs in *Pseudomonas* and *Burkholderia* strains.(Diggle et al., 2006a) Hence, this strategy allows targeting specifically these strains without affecting the residual human microbiota.

Lesic *et al.* aimed at the discovery of PqsA inhibitors based on the natural substrate anthranilic acid (**3**). (Lesic et al., 2007) Compound **3** was applied to a mouse thermal injury infection model leading to increased survival rates and limited dissemination through host tissues.(Lesic et al., 2007) This study afforded the first *in vivo* proof of principle for a *pqs* targeting antivirulence

therapy. Following a ligand-based approach our group was able to obtain the first PqsD inhibitor (**4**) which inhibited HHQ biosynthesis and affected biofilm formation.(Storz et al., 2012) The benzamidobenzoic acid derivative **5** was derived from published inhibitor of FabH, an enzyme sharing structural similarities with PqsD.(Hinsberger et al., 2014) In a comparable approach, inhibitors containing a catechol scaffold were identified.(Allegretta et al., 2015) Sahner *et al.* established the 5-aryl-ureidothiophene-2-carboxylic acid derivatives (**6**) as PqsD blockers.(Sahner et al., 2013) Notably, the high *in vitro* activities of PqsD inhibitors **5** and **6** did not translate into potent antivirulence activities in *P. aeruginosa*.(Sahner et al., 2013; Hinsberger et al., 2014)

In a parallel project, our group successfully worked on the development of the PqsR antagonists (**7**) by chemical modification of the natural ligand HHQ. Compound **7** displayed nanomolar antagonistic activity in a heterologous *E. coli* reporter gene strain but suffered from lacking antivirulence activity in *P. aeruginosa*.(Lu et al., 2012) A subsequent MS analysis elucidated that **7** undergoes enzymatic hydroxylation catalyzed by PqsH which transforms the antagonist **7** into a potent agonist. A blockade of the metabolically labile position by a carboxamide moiety led to the potent antagonist **8** which showed the expected antivirulence activities and was able to protect *Galleria mellonella* from lethal *P. aeruginosa* infections.(Lu et al., 2014) In a similar study quinazolinone derivative **9** was developed and its effect on biofilms described. Moreover, the crystal structures of the ligand binding domain (LBD) of PqsR (apo form), in complex with antagonist **9** and the native agonist NHQ (2-nonyl-4-quinolone) were resolved.(Ilangoan et al., 2013) During a phenotypic HTS campaign, over 280,000 compounds were evaluated for their effects on the PqsR regulon. Thereby, the benzamido-benzimidazole scaffold was discovered and optimized to afford PqsR antagonist **10**. Beyond its impressive antivirulence activities, this compound affected persister cell formation and showed efficacy in acute and chronic mice infection models as stand-alone or combination therapy with conventional antibiotics.(Starkey et al., 2014) All described antagonists possess a poor physico-chemical profile. In order to address these drawbacks, our group conducted a fragment-based screening initially leading to compounds containing a carboxamide moiety. A straightforward optimization approach resulted in the hydroxamic acid **11** which showed remarkable potency in *P. aeruginosa* with respect to its small molecular size.(Klein et al., 2012)

Overall, there is a high need for novel anti-infectives especially against Gram-negative pathogens like *P. aeruginosa*. Therefore, the development of compounds targeting *pqs* mediated virulence is a compelling strategy which led to first promising *in vivo* results.(Lesic et al., 2007; Lu et al., 2014; Starkey et al., 2014) Nevertheless, more research efforts are necessary to generate lead-like molecules.

1.4.4 The Transcriptional Regulator PqsR as Antivirulence Target

PqsR belongs to LTRR receptor family and consists of a *N*-terminal helix-turn-helix DNA binding motif and a *C*-terminal LBD. (Cao et al., 2001) In general, LTRRs form homodimeric complexes which bind to specific DNA regions in proximity to the regulated gene. Two dimers form a tetrameric complex leading to bending of DNA strand. The binding of autoinducer molecules results in an alteration of this bending which in turn facilitates the interaction of the RNA polymerase with the promoter region leading to enhanced transcription of the target genes. (Maddocks and Oyston, 2008) Notably, this working model has been proven for similar LTRRs but not in detail for PqsR. However, PqsR shows several characteristic features indicating that it works in a similar fashion: specific DNA binding (Cao et al., 2001), enhanced expression of *pqsABCDE* and *phnAB* operons in the presence of autoinducer molecules (Wade et al., 2005; Xiao et al., 2006) and its LBD crystallizes as homodimeric complex (Ilangoan et al., 2013).

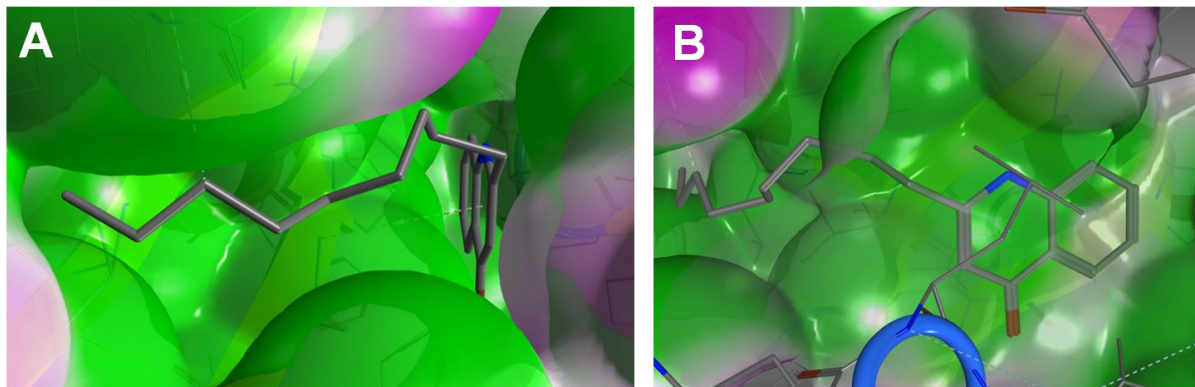


Figure 9: Crystal structure of the PqsR LBD in complex with NHQ (4JVD). Lipophilicity is plotted on the Van-der-Waals surface of the receptor as follows green: lipophilic, purple: hydrophilic. **A)** View from the dimer interface to alkyl chain pocket (in the front) **B)** Side view; quinolone pocket in the front

The crystal structure of the LBD of PqsR with the autoinducer NHQ (PDB code: 4JVD; Figure 9) revealed a L-shaped binding pocket. (Ilangoan et al., 2013) This pocket possesses a highly lipophilic environment and is divided in two subpockets: the alkyl side chain pocket (Figure 9A) located at the dimer interface and the narrow quinolone pocket (Figure 9B) pointing deeper into the protein structure.

PqsR is a key player for the expression of various *P. aeruginosa* virulence factors (Deziel et al., 2005) and *pqsR*-negative strains displayed reduced pathogenicity in several host infection models. (Rahme et al., 1997; Cao et al., 2001; Gallagher et al., 2002; Xiao et al., 2006) Furthermore, first antagonists showed efficacy in different *in vivo* models (Lu et al., 2014; Starkey et al., 2014) what underlines the potential of PqsR as drug target for the development of future anti-infectives.

1.4.5 The Enigmatic Role of PqsE

The presence of PqsE is essential for the full expression of virulence determinants like pyocyanin, elastase and rhamnolipids.(Gallagher et al., 2002; Diggle et al., 2003; Farrow et al., 2008) Knock-out complementation studies clearly demonstrated that PqsE can restore virulent phenotypes even in the absence of a functional *pqs* system.(Farrow et al., 2008; Hazan et al., 2010) Similar experiments confirmed these findings also in different *in vivo* infection models.(Rampioni et al., 2010)

Transcriptomic analysis revealed that the PqsE stimulon comprises a subset of *pqs* controlled and additional genes.(Rampioni et al., 2010) Different studies disclosed that the regulatory function of PqsE is at least partially mediated via RhlR.(Farrow et al., 2008; Hazan et al., 2010) Furthermore, PqsE down regulates the expression of its own operon leading to negative regulatory loop.(Hazan et al., 2010; Rampioni et al., 2010)

For many years, it was assumed PqsE would not take part in the HHQ biosynthesis but Drees and Fetzner showed recently that PqsE can act as pathway-specific thioesterase (Figure 7). Notably, this biosynthetic function can be bypassed by other housekeeping thioesterases.(Drees and Fetzner, 2015)

Yu *et al.* resolved the crystal structure of PqsE which revealed a beta-lactamase fold containing a dinuclear Fe(II)/Fe(III) metal center at the active site. The crystals contained a 'benzoic acid shaped ligand' in the active center (Figure 10). Subsequently, the binding of benzoic acid and anthranilate was confirmed by ITC.(Yu et al., 2009)

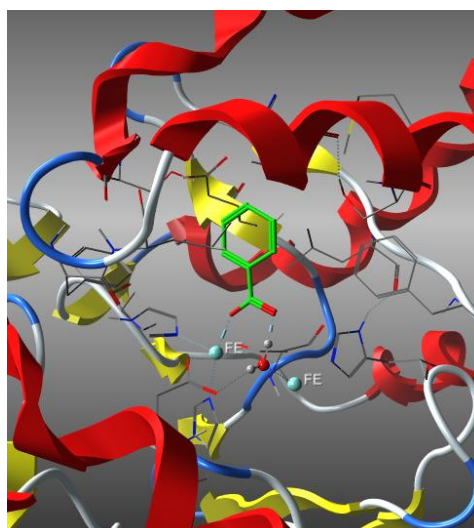


Figure 10: The crystal structure of PqsE in complex with benzoic acid depicted in green (2Q0J). View into the active site with the Fe(II)/Fe(III) metal center

Despite many research efforts, the exact molecular mechanism of PqsE for the regulation of virulence remains a mystery. However, its central role for the pathogenicity of *P. aeruginosa* makes PqsE a potentially attractive antivirulence target.

2 Objectives

There is an increasing need for novel and innovative treatment options for bacterial infections. Especially infections with Gram-negative pathogens like *P. aeruginosa* have become more and more difficult to treat due to rapid development and spreading of resistances against conventional antibiotics. Anti-infectives which block the expression of virulent phenotypes without exerting selective pressure on the bacteria might overcome these drawbacks. Following this idea, the present work aims at the development of compounds interfering with the *pqs* QS system in *P. aeruginosa*.

Antagonizing the transcriptional regulator PqsR by synthetic ligands (**8** and **10**, Figure 8) resulted in increased survival rates in different infection models. (Lu et al., 2014; Starkey et al., 2014) Hence, the 'proof-of-principle' for PqsR as an antivirulence target has been achieved. However, both compounds showed poor physicochemical properties which might hamper the further development.

The first part of this thesis deals with the development of drug-like PqsR antagonists. In doing so, fragment-based drug discovery methods are applied. Starting points for further synthesis programs are selected from the hits of an SPR fragment screening based on their thermodynamic profiles and their antagonistic activities in a heterologous *E. coli* reporter gene system. Structure-based methods as well as literature-known SAR should be incorporated into the drug design process. Subsequently, a robust synthetic route has to be developed allowing access to numerous derivatives. Selected hit scaffolds should be optimized regarding their antagonistic potencies and anti-virulence activities in *P. aeruginosa* without affecting the bacterial viability. The development process is guided by suitable efficiency metrics in order to put a special emphasis on physicochemical properties of the designed antagonists.

The fundamental role of PqsE for virulence regulation (Farrow et al., 2008) as well as the reduced pathogenicity of *pqsE* negative strains (Rampioni et al., 2010) in different infection models makes this mysterious protein attractive for future drug discovery approaches. Therefore, the second objective of this work is the discovery of synthetic PqsE ligands allowing to gain novel insights into the different protein functions. Achieving this goal involves the screening of a fragment library and the elucidation of the binding mode of the obtained hit compounds. The effects of these compounds on the PqsE enzymatic activity are evaluated in different *in vitro* assays. Subsequently, the ligands are profiled for their effect on the expression of virulence factors and signaling molecules in *P. aeruginosa*.

3 Results

3.1 Chapter A:

Discovery and Biophysical Characterization of 2-Amino-oxadiazoles as Novel Antagonists of PqsR, an Important Regulator of *Pseudomonas aeruginosa* Virulence

Michael Zender, Tobias Klein, Claudia Henn, Benjamin Kirsch, Christine K. Maurer, Dagmar Kail, Christiane Ritter, Olan Dolezal, Anke Steinbach, Rolf W. Hartmann

Reprinted (adapted) with permission from *J. Med. Chem.* **2013**, 56, 6761–6774

Copyright (2013) American Chemical Society.

ABSTRACT

The human pathogen *Pseudomonas aeruginosa* employs alkyl quinolones for cell-to-cell communication. The *Pseudomonas* Quinolone Signal (PQS) regulates various virulence factors *via* interaction with the transcriptional regulator PqsR. Therefore, we consider the development of PqsR antagonists a novel strategy to limit the pathogenicity of *P. aeruginosa*. A fragment identification approach using surface plasmon resonance screening led to the discovery of chemically diverse PqsR ligands. The optimization of the most promising hit (**5**) resulted in the oxadiazole-2-amine **37** showing pure antagonistic activity in *E. coli* (EC₅₀ 7.5 μM) and *P. aeruginosa* (38.5 μM) reporter gene assays. **37** was able to diminish the production of the PQS precursor HHQ in a PqsH deficient *P. aeruginosa* mutant. The level of the major virulence factor pyocyanin was significantly reduced in wild-type *P. aeruginosa*. In addition, site-directed mutagenesis in combination with isothermal titration calorimetry and NMR INPHARMA experiments revealed that the identified ligands bind to the same site of PqsR by adopting different binding modes. These findings will be utilized in a future fragment growing approach aiming at novel therapeutic options for the treatment of *P. aeruginosa* infections.

INTRODUCTION

Our view of bacterial lifestyle has changed drastically in the last few years. In the past, bacteria were deemed to be autonomous unicellular organisms. Nowadays, it is increasingly recognized that they have the ability to communicate with each other. A particular form of bacterial communication is referred to as *quorum sensing* (QS). QS functions *via* the release of signaling molecules. The concentration of these molecules increases as a function of cell density. After a threshold concentration has been reached they regulate gene expression in bacteria by activation of corresponding transcriptional regulators. QS cell-to-cell communication enables bacteria to monitor population density and to orchestrate their behavior on a population-wide scale.^{1,2}

Pseudomonas aeruginosa, a Gram-negative opportunistic pathogenic bacterium is an important causative agent of nosocomial infections^{3,4} and is involved in several acute and chronic infections. It is one of the major pathogens causing pneumonia e.g. in people suffering from cystic fibrosis.⁵ The ability of *P. aeruginosa* to form biofilms contributes to its low antibiotic susceptibility mainly due to lowered metabolic activity and decreased growth rate of biofilm bacteria.⁶ Moreover, during the last decades, *P. aeruginosa* strains resistant against nearly all established antibiotics have emerged, necessitating alternative therapeutic options.^{7,8}

P. aeruginosa coordinates group behaviours *via* three interconnected QS circuitries. The *las*^{9,10} and *rhl*^{11,12} communication systems operate *via* *N*-acylated homoserine lactones (AHLs), which are prevalent signaling molecules in Gram-negative bacteria. In contrast, the *pqs* system^{13,14} is restricted to particular *Pseudomonas* and *Burkholderia* strains.¹⁵ It functions *via* the 2-alkyl-4(1*H*)-quinolones (HAQ) signal molecules PQS (*Pseudomonas* Quinolone Signal; 2-heptyl-3-hydroxy-4(1*H*)-quinolone) and its precursor HHQ (2-heptyl-4(1*H*)-quinolone; Figure 1).

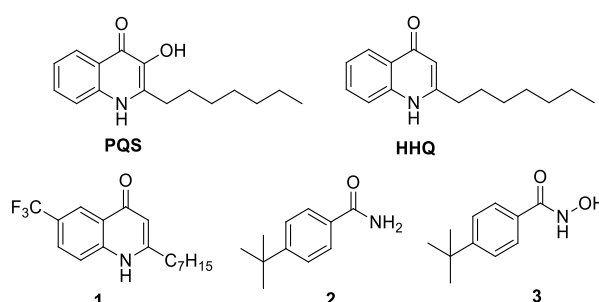


Figure 1: Structure of the *P. aeruginosa* signaling molecules PQS and HHQ as well as recently published PqsR ligands

Both interact with their receptor PqsR^{16,17} to control many genes involved in the production of various virulence factors like elastase, pyocyanin and lectins.¹⁸ Moreover, PQS enhances its own biosynthetic pathway by positively regulating the *pqsABCD(E)*^{16,19,20} and *phnAB*¹⁴ operons

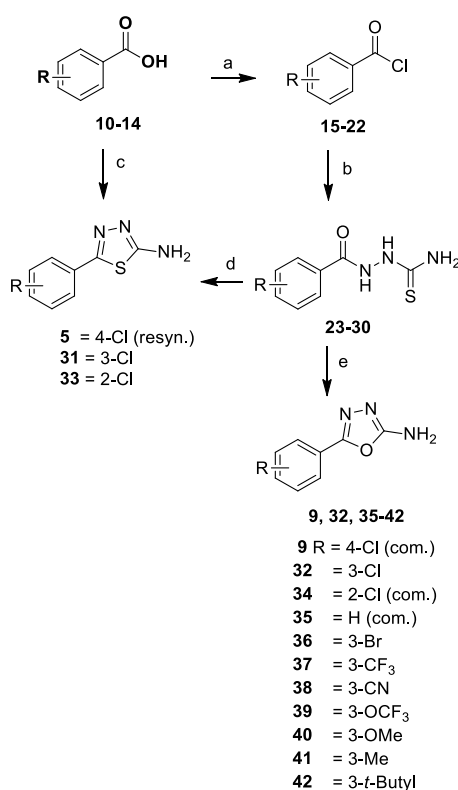
as well as it influences biofilm formation.^{18,21} The discovery of QS systems in pathogenic bacteria provides novel options for inhibiting the virulence without interfering with bacterial viability.²² The interference with QS systems by synthetic inhibitors²³ and the reduction of virulence factors by flucytosine²⁴ resulted in diminished *P. aeruginosa* pathogenicity in mouse pulmonary infection models demonstrating the in-vivo relevance of these anti-virulence strategies. Regarding *P. aeruginosa*, we consider PqsR - a key player for its pathogenicity - an attractive drug target. PqsR, also known as multiple virulence factor regulator (MvR), belongs to the family of LysR-type transcriptional regulators (LTTR).¹⁷ The N-terminal region contains a helix-turn-helix DNA binding motif and the C-terminus between amino acids 92-298 encodes for a predicted ligand binding domain (LBD).¹⁷

Recently, we have reported on the discovery of two different classes of antagonists which target PqsR (Figure 1). The HHQ derivative **1**²⁵ is a potent PqsR antagonist, but shows insufficient drug-like properties such as low aqueous solubility. Given that it is very difficult to strongly improve the physico-chemical profile of lead compounds with high logP values without losing activity,²⁶ a fragment screening was initiated as an alternative^{27,28} initially leading to the benzamide **2**.²⁹ **2** showed mixed agonistic-antagonistic properties. The introduction of a hydroxamic acid motif (**3**) provided a pure antagonistic profile.²⁹ It is noteworthy that hydroxamic acids are reported as chelating agents³⁰ and accordingly have been used as inhibitors of various metalloproteins.³¹ Furthermore, aromatic hydroxamic acids are described as potential mutagenic agents.³² In order to overcome these shortcomings and to gain chemical diversity, it was of major interest to discover PqsR antagonist with alternative scaffolds.

In this work, we present the discovery of structurally diverse, low molecular weight PqsR ligands employing surface plasmon resonance (SPR) biosensor experiments. Selected hits displaying sufficient affinity were functionally and thermodynamically characterized. Furthermore, the most promising hit compound **5** was structurally optimized and transformed into the potent PqsR antagonist **37** which was able to reduce the production of HHQ in a PqsH deficient mutant and the major virulence factor pyocyanin in wild-type *P. aeruginosa*.

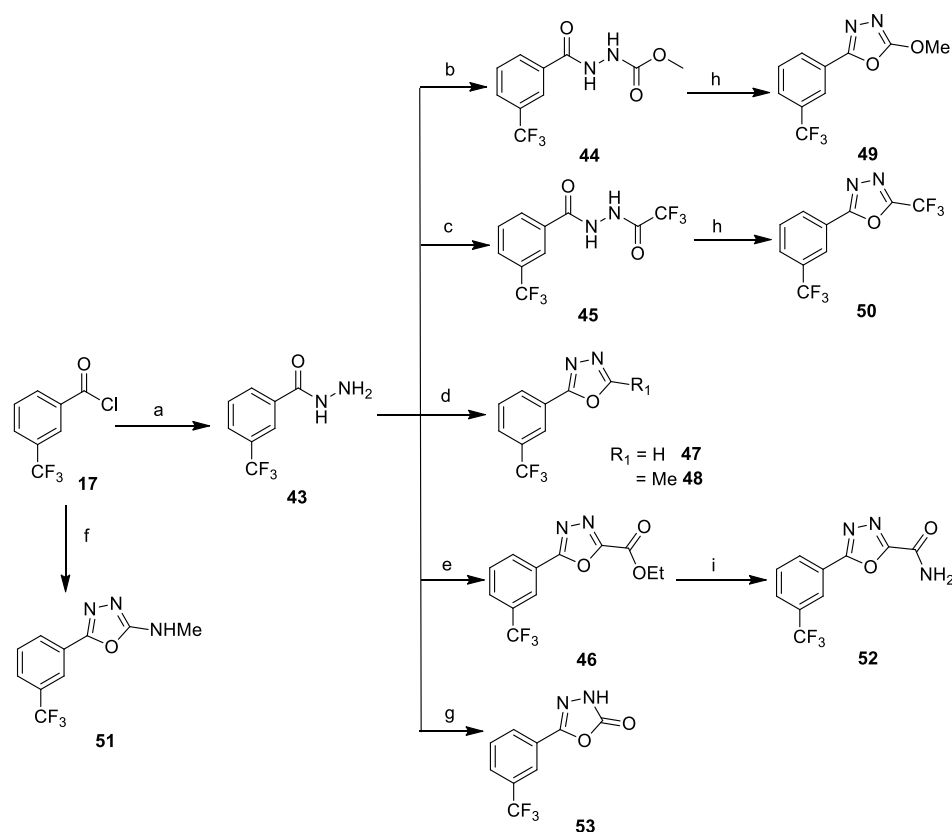
RESULTS AND DISCUSSION

Chemistry. The top screening hits **4-9** (Figure 2) were commercially available. The synthesis of the thiadiazole and oxadiazole derivatives was achieved by the use of different synthetic routes as described in the following.

Scheme 1. Synthesis of Oxadiazole-2-amine and Thiadiazole-2-amine Derivatives^a

^a Reagents and Conditions: (a) oxalyl chloride, DMF cat, DCM, reflux; (b) thiosemicarbazide, THF, 0 °C to RT; (c) thiosemicarbazide, POCl₃, 80°C; (d) H₂SO₄, RT; (e) 1,3-Dibromo-5,5-dimethylhydantoin, KI, NaOH, 2-propanol, 4 °C.

The synthesis of 1,3,4-oxadiazole-2-amine and 1,3,4-thiadiazole-2-amine derivatives is shown in Scheme 1. Thiadiazoles **5** and **33** were synthesized in a one-step procedure from commercially available benzoic acid derivatives and hydrazinecarbothioamide in POCl₃.³³ A classic coupling reaction of benzoic acid chlorides and hydrazinecarbothioamide afforded the benzoylthiosemicarbazides **23-30**.³⁴ **31** was obtained by treating the respective benzoylthiosemicarbazide **23** with concentrated sulfuric acid as dehydrating agent.³⁵ The ring closure which gives the respective 2-amino-1,3,4-oxadiazoles **32** and **35-42** was achieved under mild oxidative conditions using compounds **23-30** and employing 1,3-dibromo-5,5-dimethylhydantoin as primary oxidant in the presence of catalytic amounts of potassium iodide.³⁴

Scheme 2. Synthesis of 2-Substituted Oxadiazoles^a

^aReagents and Conditions: (a) methanol, Et₃N, RT, then hydrazine hydrate, water, 120 °C; (b) methyl chloroformate, NaHCO₃, water, dioxane, 0 °C; (c) trifluoroacetic anhydride, Et₃N, DCM, RT; (d) R₁C(OEt)₃, 150 °C; (e) ethyl oxalyl monochloride, Et₃N, DCM, 0 °C then tosyl chloride, RT; (f) *N*-methylhydrazinecarbothioamide, DCM, RT then EDC, 40 °C; (g) carbonyldiimidazole, Et₃N, DCM, RT; (h) Burgess reagent, THF, MW radiation, 100 W, 150 °C; (i) ammonia in methanol, RT.

The synthesis of compounds containing variations in the 2-position of the oxadiazole heterocycle (**47-53**) is summarized in Scheme 2. The precursor 3-(trifluoromethyl)benzohydrazide (**43**) was obtained from the corresponding benzoyl chloride **17** in a two-step procedure. Coupling of **43** with methyl chloroformate and trifluoroacetic anhydride afforded **44** and **45**. Ring-closure was carried out under microwave radiation using Burgess reagent as selective dehydrating agent yielding compounds **49** and **50**.³⁶ Heating of **43** in triethyl orthoformate or triethyl orthoacetate provided the oxadiazoles **47** and **48**, respectively.³⁷ **46** was synthesized in a one-pot two-step procedure, following the coupling of **43** with ethyl oxalyl monochloride and ring closure with tosyl chloride.³⁸ **46** was treated with ammonia in methanol to directly transform the ethyl ester in the corresponding carboxamide **52**.³⁹ The *N*-methylated analog **51** was obtained in a one-pot two-step protocol: the benzoyl chloride was coupled with *N*-methylhydrazinecarbothioamide and ring closure was carried out by employing EDC.⁴⁰ Oxadiazol-2-one **53** was prepared by conversion of **43** with carbonyldiimidazole.⁴¹

Identification of PqsR Ligands by Fragment Screening. The detection and analysis of biomolecular interactions is one of the key issues in the hit identification phase of a drug discovery project. Surface plasmon resonance spectroscopy represents a powerful tool to monitor and characterize binding events in real-time.⁴² We have applied this technology to screen a library containing 720 compounds with a molecular weight ranging from 100 to 350 g/mol (for details see SI; Table S2). PqsR was immobilized on the sensor chip surface *via* biotin-streptavidin specific interaction and compounds were initially screened at a single concentration of 100 μ M. Approximately 40 binding compounds were selected based on affinity and selectivity against negative control (bovine carbonic anhydrase II). Compounds showing undesirable SPR binding characteristics as described by Giannetti *et al.*⁴³ were not taken into consideration. These included fragments displaying binding irregularities, fragments with non-typical slow dissociation and compounds producing super-stoichiometric binding responses. The obtained hit rate of 5-6% can be regarded as excellent compared to the screening of more complex structures.²⁸ The best fragments were further subjected to SPR dose-ranging experiments to accurately determine dissociation constants (K_D values). The five top candidates displayed K_D values below 11 μ M (**4-8**, Figure 2 and Table 1). To further evaluate binding of the best screening hits we performed SPR competition experiments similar to those described previously.⁴⁴ Dose binding experiments with mixtures consisting of various concentrations of either compound **4** or **5** and constant concentrations of PQS showed no overall additivity in the SPR response (SI, Figure S2). Increasing the PQS concentration did not exceed the maximal binding capacity of the chip surface (R_{max} ; experimentally determined for the different fragments). These results show that both fragments compete with PQS for binding to PqsR.

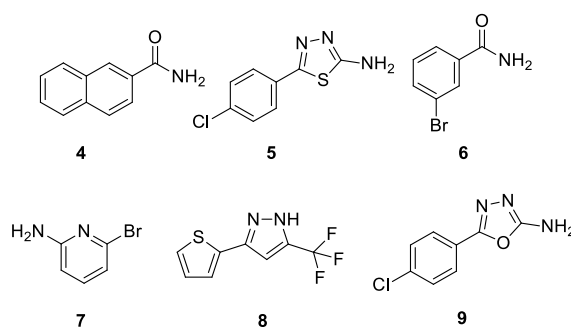


Figure 2: Chemical structures of highest affinity compounds **4-8** and compound **9**

As evaluation of the K_D values alone gives no clear indication of which ligands to select for further progression,⁴⁵ the thermodynamic parameters, which allow a more detailed understanding of biomolecular interactions,⁴⁶ were determined (Table 1) using isothermal titration calorimetry (ITC).

Table 1: Biophysical characterization of PqsR ligands.^a

Comp.	K_D (SPR) [μM] ^b	K_D (ITC) [μM]	ΔG [kcal mol ⁻¹]	ΔH [kcal mol ⁻¹]	$-\Delta S$ [kcal mol ⁻¹]	LE [kcal mol ⁻¹]
2	-	0.9±0.0	-8.3±0.0	-9.7±0.3	1.5±0.3	0.63
4	0.8±0.2	1.8±0.2	-7.9±0.1	-8.6±0.2	0.7±0.2	0.60
5	4.5±0.0	3.7±0.1	-7.4±0.0	-8.2±0.9	0.7±0.9	0.57
6	6.8±3.5	7.6±0.7	-7.0±0.1	-6.9±0.1	0.1±0.1	0.70
7	6.8±3.8	10.0±1.3	-6.8±0.1	-9.3±0.4	2.5±0.4	0.85
8	10.7±6.5	8.5±0.7	-6.9±0.0	-8.6±0.0	1.6±0.1	0.49
9	200-500	-	-	-	-	-
37	-	1.3±0.3	-8.0±0.1	-8.5±0.5	0.4±0.5	0.50
41	-	12.4±1.0	-6.7±0.0	-4.0±0.1	-2.6±0.1	0.51
42	-	3.1±0.6	-7.5±0.1	-7.6±0.0	0.0±0.1	0.47
47	-	6.5±0.5	-7.1±0.0	-9.0±0.5	1.9±0.3	0.47
48	-	12.9±2.4	-6.7±0.1	-3.8±0.2	-2.8±0.3	0.42

^aSPR measurements and ITC titrations were performed at 20 °C and 25 °C, respectively. Data represent mean ± SD from at least two independent experiments. ^b K_D (SPR), PQS: 0.21±0.0 μM

The ITC derived K_D values were in good accordance with the ones determined by SPR experiments. The naphthalene-2-carboxamide **4** and the thiadiazole derivative **5** displayed the highest affinities (Table 1). Analysis of the thermodynamic signatures revealed that **4-8** are enthalpy-driven binders (Table 1) indicating a good non-covalent bond complementarity between the protein site and the compounds.⁴⁵ Given that it is harder to improve the ΔH contribution than to improve the ΔS contribution, enthalpy driven binders are usually preferred for further optimization.⁴⁵ Moreover, we determined the ratio of Gibb's free binding energy to the number of non-hydrogen atoms termed ligand efficiency (LE) that enables a better comparison of hits with widely differing structures and activities.⁴⁷ Compounds **4-8** showed LEs ranging from 0.49 to 0.85 kcal/mol and are above the threshold value of 0.33 kcal/mol, which should be exceeded for an efficient optimization.⁴⁷ In order to evaluate the agonistic and antagonistic activities of **4-8**, we examined the PqsR-mediated transcriptional effect in a reporter gene assay by measuring the β -galactosidase activity in *E. coli* the pEAL08-2 plasmid containing the *tacP-pqsR* and *pqsA_P-lacZ* fusion genes (Table 2).⁴⁸ *E. coli* was used, as it provides a system to characterize the functionality of PqsR ligands independent of the entire *pqs* system and the low outer membrane permeability⁴⁹ characteristic for *P. aeruginosa*. While **6-8** showed no or only weak antagonistic activity, compounds **4** and **5** exhibited marked antagonistic properties. In contrast to compound **4**, compound **5** provided only moderate agonistic activity. Overall, the screening process afforded thiadiazole **5** which combines a remarkably high affinity with regard to its low molecular weight with superior functional properties in the *E. coli* reporter gene assay and was therefore selected for further optimization.

Fragment Optimization. Another hit compound sharing a high degree of similarity with **5**, compound **9** (Figure 2), which had shown lower affinity in the SPR screen, but pure antagonistic activity (Table 2) was included in the optimization strategy (Figure 3).

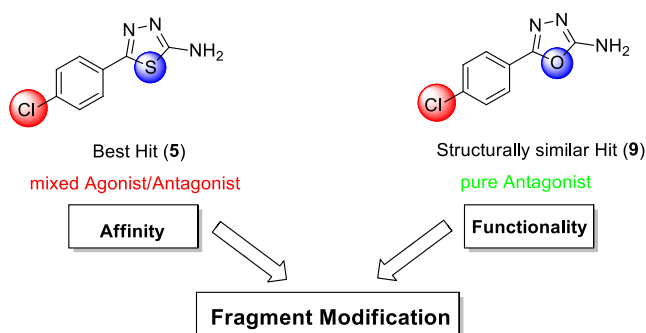
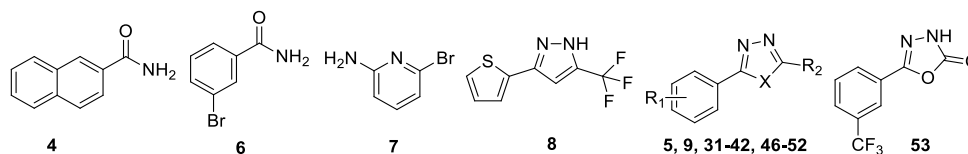


Figure 3: Fragment modification strategy

In the first modification step the position of the Cl substituent was shifted into the *meta* and *ortho* position (Table 2), as we had observed that the antagonistic properties in the quinolone class of PqsR antagonists strongly depended on the position of the aromatic substituents.²⁵ The compounds with Cl in *meta* position showed an opposed functional profile in case of both heterocycles: the thiadiazole **31** displayed pure agonistic properties, while the oxadiazole **32** turned out to be a pure antagonist. The Cl substituent in *ortho* position (**33**, **34**) led to a moderate agonistic activity without antagonistic properties for both heterocycles.

Compound **32** was used for further optimization. The Cl group was exchanged for substituents providing different electronic properties (**35-42**, Table 2). Omitting the Cl substituent (**35**) led to a moderate agonistic activity. The bioisosteric exchange of Cl for electron-withdrawing moieties in *meta* position (**36-39**) resulted in pure antagonists with the Br compound **36** and the CF₃ derivative **37** as the most potent ones (EC₅₀ 7.5 μM). Interestingly, in the class of HHQ derived antagonist a CF₃ substituted quinolone also showed the strongest antagonistic properties.²⁵ The introduction of a methoxy group (**40**) was accompanied by a complete loss of activity. In contrast, the introduction of a methyl substituent resulted in a partial antagonist (**41**, SI, Figure S5). In the case of the benzamide scaffold reported by Klein *et al.* (**2**, Figure 1) the exchange of Cl for *tert*-butyl resulted in an increased affinity due to an enthalpic gain.²⁹ Assuming a similar binding mode of **2** and **37** (discussed in detail below) this structural modification was deemed to have a similar effect in the oxadiazole class. Compound **42**, however, showed a slightly reduced affinity according to ITC analysis (Table 1) and more importantly a diminished antagonistic activity. Overall, **37** showing a favorable logP of 2.12 (ACD Perspecta 14.0.0 consensus logP) and a better aqueous solubility compared to **36** emerged as the most promising compound. Accordingly, **37** was tested in the *P. aeruginosa* reporter gene assay. As the outer membrane is much less permeable in *P. aeruginosa*⁴⁹ the observed antagonistic activity being only 5-fold reduced (EC₅₀s: 7.5 μM in *E. coli*, 38.5 μM in *P. aeruginosa*; SI Figure S6) was remarkably high.

Table 2: Agonistic and antagonistic activities of PqsR ligands^a

Compd.	Pos	X	R ₁	R ₂	Agonistic activity [%]	Antagonistic activity [%]	EC ₅₀ ^b [μM]
4	-	-	-	NH ₂	52±12	41±12	-
5	4	S	Cl	NH ₂	28±1	43±16	-
6	-	-	-	NH ₂	n.a.	n.i.	-
7	-	-	-	NH ₂	n.a.	22±17	-
8	-	-	-	NH ₂	n.a.	n.i.	-
9	4	O	Cl	NH ₂	n.a.	40±9	-
31	3	S	Cl	NH ₂	105±11	n.i.	-
32	3	O	Cl	NH ₂	n.a.	76±12	26.7
33	2	S	Cl	NH ₂	48±1	n.i.	-
34	2	O	Cl	NH ₂	22±5	n.i.	-
35	3	O	H	NH ₂	28±3	n.i.	-
36	3	O	Br	NH ₂	n.a.	105±6	7.5
37	3	O	CF ₃	NH ₂	n.a.	111±13	7.5
38	3	O	CN	NH ₂	n.a.	84±1	17.8
39	3	O	OCF ₃	NH ₂	n.a.	69±6	46.5
40	3	O	OMe	NH ₂	n.a.	n.i.	-
41	3	O	Me	NH ₂	n.a.	55±20	57.8 ^c
42	3	O	t-Butyl	NH ₂	n.a.	42±11	-
47	3	O	CF ₃	H	n.a.	49±22	101.2
48	3	O	CF ₃	Me	n.a.	n.i.	-
49	3	O	CF ₃	OMe	n.a.	n.i.	-
50	3	O	CF ₃	CF ₃	n.a.	n.i.	-
51	3	O	CF ₃	NHMe	n.a.	n.i.	-
52	3	O	CF ₃	CONH ₂	39±6	n.i.	-
53	-	-	-	-	41±4	n.i.	-

^aAgonistic and Antagonistic properties were evaluated in an *E. coli* reporter gene assay. Agonistic activity was determined by measuring the PqsR stimulation induced by 100 μM of the test compound compared to 50 nM PQS (= 100%); n.a. = no agonism (agonistic activity ≤ 20%). Antagonistic activity was determined by measuring the inhibition of the PqsR stimulation induced by 50 nM PQS in the presence of 100 μM test compound (full inhibition = 100%); n.i. = no inhibition (antagonistic activity ≤ 20%). Mean values of at least two independent experiments with n = 4. ^bConcentration of the half maximal antagonistic activity. Mean values of at least two independent experiments with compounds tested in at least 6 different concentrations and n = 4. ^cpartial antagonist

Characterization of Fragment Binding Mode. Despite many efforts,^{50,51} the 3D structure of the PqsR protein is not available. The amino acids Q194 and F221 are located within the LBD of PqsR and are potential partners for non-covalent interactions.²⁹ We could clearly show that Q194 and F221 are involved in the binding of benzamide **2** employing site-directed mutagenesis in combination with ITC analysis.²⁹ Accordingly, the optimized compound **37** and the screening hit naphthalene-2-carboxamid **4** showing highest affinity were evaluated for their binding to the Q194A and F221A PqsR mutants by ITC (Table 3).

Table 3: Effect of site-directed mutations on the thermodynamic parameters of PqsR ligands.

Ligand	Q194A			F221A		
	$\Delta\Delta G$ [kcal mol ⁻¹]	$\Delta\Delta H$ [kcal mol ⁻¹]	$-T\Delta\Delta S$ [kcal mol ⁻¹]	$\Delta\Delta G$ [kcal mol ⁻¹]	$\Delta\Delta H$ [kcal mol ⁻¹]	$-T\Delta\Delta S$ [kcal mol ⁻¹]
2	-1.3±0 [*]	-4.4±0.3 [*]	3.1±0.3 [*]	-1.0±0.1 [*]	-7.6±0.3 [*]	6.6±0.4 [*]
4	-1.1±0.1 [*]	-3.2±0.2 [*]	2.1±0.2 [*]	-0.4±0.1 [*]	-7.1±0.2 [*]	6.7±0.2 [*]
37	-0.6±0.1 [*]	-0.3±0.6	-0.3±0.7	-0.6±0.1 [*]	-7.1±0.5 [*]	6.5±0.6 [*]

$\Delta\Delta G$, $\Delta\Delta H$, and $-T\Delta\Delta S$ are $\Delta G_{WT} - \Delta G_{mutant}$, $\Delta H_{WT} - \Delta H_{mutant}$, and $-T(\Delta S_{WT} - \Delta S_{mutant})$, respectively. Negative values indicate a loss, positive values a gain compared to wild-type. Errors indicate SD calculated via Gaussian error propagation. Significance: effect of the point mutation on the thermodynamic parameters of ligand binding compared to the wild-type. ☆ $p < 0.003$; ★ $p < 0.05$.

Comparing the thermodynamic signatures of **4** binding to Q194A mutant and wild-type PqsR a loss in ΔH of 3.2 kcal/mol was observed. Given that a well-placed H-bond makes a favorable enthalpic contribution in a range from 4 to 5 kcal/mol,⁵² this value indicates the presence of a weak H-bond between **4** and Gln194. The enthalpic contribution of **4** binding to the F221A mutant was significantly reduced compared to the wild-type ($\Delta\Delta H = -7.1$ kcal/mol). F221 might be involved in a π - π interaction with the naphthalene core of **4**. However, theoretical investigations revealed an interaction energy of only 4.0 to 4.2 kcal/mol for the benzene-naphthalene complex.⁵³ In all cases the loss in enthalpy is partly compensated by a gain in entropy. This might be due to a higher conformational flexibility of the complex in the absence of specific non-covalent interactions. Overall, the measured data indicate that naphthalene-2-carboxamide **4** adopts the same binding mode as the benzamide **2**.

In contrast, there was no significant difference in the enthalpic contribution observed for the oxadiazole **37** when binding to Q194A mutant and wild-type PqsR. This indicates that the side-chain of Gln194 is not directly involved in the binding of **37**. As observed for **4**, the binding of **37** was also affected by the F221A mutation ($\Delta\Delta H = -7.1$ kcal/mol). The phenyl moiety of **37** might be involved in a π -stacking interaction with F221. Overall, these data lead to the conclusion that aromatic carboxamides **2** and **4** as well as the oxadiazole **37** interact with different amino acids within the LBD by adopting different binding modes.

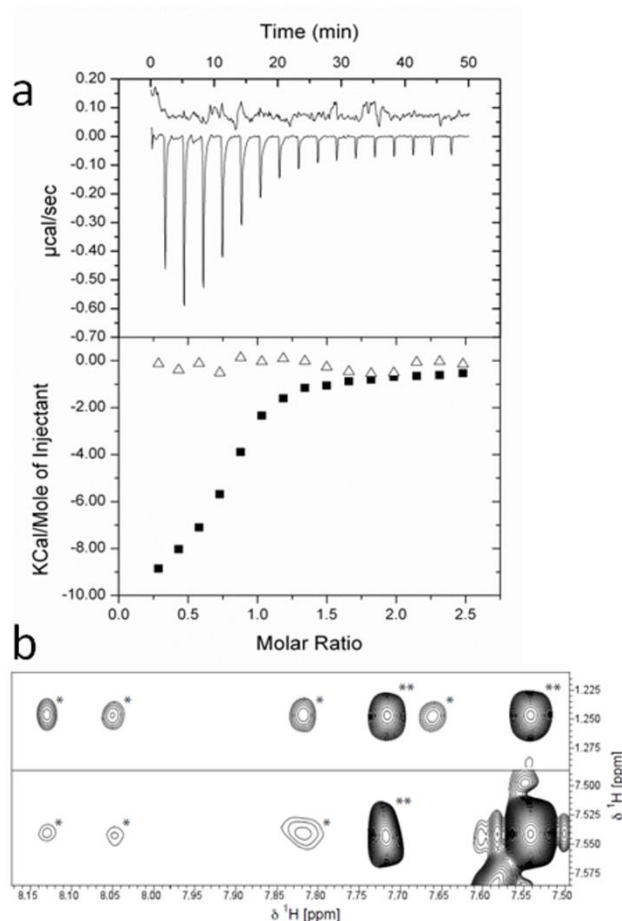


Figure 4. Competitive binding of **2** and **37** to PqsR (a) Raw ITC data (top) and integrated normalized data (bottom) for titrations of 43 μM PqsR with 500 μM **37** in the absence of **2** (■) and in the presence of 500 μM compound **2** (Δ). (b) NOESY spectrum of a mixture of 500 μM **2** and 400 μM **37** in the presence of 10 μM PqsR; interligand NOEs between the tert-butyl moiety of **2** and the phenyl ring of **37** (top), between the two phenyl rings (bottom); (*) indicates interligand INPHARMA NOEs mediated by PqsR; (**) indicates intramolecular transferred NOEs. Signals marked with (*) or (**) were not detected in a control experiment recorded under identical conditions in the absence of PqsR.

ITC analysis was applied to analyze whether both fragments bind to the same site. PqsR was saturated with an excess of **2** and **37** was titrated subsequently into the same solution (Figure 4a). No additional heat release was detected which gives strong evidence that both compounds compete for binding to PqsR. Additionally, the *vice versa* experiment was performed to exclude that the binding of **2** induces a conformational change which hinders the binding of **37**. This experiment led to the same result (SI Figure S4) confirming that both fragments bind to the same site. In order to further validate the competitive binding (**2**, **37**) we applied NMR INPHARMA experiments.⁵⁴ This technique allows to detect protein-mediated interligand NOEs, if both compounds bind competitively to the same site of the protein. When we conducted a 2D NOESY experiment of a mixture of **2** and **37** in the presence of PqsR, clear interligand NOEs between the tert-butyl group of **2** and the phenyl ring of **37** were observed (Figure 4b, upper panel). Additionally, weaker interligand NOEs between the two phenyl moieties of **2** and **37** were detected (Figure 4b, lower panel). These findings corroborated our ITC data that both

ligands bind competitively to the same site of PqsR. Given that both fragments interact with F221 and compete with PQS as shown for the structural analogs **4** and **5** in SPR competition experiments, we conclude that **2** and **37** have overlapping binding sites within the LBD.

Biophysically Guided Structural Modifications. Structural modifications of **37** in combination with thermodynamic analysis were performed to evaluate the relative contributions of the different functional groups. The CF_3 moiety was replaced by a methyl group and the thermodynamic signature of the resulting compound **41** was compared to that of **37** (Figure 5).

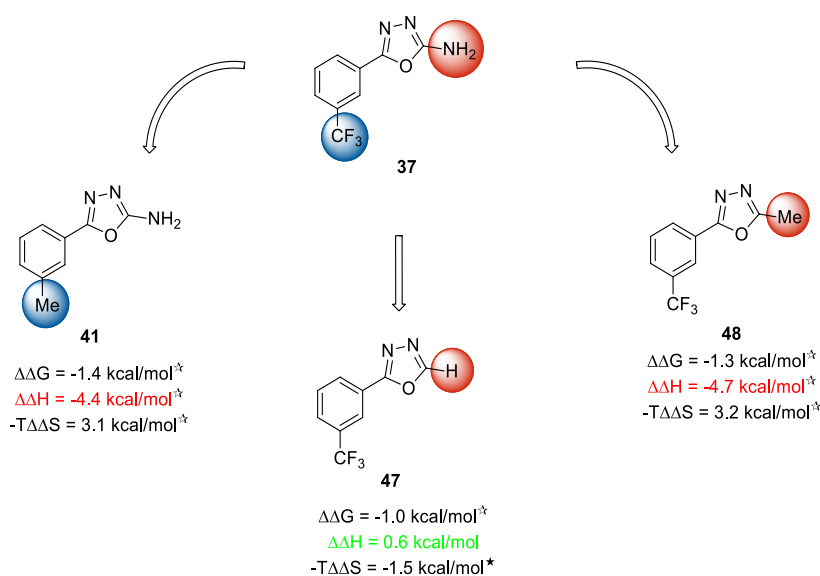


Figure 5. Relative thermodynamic contributions of functional groups. Negative values indicate a loss; positive values a gain compared to compound **37**; $\star p < 0.003$; $\star p < 0.05$

Compound **41** showed a reduced affinity for PqsR compared to **37** (Table 1), which was due to a significant loss in ΔH of 4.4 kcal/mol (Figure 5). This corroborates the proposed π -stacking between F221 and the phenyl moiety of the oxadiazole **37** as electron-withdrawing groups like CF_3 can intensify such interactions either through enhanced electrostatic^{55,56} or direct effects of the substituents.⁵⁷ Considering the loss in enthalpy that is caused by the F221A mutation (7.1 kcal/mol) and the loss in enthalpy that is due to the exchange of the CF_3 by CH_3 (4.4 kcal/mol), the enthalpic contribution of a possible π - π interaction between **37** and Phe221 might be 2.7 kcal/mol. Remarkably, this is consistent with the binding energy of the gas-phase benzene dimer ranging from 2.0 to 3.0 kcal/mol.⁵⁸

The thermodynamic profile of compound **37** binding to Q194A suggested that the amino group of **37** does not make an H-bond with the polar side-chain of Gln194. To investigate whether the amino group is involved in the formation of an H-bond with polar backbone atoms or other side-chains in the LBD of PqsR it was replaced by hydrogen. The binding affinity of the resulting compound **47** was reduced (Table 1). The same tendency was observed for the functional

properties (Table 2). But even more interesting, there was no significant difference in the enthalpic contributions (Figure 5). These findings initially led us to the conclusion that the amino group is not involved in a specific non-covalent interaction (e.g. H-bond) with PqsR. Hence, we decided to replace the amino function for apolar moieties with different electronic properties like methyl (**48**), methoxy (**49**) and CF₃ (**50**) in order to overcome the enthalpy penalty associated with desolvation of the polar amino group.⁵² In contrast to our assumption, compound **48** displayed a reduced affinity toward PqsR (Table 1), which results from a significant decrease in ΔH of 4.7 kcal/mol (Figure 5) typical for a loss of a well-placed H-bond.⁵² Furthermore, these modifications (**48-50**) completely abolished the antagonistic activity (Table 2). These findings led us reconsider our hypothesis of a non-interacting amino function: the C-H bond in 2-position of the 1,3,4-oxadiazole (**47**) is highly polarized and can interact through a non-classical hydrogen bond.⁵⁹ In our case such an interaction could be mediated by a water molecule that is displaced in the presence of an amino function (**37**). This explanation is sustained by the loss in entropy (-1.5 kcal/mol) due to the exchange of NH₂ by H. Theoretical investigations revealed an interaction energy for highly similar 5-membered heterocycles like oxazoles and isoxazoles in the range of 3.0 to 3.5 kcal/mol.⁵⁹ Such an interaction might compensate the loss in enthalpy by omitting the amino group.

In order to evaluate whether both hydrogen atoms of the amino substituent (**37**) are involved in ligand-receptor interaction we synthesized the *N*-methylated analogue **51**. The latter showed no antagonistic activity (Table 2) as did the carboxamide (**52**) and oxadiazol-2-on (**53**) indicating that the amino group is essential for full antagonistic activity even if the exact function in the ligand-receptor interaction remains speculative.

Effects on alkylquinolone signaling and virulence factor pyocyanin formation in *P. aeruginosa*. Following our strategy of inhibiting *P. aeruginosa* pathogenicity, we evaluated the effect of different oxadiazole derivatives on the production of alkylquinolones and the major virulence factor pyocyanin in the highly virulent clinical isolate *P. aeruginosa* PA14. The activation of PqsR upregulates the *pqsABCD(E)* operon which is essential for HHQ and PQS biosynthesis.^{16,19,20} Furthermore, PQS is reported to influence biofilm shape.²¹ Accordingly, we examined the effect of **37** on extracellular levels of PQS in wild-type *P. aeruginosa*. As we reported for the HHQ derived antagonist²⁵ no remarkable reduction of PQS levels was observed (data not shown). We assumed that the autoinductive effect of high intrinsic PQS levels ranging from 30 to 60 μ M in the culture supernatant might compensate the antagonistic activity of **37**. Therefore, we further investigated the effect of compound **37** on HHQ formation in the absence of PQS.¹⁷ We employed a *P. aeruginosa* isogenic strain lacking PqsH, a monooxygenase catalyzing the conversion of HHQ to PQS.^{19,20} Interestingly, we observed a reduction of extracellular HHQ (42 \pm 0% at 250 μ M of **37**). The level of HQNO (2-heptyl-4-hydroxy quinoline-*N*-oxide), another alkylquinolone under the control of PqsR,²⁰ was also clearly decreased

(43±3% at 250 µM of **37**). The reduction of both alkylquinolones demonstrates that PqsR antagonists block the QS system in *P. aeruginosa*. Future experiments will extend the fragment structure aiming at antagonists with improved affinity. Such compounds would hopefully disrupt the self-inductive effect of high intrinsic PQS levels and potentially affect biofilm shape in wild-type *P. aeruginosa*.

The biological effects on the major virulence factor pyocyanin were examined subsequently. Pyocyanin is a redox-active secondary metabolite released by *P. aeruginosa* that plays a critical role during acute infections by provoking oxidative stress and inflammatory responses in host cell tissue.⁶⁰ Biological studies indicate a connection between the PQS system and pyocyanin production,^{18,61} supported by the fact that a PqsR deficient mutant (*pqsR*) is incapable to produce pyocyanin.^{20,62} Analogously, the HHQ derived antagonist **1**²⁵ and the hydroxamic acid **3**²⁹ diminish pyocyanin in *P. aeruginosa*. The PqsR antagonist **37** likewise clearly reduced the pyocyanin level (46±9% at 250 µM). The weaker antagonists **38** and **41** showed a moderate or only little reduction, respectively (32±3% at 250 µM of **38**; 18±3% at 250 µM of **41**). In contrast the inactive compound **40** showed no effect. The correlation of these data with the antagonistic properties indicates that the reduction of pyocyanin is caused by PqsR antagonism. A growth curve of *P. aeruginosa* incubated with **37** confirmed that the observed effects are not due to an antibacterial activity of the compound (SI, Figure S6). While in the absence of functional PqsR (*pqsR*) no significant levels of pyocyanin and PQS were detected,²⁰ our results show that in the presence of weaker antagonists pyocyanin production is more sensitive to PqsR antagonism than PQS biosynthesis. This finding might facilitate a more detailed understanding of the underlying mechanisms. Overall these results demonstrate that the interference with the PQS system by the oxadiazole type antagonists is a suitable approach to reduce *P. aeruginosa* pathogenicity.

CONCLUSION

Considering the hydrophobic character of the natural effectors HHQ and PQS, the LBD of PqsR is expected to be a mainly lipophilic pocket. This renders the transcriptional regulator PqsR a quite challenging drug target. Nevertheless, we identified chemically diverse PqsR ligands by employing an SPR fragment screening. The thermodynamic profiles of the top five hit compounds were evaluated using ITC methodology. The discovered hits showed enthalpy driven binding and excellent LEs. Furthermore, the functional properties of the best fragments were analyzed in a β -galactosidase reporter gene assay as an additional guidepost for hit selection. The thiadiazole-2-amine derivative **5** displayed a mixed agonistic/antagonistic profile and was chosen as starting point for structural modification. A functionality-guided optimization process afforded the pure antagonist **37** showing improved affinity and potency with consistently high LE (**5**, LE = 0.57 kcal/mol vs. **37**, LE = 0.50 kcal/mol). In contrast to the HHQ derived antagonists (for example **1**, Figure 1), **37** showed a more favorable logP and higher aqueous solubility. The 2-amino-1,3,4-oxadiazole moiety present in the optimized ligand **37** has not been reported as a chelating agent for metal ions, contrary to the hydroxamic acid motif of fragment **3** (Figure 1). Furthermore, an *in-silico* toxicology prediction (Derek Nexus, Version 2.0.3.201206121715) of compound **37** revealed no safety issues.⁶³ Taken together these data emphasize the high potential of the optimized fragment **37**.

To shed light on the binding mode of different fragment classes, site-directed mutagenesis in combination with thermodynamic analysis was applied. The oxadiazole **37** and the carboxamides **2** and **4** bind competitively to PqsR but do not cover exactly the same space in the LBD. This provides the potential for hit-to-lead optimization using fragment growing strategies. Additionally, structural modifications of **37** together with calorimetric evaluation were performed to evaluate the relative importance of the functional groups in order to guide future optimization strategies. Furthermore, compound **37** is able to reduce the virulence factor pyocyanin in wild-type *P. aeruginosa* without affecting bacterial growth. Thus, the identified PqsR antagonists represent an interesting starting point for the development of novel anti-infectives.

Future experiments will aim at merging the best features of the different fragments to develop drug-like molecules which may provide novel therapeutic options to counter the burden of *P. aeruginosa* infections.

EXPERIMENTAL SECTION

Surface Plasmon Resonance. SPR binding studies were performed using a Biacore T100 instrument optical biosensor (GE Healthcare). CSIRO fragment library collection consisted of 720 compounds with a molecular weight range of 100 to 350 Da. The expression, purification and minimal biotinylation of H₆SUMO-PqsR^{C87} as well as the immobilization onto the streptavidin chip surface and is described in detail in the Supporting Information.

SPR Library Screening. 10 mM DMSO stock solutions of compounds were diluted in 1.05 x DMSO free screening buffer (52.5 mM HEPES, pH 7.4, 157.5 mM NaCl, 0.0525% Tween-20 (v/v)) to 500 μM. Final ligand concentrations (100 μM) were achieved by diluting 1:5 (v/v) in the instrument running buffer (50 mM HEPES, pH 7.4, 150 mM NaCl, 0.05% Tween-20 (v/v) and 5% DMSO (v/v)). Two separate fragment screens were performed each time screening 360 fragments against protein targets immobilized on chips I and II. Fragment solutions (100 μM) were injected over the protein sensor surface for 30 s at 60 μL/min at 4 °C. After every 120 injections, a positive control compound (PQS in the first 360 compound screen and fragment **4** in the second screen) was injected for control binding purposes. Regeneration of the surfaces between subsequent binding experiments was achieved by washing the surface at 60 μL/min for 30 s with the instrument running buffer as well as by using a “carry-over injection” of running buffer at 40 μL/min for further 30 s. To determine binding affinity, candidate hit fragments were analyzed using dosage experiments. Fresh 100 mM DMSO fragment solutions were diluted directly into instrument running buffer to a final concentration of 81 μM and then diluted 3-fold down to 1 μM aiming for a 5-point concentration series range. Each compound was injected for 30 s association- and 60 s dissociation time at 20 °C at a constant flow rate of 60 μL/min. Scrubber 2 (www.biologic.com.au) and Microsoft Excel software packages were utilized for data processing and analysis. Using Scrubber software, SPR signals were referenced against the blank surface (streptavidin + D-biotin) and further corrected for DMSO refractive index change as previously described.⁶⁴ A normalization scheme of Giannetti *et al.*⁴³ was applied to the processed data based on the maximal binding response (R_{max}) that has been determined from experiments with the control compound (initially PQS and later fragment **4**). For the initial ranking of the best hits, the K_D values were estimated using equation derived from the Langmuir adsorption isotherm (1):

$$K_D = \frac{R_{max} * C}{R} - C \quad (1)$$

R_{\max} , R , and C correspond to the normalized saturation response of the compound, the normalized response of the test compound, and the concentration of the test solution, respectively.

To determine binding affinities (K_D) from dosage experiments, binding responses at equilibrium were fit to a 1:1 steady state affinity model available within Scrubber. As described above, normalized saturation response (R_{\max}), derived using reference compound(s), was applied to response curves obtained with fragment hits at non-saturating concentration. Equilibrium isotherm containing the assumed R_{\max} was used to determine K_D values (SI, Figure S1).

Isothermal Titration Calorimetry ITC titrations were carried out as previously reported²⁹ and a detailed protocol as well as representative titration curves are included in the Supporting Information.

INPHARMA NMR Experiments To detect interligand NOEs, 10 μM $\text{H}_6\text{SUMO-PqsR}^{\text{C87}}$ was mixed with 500 μM **2** and 400 μM **37** in PBS buffer (50 mM potassium phosphate, pH 7.4, 150 mM NaCl, 5% DMSO- d_6 (v/v), 5 % D_2O (v/v)). Spectra were acquired at 25 °C on a 700 MHz Bruker Avance III spectrometer equipped with a cryoprobe. Two-dimensional NOESY spectra were recorded with a mixing time of 600 ms, 16 scans for each of 400 complex points in the indirect dimension and 512 complex points in the direct dimension, a sweep width of 9 ppm and a recycle delay of 1.5 sec. Dephasing of water signals was achieved by a WATERGATE sequence. A control experiment under identical conditions without $\text{H}_6\text{SUMO-PqsR}^{\text{C87}}$ was carried out. Data were processed using Bruker TOPSPIN 3.1 software using squared sine bell functions and zero filling to 2048 and 1024 complex points in the direct and indirect dimension, respectively, for apodization.

Reporter Gene Assay in *E. coli*. The ability of the compounds to either stimulate or antagonize the PqsR-dependent transcription was analysed as previously described²⁵ using a β -galactosidase reporter gene assay in *E. coli* expressing PqsR with some modifications to enable a higher throughput.⁶⁵ Briefly, a culture of *E. coli* DH5 α cells containing the plasmid pEAL08-2⁴⁸ which encodes PqsR under the control of the *tac* promoter and the β -galactosidase reporter gene *lacZ* controlled by the *pqsA* promoter were co incubated with test compound. Antagonistic effects of compounds were assayed in the presence of 50 nM PQS. After incubation galactosidase activity was measured photometrically using POLARstar Omega (BMG Labtech) and expressed as ratio of controls. For the determination of EC_{50} value, compounds were tested at least in six different concentrations. The given data represent mean of at least two experiments with $n = 4$. The log (inhibitor) vs. response model (Prism 5.0) was applied for nonlinear regression and determination of EC_{50} -values.

Reporter Gene Assay in *P. aeruginosa*. In order to evaluate the antagonistic properties of compound **37**, the PqsR-dependent transcription was evaluated as previously described²⁵ using

a β -galactosidase reporter gene assay system⁴⁸ in *P. aeruginosa*. In brief, a *P. aeruginosa* PA14 strain carrying a nonfunctional *pqsA* gene was used to eliminate intrinsic HHQ and PQS production. A culture of *P. aeruginosa* PA14 Δ *pqsA* cells containing the plasmid pEAL08-2⁴⁸ were co incubated with **37** and 50 nM PQS. After incubation galactosidase activity was measured photometrically using POLARstar Omega (BMG Labtech) and expressed as ratio of controls. For the determination of EC₅₀ value, **37** was tested at nine different concentrations. The given data represent mean of two experiments with n = 4. The log (inhibitor) vs. response model (Prism 5.0) was applied for nonlinear regression and determination of EC₅₀-values.

Pyocyanin Assay. Pyocyanin produced by *P. aeruginosa* PA14 was determined as described previously⁶⁶ according to the method of Essar *et al.*⁶⁷ In short, cultures inoculated with a starting OD₆₀₀ of 0.02 were grown in the presence of inhibitors or DMSO as a control in PPGAS medium at 37 °C, 200 rpm and a humidity of 75% for 16 h. For pyocyanin determination, cultures were extracted with chloroform and re-extracted with 0.2 M HCl. The OD₅₂₀ was determined using FLUOstar Omega (BMG Labtech) and normalized to cell growth measured as OD₆₀₀. For each sample, cultivation and extraction were performed in triplicates.

Determination of Extracellular HHQ and HQNO Levels. Extracellular levels of HHQ and HQNO were determined according to the methods of Lépine *et al.*^{68,69} with some modifications: Briefly, cultures of *P. aeruginosa* PA14 Δ *pqsH* mutant were inoculated with a starting OD₆₀₀ of 0.02 and grown in LB medium in the presence of DMSO as a control or DMSO solutions of inhibitors at 37 °C, 200 rpm and a humidity of 75 % for 17 h. For HHQ and HQNO analysis, 500 μ L of bacterial cultures were supplemented with 50 μ L of a 10 μ M methanolic solution of the internal standard (IS) 5,6,7,8-tetradeutero-2-heptyl-4(1*H*)-quinolone (HHQ-*d*₄) and extracted with 1 mL of ethyl acetate by vigorous shaking. After centrifugation (14, 000 rpm, 12 min), 400 μ L of the organic phase were evaporated to dryness in LC glass vials and dissolved in methanol. For each sample, cultivation and extraction were performed in triplicates. UHPLC-MS/MS analysis was performed as described in detail by Storz *et al.*⁶⁷ The following ions were monitored (mother ion [m/z], product ion [m/z], scan time [s], scan width [m/z], collision energy [V], tube lens offset [V]): HHQ: 244, 159, 0.5, 0.01, 30, 106; HQNO: 260, 159, 0.1, 0.01, 25, 88; HHQ-*d*₄ (IS): 248, 163, 0.1, 0.01, 32, 113. Xcalibur software was used for data acquisition and quantification with the use of a calibration curve relative to the area of the IS.

Chemical and Analytical Methods. ¹H and ¹³C NMR spectra were recorded on a Bruker DRX-500 instrument. Chemical shifts are given in parts per million (ppm), and referenced against the residual solvent peak. Coupling constants (*J*) are given in hertz. Purity control of final compounds was carried out using a SpectraSystems-MSQ LCMS system (Thermo Fisher Scientific) consisting of a pump, an autosampler, VWD detector and a ESI quadrupole mass

spectrometer by determination of the relative peak area in the UV trace. Purities were greater than 95%. Mass spectrometry was performed on an MSQ electro spray mass spectrometer (Thermo Fisher Scientific). High resolution mass spectra were recorded on a maXis 4G hr-ToF mass spectrometer (Bruker Daltonics). Reagents were used as obtained from commercial suppliers without further purification. Procedures were not optimized regarding yield. Microwave assisted synthesis was carried out in a Discover microwave synthesis system (CEM). Column chromatography was performed using the automated flash chromatography system Combiflash Companion (Teledyne Isco) equipped with RediSepRf silica columns. Final products were dried under reduced pressure at 40 °C or in high vacuum. Melting points were determined using the melting point apparatus SMP3 (Stuart Scientific) and are uncorrected.

Screening hits **4-8** were obtained from the CSIRO fragment library and used for biological studies. **5** was resynthesized as described below. **2** was purchased from Alfa Aesar; **9, 34** and **35** were purchased from Sigma Aldrich.

Preparation of Thiodiazole-2-amines (General Procedure 1)³³ Benzoic acid (1 mmol) and hydrazinecarbothioamide (1 mmol) were filled into a sealed reaction vial. Phosphorus oxychloride (4 mmol) was added while cooling on an ice bath. Afterwards, the mixture was heated to 80 °C for 2.5 h in a metal block. Built up pressure was released every hour. The reaction mixture was poured into water at 0 °C and stirred vigorously for 30 min. The mixture was alkalinized using a 10 M solution of KOH. The resulting suspension was extracted with ethyl acetate (3 times). The combined organic layers were washed with brine, dried over MgSO₄, and concentrated to yield the expected 5-phenyl-[1,3,4]-thiadiazole-2-amine.

Preparation of benzoylthiosemicarbazides (General Procedure 2)³⁴ Hydrazinecarbothioamide (3 mmol) and THF (5 ml) were filled into a three necked round bottom flask. Benzoyl chloride (1 mmol) was added through a dropping funnel at 0 °C (ice-bath). The mixture was stirred at RT under nitrogen atmosphere for 24 h. The mixture was quenched by the addition of water and alkalinized using a saturated aqueous solution of NaHCO₃. Afterwards, THF was evaporated under reduced pressure until precipitation of a solid. The suspension was filtered and the resulting cake was washed with water to afford the expected benzoylthiosemicarbazide.

Preparation of Oxadiazole-2-amines (General Procedure 3)³⁴ Benzoylthiosemicarbazide (1 mmol) was filled into a three necked flask and suspended in IPA (7 ml). The suspension was mixed with a solution of potassium iodide (0.3 mmol) in water (0.5 mL). The reaction was cooled to 0 °C on an ice-bath and a 5 M solution of NaOH (1.5 mmol) was added. Dibromodimethylhydantoin (0.75 mmol) dissolved in ACN (3 ml) was added through a dropping funnel over 1 h while maintaining the temperature below 10 °C. Afterwards, the reaction was aged for 1 h below 10 °C. The reaction mixture was quenched using NaHSO₃ sat.

(0.25 mL) and water was added. The pH was adjusted to >12 using a saturated solution of NaHCO₃. The suspension was filtered and low boiling solvents were removed from the filtrate under reduced pressure to give a precipitate. The suspension was filtered and the cake rinsed with water and IPA to give the 5-phenyl-[1,3,4]-oxadiazole-2-amine.

5-(4-Chlorophenyl)-1,3,4-thiadiazol-2-amine (5) was prepared according to General Procedure 1 starting from 4-chlorobenzoic acid (**10**, 1.00 g, 6.39 mmol) and hydrazinecarbothioamide (0.582 g, 6.39 mmol). The obtained solid was recrystallized from ethanol to give the pure product as white needles (0.51 g, 2.44 mmol, 38% yield). ¹H NMR (500 MHz, DMSO-*d*₆) δ ppm 7.47 (s, 2 H), 7.50 - 7.55 (m, 2 H), 7.73 - 7.79 (m, 2 H); ¹³C NMR (126 MHz, DMSO-*d*₆) δ ppm 127.88 (2 C), 129.13 (2 C), 129.82, 133.92, 155.08, 168.81; mp 231-232 °C; LC-MS (ESI): *m/z*: 252.88 (M+H+CH₃CN)⁺; 98%

5-(3-Chlorophenyl)-1,3,4-thiadiazol-2-amine (31)³⁵ 2-(3-chlorobenzoyl)hydrazinecarbothioamide (**23**, 0.50 g, 2.18 mmol) was dissolved in sulfuric acid (3 ml). The mixture was stirred for 2 h at RT. The reaction mixture was slowly poured into water and basified using ammonia solution 20% while cooling on an ice bath. The resulting suspension was filtered and the resulting cake was washed with water to give the pure product as a white solid (0.37 g, 1.75 mmol, 80% yield). ¹H NMR (500 MHz, DMSO-*d*₆) δ ppm 7.47 - 7.50 (m, 2 H), 7.52 (s, 2 H), 7.66 - 7.72 (m, 1 H), 7.77 - 7.81 (m, 1 H); ¹³C NMR (126 MHz, DMSO-*d*₆) δ ppm 125.07, 125.39, 129.23, 131.04, 132.87, 133.78, 154.72, 169.05; mp 214-218°C; MS (ESI): *m/z*: 212.00 (M+H)⁺, 252.82 (M+H+CH₃CN)⁺; 96%.

5-(3-Chlorophenyl)-1,3,4-oxadiazol-2-amine (32) was prepared according to General Procedure 3 starting from 2-(3-(chloro)benzoyl)hydrazinecarbothioamide (**23**, 0.500 g, 2.18 mmol). The titled product was obtained as yellow solid (0.199 g, 1.02 mmol, 47% yield). ¹H NMR (500 MHz, DMSO-*d*₆) δ ppm 7.34 (s, 2 H) 7.56 - 7.58 (m, 2 H) 7.71 - 7.77 (m, 2 H); ¹³C NMR (126 MHz, DMSO-*d*₆) δ ppm 123.60, 124.43, 126.23, 130.10, 131.31, 133.81, 156.12, 164.08; mp 251-255°C; MS (ESI): *m/z*: 236.81 (M+H+CH₃CN)⁺; 95%.

5-(2-Chlorophenyl)-1,3,4-thiadiazol-2-amine (33) was prepared according to General Procedure 1 starting from 2-chlorobenzoic acid (**12**, 1.00 g, 6.39 mmol) and hydrazinecarbothioamide (0.582 g, 6.39 mmol). The obtained solid was adsorbed on silica gel and purified by flash-chromatography using a gradient of hexane/ethyl acetate (7:3) to ethyl acetate to give the expected product as a white solid (0.482 g, 2.28 mmol, 36% yield). ¹H NMR (500 MHz, DMSO-*d*₆) δ ppm 7.39 - 7.52 (m, 4 H), 7.53 - 7.66 (m, 1 H), 7.92 - 8.04 (m, 1 H); ¹³C NMR (126 MHz, DMSO-*d*₆) δ ppm 127.65, 129.57, 130.27, 130.41, 130.43, 130.90, 151.58, 170.10; mp 191-192 °C; MS (ESI): *m/z*: 211.99 (M+H)⁺, 252.89 (M+H+CH₃CN)⁺; 98%.

5-(3-Bromophenyl)-1,3,4-oxadiazol-2-amine (36) was prepared according to General Procedure 3 starting from 2-(3-bromobenzoyl)hydrazinecarbothioamide (**24**, 0.506 g, 1.85 mmol). The crude product was triturated with DCM/MeOH and filtered to afford a yellow solid as the pure product (0.225 g, 0.890 mmol, 48% yield) ^1H NMR (500 MHz, DMSO- d_6) δ ppm 7.34 (br. s, 2 H), 7.49 (t, $J=7.9$ Hz, 1 H), 7.71 (ddd, $J=8.0, 2.8, 0.9$ Hz, 1 H), 7.78 (ddd, $J=7.9, 2.5, 0.9$ Hz, 1 H), 7.90 (t, $J=1.6$ Hz, 1 H); ^{13}C NMR (126 MHz, DMSO- d_6) δ ppm 122.21, 123.94, 126.45, 127.29, 131.50, 132.97, 155.98, 164.08; mp 240-243°C; MS (ESI): m/z 239.84 (M+H) $^+$, 280.87 (M+H+CH $_3$ CN) $^+$; 98%.

5-(3-(Trifluoromethyl)phenyl)-1,3,4-oxadiazol-2-amine (37) was prepared according to General Procedure 3 starting from 2-(3-(trifluoromethyl)benzoyl)hydrazinecarbothioamide (**25**, 2.00 g, 7.60 mmol). The precipitate was triturated with ethyl acetate and filtered. The resulting solid was purified by flash chromatography on silica gel using DCM:MeOH (98:2 to 97:3) to afford the product as a white solid (0.741 g, 3.23 mmol, 43% yield). ^1H NMR (500 MHz, DMSO- d_6) δ ppm 7.39 (s, 2 H), 7.78 (t, $J=7.9$ Hz, 1 H), 7.87 (d, $J=7.9$ Hz, 1 H), 8.01 (s, 1 H), 8.08 (d, $J=7.9$ Hz, 1 H); ^{13}C NMR (126 MHz, DMSO- d_6) δ ppm 121.16, 123.70 (d, $^1J(\text{C},\text{F})=270.4$ Hz, 1 C), 125.35, 126.73 (q, $^3J(\text{C},\text{F})=3.7$ Hz, 1 C), 128.80, 129.79 (q, $^2J(\text{C},\text{F})=31.2$ Hz, 1 C), 130.67, 156.17, 164.19; mp 219-224 °C; MS (ESI): m/z 229.95 (M+H) $^+$, 270.88 (M+H+CH $_3$ CN) $^+$; 99%.

3-(5-Amino-1,3,4-oxadiazol-2-yl)benzonitrile (38) was prepared according to General Procedure 3 starting from 2-(3-cyanobenzoyl)hydrazinecarbothioamide (**26**, 0.500 g, 2.27 mmol). The crude product was purified by flash-chromatography on silica gel using ethyl acetate:THF (9:1). The resulting yellow solid was triturated with ethyl acetate and a few drops of MeOH. The suspension was filtered to give the product as yellow solid (80 mg, 0.430 mmol, 19% yield). ^1H NMR (500 MHz, DMSO- d_6) δ ppm 7.40 (s, 2 H), 7.74 (t, $J=7.9$ Hz, 1 H), 7.96 (d, $J=7.9$ Hz, 1 H), 8.08 (d, $J=7.9$ Hz, 1 H), 8.13 (s, 1 H); ^{13}C NMR (126 MHz, DMSO- d_6) δ ppm 112.43, 117.97, 125.52, 128.26, 129.36, 130.59, 133.65, 155.82, 164.23; mp 242-244; MS (ESI): m/z 227.94 (M+H+CH $_3$ CN) $^+$; 99%.

5-(3-(Trifluoromethoxy)phenyl)-1,3,4-oxadiazol-2-amine (39) was prepared according to General Procedure 3 starting from 2-(3-(trifluoromethoxy)benzoyl)hydrazinecarbothioamide (**27**, 0.500 g, 1.79 mmol). The product was obtained as yellow solid (90 mg, 0.349 mmol, 20% yield). ^1H NMR (500 MHz, DMSO- d_6) δ ppm 7.37 (s, 2 H), 7.52 (d, $J=8.2$ Hz, 1 H), 7.63 - 7.71 (m, 2 H), 7.81 (dt, $J=7.8, 1.3$ Hz, 1 H); ^{13}C NMR (126 MHz, DMSO- d_6) δ ppm 116.98, 121.01 (t, $^1J(\text{C},\text{F})=257.50$ Hz, 1 C), 122.72, 123.99, 126.38, 131.65, 148.68 (q, $^3J(\text{C},\text{F})=1.80$ Hz, 1 C), 156.30, 164.30; mp 197-200°C; MS (ESI): m/z 286.87 (M+H+CH $_3$ CN) $^+$; 95%.

5-(3-Methoxyphenyl)-1,3,4-oxadiazol-2-amine (40) was prepared according to General Procedure 3 starting from 2-(3-methoxybenzoyl)hydrazinecarbothioamide (**28**, 0.500 g, 2.22 mmol). The crude product was purified by flash-chromatography using ethyl acetate to obtain

the pure product as a white solid (152 mg, 0.795 mmol, 36% yield). ^1H NMR (500 MHz, $\text{DMSO}-d_6$) δ ppm 3.81 (s, 3 H), 7.07 (dd, $J=8.20, 2.52$ Hz, 1 H), 7.25 (s, 2 H), 7.29 (dd, $J=2.52, 1.26$ Hz, 1 H), 7.37 (dt, $J=7.80, 1.14$ Hz, 1H), 7.44 (t, $J=7.88$ Hz, 1 H); ^{13}C NMR (126 MHz, $\text{DMSO}-d_6$) δ ppm 55.23, 109.83, 116.34, 117.33, 125.57, 130.48, 157.18, 159.53, 163.86; mp 192-195°C; MS (ESI): m/z 192.02 ($\text{M}+\text{H}$) $^+$; 99%.

5-(4-Tolyl)-1,3,4-oxadiazol-2-amine (41) was prepared according to General Procedure 3 starting from 2-(3-(methyl)benzoyl)hydrazinecarbothioamide (**29**, 0.500 g, 2.39 mmol). The crude product was recrystallized from ethanol to obtain the product as a pale yellow solid (86 mg, 0.466 mmol, 20% yield). ^1H NMR (500 MHz, $\text{DMSO}-d_6$) δ ppm 2.37 (s, 3 H), 7.21 (s, 2 H), 7.27 - 7.34 (m, 1 H), 7.41 (t, $J=7.6$ Hz, 1 H), 7.56 - 7.60 (m, 1 H), 7.60 - 7.62 (m, 1 H); ^{13}C NMR (126 MHz, $\text{DMSO}-d_6$) δ ppm 20.87, 122.19, 124.31, 125.39, 129.11, 130.99, 138.54, 157.37, 163.78; mp 213-216 °C; MS (ESI): m/z 176.06 ($\text{M}+\text{H}$) $^+$, 217.07 ($\text{M}+\text{H}+\text{CH}_3\text{CN}$) $^+$; 96%.

5-(3-(Tert-butyl)phenyl)-1,3,4-oxadiazol-2-amine (42) was prepared according to General Procedure 3 starting from 3-(tert-butyl)benzoyl thiosemiamidecarbazide (**30**, 1.00 g, 3.98 mmol). The quenched reaction mixture was extracted twice with ethyl acetate. The combined organic phases were washed with a saturated solution of NaHCO_3 and brine. The organic layer was dried over MgSO_4 and filtered. Heptane was added and ethyl acetate was evaporated to give a yellow suspension. The suspension was filtered and the cake washed with heptane/ethyl acetate to yield a white solid as the pure product (0.265 g, 1.22 mmol, 31% yield). ^1H NMR (500 MHz, $\text{DMSO}-d_6$) δ ppm 1.31 (s, 9 H), 7.23 (s, 2 H), 7.45 (t, $J=7.7$ Hz, 1 H), 7.55 (d, $J=7.9$ Hz, 1 H), 7.61 (d, $J=7.6$ Hz, 1 H), 7.79 (s, 1 H); ^{13}C NMR (126 MHz, $\text{DMSO}-d_6$) δ ppm 30.90 (3 C), 34.48, 121.49, 122.36, 124.15, 127.48, 129.04, 151.60, 157.59, 163.80; mp 216-219°C; MS (ESI): m/z 218.12 ($\text{M}+\text{H}$) $^+$, 259.09 ($\text{M}+\text{H}+\text{CH}_3\text{CN}$) $^+$; 96%.

2-(3-(Trifluoromethyl)phenyl)-1,3,4-oxadiazole (47)³⁷ A sealed reaction vial was charged with 3-(trifluoromethyl)benzohydrazide (**43**, 0.400 g, 1.96 mmol) and triethyl orthoformate (4.00 mL, 24.0 mmol). The mixture was heated under an argon atmosphere for 2 h at 160 °C. The reaction mixture was poured into a precooled saturated aqueous solution of Na_2CO_3 while stirring vigorously at 0 °C. The aqueous phase was extracted twice with ethyl acetate and the combined organic phases were washed with brine (2 times). The organic phase was dried over MgSO_4 and concentrated. The resulting yellow oil was adsorbed on silica gel and purified by flash chromatography using hexane/ethyl acetate (95:5) to (8:2) to give a colorless oil, which crystallized in the fridge (0.262 g, 1.22 mmol, 62% yield). ^1H NMR (500 MHz, $\text{DMSO}-d_6$) δ ppm 7.87 (t, $J=7.9$ Hz, 1 H), 8.00 - 8.04 (m, 1 H), 8.26 (s, 1 H), 8.30 - 8.34 (m, 1 H), 9.44 (s, 1 H); ^{13}C NMR (126 MHz, $\text{DMSO}-d_6$) δ ppm 123.6 (q, $^1J(\text{C},\text{F})=272.2$ Hz, 1 C), 123.0 (q, $^3J(\text{C},\text{F})=3.7$ Hz, 1 C), 124.3, 128.5 (q, $^3J(\text{C},\text{F})=3.7$ Hz, 1 C), 130.1 (q, $^2J(\text{C},\text{F})=32.1$ Hz, 1 C), 130.7, 130.9, 155.0, 162.6; mp 35°C; MS (ESI): m/z 255,91 ($\text{M}+\text{H}+\text{CH}_3\text{CN}$) $^+$; 97%.

2-Methyl-5-(3-(trifluoromethyl)phenyl)-1,3,4-oxadiazole (48)³⁷ 3-(Trifluoromethyl)-benzohydrazide (**43**, 0.500 g, 2.45 mmol) was filled into a sealed reaction vial. Triethyl orthoacetate (8.00 mL, 43.4 mmol) was added to give a clear solution. The solution was heated to 150 °C in a metal block over-night. The reaction mixture was poured into a precooled saturated solution of Na₂CO₃ while stirring vigorously at 0 °C. The water phase was extracted twice with ethyl acetate and the combined organic layers were washed with brine. The organic phase was dried over MgSO₄ and concentrated to obtain a pale yellow oil. Scratching with a spatula afforded a white solid. The white solid was triturated with hexane and filtered. The resulting cake was washed with hexane to give the pure product as white crystals (0.230 g, 1.01 mmol, 41% yield). ¹H NMR (500 MHz, DMSO-*d*₆) δ ppm 2.61 (s, 3 H), 7.84 (t, *J*=7.9 Hz, 1 H), 7.99 (d, *J*=7.9 Hz, 1 H), 8.19 (s, 1 H), 8.26 (d, *J*=7.9 Hz, 1 H); ¹³C NMR (126 MHz, DMSO-*d*₆) δ ppm 10.33, 123.58 (q, ¹*J*(C,F)=273.1 Hz, 1 C), 128.19 (q, ³*J*(C,F)=3.7 Hz, 1 C), 130.06 (q, ²*J*(C,F)=33.9 Hz, 1 C), 130.23, 130.83, 162.81, 164.49; mp 79-82°C; MS (ESI): *m/z* 228.96 (M+H)⁺, 270.00 (M+H+CH₃CN)⁺.

2-Methoxy-5-(3-(trifluoromethyl)phenyl)-1,3,4-oxadiazole (49)³⁶ Methyl 2-(3-(trifluoromethyl)benzoyl)hydrazinecarboxylate (**44**, 0.500 g, 1.91 mmol) and Burgess reagent (0.680 g, 2.86 mmol) were dissolved in dry THF (9 mL) in a MW vial flushed with argon. The reaction mixture was heated in the MW for 2 min (dynamic heating 100W max power, 150 °C safe temperature). The reaction mixture was poured into a saturated aqueous solution of NaHCO₃. The aqueous phase was extracted twice with ethyl acetate. The combined organic layers were percolated through a filter loaded with silica gel. The filtrate was concentrated to give a yellow oil. The oil was triturated with diethyl ether to afford a suspension. The solid was removed by filtration. The filtrate was adsorbed on silica gel and purified by flash chromatography with DCM:hexane (1:1) to yield the product as colorless needles (167 mg, 0.684 mmol, 36% yield). ¹H NMR (500 MHz, DMSO-*d*₆) δ ppm 4.20 (s, 3 H), 7.82 (t, *J*=7.9 Hz, 1 H), 7.96 (d, *J*=7.9 Hz, 1 H), 8.11 (s, 1 H), 8.17 (d, *J*=7.9 Hz, 1 H); ¹³C NMR (126 MHz, DMSO-*d*₆) δ ppm 59.88, 121.94 (q, ³*J*(C,F)=3.7 Hz, 1 C), 123.58 (d, ¹*J*(C,F)=272.2 Hz, 1 C), 124.64, 127.89 (q, ³*J*(C,F)=3.7 Hz, 1 C), 129.61, 130.01 (d, ²*J*(C,F)=32.1 Hz, 1 C), 130.75, 158.64, 166.11; mp 42-43 °C; HRMS: *m/z* calcd 245.0532 (M+H)⁺ found 245.0557.

2-(Trifluoromethyl)-5-(3-(trifluoromethyl)phenyl)-1,3,4-oxadiazole (50)³⁶ *N*-(2,2,2-trifluoroacetyl)-3-(trifluoromethyl)benzohydrazide (**45**, 0.500 g, 1.66 mmol) and Burgess reagent (0.595 g, 2.50 mmol) were dissolved in dry THF (9 mL) in a MW vial flushed with argon. The reaction mixture was heated in the MW for 2 min (dynamic heating 100W max power, 150 °C safe temperature). The reaction mixture was poured into a saturated aqueous solution of NaHCO₃. The aqueous phase was extracted twice with ethyl acetate. The combined organic layers were percolated through a filter loaded with silica gel. The filtrate was concentrated to give a yellow oil. The oil was triturated with ethyl acetate and DCM. The resulting suspension

was cooled in the fridge and filtered. The filtrate was adsorbed on silica gel and purified by flash chromatography using a gradient of hexane/ethyl acetate (95:5) to (70:30) to yield a yellow oil. The oil crystallized in the fridge to give the pure product as yellow needles (205 mg, 0.730 mmol, 43% yield). ^1H NMR (500 MHz, $\text{DMSO}-d_6$) δ ppm 7.91 (t, $J=7.9$ Hz, 1 H), 8.10 (d, $J=7.9$ Hz, 1 H), 8.31 (s, 1 H), 8.39 (d, $J=7.9$ Hz, 1 H); ^{13}C NMR (126 MHz, $\text{DMSO}-d_6$) δ ppm 116.14 (d, $^1J(\text{C},\text{F})=272.2$ Hz, 1 C), 123.45 (d, $^1J(\text{C},\text{F})=271.3$ Hz, 1 C), 123.26, 123.71 (q, $^3J(\text{C},\text{F})=3.7$ Hz, 1 C), 129.56 (q, $^3J(\text{C},\text{F})=3.7$ Hz, 1 C), 130.20 (q, $^2J(\text{C},\text{F})=32.1$ Hz, 1 C), 131.05, 131.40, 154.33 (d, $^2J(\text{C},\text{F})=44.0$ Hz, 1 C), 164.92; mp 25 °C; MS (ESI): m/z not found $(\text{M}+\text{H})^+$, 99%; HRMS: m/z calcd 283.0300 $(\text{M}+\text{H})^+$ found 283.0313.

***N*-methyl-5-(3-(trifluoromethyl)phenyl)-1,3,4-oxadiazol-2-amine (51)**⁴⁰ *N*-methylhydrazine-carbothioamide (186 mg, 1.770 mmol) was dissolved in DCM (8 ml). 3-(trifluoromethyl)benzoyl chloride (**17**, 0.250 mL, 1.770 mmol) was added. The resulting suspension was stirred for 15 min at RT, then EDC (0.500 mL, 3.81 mmol) was added to give a yellow solution. The solution was stirred for 24 h at RT. Another amount of EDC (0.25 ml, 1.905 mmol) was added and the solution stirred over night at 40 °C. The reaction mixture was added dropwise to an aqueous citric acid solution (10%). The aqueous layer was extracted with ethyl acetate (3 times). The combined ethyl acetate layers were washed with saturated aqueous NaHCO_3 solution (2 times) and brine (2 times). The organic layer was concentrated to dryness and purified by flash-chromatography (hexane/ethyl acetate 1:1) to give the product as white solid (60 mg, 0.247 mmol, 14% yield). ^1H NMR (500 MHz, $\text{DMSO}-d_6$) δ ppm 2.88 (d, $J=4.7$ Hz, 3 H) 7.73 - 7.81 (m, 2 H) 7.88 (dt, $J=7.9, 0.8$ Hz, 1 H) 8.03 (s, 1 H) 8.08 - 8.12 (m, 1 H); ^{13}C NMR (126 MHz, $\text{DMSO}-d_6$) δ ppm 28.99, 121.22 (q, $^3J(\text{C},\text{F})=3.7$ Hz, 1 C), 124.78 (d, $^1J(\text{C},\text{F})=272.2$ Hz, 1 C), 122.62, 125.28, 126.79 (q, $^3J(\text{C},\text{F})=3.7$ Hz, 1 C), 128.88, 129.92 (q, $^2J(\text{C},\text{F})=33.9$ Hz, 1 C), 130.65, 156.46, 164.42; mp 190-192°C; MS (ESI): m/z 243,89 $(\text{M}+\text{H})^+$, 96%

5-(3-(Trifluoromethyl)phenyl)-1,3,4-oxadiazole-2-carboxamide (52)³⁹ Ethyl 5-(3-(trifluoromethyl)phenyl)-1,3,4-oxadiazole-2-carboxylate (**46**, 0.800 g, 2.80 mmol) was dissolved in MeOH (6 mL) and diethyl ether (3 mL) in a sealed reaction vial. Ammonia in MeOH (4.00 mL, 28.0 mmol) was added, the reaction mixture was agitated and aged at RT without stirring for 48 h. The reaction mixture was concentrated to dryness to give the product as white solid (720 mg, 2.80 mmol, 100 % yield). ^1H NMR (500 MHz, $\text{DMSO}-d_6$) δ ppm 7.90 (t, $J=7.9$ Hz, 1 H), 8.07 (d, $J=7.9$ Hz, 1 H), 8.30 (br. s, 1 H), 8.34 (s, 1 H), 8.39 (d, $J=7.9$ Hz, 1 H), 8.74 (br. s, 1 H); ^{13}C NMR (126 MHz, $\text{DMSO}-d_6$) δ ppm 123.57 (q, $^2J(\text{C},\text{F})=272.2$ Hz, 1 C), 123.45 (q, $^3J(\text{C},\text{F})=4.6$ Hz, 1 C), 124.04, 128.98 (q, $^3J(\text{C},\text{F})=4.6$ Hz, 1 C), 130.12 (q, $^2J(\text{C},\text{F})=32.9$ Hz, 1 C), 130.92, 130.99, 154.27, 158.83, 163.75; mp: 151-153 °C; MS (ESI): m/z not found $(\text{M}+\text{H})^+$, 98%; HRMS: calcd m/z 258.0484 $(\text{M}+\text{H})^+$ found 258.0494.

5-(3-(Trifluoromethyl)phenyl)-1,3,4-oxadiazol-2(3H)-one (53)⁴¹ 3-(Trifluoromethyl) benzohydrazide (**43**, 0.500 g, 2.45 mmol) was dissolved in DCM (25 mL) and triethylamine

(0.512 mL, 3.67 mmol). Carbonyldiimidazole (0.596 g, 3.67 mmol) was added under constant stirring. The reaction mixture was aged at RT for 30 min. The reaction mixture was washed with a 5% aqueous solution of citric acid (2 times) and twice with brine. The organic layer was dried over MgSO_4 , filtered and concentrated to give a white solid. The solid was triturated with DCM/hexane, filtered and the resulting cake was washed with DCM/hexane to afford the product as a white solid (0.206 g, 0.895 mmol, 37% yield). ^1H NMR (500 MHz, $\text{DMSO}-d_6$) δ ppm 7.80 (t, $J=7.9$ Hz, 1 H), 7.94 (d, $J=7.9$ Hz, 1 H), 8.00 (s, 1 H), 8.08 (d, $J=7.9$ Hz, 1 H), 12.75 (br. s, 1 H); ^{13}C NMR (126 MHz, $\text{CHLOROFORM}-d$) δ ppm 123.40 (q, $^1J(\text{C},\text{F})=271.3$ Hz, 1 C), 122.74 (q, $^3J(\text{C},\text{F})=3.7$ Hz, 1 C), 124.61, 128.29 (q, $^3J(\text{C},\text{F})=3.7$ Hz, 1 C), 128.84, 129.74, 131.81 (q, $^2J(\text{C},\text{F})=33.0$ Hz, 1 C), 154.09, 154.67; mp 112-123 °C; HRMS: m/z calcd 231.0375 found 231.0380.

ACKNOWLEDGMENT

The authors would like to thank Simone Amann for performing the in-vitro assays, Dr. Johannes C. de Jong for synthesis of HHQ and HHQ-*d*₄, Michael Hoffmann, Dr. Stefan Boettcher and Dr. Josef Zapp for assistance with chemical analytics and Meghan Hattarki and Lesley Pearce for assisting during SPR experiments. The *P. aeruginosa* strain PA14 and its isogenic transposon mutant strains were obtained from Prof. Dr. Susanne Häussler (Twincore Hannover, Germany) and HQNO from Prof. Dr. Friedrich Hammerschmidt (Institute of Organic Chemistry, Vienna, Austria)

REFERENCES

- 1) Williams, P.; Winzer, K.; Chan, W. C.; Cámara, M. Look who's talking: communication and quorum sensing in the bacterial world. *Philos. Trans. R. Soc., B* **2007**, *362*, 1119–1134.
- 2) Whitehead, N. A.; Barnard, A. M. L.; Slater, H.; Simpson, N. J. L.; Salmond, G. P. C. Quorum-sensing in Gram-negative bacteria. *FEMS Microbiol. Rev.* **2001**, *25*, 365–404.
- 3) Bertrand, X.; Thouverez, M.; Patry, C.; Balvay, P.; Talon, D. *Pseudomonas aeruginosa*: antibiotic susceptibility and genotypic characterization of strains isolated in the intensive care unit. *Clin. Microbiol. Infect.* **2001**, *7*, 706–708.
- 4) Vincent, J. L.; Bihari, D. J.; Suter P. M.; Bruining H. A.; White, J.; Nicolas-Chanoin, M.H.; Wolff, M.; Spencer, R.C.; Hemmer, M. The prevalence of nosocomial infection in intensive care units in Europe: Results of the European prevalence of infection in intensive care (epic) study. *J. Am. Med. Assoc.* **1995**, *274*, 639–644.
- 5) Koch, C.; Høiby N. Pathogenesis of cystic fibrosis. *The Lancet* **1993**, *341*, 1065–1069.
- 6) Walters, M. C.; Roe, F.; Bugnicourt, A.; Franklin, M. J.; Stewart, P. S. Contributions of Antibiotic Penetration, Oxygen Limitation, and Low Metabolic Activity to Tolerance of *Pseudomonas aeruginosa* Biofilms to Ciprofloxacin and Tobramycin. *Antimicro. Agents Chemother.* **2003**, *47*, 317–323.
- 7) Aloush, V.; Navon-Venezia, S.; Seigman-Igra, Y.; Cabili, S.; Carmeli, Y. Multidrug-Resistant *Pseudomonas aeruginosa*: Risk Factors and Clinical Impact. *Antimicro. Agents Chemother.* **2006**, *50*, 43–48.
- 8) Boucher, H. W.; Talbot, G. H.; Bradley, J. S.; Edwards, J. E.; Gilbert, D.; Rice, L. B.; Scheld, M.; Spellberg, B.; Bartlett, J. Bad Bugs, No Drugs: No ESCAPE! An Update from the Infectious Diseases Society of America. *Clin. Infect. Dis.* **2009**, *48*, 1–12.
- 9) Gambello, M. J.; Iglewski, B. H. Cloning and characterization of the *Pseudomonas aeruginosa* lasR gene, a transcriptional activator of elastase expression. *J. Bacteriol.* **1991**, *173*, 3000–3009.
- 10) Passador, L.; Cook, J. M.; Gambello, M. J.; Rust, L.; Iglewski, B. H. Expression of *Pseudomonas aeruginosa* virulence genes requires cell-to-cell communication. *Science* **1993**, *260*, 1127–1130.
- 11) Ochsner, U. A.; Koch, A. K.; Fiechter, A.; Reiser, J. Isolation and characterization of a regulatory gene affecting rhamnolipid biosurfactant synthesis in *Pseudomonas aeruginosa*. *J. Bacteriol.* **1994**, *176*, 2044–2054.
- 12) Ochsner, U. A.; Reiser, J. Autoinducer-mediated regulation of rhamnolipid biosurfactant synthesis in *Pseudomonas aeruginosa*. *Proc. Natl. Acad. Sci. U.S.A.* **1995**, *92*, 6424–6428.
- 13) Pesci, E. C.; Milbank, J. B. J.; Pearson, J. P.; McKnight, S.; Kende, A. S.; Greenberg, E. P.; Iglewski, B. H. Quinolone signaling in the cell-to-cell communication system of *Pseudomonas aeruginosa*. *Proc. Natl. Acad. Sci. U.S.A.* **1999**, *96*, 11229–11234.
- 14) Cao, H.; Krishnan, G.; Goumnerov, B.; Tsongalis, J.; Tompkins, R.; Rahme, L. G. A quorum sensing-associated virulence gene of *Pseudomonas aeruginosa* encodes a LysR-like transcription regulator with a unique self-regulatory mechanism. *Proc. Natl. Acad. Sci. U.S.A.* **2001**, *98*, 14613–14618.
- 15) Diggle, S. P.; Lumjiaktase, P.; Dipilato, F.; Winzer, K.; Kunakorn, M.; Barrett, D. A.; Chhabra, S. R.; Cámara, M.; Williams, P. Functional Genetic Analysis Reveals a 2-Alkyl-4-Quinolone Signaling System in the Human Pathogen *Burkholderia pseudomallei* and Related Bacteria. *Chem. Biol.* **2006**, *13*, 701–710.
- 16) Wade, D. S.; Calfee, M. W.; Rocha, E. R.; Ling, E. A.; Engstrom, E.; Coleman, J. P.; Pesci, E. C. Regulation of *Pseudomonas aeruginosa* Quinolone Signal Synthesis in *Pseudomonas aeruginosa*. *J. Bacteriol.* **2005**, *187*, 4372–4380.
- 17) Xiao, G.; Déziel, E.; He, J.; Lépine, F.; Lesic, B.; Castonguay, M.-H.; Milot, S.; Tampakaki, A. P.; Stachel, S. E.; Rahme, L. G. MvR, a key *Pseudomonas aeruginosa* pathogenicity LTTR-class regulatory protein, has dual ligands. *Mol. Microbiol.* **2006**, *62*, 1689–1699.
- 18) Diggle, S. P.; Winzer, K.; Chhabra, S. R.; Worrall, K. E.; Cámara, M.; Williams, P. The *Pseudomonas aeruginosa* quinolone signal molecule overcomes the cell density-dependency of the quorum sensing hierarchy, regulates rhl-dependent genes at the onset of stationary phase and can be produced in the absence of LasR. *Mol. Microbiol.* **2003**, *50*, 29–43.

- (19) Gallagher, L. A.; McKnight, S. L.; Kuznetsova, M. S.; Pesci, E. C.; Manoil, C. Functions Required for Extracellular Quinolone Signaling by *Pseudomonas aeruginosa*. *J. Bacteriol.* **2002**, *184*, 6472–6480.
- (20) Déziel, E.; Lépine, F.; Milot, S.; He, J.; Mindrinos, M. N.; Tompkins, R. G.; Rahme, L. G. Analysis of *Pseudomonas aeruginosa* 4-hydroxy-2-alkylquinolines (HAQs) reveals a role for 4-hydroxy-2-heptylquinoline in cell-to-cell communication. *Proc. Natl. Acad. Sci. U.S.A.* **2004**, *101*, 1339–1344.
- (21) Yang, L.; Nilsson, M.; Gjermansen, M.; Givskov, M.; Tolker-Nielsen, T. Pyoverdine and PQS mediated subpopulation interactions involved in *Pseudomonas aeruginosa* biofilm formation. *Mol. Microbiol.* **2009**, *74*, 1380–1392.
- (22) Hartman, G.; Wise, R. Quorum sensing: potential means of treating Gram-negative infections? *The Lancet* **1998**, *351*, 848–849.
- (23) Hentzer, M.; Wu, H.; Andersen, J. B.; Riedel, K.; Rasmussen, T. B.; Bagge, N.; Kumar, N.; Schembri, M. A.; Song, Z.; Kristoffersen, P.; Manefield, M.; Costerton, J. W.; Molin, S.; Eberl, L.; Steinberg, P.; Kjelleberg, S.; Hoiby, N.; Givskov, M. Attenuation of *Pseudomonas aeruginosa* virulence by quorum sensing inhibitors. *EMBO J.* **2003**, *22*, 3803–3815.
- (24) Imperi, F.; Massai, F.; Facchini, M.; Frangipani, E.; Visaggio, D.; Leoni, L.; Bragonzi, A.; Visca, P. Repurposing the antimycotic drug flucytosine for suppression of *Pseudomonas aeruginosa* pathogenicity. *Proc. Natl. Acad. Sci. U.S.A.* **2013**, *110*, 7458–7463.
- (25) Lu, C.; Kirsch, B.; Zimmer, C.; Jong, J. C. de; Henn, C.; Maurer, C. K.; Müsken, M.; Häussler, S.; Steinbach, A.; Hartmann, R. W. Discovery of Antagonists of PqsR, a Key Player in 2-Alkyl-4-quinolone-Dependent Quorum Sensing in *Pseudomonas aeruginosa*. *Chem. Biol.* **2012**, *19*, 381–390.
- (26) Leeson, P. D.; Springthorpe, B. The influence of drug-like concepts on decision-making in medicinal chemistry. *Nat. Rev. Drug Discovery* **2007**, *6*, 881–890.
- (27) Waldrop, G. L. Smaller Is Better for Antibiotic Discovery. *ACS Chem. Biol.* **2009**, *4*, 397–399.
- (28) Hajduk, P. J.; Greer, J. A decade of fragment-based drug design: strategic advances and lessons learned. *Nat. Rev. Drug Discovery* **2007**, *6*, 211–219.
- (29) Klein, T.; Henn, C.; Jong, J. C. de; Zimmer, C.; Kirsch, B.; Maurer, C. K.; Pistorius, D.; Müller, R.; Steinbach, A.; Hartmann, R. W. Identification of Small-Molecule Antagonists of the *Pseudomonas aeruginosa* Transcriptional Regulator PqsR: Biophysically Guided Hit Discovery and Optimization. *ACS Chem. Biol.* **2012**, *7*, 1496–1501.
- (30) Kurzak, B.; Kozłowski, H.; Farkas, E. Hydroxamic and aminohydroxamic acids and their complexes with metal ions. *Coord. Chem. Rev.* **1992**, *114*, 169–200.
- (31) Muri, E. M. F.; Nieto, M. J.; Sindelar, R. D.; Williamson, J. S. Hydroxamic acids as pharmacological agents. *Curr. Med. Chem.* **2002**, *9*, 1631–1653.
- (32) Ching Yung Wang. Mutagenicity of hydroxamic acids for *Salmonella typhimurium*. *Mutat. Res., Fundam. Mol. Mech. Mutagen.* **1977**, *56*, 7–12.
- (33) Ferrari, S.; Morandi, F.; Motiejunas, D.; Nerini, E.; Henrich, S.; Luciani, R.; Venturelli, A.; Lazzari, S.; Calò, S.; Gupta, S.; Hannaert, V.; Michels, P. A. M.; Wade, R. C.; Costi, M. P. Virtual Screening Identification of Nonfolate Compounds, Including a CNS Drug, as Antiparasitic Agents Inhibiting Pteridine Reductase. *J. Med. Chem.* **2010**, *54*, 211–221.
- (34) Rivera, N. R.; Balsells, J.; Hansen, K. B. Synthesis of 2-amino-5-substituted-1,3,4-oxadiazoles using 1,3-dibromo-5,5-dimethylhydantoin as oxidant. *Tetrahedron Lett.* **2006**, *47*, 4889–4891.
- (35) Oruç, E. E.; Rollas, S.; Kandemirli, F.; Shvets, N.; Dimoglo, A. S. 1,3,4-Thiadiazole Derivatives. Synthesis, Structure Elucidation, and Structure-Antituberculosis Activity Relationship Investigation. *J. Med. Chem.* **2004**, *47*, 6760–6767.
- (36) Brain, C. T.; Paul, J. M.; Loong, Y.; Oakley, P. J. Novel procedure for the synthesis of 1,3,4-oxadiazoles from 1,2-diacylhydrazines using polymer-supported Burgess reagent under microwave conditions. *Tetrahedron Lett.* **1999**, *40*, 3275–3278.
- (37) Ainsworth, C.; Hackler, R. E. Alkyl-1,3,4-oxadiazoles. *J. Org. Chem.* **1966**, *31*, 3442–3444.
- (38) Huguet, F.; Melet, A.; Alves de Sousa, R.; Lieutaud, A.; Chevalier, J.; Maigre, L.; Deschamps, P.; Tomas, A.; Leulliot, N.; Pages, J.-M.; Artaud, I. Hydroxamic Acids as Potent Inhibitors of Fell and

- MnII *E.coli* Methionine Aminopeptidase: Biological Activities and X-ray Structures of Oxazole Hydroxamate–EcMetAP–Mn Complexes. *ChemMedChem* **2012**, *7*, 1020–1030.
- (39) Dost, J.; Heschel, M.; Stein, J. Zur Herstellung von 1,3,4-Oxadiazol-2-carbonsäurederivaten. *J. Prakt. Chem.* **1985**, *327*, 109–116.
- (40) Piatnitski Chekler, E. L.; ElokDAH, H. M.; Butera, J. Efficient one-pot synthesis of substituted 2-amino-1,3,4-oxadiazoles. *Tetrahedron Lett.* **2008**, *49*, 6709–6711.
- (41) Flechter, J. M.; Fong Tung M.; Hagmann W. K.; Vachal P. Sufonylated Piperazines as Cannabinoid-1 Receptor Modulators. WO2008/024284, **2008**.
- (42) Myszka, D. G.; Rich, R. L. Implementing surface plasmon resonance biosensors in drug discovery. *Pharm. Sci. Technol. Today* **2000**, *3*, 310–317.
- (43) Giannetti, A. M.; Koch, B. D.; Browner, M. F. Surface plasmon resonance based assay for the detection and characterization of promiscuous inhibitors. *J. Med. Chem.* **2008**, *51*, 574–580.
- (44) Perspicace, S.; Banner, D.; Benz, J.; Müller, F.; Schlatter, D.; Huber, W. Fragment-Based Screening Using Surface Plasmon Resonance Technology. *J. Biomol. Screening* **2009**, *14*, 337–349.
- (45) Ladbury, J. E.; Klebe, G.; Freire, E. Adding calorimetric data to decision making in lead discovery: a hot tip. *Nat. Rev. Drug Discovery* **2010**, *9*, 23–27.
- (46) Ladbury, J. E.; Chowdhry, B. Z. Sensing the heat: the application of isothermal titration calorimetry to thermodynamic studies of biomolecular interactions. *Chem. Biol.* **1996**, *3*, 791–801.
- (47) Hopkins, A. L.; Groom, C. R.; Alex, A. Ligand efficiency: a useful metric for lead selection. *Drug Discovery Today* **2004**, *9*, 430–431.
- (48) Cugini, C.; Calfee, M. W.; Farrow, J. M.; Morales, D. K.; Pesci, E. C.; Hogan, D. A. Farnesol, a common sesquiterpene, inhibits PQS production in *Pseudomonas aeruginosa*. *Mol. Microbiol.* **2007**, *65*, 896–906.
- (49) Nicas, T. I.; Hancock, P. *Pseudomonas aeruginosa* outer membrane permeability: isolation of a porin protein F-deficient mutant. *J. Bacteriol.* **1983**, *153*, 281–285.
- (50) Kefala, K.; Kotsifaki, D.; Providaki, M.; Kapetaniou, E. G.; Rahme, L.; Kokkinidis, M. Purification, crystallization and preliminary X-ray diffraction analysis of the C-terminal fragment of the MvR protein from *Pseudomonas aeruginosa*. *Acta Crystallogr., Sect. F: Struct. Biol. Cryst. Commun.* **2012**, *68*, 695–697.
- (51) Xu, N.; Yu, S.; Moniot, S.; Weyand, M.; Blankenfeldt, W. Crystallization and preliminary crystal structure analysis of the ligand-binding domain of PqsR (MvR), the *Pseudomonas* quinolone signal (PQS) responsive quorum-sensing transcription factor of *Pseudomonas aeruginosa*. *Acta Crystallogr., Sect. F: Struct. Biol. Cryst. Commun.* **2012**, *68*, 1034–1039.
- (52) Freire, E. Do enthalpy and entropy distinguish first in class from best in class? *Drug Discovery Today* **2008**, *13*, 869–874
- (53) Rubeš, M.; Bludský, O.; Nachtigall, P. Investigation of the Benzene-Naphthalene and Naphthalene–Naphthalene Potential Energy Surfaces: DFT/CCSD(T) Correction Scheme. *ChemPhysChem* **2008**, *9*, 1702–1708.
- (54) Sánchez-Pedregal, V. M.; Reese, M.; Meiler, J.; Blommers, M. J. J.; Griesinger, C.; Carlomagno, T. The INPHARMA Method: Protein-Mediated Interligand NOEs for Pharmacophore Mapping. *Angew. Chem., Int. Ed.* **2005**, *117*, 4244–4247.
- (55) Cozzi, F.; Cinquini, M.; Annunziata, R.; Dwyer, T.; Siegel, J. S. Polar/ π interactions between stacked aryls in 1,8-diarylnaphthalenes. *J. Am. Chem. Soc.* **1992**, *114*, 5729–5733.
- (56) Gung, B. W.; Xue, X.; Zou, Y. Enthalpy (ΔH) and Entropy (ΔS) for π -Stacking Interactions in Near-Sandwich Configurations: Relative Importance of Electrostatic, Dispersive, and Charge-Transfer Effects. *J. Org. Chem.* **2007**, *72*, 2469–2475.
- (57) Wheeler, S. E.; Houk, K. N. Substituent Effects in the Benzene Dimer are Due to Direct Interactions of the Substituents with the Unsubstituted Benzene. *J. Am. Chem. Soc.* **2008**, *130*, 10854–10855.
- (58) Sinnokrot, M. O.; Valeev, E. F.; Sherrill, C. D. Estimates of the Ab Initio Limit for π - π Interactions: The Benzene Dimer. *J. Am. Chem. Soc.* **2002**, *124*, 10887–10893.

- (59) Pierce, A. C.; Sandretto, K. L.; Bemis, G. W. Kinase inhibitors and the case for CH...O hydrogen bonds in protein-ligand binding. *Proteins* **2002**, *49*, 567–576.
- (60) Rada, B.; Gardina, P.; Myers, T. G.; Leto, T. L. Reactive oxygen species mediate inflammatory cytokine release and EGFR-dependent mucin secretion in airway epithelial cells exposed to *Pseudomonas* pyocyanin. *Mucosal Immunol.* **2011**, *4*, 158–171.
- (61) Déziel, E.; Gopalan, S.; Tampakaki, A. P.; Lépine, F.; Padfield, K. E.; Saucier, M.; Xiao, G.; Rahme, L. G. The contribution of MVR to *Pseudomonas aeruginosa* pathogenesis and quorum sensing circuitry regulation: multiple quorum sensing-regulated genes are modulated without affecting *lasRI*, *rhlRI* or the production of *N*-acyl-L-homoserine lactones. *Mol. Microbiol.* **2005**, *55*, 998–1014.
- (62) Hazan, R.; He, J.; Xiao, G.; Dekimpe, V.; Apidianakis, Y.; Lesic, B.; Astrakas, C.; Déziel, E.; Lépine, F.; Rahme, L. G. Homeostatic Interplay between Bacterial Cell-Cell Signaling and Iron in Virulence. *PLoS Pathog.* **2010**, *6*, e1000810 EP.
- (63) Merlot, C. Computational toxicology—a tool for early safety evaluation. *Drug Discovery Today* **2010**, *15*, 16–22.
- (64) Papalia, G. A.; Leavitt, S.; Bynum, M. A.; Katsamba, P. S.; Wilton, R.; Qiu, H.; Steukers, M.; Wang, S.; Bindu, L.; Phogat, S.; Giannetti, A. M.; Ryan, T. E.; Pudlak, V. A.; Matusiewicz, K.; Michelson, K. M.; Nowakowski, A.; Pham-Baginski, A.; Brooks, J.; Tieman, B. C.; Bruce, B. D.; Vaughn, M.; Baksh, M.; Cho, Y. H.; Wit, M. de; Smets, A.; Vandersmissen, J.; Michiels, L.; Myszka, D. G. Comparative analysis of 10 small molecules binding to carbonic anhydrase II by different investigators using Biacore technology. *Anal. Biochem.* **2006**, *359*, 94–105.
- (65) Griffith, K. L.; Wolf, R. E. Measuring beta-galactosidase activity in bacteria: cell growth, permeabilization, and enzyme assays in 96-well arrays. *Biochem. Biophys. Res. Commun.* **2002**, *290*, 397–402.
- (66) Storz, M. P.; Maurer, C. K.; Zimmer, C.; Wagner, N.; Brengel, C.; Jong, J. C. de; Lucas, S.; Müsken, M.; Häussler, S.; Steinbach, A.; Hartmann, R. W. Validation of PqsD as an Anti-biofilm Target in *Pseudomonas aeruginosa* by Development of Small-Molecule Inhibitors. *J. Am. Chem. Soc.* **2012**, *134*, 16143–16146.
- (67) Essar, D. W.; Eberly, L.; Hadero, A.; Crawford, I. P. Identification and characterization of genes for a second anthranilate synthase in *Pseudomonas aeruginosa*: interchangeability of the two anthranilate synthases and evolutionary implications. *J. Bacteriol.* **1990**, *172*, 884–900.
- (68) Lépine, F.; Déziel, E.; Milot, S.; Rahme, L. G. A stable isotope dilution assay for the quantification of the *Pseudomonas* quinolone signal in *Pseudomonas aeruginosa* cultures. *Biochim. Biophys. Acta, Gen. Subj.* **2003**, *1622*, 36–41.
- (69) Lépine, F.; Milot, S.; Déziel, E.; He, J.; Rahme, L. G. Electrospray/mass spectrometric identification and analysis of 4-hydroxy-2-alkylquinolines (HAQs) produced by *Pseudomonas aeruginosa*. *J. Am. Soc. Mass Spectrom.* **2004**, *15*, 862–869.

3.2 Chapter B:

Flexible-Fragment-Growing Boosts Potency of Quorum Sensing Inhibitors against *Pseudomonas aeruginosa* virulence

The coworkers listed below made the following experimental contributions to this chapter:

Florian Witzgall:	Performed PqsR crystallization experiments, built and refined PqsR models.
Alexander Kiefer:	Performed parts of the chemical synthesis work
Benjamin Kirsch:	Established and planed <i>E. coli</i> reporter gene assays
Christine K. Maurer:	Established and planed alkylquinolone and pyocyanin assays
Andreas Kany:	Performed parts of the ITC measurements
Ningna Xu:	Performed parts of the PqsR crystallization experiments
Carsten Börger:	Performed parts of compound purification work and MS analytics
Martin Empting:	Performed the in silico experiments

INTRODUCTION

Pseudomonas aeruginosa is an opportunistic Gram-negative pathogen. It provokes different acute and chronic infections especially in immune-compromised and hospitalized patients.¹ Alarmingly, the occurrence of multi-resistant and pan-resistant strains renders currently available antibiotics ineffective and leads to an urgent need for novel treatment options.² *P. aeruginosa* employs an arsenal of virulence-associated factors that allow this pathogen to be effective in various host organisms.³ The release of many virulence factors is controlled and synchronized by a process called quorum sensing (QS).⁴ QS allows bacteria to collectively regulate gene expression depending on their population density. Small diffusible molecules (auto-inducers) are secreted from the cells and once a certain threshold concentration has been achieved, transcriptional regulators are activated. This leads to a population-wide alteration of gene expression, resulting in concerted phenotypic actions.⁵ This ability is essential during the course of acute and chronic infections⁶ as well as for lowered antibiotic susceptibility⁷.

Respective cell-to-cell communication in *P. aeruginosa* is mainly based on three distinct QS circuitries. The las⁸ and the rhl⁹ QS systems use different N-acylated homoserine lactones (AHLs) as signaling molecules¹⁰. AHLs-based communication is most widespread 'language' found in Gram-negative bacteria.¹¹ On the contrary, the third system called pqs¹² employs 4-hydroxy-2-alkylquinolones (HAQs)^{13,14} and occurs only in *Pseudomonas* and *Burkholderia* strains (Figure 1).¹⁵ The signaling molecules PQS (*Pseudomonas* Quinolone Signal; 3,4-

dihydroxy-2-heptylquinoline) and its precursor HHQ (4-hydroxy-2-heptylquinoline) activate the receptor.

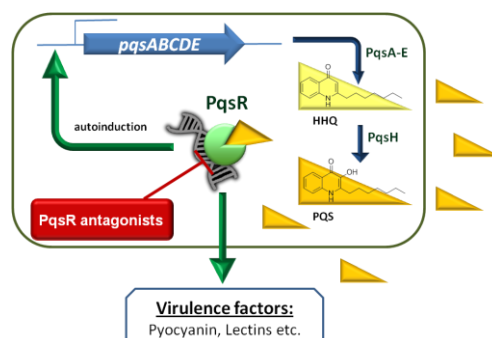


Figure 1: Schematic representation of the PQS quorum sensing system.

Our group has previously obtained the first PqsR antagonists by chemical modification of the natural ligand HHQ.²¹ These compounds were further improved regarding their efficacy in *P. aeruginosa*.^{22,23} In a similar approach, antagonists containing a quinazolinone scaffold were developed and helped resolving the crystal structure of the ligand binding domain of PqsR.²⁴ Very recently, an HTS campaign led to benzamide-benzimidazole antagonists showing efficacy in different mouse models, which emphasizes the *in vivo* relevance of targeting PqsR in infectious diseases.²⁵ To overcome the poor physico-chemical profiles of the HHQ-derived antagonists, we initiated two fragment screenings using surface plasmon resonance (SPR) technology.^{26,27} These approaches led to the hydroxamic acid **1** and the 2-amino-oxadiazole **2** (Table 1). First attempts to enlarge these structures have not been successful so far or led to compounds lacking activity in *P. aeruginosa* (data not shown).

Here, we applied enthalpic efficiency^{28,29} as a metric to select screening hit **3** as alternative starting point. During initial fragment–growing efforts, we were successful in stepwisely enlarging the fragment structure. Notably, we determined the crystal structure of a ligand–receptor complex. This enabled us to devise an elegant structure-guided optimization strategy considering the binding pose of the natural ligand HHQ. The introduction of a flexible linker finally led to compounds with nanomolar antagonistic activities in an *E. coli* reporter gene assay and complete pyocyanin inhibition in *P. aeruginosa*.

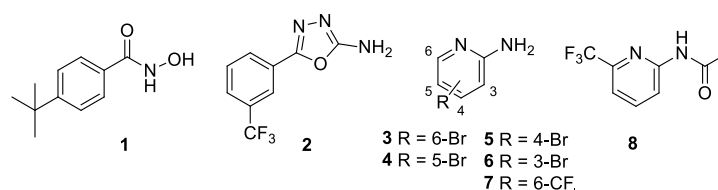
RESULTS AND DISCUSSION

Selection of an optimal starting point. Selecting the best starting point is a pivotal decision in the early stage of a drug discovery project. In previous projects, ligand efficiency³⁰ (LE) was used as major criterion for hit selection.²⁷ The LE values represent the mean binding contribution per heavy atom ($LE = \Delta G/N$) allowing to compare hits of different sizes.³⁰ Taken into account that the ligand binding site of PqsR is highly lipophilic,²⁴ the engineering of well-placed

hydrogen bonds will be a difficult task. Hence, an ideal screening hit should establish most effective non-covalent interactions. Enthalpic contribution (ΔH) is a convenient indicator for the establishment and the breaking of specific interactions during the formation of the protein-ligand complex.^{28,29} In a simple model, ΔH describes the sum of bond breaks between solvent and ligand and on the other hand bond formation between ligand and protein.²⁸ Hence, enthalpic efficiency (EE) was used as guideline to derive an alternative starting point.²⁸ EE normalizes the enthalpic contribution for the heavy atom count (EE= $\Delta H/N$). Hence, this concept allows comparing ligands of different sizes.

During two previously reported fragment optimization approaches, antagonists **1**²⁷ and **2**²⁶ (Table 1) were discovered. The thermodynamic profiles of these optimized fragments were compared to the best screening hits derived from previously reported SPR screenings.^{26,27} Initially, compound **3** was ranked lower due to its lower affinity, even if it showed strikingly better EE and LE values (Table 1). In the light of these considerations, fragment **3** was evaluated as a promising alternative starting point.

Table 1: Thermodynamic profiling of fragment-sized PqsR ligands guiding the selection of the optimal starting point for further compound development.



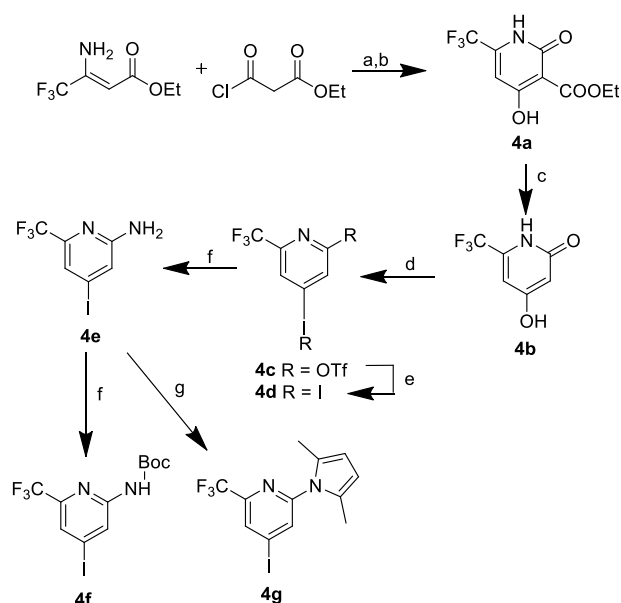
Comp	K_D (ITC) [μM]	ΔG [kcal mol ⁻¹]	ΔH [kcal mol ⁻¹]	$-T\Delta S$ [kcal mol ⁻¹]	EE ^a [kcal mol ⁻¹]	LE ^b [kcal mol ⁻¹]
1	4.1 ± 0.6	-7.4 ± 0.1	-8.9 ± 0.2	1.5 ± 0.3	0.63	0.53
2	1.3 ± 0.3	-8.0 ± 0.1	-8.5 ± 0.5	0.4 ± 0.6	0.53	0.50
3	10.0 ± 1.3	-6.8 ± 0.1	-9.3 ± 0.4	2.5 ± 0.4	1.17	0.85
4	> 50 ^c	-	-	-	-	-
5	21.3 ± 3.4	-6.4 ± 0.1	-5.8 ± 0.1	-0.6 ± 0.2	0.72	0.80
6	> 50 ^c	-	-	-	-	-
7	3.1 ± 0.5	-7.5 ± 0.1	-11.5 ± 0.9	3.7 ± 1	1.05	0.70
8	> 50 ^a	-	-	-	-	-

ITC titrations were performed at 298 K. Data represent mean ± SD from at least two independent experiments; ^aEE = $-\Delta H/(\text{heavy atom count})$; ^bLE = $-\Delta G/(\text{heavy atom count})$. ^cno heat release detectable at solubility maximum.

Chemistry. Compounds **3-8** (Table 1) were obtained from commercial suppliers. The synthesis to access the key intermediate **4e** is outlined in Scheme 1. The de-novo construction of the 2,4,6 substituted pyridine ring followed a modified protocol described by Adam et al.³¹ starting with the acetylation of ethyl-3-amino-4,4,4-trifluorocrotonate with ethyl-malonyl-chloride. Ring closing was achieved using potassium *tert*-butoxide to obtain **4a**. Hydrolysis and

decarboxylation of **4a** by hydrochloric acid and reflux provided **4b**. **4b** was reacted with triflic anhydride to give **4c**, which was further converted into the corresponding 2,4-diiodo-pyridine (**4d**) by substitution with iodide after protonation of the pyridine with triflic acid. Both steps can also be performed as a one-pot procedure.³² For the introduction of the amino group in position two of the pyridine ring, aqueous ammonia and copper/phenanthroline as catalyst were applied, which yielded compound **4e** in 65% isolated yield, while the reaction provided a 84:16 regioselectivity for the desired product. Additionally, the protected precursors **4f** and **4g** were synthesized by standard protocols.

Scheme 1. Synthesis of key intermediates



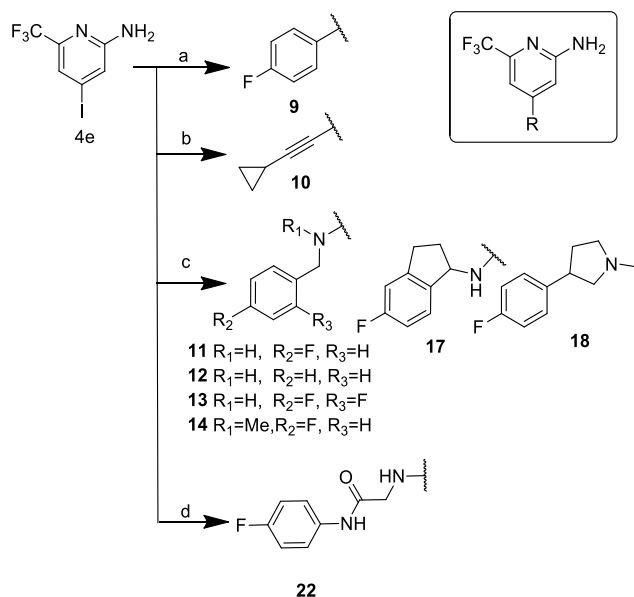
Reagents and Conditions: (a) Pyridine, DCM, RT; (b) potassium tert-butoxide, EtOH, 70°C to RT; (c) 6M HCl, RF; (d) Triflic anhydride, pyridine, acetonitrile 5°C to RT (e) KI, triflic acid, RT; (f) $\text{NH}_{3\text{aq}}$, 1,10-phenanthroline, Cu_2O , DMSO, 15°C to RT (f) Boc anhydride, Et₃N, DMAP, t-BuOH; 35°C (g) hexane-2,5-dione, pTsOH, toluene, RF.

Key building block **4e** was suitable for palladium- and copper-catalyzed coupling reactions as shown in Scheme 2. **4e** and 4-fluorophenylboronic acid were reacted under standard Suzuki coupling conditions using $\text{Pd}(\text{dppf})\text{Cl}_2$ as catalyst to obtain **9**. **4e** and cyclopropylacetylene were coupled by modified Sonogashira coupling protocol³³ using a combination of $\text{Pd}(\text{PPh}_3)_2\text{Cl}_2$ and TBAF to give **10**. The introduction of the particular amines was achieved using Buchwald-Hartwig conditions. 2-amino pyridines are known to be challenging substrates for most palladium-catalyst reactions; hence various protocols had to be tested. However, the procedure of Marion et al.³⁴ using a Pd NHC catalyst was the only one which allowed access to amines **11-14** and **17,18**. Compound **22** was synthesized via a copper-catalyzed amination reaction.³⁵

As outlined in Scheme 3, the benzyl alcohol was attached to **4g** by $\text{S}_{\text{N}}\text{Ar}$ reaction using sodium hydride as base to give **15a**. Deprotection was achieved using hydroxylamine hydrochloride and

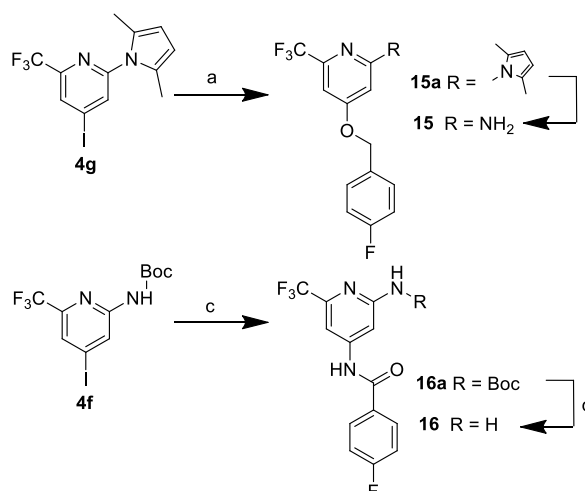
triethylamine to afford **15**.³⁶ The synthesis of **16** required the use of the Boc protected precursor **4f** and modified Buchwald-Hartwig conditions. **16** was obtained following a standard deprotection procedure using TFA/DCM. Compounds **19-21** were not accessible with the Pd NHC catalyst mentioned before. The particular amines were introduced to **4d** by a microwave assisted S_NAr reaction (Scheme 4). Copper-mediated amination of the aryl iodines (**19a-21a**) led to final products (**19-21**).

Scheme 2. Reactions applied for fragment growing

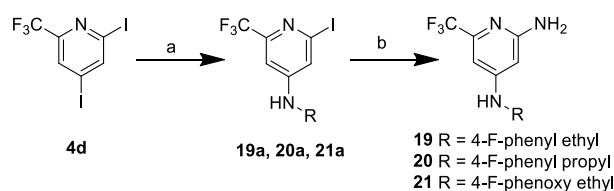


Reagents and Conditions: (a) (4-fluorophenyl) boronic acid, Pd(dppf)Cl₂, Na₂CO₃, DME/water 1:1 (v/v), 80°C; (b) cyclopropylacetylene, Pd(PPh₃)₂Cl₂, TBAF (neat), 80°C; (c) amine, (SIPR)Pd(cinnamyl)Cl, KOtBu, DME, 80°C (d) 2-amino-*N*-(4-fluorophenyl)acetamide, CuI, dimethylaminoethanol, K₃PO₄, ACN/H₂O(2/1), 90°C.

Scheme 3. Synthesis of **15** and **16**

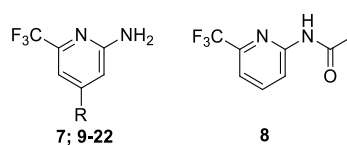


Reagents and Conditions: (a) (4-fluorophenyl)methanol, NaH, DMF, 50°C (b) hydroxylamine·HCl, Et₃N, EtOH/H₂O, RF (c) 4-fluorobenzamide, Cs₂CO₃; Pd₂(dba)₃, Xantphos, dioxane, 80°C (d) TFA, DCM, 0°C to RT.

Scheme 4. Route towards compounds **19-21**

Reagents and Conditions: (a) amine, Huenig's base, ACN, MW 130°C; (b) $\text{NH}_{3\text{aq}}$, 1,10-phenanthroline, Cu_2O , NMP/water RT.

Fragment Growing. The combination of fragment-based screening and structure-based drug design strategies improves the chances to develop highly active lead molecules tremendously.³⁷ For **3** no crystal structure in complex with PqsR could be obtained. In order to derive a first SAR and to find a potential vector for growing the fragment, close commercial analogs (**4-8**) were investigated for their affinity to PqsR by ITC analysis (Table 1). This revealed that the position of the bromine substituent was fundamental for affinity. A bromo substituent in 3- and 5-position (**4** and **6**) abolished the affinity, whereas in 4-position (**5**) the affinity was slightly decreased, which promoted the 4-position as potential growth vector. The exchange of the bromine for a sterically more demanding trifluoromethyl group in 6-position (**7**) led to a threefold increase of affinity caused by a gain in the enthalpic term. Candidate compounds were tested in an *E. coli* lacZ reporter gene system for their ability to antagonize or agonize PqsR.³⁸ This heterologous system provides higher sensitivity and a clear-cut readout due to the absence of the entire *pqs* system present in *P. aeruginosa*. Our previous studies indicated that the system employing an *E. coli* laboratory strain poses a smaller biological barrier to small molecules for reaching the intracellular target.²² Hence, it facilitates a straightforward evaluation and comparison of PqsR antagonists regarding their on-target activities. Noteworthy, this assay system provides a more reliable estimation of cellular effectivity than cell-free affinity measurements. For example, the reported affinity of the native agonist PQS towards the ligand binding domain is rather low ($K_D = 1.2 \pm 0.3 \mu\text{M}$).³⁹ In contrast, the PQS-mediated effect in *E. coli*-based assays and *P. aeruginosa* occurs at drastically lower concentrations ($EC_{50(E. coli)} = 6.3 \text{ nM}$ ²², $EC_{50(P. aeruginosa)} = 24 \text{ nM}$). This discrepancy might be explained by the fact that functional PqsR is a homotetramer capable of binding to DNA and adopting different conformational states.⁴⁰ This higher-ordered architecture of the bacterial target is not resembled in cell-free assays employing only a monomeric N-terminally truncated protein.

Table 2: Antagonistic activity of PqsR antagonists^a

	Structure	IC ₅₀ [μ M] ^b	clogD _{7.4} ^c
7	H	33.6 \pm 8.2	1.7
8	-	n.i.	1.6
9		n.i.	3.1
10		29 % @ 100 μ M	3.7
11		2.6 \pm 0.8	3.5
12		5.1 \pm 0.5	3.1
13		5.9 \pm 0.9	3.6
14		4.9 \pm 0.9	3.9
15		18.5 \pm 7.3	3.6
16		35 \pm 5 % @ μ M	3.3
17		42.8 \pm 19.5	4.2
18		n.i.	4.3
19		3.4 \pm 0.2	3.4
20		0.14 \pm 0.04	3.8
21		3.6 \pm 1.1	3.6
22		0.49 \pm 0.17	2.8

^aAgonistic and antagonistic activities were evaluated in an *E. coli* reporter gene assay.

^bAntagonistic activity was determined in the presence of 50 nM PQS; n.i. = no inhibition (antagonistic activity \leq 15%). IC₅₀ represents the concentration of the half maximal antagonistic activity. ^ccalculated using ACD/Percepta 2015

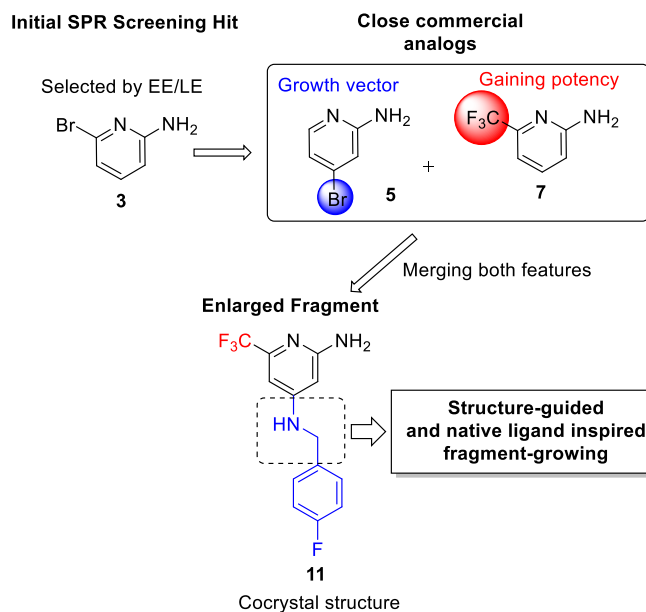


Figure 2: Fragment optimization approach

Taken together, these findings led to the decision to keep the scaffold **7** constant and to introduce further substituents into the 4-position (Figure 2). At first, rigid cyclopropyl-ethynyl (**9**) and 4-fluorophenyl (**10**) moieties were attached as molecular probes. Both modifications abolished the antagonistic activity almost completely. A closer look at the thermodynamic profile of **9** disclosed a significant loss in the enthalpic contribution (SI Table1: **7**: $\Delta H = -11.5$ kcal/mol vs. **9**: $\Delta H = -3.7$ kcal/mol) that is partially compensated by a gain in entropy. These findings suggest that the formation of specific interactions were hindered due to the attached moiety. Hence, we introduced a more flexible linker into the 4-position with the aim to regain specific interactions of the amino-pyridine headgroup. For this purpose, several compounds enlarged with different benzylamine moieties (**11-13**) were synthesized. Indeed, these compounds (**11-12**) displayed up to 12-fold increase in the antagonistic activities. Overall, the 4-fluoro substituted compound **11** evolved as the most potent antagonist of this series. Notably, also the affinity measured by ITC was improved up to 5-fold. (SI, Table S1). Taken together, the following general concept was derived from these previous findings (Figure 2): the amino-pyridine headgroup is connected via a flexible linker part to another aromatic moiety.

We determined a co-crystal structure of **11** in complex with the ligand binding domain of PqsR (Figure 3a), clearly showing that the linker establishes an angled connection between the 2-amino-pyridine headgroup, which occupies the space of the quinolone core of the natural ligands while the 4-fluorophenyl ring which points into the alkyl-chain pocket. Both aromatic systems of **11** are flanked by the alkyl side chains of isoleucine residues enabling CH- π interactions. The 2-amino moiety can form an H-bond interaction with the backbone carbonyl of

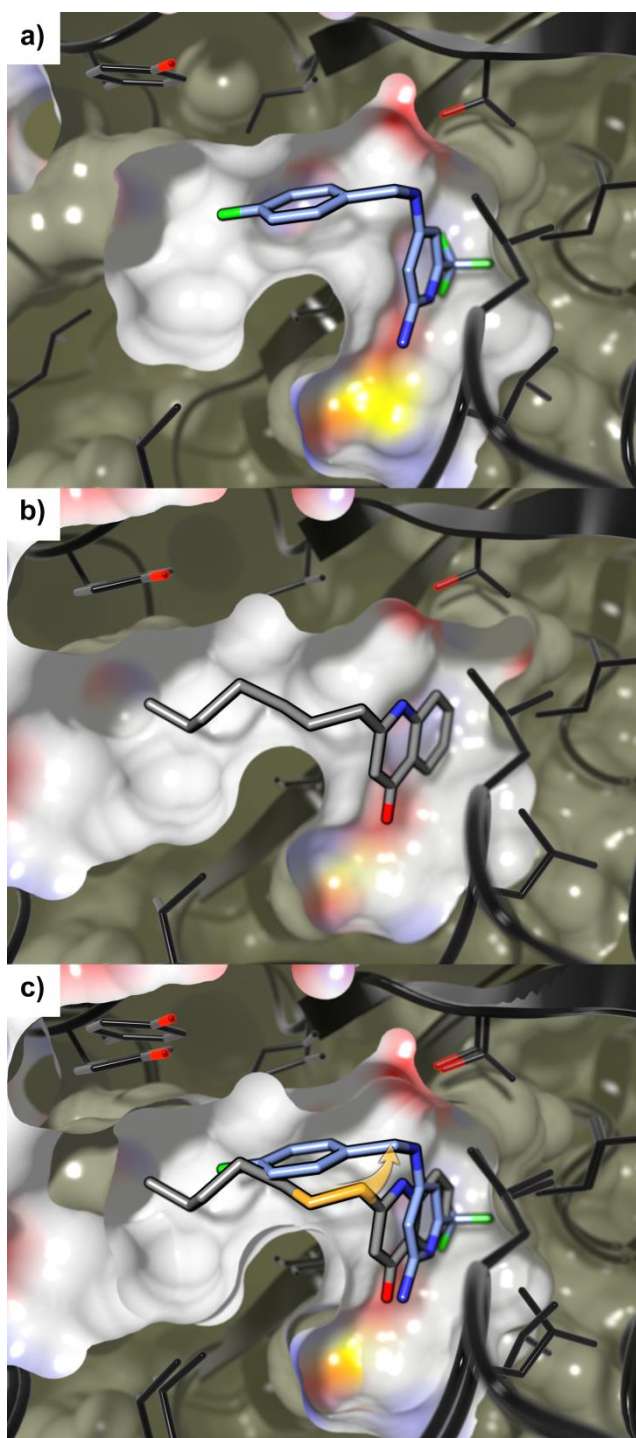


Figure 3: **a)** Crystal structure of **11** (light blue carbon) in complex with PqsR_{c91} (ribbon: black carbon; surface: white carbon). **b)** Crystal structure of HHQ (grey carbon) in complex with PqsR_{c91} (ribbon: black carbon; surface: white carbon). **c)** Overlay of a) and b). The orange arrow indicates the applied rationale for linker modification toward **20**. Fluorine: green, nitrogen: blue, oxygen: red, sulfur: yellow. Hydrogen omitted for clarity.

Leu207 and the NH of the benzylamine linker interacted with the hydroxyl moiety of Thr265. However, a comparison of the thermodynamic signatures of **11** binding to PqsR_{wt} and PqsRT265A, respectively (SI, Figure S3) displayed no significant difference in the enthalpic contribution which argues against a beneficial H-bond interaction. Notably, we detected an additional putative H-bond between the pyridine nitrogen lone pair and a water molecule (Figure

S1) that had been observed in ligand-receptor-complexes of the congener **22** (described below) and PDB entry 4JVC.²⁴In the further proceeding, modifications of the linker part were prioritized (Figure 2) in order to develop preferably small and efficient antagonist. Following this strategy, we evaluated the role of the NH within the linker; the *N*-methylated derivative **14** and the benzyl alcohol **15** were synthesized. Compound **14** showed a slightly decreased antagonistic activity corroborating the notion that the H-bond observed in the X-ray structure does not translate into a significant gain in binding affinity, whereas the exchanged of NH to O (**16**) led to a more significant drop in potency. Usually, unfavorable entropic penalties resulting from ligand flexibility are addressed by rigidization of compounds through reduction of rotatable bonds.⁴² Hence, we made several efforts to introduce less flexible and cyclic structures into the linker region (**16-18**). However, none of these modifications led to improved potency. For example, the rigidized amide linker (**16**) is not able to adapt the angled conformation of **11**; as a consequence the antagonistic activity was almost abolished. The same trend was observed for cyclized derivatives **17** and **18**. Especially in the case of the indane derivative **17**, this loss of activity was surprising. Based on the crystal structure of **11** we assumed that neither the angled conformation nor the observed interactions would be affected by introduction of this 5-membered ring (SI, Figure S2). These findings underline that the optimal geometric arrangement of the pyrimidine headgroup and the second aromatic system is difficult to be mimicked by rigid ligand structures. In this regard we used the crystal structure in complex with the native ligand HHQ was resolved (Figure 3b). A superimposition with HHQ and **11** (Figure 3C) raised the idea to introduce a prolonged, even more flexible linker to mimic the alkyl sidechain of these compounds. Therefore, compounds **19-22** were synthesized. The antagonistic activity of **19** was unchanged compared to **11**.

Interestingly, introduction of four-atom linkers resulted in remarkable antagonistic potencies in the heterologous reporter gene assay (**20-22**). The *n*-propyl amine linker (**20**) showed a 20-fold boost in potency (Table 2; **11** IC₅₀ = 2.6±0.8 μM vs. **20** IC₅₀ = 0.14±0.04 μM). A co-crystal structure of **20** in complex with PqsR_{c91} showed that the extended linker pointed deeper into the pocket occupied by the alkyl chain of the natural ligand, enabling additional CH-π interactions with Tyr258 while the interactions of the aminopyridine head group were retained (Figure 4). However, the affinity of **20** was reduced according to ITC analysis (SI, Table S1; **11**: *K_D* = 0.6±0.2 μM vs. **20** *K_D* = 2.8±0.5 μM). As described above, this discrepancy might be explained by the use of an artificial PqsR construct (H₆SUMOPqsR_{c87}) for ITC measurements which is not able to form the native tetrameric structure of the receptor.

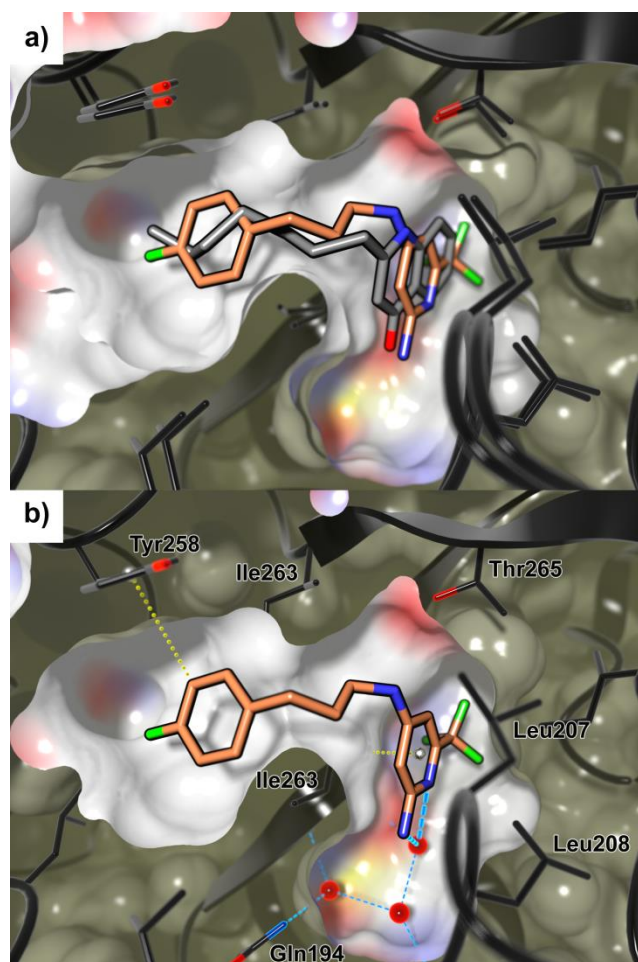


Figure 4: **a)** Overlay of crystal structures of **20** (orange carbon) and HHQ (grey carbon) in complex with PqsR_{c91} (ribbon: black carbon; surface: white carbon). **b).** Crystal structure of **20** highlighting the main interactions with PqsR (hydrogen bonds: light blue, CH- π interactions: yellow). Fluorine: green, nitrogen: blue, oxygen: red, sulfur: yellow. Hydrogen omitted for clarity.

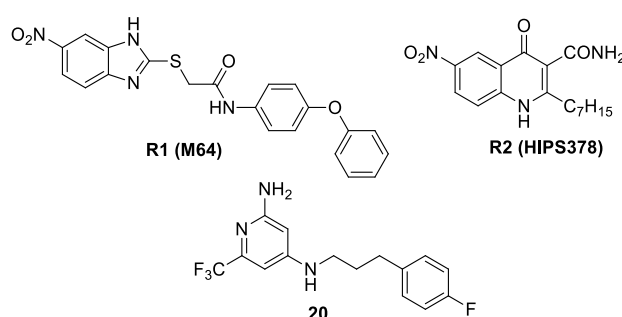
The alkyl chain (**20**) was exchanged by an ethanolamine (**21**) and glycine (**22**) linker moiety to lower clogD; the latter was inspired by the recently discovered benzamide-benzimidazole antagonists.²⁵ Compound **22** showed only a slightly reduced antagonistic activity, whereas **21** showed a significant drop. Overall, **20** emerged as the top candidate from this fragment-growing approach, showing a superior combination of nanomolar antagonistic activity, enthalpy-driven binding (EE = 0.50 kcal/mol) and reasonable physico-chemical properties (clogD=3.8). Remarkably, in contrast to the usual drug optimization process relying on reducing the amount of rotatable bonds, we gained potency through allowing ligand flexibility here.

Effects in *P. aeruginosa*

P. aeruginosa applies an arsenal of quorum sensing controlled virulence factors. Knock-out studies^{19,43} and synthetic antagonists^{22,25} clearly showed that inhibition of PqsR-mediated transcription leads to reduced *P. aeruginosa* pathogenicity. Therefore, the most interesting compounds during the development process were tested for their effect on virulence factor pyocyanin as well as on the alkylquinolons HHQ and HQNO (2-heptyl-4-hydroxy quinoline-*N*-

oxide). Pyocyanin is the most prominent and characteristic virulence factors released by *P. aeruginosa* during acute and chronic infections.⁴⁴ The redox-active blue pigment has cytotoxic and immunomodulating properties.⁴⁴ Moreover, it has been clearly demonstrated that pyocyanin promotes the development of a pulmonary pathophysiology in mice similar to the lung of infected cystic fibrosis patients.⁴⁵ Hence, it was of major interest to demonstrate that 2-amino-pyridines were able to translate the antagonistic activity measured in *E.coli* into antivirulence activity in *P. aeruginosa* as early as possible. In this regard, it is important to point out, that *P. aeruginosa* shows low intrinsic outer-membrane permeability for xenobiotics and applies a multitude of different efflux pumps.⁴⁴

Table 3: Effects on pyocyanin in *P. aeruginosa*



	Pyocyanin ^a IC ₅₀ [μM]	PEI ^b	MW
R1	0.12	0.0165	420.4
R2	2.0	0.0172	331.4
7	43% @ 250 μM	-	162.1
11	102	0.0140	285.2
20	5.9	0.0168	313.3
21	58% @ 100 μM	-	315.3
22	37% @ 100 μM	-	328.3

^aPhotometric quantification of Pyocyanin from PA14 cultures; given values represent the mean of at least two independent experiments; SD<25%. ^bPEI Pyocyanin Efficiency Index PEI=pIC₅₀/MW.

Therefore, compounds **7**, **11** and **20-22** were evaluated for the inhibition of pyocyanin in the highly virulent clinical isolate PA14 (Table 3). Compound **7** showed albeit in high concentration a significant effect on pyocyanin. Antagonist **11** showed low micromolar antagonistic activity in the *E.coli* assay (**11** IC₅₀=2.6±0.8 μM) and inhibited pyocyanin with an IC₅₀ = 105±13 μM. Antagonist **20** displayed the highest cellular efficacy (IC₅₀ = 5.9±0.7 μM). The literature-known compounds **R1-R2** were included as references in Table 3. The PqsR antagonist **R1** originated from an HTS screening.²⁵ **R2** was developed in-house by modification of HHQ.²² We established a metric called PEI (pyocyanin efficiency index; Table 3) which normalized the effect on pyocyanin for the molecular weight of the inhibitors to enable a better comparison. The

antagonist **20** clearly displayed efficiency in the range of the benchmark compounds **R1** and **R2**. This clearly emphasized the high potential of the developed antagonist **20**. In contrast, the slightly less active compounds **21** and **22** were not able to inhibit pyocanin to the same extent. This might be due to efflux or permeation problems. The phenomenon that even small changes within a molecule can have drastic effects on the activity in *P. aeruginosa* was also observed in other projects and emphasizes the need for further insights on the requirement for intracellular activity, especially in the case of Gram-negative pathogens.^{22,46}

The activation of PqsR drives the expression of the HHQ biosynthesis operon *pqsA-E*, leading to enhanced AHQ levels and finally to an auto-inductive loop. *P. aeruginosa* produces more than 50 different AHQ congeners.⁴⁷ Among others HHQ and HQNO are most prevalent.⁴⁷ HQNO showed Gram-positive antibacterial activity that promotes a growth advantage for *P. aeruginosa* in mixed microbial communities.⁴⁸ Subsequently, the most interesting antagonists were also evaluated for their effect on HHQ and HQNO levels in a PA14*pqsH* strain. Antagonist **11** was able to significantly affect HHQ (48±4% inhibition at 200 µM) and HQNO (36±3% inhibition at 200 µM). The enlarged compound **20** showed a HHQ (56±4% inhibition at 100 µM) and HQNO (48±1 inhibition at 100 µM). These results were in line with already reported data showing that the expression of virulence factors and the levels of Aqs are differently sensitive to the antagonization of PqsR.^{22,25}

Conclusion

The rapid development and spreading of resistances against conventional antibiotics has raised the awareness of a broader public in recent years. This ability of pathogens demonstrates the power of evolutionary adaption processes.⁴⁹ The development of PqsR antagonists pursues the strategy to limit *P. aeruginosa*'s virulence without affecting bacterial fitness. Hence, these antivirulence compounds might be more robust to adaptive evolution because they avoid exerting selective pressure.⁵⁰ Herein, we report on the discovery and development of 2-amino-pyridines as potent PqsR antagonists. Starting from an SPR fragment screening²⁶ ligand **3** was selected based on its unique EE, although it did not show significant antagonistic activity. Successfully growing and improving a fragment screening hit without structural information is a challenging approach and only rarely reported in the literature. Therefore, close commercial analogs were investigated, leading to compound **7**. **7** showed improved affinity and comparable EE. Furthermore, **7** possessed moderate antagonistic activity. By the introduction of a flexible benzyl-amine linker into the 4-position (**11**) affinity and antagonistic activity were significantly improved. The solution of the crystal structure of **11** in complex with PqsR_{c87} facilitated further structure-guided optimization. Notably, the ligand assumed an angled conformation spanning over the quinolone- and alkylchain-pocket. Inspired by the alkyl chain of the natural ligand HHQ, we extended the linker moiety, which led to the top candidate **20** showing antagonistic activity in

the nanomolar range. The rather unusual approach of allowing more flexibility instead of rigidifying the ligand might be also applicable to a broader scope of drugable proteins. Especially in cases where the biological function of the drug target depends on different conformational states (e.g. inducible transcriptional regulators), this flexible fragment growing strategy might be a valuable tool to rapidly generate lead-like molecules. Usually, a selected fragment-sized hit already provides efficient directed interactions with the target. Allowing compound flexibility during the enlargement process could help to retain the beneficial binding geometry while granting access to additional sites of the binding pocket resulting in enhanced potency.

The developed PqsR antagonist is a remarkably small compound and efficiently reduces pyocyanin in *P. aeruginosa* without affecting bacterial viability. Compound **20** represents an excellent starting point for further lead optimization studies. With these findings we try to fill the gap of lacking treatment options against severe *P. aeruginosa* infections by following an innovative approach towards novel anti-infectives which are less prone to resistance development.

EXPERIMENTAL SECTION

PqsR Reportergeneassay in *E. coli* The agonistic and antagonistic activity of potential PqsR ligands was evaluated in a β -galactosidase reporter gene assay in *E. coli* as previously described.²¹ In short, test compounds were co-incubated with *E. coli* DH5 α cells containing the plasmid pEAL08-2³⁸, which expresses PqsR and the β -galactosidase LacZ under the control of the *pqsA* promoter. The antagonistic activity of compounds was measured in the presence of 50 nM PQS. After incubation, galactosidase activity was quantified photometrically and expressed as ratio of controls. The given IC₅₀ values represent the mean of at least two independent experiments using at least eight different concentrations of test compound with n = 4. Non-linear regression analysis was done using the log (inhibitor) vs. response model included in the GrapPad Prism 5.0 software package.

Protein crystallization, Data Collection and Structure Solution. Initial crystals of PqsR₉₁₋₃₁₉ in complex with HHQ, fragment **11** or **20** were obtained by co-crystallization in a sitting drop vapor diffusion set-up using the commercially available JCSG Core Suites I-IV (Qiagen), Cryos Suite (Qiagen) and Index HT screen (Hampton Research) at 20°C. Initial screening hits were optimized in 96 well plates using a Formulatrix liquid handling station (Formulatrix). Crystallization drops consisted of 0.2 μ l protein-ligand solution and 0.2 μ l mother liquor and were prepared with a Honeybee 961 robot (Digilab). The morphology of PqsR₉₁₋₃₁₉-HHQ crystals was improved with the Additive Screen (Hampton Research) by the addition of 0.1 M CsCl.

Protein/ligand concentrations and final crystallization conditions that yielded diffraction quality crystals are described in Table S1 for each ligand. The crystals were flash-frozen in liquid nitrogen, and X-ray diffraction data were collected at 100 K at beamlines BL14.1/BL14.2 of the BESSY II synchrotron and at beamline X06DA of the Swiss Light Source (Table S1). Diffraction data were processed with XDS⁵¹ and AIMLESS⁵² from the CCP4 suite.⁵³ The dataset of PqsR₉₁₋₃₁₉ in complex with compound **11** was corrected for anisotropy using the UCLA Diffraction Anisotropy Server⁵⁴ (<http://services.mbi.ucla.edu/anisotropy/>) with the resolution limits of 3.4 Å, 3.2 Å and 2.8 Å along the a*, b*, and c* directions for ellipsoidal truncation. The structures were determined by molecular replacement with PHASER⁵⁵ or rigid-body refinement with REFMAC5⁵⁶ using the PDB entry 4JVC. Model building and refinement were performed with COOT⁵⁷ and with phenix.refine⁵⁸ from the PHENIX suite.⁵⁹

Ligand-receptor-interaction studies. Complex structures of HHQ as well as compounds **11** and **20** bound to the ligand-binding domain of PqsR were analyzed using *Molecular Operating Environment MOE* (Chemical Computing Group) after applying the “QuickPrep” protocol using the MMFF94x force field (see Figure S1 in the Supporting Information). Default parameters were used, while receptor, ligands, and solvents were tethered (“strength” parameter of 10). A prominent water molecule observed in crystal structure of PqsR in complex with **20** was also considered when investigating the interactions of compound **11**. Figures 3 and 4 of the main text were rendered with PovRay.

Pyocyanin Assay The inhibition of virulence factor pyocyanin was measured as described previously²¹ following a procedure established by Essar *et al.*⁶² Briefly, *Pseudomonas aeruginosa* PA14 cultures were grown in the presence of inhibitors or DMSO as control for 16 h. Pyocyanin was determined photometrically after extraction of the cultures with chloroform and re-extraction with 0.2 M HCl. Values were expressed in relation to the DMSO control. Each value is the mean of at least two independent experiments with n=3. The given IC₅₀ values represent the mean of at least two experiments using at least five different concentrations. Curve fitting was performed using the log (inhibitor) vs. response model with constrained bottom = 0 and top =100 (GraphPad Prism 5.0).

HHQ and HQNO Quantification Extracellular HHQ and HQNO were measured as previously reported²² following a modified procedure of Lépine *et al.*^{47,63}. Briefly, *P. aeruginosa* PA14 cultures were grown in the presence of DMSO as a control or DMSO solutions of inhibitors for 17 h. HHQ and HQNO were quantified from ethyl acetate extracts using 5,6,7,8-tetradeutero-2-heptyl-4(1*H*)-quinolone (HHQ-*d*₄) as internal standard (IS). UHPLC-MS/MS analysis was performed as described in detail by Storz *et al.*⁶⁴ The following ions were monitored (mother ion [m/z], product ion [m/z], scan time [s], scan width [m/z], collision energy [V], tube lens offset [V]): HHQ: 244, 159, 0.5, 0.01, 30, 106; HQNO: 260, 159, 0.1, 0.01, 25, 88; HHQ-*d*₄ (IS): 248, 163,

0.1, 0.01, 32, 113. Data acquisition and quantification was performed using Xcalibur software with the use of a calibration curve relative to the area of the IS. Given data represent the mean of at least two independent experiments with $n=3$ and were expressed as percentage inhibition relative to DMSO control.

Chemical and Analytical Methods. ^1H and ^{13}C NMR spectra were recorded as indicated on a Bruker DRX-500 or a Bruker Fourier 300 instrument. Chemical shifts are given in parts per million (ppm), and referenced against the residual solvent peak. Coupling constants (J) are given in hertz. Low resolution mass analytics and purity control of final compounds was carried out either using a SpectraSystems-MSQ LCMS system (Thermo Fisher Scientific) consisting of a pump, an autosampler, VWD detector and a ESI quadrupole mass spectrometer or a Waters LCMS-Sytsem consisting of a 767 sample Manager, a 2545 binary gradient pump, a 2998 PDA detector and a 3100 electron spray mass spectrometer. High resolution mass spectra were recorded on a maXis 4G hr-ToF mass spectrometer (Bruker Daltonics). Reagents were used as obtained from commercial suppliers without further purification. Procedures were not optimized regarding yield. Microwave assisted synthesis was carried out in a Discover microwave synthesis system (CEM). Column chromatography was performed using the automated flash chromatography system CombiFlash Rf 150 (Teledyne Isco) equipped with RediSepRf silica columns. Final products were dried at high vacuum.

Method A: General Procedure for Buchwald-Hartwig cross coupling reactions:³⁴

Heteroaryl halide (0.35 mmol), potassium tert-butoxide (1.1 mmol) and (SIPr)Pd(cinnamyl)Cl (3 mol%) were combined into MW-vial (Biotage). The vial was evacuated and flushed with argon (3 times). Dry dimethoxyethane (1 ml) was added. The reaction mixture was purged with argon and the amine (1.1 mmol) was slowly added. The reaction was stirred over night at 80°C. The mixture quenched with diethyl ether, filtered through Cellite and the filtrate was concentrated to dryness. The crude was further purified by preparative HPLC or chromatography on silica gel.

Method B: Copper-mediated amination reaction 2-iodo-6-(trifluoromethyl)pyridin-4-amine (0.3 mmol) was dissolved in NMP/water (3ml; 2/1(V/V)) using crimp reaction vial. (Biotage). 1,10-phenanthroline (0.1 mmol) and copper (I) oxide (0.1 mmol) were added. The reaction mixture was purged with argon and $\text{NH}_{3(\text{aq})}$ 28% (~5 mmol) was added. The mixture was stirred over night at RT. The crude product was purified by automated flash chromatography.

4-(cyclopropylethynyl)-6-(trifluoromethyl)pyridin-2-amine (9): -iodo-6-(trifluoromethyl)pyridin-2-amine (**4e**; 100 mg, 0.415 mmol), $\text{PdCl}_2(\text{PPh}_3)_2$ (7 mg, 10 μmol), tetrabutylammonium fluorid (1.0 mmol) and ethynylcyclopropane (34 mg, 0.52 mmol) were filled into a crimp vial (neat reation). The vial was evacuated and purged with argon (3 times). The reaction mixture was heated at 80°C overnight. The reaction was quenched by addition of water. The aqueous layer was extracted with ethylacetat (3 times). Combined organics were washed with brine,

dried over MgSO_4 and concentrated. The crude product was purified by automated flash chromatography (PE:EA 95:5 to PE:EA 80:20) to give the titled compound (74 mg, 0.33 mmol, 94 % yield) as pale yellow solid. ^1H NMR (500 MHz, CHLOROFORM-*d*) δ ppm 0.82 - 0.87 (m, 2 H), 0.91 - 0.96 (m, 2 H), 1.42 - 1.48 (m, 1 H), 4.75 (br. s., 2 H), 6.59 (d, $J=0.6$ Hz, 1 H), 6.95 (d, $J=0.9$ Hz, 1 H); ^{13}C NMR (126 MHz, CHLOROFORM-*d*) δ ppm 1.00, 8.94 (2 C), 73.19, 99.37, 112.76 (d, $^3J(\text{C},\text{F})=3.7$ Hz, 1 C), 113.34, 121.35 (q, $^1J(\text{C},\text{F})=274.0$ Hz, 1 C), 134.77, 146.53 (q, $^2J(\text{C},\text{F})=33.9$ Hz, 1 C), 158.46; MS (ESI+) m/z 268 (M+ACN+H) $^+$.

(4-fluorophenyl)-6-(trifluoromethyl)pyridin-2-amine (10): 4-iodo-6-(trifluoromethyl)pyridin-2-amine (**4e**; 100 mg, 0.35 mmol), (4-fluorophenyl)boronic acid (73 mg, 0.52 mmol) and $\text{Pd}(\text{dppf})\text{Cl}_2$ (12 mg, 0.016 mmol) were filled into a crimp reaction vial. The vial was evacuated and flushed with argon (2 times). Na_2CO_3 (3 ml, 3.0 mmol) 1M solution were added. The mixture was purged with argon and stirred at 80°C for overnight. The mixture was quenched by addition of water and extracted by ether. The combined organics were washed with brine, dried over MgSO_4 and concentrated. The crude was attached purified by automated flash chromatography (PE to PE:EA 80:20) to give the titled compound (67 mg, 0.262 mmol, 75 % yield) as a white solid. ^1H NMR (300 MHz, CHLOROFORM-*d*) δ ppm 4.92 (br. s., 2 H), 6.78 (s, 1 H), 7.07 - 7.24 (m, 3 H), 7.49 - 7.65 (m, 2 H); ^{13}C NMR (75 MHz, CHLOROFORM-*d*) δ ppm 108.89, 108.92 (q, $^3J(\text{C},\text{F})=3.0$ Hz, 1 C), 116.16 (d, $^2J(\text{C},\text{F})=22.4$ Hz, 2 C), 121.61 (q, $^1J(\text{C},\text{F})=274.2$ Hz, 1 C), 128.74 (d, $^3J(\text{C},\text{F})=8.9$ Hz, 2 C), 133.80 (d, $^4J(\text{C},\text{F})=3.7$ Hz, 1 C), 147.24 (q, $^2J(\text{C},\text{F})=33.5$ Hz, 1 C), 150.51, 159.12, 163.60 (d, $^2J(\text{C},\text{F})=249.6$ Hz, 1 C); MS (ESI+) m/z 257 (M+H) $^+$; 298 (M+ACN+H) $^+$.

N4-(4-fluorobenzyl)-6-(trifluoromethyl)pyridine-2,4-diamine (11) was synthesized according to Method A from 4-iodo-6-(trifluoromethyl)pyridin-2-amine (**4e**; 100 mg, 0.35 mmol) and (4-fluorophenyl)methanamine (130 mg, 1.04 mmol). The crude was purified by combyflash (PE:diethylether 80:20 to 60:40) to give a pale brown solid. The solid was titrated with diethyl ether/pentane and filtered to give the titled compound (27 mg, 0.095 mmol, 27% yield) as a brown-white solid. ^1H NMR (500 MHz, CHLOROFORM-*d*) δ ppm 4.33 (d, $J=5.4$ Hz, 2 H), 4.46 (br. s., 2 H), 4.56 (br. s., 1 H), 5.68 (d, $J=1.6$ Hz, 1 H), 6.37 (d, $J=1.9$ Hz, 1 H), 7.00 - 7.12 (m, 2 H), 7.20 - 7.35 (m, 2 H); ^{13}C NMR (126 MHz, CHLOROFORM-*d*) δ ppm 46.17, 90.66, 98.52, 115.56 (d, $^2J(\text{C},\text{F})=21.1$ Hz, 2 C), 121.36 (d, $^1J(\text{C},\text{F})=273.1$ Hz, 1 C), 128.62 (d, $^3J(\text{C},\text{F})=8.2$ Hz, 2 C), 132.83 (d, $^4J(\text{C},\text{F})=3.7$ Hz, 1 C), 146.65 (q, $^2J(\text{C},\text{F})=33.0$ Hz, 1 C), 154.83, 159.57, 162.04 (d, $^1J(\text{C},\text{F})=246.5$ Hz, 1 C); MS (ESI+) m/z 286 (M+H) $^+$.

N4-benzyl-6-(trifluoromethyl)pyridine-2,4-diamine (12) was synthesized according to Method A from 4-iodo-6-(trifluoromethyl)pyridin-2-amine (**4e**; 100 mg, 0.35 mmol) and phenylmethanamine (112 mg, 1.04 mmol). The crude product was purified by combyflash (PE:diethylether gradient, elution 30:70 PE:ether) to give the titled compound as pale yellow

solid (48 mg, 0.18 mmol, 52% yield). ^1H NMR (500 MHz, CHLOROFORM-*d*) δ ppm 4.34 (d, $J=5.7$ Hz, 2 H), 4.43 - 4.93 (m, 1 H), 5.68 (d, $J=1.9$ Hz, 1 H), 6.35 (d, $J=1.9$ Hz, 1 H), 7.28 - 7.34 (m, 3 H), 7.34 - 7.41 (m, 2 H); ^{13}C NMR (126 MHz, CHLOROFORM-*d*) δ ppm 47.01, 90.83, 98.68 (d, $^3J(\text{C},\text{F})=3.7$ Hz, 1 C), 121.71 (q, $^1J(\text{C},\text{F})=274.9$ Hz, 1 C), 127.21 (2 C), 127.68, 128.84 (2 C), 137.48, 146.78 (q, $^2J(\text{C},\text{F})=33.0$ Hz, 1 C), 155.20, 159.85; MS (ESI+) m/z 259 (M+H) $^+$ 299 (M+ACN+H) $^+$

N4-(2,4-difluorobenzyl)-6-(trifluoromethyl)pyridine-2,4-diamine (13) was synthesized according to Method A from 4-iodo-6-(trifluoromethyl)pyridin-2-amine (**4e**; 100 mg, 0.35 mmol) and (2,4-difluorophenyl)methanamine (149 mg, 1.04 mmol). The crude product was purified by preparative HPLC to give the titled compound (21 mg, 0,069 mmol, 20 % yield) as brown oil. ^1H NMR (500 MHz, METHANOL-*d*₄) δ ppm 4.37 (s, 2 H), 5.78 (d, $J=1.6$ Hz, 1 H), 6.42 (d, $J=1.9$ Hz, 1 H), 6.87 - 7.02 (m, 2 H), 7.36 (td, $J=8.2, 6.6$ Hz, 1 H); ^{13}C NMR (126 MHz, METHANOL-*d*₄) δ ppm 40.61 (d, $^3J(\text{C},\text{F})=4.6$ Hz, 1 C), 90.70, 99.84, 104.68 (t, $^2J(\text{C},\text{F})=25.7$ Hz, 1 C), 112.30 (dd, $^2J(\text{C},\text{F})=20.2, 3.7$ Hz, 1 C), 123.07 (q, $^1J(\text{C},\text{F})=273.1$ Hz, 1 C), 122.55 (dd, $^3J(\text{C},\text{F})=14.7, 3.7$ Hz, 1 C), 131.47 (dd, $^3J(\text{C},\text{F})=9.6, 6.0$ Hz, 1 C), 145.77 (q, $^2J(\text{C},\text{F})=33.9$ Hz, 1 C), 157.12, 162.26 (dd, $^1J(\text{C},\text{F})=243.8, 11.9$ Hz, 1 C), 161.74, 163.84 (dd, $^1J(\text{C},\text{F})=246.5, 12.8$ Hz, 1 C); MS (ESI +) m/z 304 (M+H) $^+$.

N4-(4-fluorobenzyl)-N4-methyl-6-(trifluoromethyl)pyridine-2,4-diamine (14) was synthesized according to Method A from 4-iodo-6-(trifluoromethyl)pyridin-2-amine (**4e**; 100 mg, 0.35 mmol) and 1-(4-fluorophenyl)-N-methylmethanamine (145 mg, 1,042 mmol). The crude product was purified by automated flash chromatography using a gradient of Hex:EA (8:2 to 6:4) to give the titled compound (19 mg, 0.063 mmol, 18% yield) as white solid. ^1H NMR (300 MHz, CHLOROFORM-*d*) δ ppm 3.04 (s, 3 H), 4.52 (s, 4 H), 5.76 (d, $J=2.0$ Hz, 1 H), 6.48 (d, $J=2.1$ Hz, 1 H), 6.97 - 7.07 (m, 2 H), 7.08 - 7.16 (m, 2 H); ^{13}C NMR (75 MHz, CHLOROFORM-*d*) δ ppm 37.94, 54.57, 90.92, 96.73 (d, $^3J(\text{C},\text{F})=3.7$ Hz, 1 C), 115.80 (d, $^2J(\text{C},\text{F})=20.9$ Hz, 1 C), 121.88 (q, $^1J(\text{C},\text{F})=274.2$ Hz, 1 C), 127.99 (d, $^3J(\text{C},\text{F})=8.2$ Hz, 2 C), 132.48 (d, $^4J(\text{C},\text{F})=3.7$ Hz, 1 C), 147.34 (q, $^2J(\text{C},\text{F})=32.8$ Hz, 1 C), 156.08, 159.78, 162.14 (d, $^1J(\text{C},\text{F})=245.9$ Hz, 1 C); MS (ESI +) m/z 300 (M+H) $^+$.

4-((4-fluorobenzyl)oxy)-6-(trifluoromethyl)pyridin-2-amine (15) 2-(2,5-dimethyl-1H-pyrrol-1-yl)-4-((4-fluorobenzyl)oxy)-6-(trifluoromethyl)pyridine (**15a**; 80 mg, 0.22 mmol), triethylamine (0.061 ml, 0.44 mmol) and hydroxylamine hydrochloride (153 mg, 2.20 mmol) were dissolved in EtOH/water 3/1 and the solution was refluxed overnight. An additional amount of hydroxylamine hydrochloride (153 mg, 2.20 mmol) and triethylamine (0.061 ml, 0.44 mmol) was added and again refluxed overnight. The mixture was quenched by addition of EA and water. The aqueous phase was extracted (EA 3 times). Combined organics were washed with brine, dried (MgSO₄) filtered and concentrated. The crude was purified by column chromatography (step gradient 9:1

to 1:1 PE:EA) to give the titled compound (40 mg, 0.14 mmol, 64 % yield) as pale yellow crystals. ^1H NMR (300 MHz, DMSO- d_6) δ ppm 5.12 (s, 2 H), 6.22 (d, $J=1.8$ Hz, 1 H), 6.44 (s, 2 H), 6.59 (d, $J=2.0$ Hz, 1 H), 7.13 - 7.33 (m, 2 H), 7.50 (dd, $J=8.7, 5.5$ Hz, 1 H); ^{13}C NMR (75 MHz, DMSO- d_6) δ ppm 68.58, 94.36, 98.49 (d, $^4J(\text{C},\text{F})=3.0$ Hz, 1 C), 115.31 (d, $^2J(\text{C},\text{F})=22.4$ Hz, 2 C), 121.61 (q, $^1J(\text{C},\text{F})=274.2$ Hz, 1 C), 130.13 (d, $^3J(\text{C},\text{F})=8.2$ Hz, 2 C), 132.21 (d, $^4J(\text{C},\text{F})=3.0$ Hz, 1 C), 146.25 (q, $^2J(\text{C},\text{F})=33.5$ Hz, 1 C), 161.89 (d, $^1J(\text{C},\text{F})=244.4$ Hz, 1 C), 161.80, 165.70; MS (ESI+) m/z 287 (M+H) $^+$; 328 (M+ACN+H) $^+$.

N-(2-amino-6-(trifluoromethyl)pyridin-4-yl)-4-fluorobenzamide (16): tert-butyl (4-(4-fluorobenzamido)-6-(trifluoromethyl)pyridin-2-yl)carbamate (**16a**; 46 mg, 0.11 mmol) was dissolved in DCM (4 ml) and cooled on an ice bath. Trifluoroacetic acid (1 ml) was added and the mixture was aged at RT for 3 h. The reaction was quenched by addition of DCM and Na_2CO_3 saturated solution. The aqueous layer was extracted with DCM (3 times) and EtOAc (3 times). Both organics were dried over MgSO_4 , filtered and concentrated. The crude was purified by automated flash chromatography (PE:EA 75:25) to give the titled compound (11 mg, 0.04 mmol, 32% yield) as white solid. ^1H NMR (300 MHz, DMSO- d_6) δ ppm 6.53 (br. s, 2 H), 7.26 - 7.33 (m, 2 H), 7.33 - 7.44 (m, 2 H), 7.93 - 8.12 (m, 2 H), 10.50 (br. s, 1 H); ^{13}C NMR (75 MHz, DMSO- d_6) δ ppm 100.07, 101.06 (q, $^3J(\text{C},\text{F})=3.0$ Hz, 1 C), 115.93 (d, $^2J(\text{C},\text{F})=21.6$ Hz, 2 C), 122.28 (q, $^1J(\text{C},\text{F})=273.4$ Hz, 1 C), 131.06, 131.13 (d, $^3J(\text{C},\text{F})=8.9$ Hz, 1 C), 145.91 (q, $^2J(\text{C},\text{F})=32.0$ Hz, 1 C), 147.88, 161.61, 164.84 (d, $^1J(\text{C},\text{F})=248.9$ Hz, 1 C), 165.77; MS (ESI+) m/z 300 (M+H) $^+$, 341 (M+ACN+H) $^+$

N4-(5-fluoro-2,3-dihydro-1H-inden-1-yl)-6-(trifluoromethyl)pyridine- 2,4-diamine (17) was synthesized according to Method A from 4-iodo-6-(trifluoromethyl)pyridin-2-amine (**4e**; 100 mg, 0.35 mmol) and 5-fluoro-2,3-dihydro-1H-inden-1-amine (157 mg, 1.04 mmol). The crude product was purified by preparative HPLC to give the titled compound (48 mg, 0.15 mmol, 44 % yield) as brown solid. ^1H NMR (300 MHz, CHLOROFORM- d) δ ppm 1.87 - 2.08 (m, 1 H), 2.53 - 2.69 (m, 1 H), 2.80 - 3.11 (m, 2 H), 4.41 (d, $J=7.8$ Hz, 1 H), 4.53 (br. s., 2 H), 4.97 (q, $J=6.9$ Hz, 1 H), 5.83 (d, $J=1.8$ Hz, 1 H), 6.37 (d, $J=1.9$ Hz, 1 H), 6.82 - 7.04 (m, 2 H), 7.16 - 7.37 (m, 1 H); ^{13}C NMR (75 MHz, CHLOROFORM- d) δ ppm 30.21, 33.84, 57.04, 91.04, 98.78 (d, $^3J(\text{C},\text{F})=3.7$ Hz, 1 C), 112.03 (d, $^2J(\text{C},\text{F})=23.1$ Hz, 1 C), 114.05 (d, $^2J(\text{C},\text{F})=23.1$ Hz, 1 C), 121.70 (d, $^1J(\text{C},\text{F})=273.4$ Hz, 1 C), 125.28 (d, $^3J(\text{C},\text{F})=8.9$ Hz, 1 C), 138.39 (d, $^4J(\text{C},\text{F})=2.2$ Hz, 1 C), 145.89 (d, $^3J(\text{C},\text{F})=8.2$ Hz, 1 C), 147.33 (q, $^2J(\text{C},\text{F})=32.0$ Hz, 1 C), 154.73, 159.80, 163.24 (d, $^1J(\text{C},\text{F})=245.9$ Hz, 1 C); MS (ESI+) m/z 312 (M+H) $^+$.

4-(3-(4-fluorophenyl)pyrrolidin-1-yl)-6-(trifluoromethyl)pyridin-2-amine (18) was synthesized according to Method A from 4-iodo-6-(trifluoromethyl)pyridin-2-amine (**4e**, 100 mg, 0.35 mmol) and 3-(4-fluorophenyl)pyrrolidine (172 mg, 1.04 mmol). The crude product was purified by automated flash chromatography (PE:Diethylether gradient) to give the titled compound (90 mg,

0.28 mmol, 80 % yield) as pale yellow solid. ^1H NMR (300 MHz, CHLOROFORM-*d*) δ ppm 2.02 - 2.21 (m, 1 H), 2.43 (m, 1 H), 3.33 (t, $J=9.0$ Hz, 1 H), 3.38 - 3.61 (m, 3 H), 3.74 (dd, $J=9.3, 7.7$ Hz, 1 H), 4.49 (br. s., 2 H), 5.65 (d, $J=1.8$ Hz, 1 H), 6.34 (d, $J=1.9$ Hz, 1 H), 6.93 - 7.11 (m, 2 H), 7.14 - 7.26 (m, 2 H); ^{13}C NMR (75 MHz, CHLOROFORM-*d*) δ ppm 32.47, 42.64, 46.70, 53.42, 90.23 (d, $J=6.0$ Hz, 1 C), 96.76 (d, $^3J(\text{C},\text{F})=3.7$ Hz, 1 C), 115.11 (d, $^2J(\text{C},\text{F})=18.6$ Hz, 2 C), 121.49 (d, $^1J(\text{C},\text{F})=274.2$ Hz, 1 C), 128.03 (d, $J=7.4$ Hz, 2 C), 136.52 (d, $^3J(\text{C},\text{F})=3.7$ Hz, 1 C), 146.63 (q, $^2J(\text{C},\text{F})=32.8$ Hz, 1 C), 153.15, 158.97, 161.37 (d, $^1J(\text{C},\text{F})=245.1$ Hz, 1 C); MS (ESI+) m/z 326 (M+H) $^+$, 367 (M+ACN+H) $^+$

N4-(4-fluorophenethyl)-6-(trifluoromethyl)pyridine-2,4-diamine (19) was synthesized according to Method B from N-(4-fluorophenethyl)-2-iodo-6-(trifluoromethyl)-pyridin-4-amine (100 mg, 0.24 mmol). The crude product was purified by automated flash chromatography (PE:DE 7:3 to 3:7) to give the titled compound (55 mg, 0.18 mmol, 75 % yield) as white solid. ^1H NMR (500 MHz, DMSO-*d*₆) δ ppm 2.80 (t, $J=7.4$ Hz, 2 H), 3.18 - 3.26 (m, 2 H), 5.72 (d, $J=1.6$ Hz, 1 H), 5.95 (br. s., 2 H), 6.27 (d, $J=1.6$ Hz, 1 H), 6.67 (br. s., 1 H), 7.08 - 7.16 (m, 2 H), 7.27 - 7.34 (m, 2 H); ^{13}C NMR (126 MHz, DMSO-*d*₆) δ ppm 33.43, 43.65, 88.92, 97.12, 115.02 (d, $^2J(\text{C},\text{F})=20.2$ Hz, 2 C), 122.09 (q, $^1J(\text{C},\text{F})=274.0$ Hz, 1 C), 130.53 (d, $^3J(\text{C},\text{F})=8.2$ Hz, 2 C), 135.51 (d, $^3J(\text{C},\text{F})=2.8$ Hz, 1 C), 144.59 (q, $^2J(\text{C},\text{F})=30.2$ Hz, 1 C), 154.92, 160.92 (d, $^1J(\text{C},\text{F})=241.9$ Hz, 1 C), 160.70; MS (ESI+) m/z 300 (M+H) $^+$; HRMS found 300.11091 calc. 300.11184 (M+H) $^+$.

N4-(3-(4-fluorophenyl)propyl)-6-(trifluoromethyl)-pyridine-2,4-diamine (20) was synthesized according to Method B from N-(3-(4-fluorophenyl)propyl)-2-iodo-6-(trifluoromethyl)pyridin-4-amine (130 mg, 0.31 mmol). The crude product was purified by automated flash chromatography (gradient PE:diethylether) to give the titled compound (45 mg, 0.14 mmol, 47 % yield) as pale yellow solid. ^1H NMR (500 MHz, DMSO-*d*₆) δ ppm 1.80 (quin, $J=7.3$ Hz, 1 H), 2.65 (t, $J=7.3$ Hz, 2 H), 2.93 - 3.03 (m, 2 H), 5.62 (d, $J=1.3$ Hz, 1 H), 5.88 (s, 2 H), 6.25 (d, $J=1.9$ Hz, 1 H), 6.55 (t, $J=5.2$ Hz, 1 H), 7.07 - 7.14 (m, 2 H), 7.21 - 7.28 (m, 2 H); ^{13}C NMR (126 MHz, DMSO-*d*₆) δ ppm 30.00, 31.57, 41.20, 88.82, 96.79, 114.93 (d, $^2J(\text{C},\text{F})=21.1$ Hz, 2 C), 122.15 (q, $^1J(\text{C},\text{F})=274.0$ Hz, 1 C), 129.97 (d, $^3J(\text{C},\text{F})=7.3$ Hz, 2 C), 137.63 (d, $^3J(\text{C},\text{F})=3.7$ Hz, 1 C), 144.95 (q, $^2J(\text{C},\text{F})=32.1$ Hz, 1 C), 155.03, 160.58 (d, $^1J(\text{C},\text{F})=241.0$ Hz, 1 C), 160.88; MS (ESI+) 314 (M+H) $^+$; HRMS found 314.12708 calc 314.12749 (M+H) $^+$.

N4-(2-(4-fluorophenoxy)ethyl)-6-(trifluoromethyl)-pyridine-2,4-diamine (21) was synthesized according to Method B from N-(2-(4-fluorophenoxy)ethyl)-2-iodo-6-(trifluoromethyl)pyridin-4-amine (**21a**; 30,0 mg, 0.07 mmol). The crude product was purified by automated flash chromatography (PE:EA gradient). The isolated product was further purified by preparative HPLC to give the titled compound (7 mg, 0.022 mmol, 31% yield) as white solid. ^1H NMR (500 MHz, METHANOL-*d*₄) δ ppm 3.52 (t, $J=5.4$ Hz, 2 H), 4.12 (t, $J=5.5$ Hz, 2 H), 5.88 (d,

$J=1.9$ Hz, 1 H), 6.41 (d, $J=1.9$ Hz, 1 H), 6.91 - 6.97 (m, 2 H), 6.97 - 7.04 (m, 2 H); ^{13}C NMR (126 MHz, METHANOL- d_4) δ ppm 43.01, 68.05, 90.74, 99.48, 116.69 (d, $^2J(\text{C},\text{F})=22.9$ Hz, 2 C), 116.82 (d, $^3J(\text{C},\text{F})=7.8$ Hz, 2 C), 123.34 (q, $^1J(\text{C},\text{F})=273.1$ Hz, 1 C), 146.79 (q, $^2J(\text{C},\text{F})=33.0$ Hz, 1 C), 156.43 (d, $^4J(\text{C},\text{F})=1.8$ Hz, 1 C), 157.39, 158.81 (d, $^1J(\text{C},\text{F})=236.4$ Hz, 1 C); MS (ESI+) 316 (M+H) $^+$; HRMS found 316.10667 calc. 316.10675 (M+H) $^+$.

2-((2-amino-6-(trifluoromethyl)pyridin-4-yl)amino)-N-(4-fluorophenyl)acetamide (22) 4-iodo-6-(trifluoro methyl)pyridin-2-amine (**22a**; 150 mg, 0.52 mmol), 2-amino-N-(4-fluorophenyl)acetamide (131 mg, 0.78 mmol), copper (I) iodide (99 mg, 0.52 mmol), K_3PO_4 (221 mg, 1.04 mmol) and 2-(dimethylamino)ethanol (46 mg, 0.5 mmol) were filled into a crimp vial. The vial was evacuated and backfilled with argon (3 times). Acetonitrile (4 ml) and water (2 ml) were added and the mixture degassed with argon. The reaction was heated at 90 °C over night. The mixture was poured into saturated NH_4Cl solution. The aqueous phase was extracted using EtOAc (3 times). The combined organics were washed with brine, dried (MgSO_4), filtered and adsorbed onto silica gel. The crude product was first purified by automated flash chromatography (PE:EA gradient) and further by prep HPLC to give the titled compound (25 mg, 0,076 mmol, 15 % yield) as white solid. ^1H NMR (500 MHz, DMSO- d_6) δ ppm 3.89 (d, $J=6.0$ Hz, 2 H), 5.62 (s, 1 H), 5.97 (s, 2 H), 6.37 (d, $J=1.9$ Hz, 1 H), 6.87 (t, $J=6.1$ Hz, 1 H), 7.05 - 7.22 (m, 2 H), 7.54 - 7.66 (m, 2 H), 10.12 (s, 1 H). ^{13}C NMR (126 MHz, DMSO- d_6) δ ppm 45.79, 89.55, 97.15, 115.28 (d, $J=20.2$ Hz, 2 C), 122.11 (q, $^1J(\text{C},\text{F})=274.0$ Hz, 1 C), 121.03 (d, $J=7.3$ Hz, 2 C), 135.14 (d, $J=2.8$ Hz, 1 C), 144.99 (q, $J=32.1$ Hz, 1 C), 155.07, 158.01 (d, $^1J(\text{C},\text{F})=239.2$ Hz, 1 C), 160.80, 167.91; MS (ESI+) 329.2 (M+H) $^+$. HRMS found 329.10171 calc. 329.10200 (M+H) $^+$

REFERENCES

- (1) Bodey, G. P.; Bolivar, R.; Fainstein, V.; Jadeja, L. *Rev. Infect. Dis.* **1983**, *5*, 279–313.
- (2) Aloush, V.; Navon-Venezia, S.; Seigman-Igra, Y.; Cabili, S.; Carmeli, Y. *Antimicrob. Agents Chemother.* **2006**, *50*, 43–48.
- (3) Rahme, L. G.; Ausubel, F. M.; Cao, H.; Drenkard, E.; Goumnerov, B. C.; Lau, G. W.; Mahajan-Miklos, S.; Plotnikova, J.; Tan, M. W.; Tsongalis, J.; Walendziewicz, C. L.; Tompkins, R. G. *Proc. Natl. Acad. Sci. U.S.A.* **2000**, *97*, 8815–8821.
- (4) van Delden, C.; Iglewski, B. H. *Emerging Infect. Dis.* **1998**, *4*, 551–560.
- (5) Whitehead, N. A.; Barnard, A. M. L.; Slater, H.; Simpson, N. J. L.; Salmond, G. P. C. *FEMS Microbiol. Rev.* **2001**, *25*, 365–404.
- (6) a) Parker, C. T.; Sperandio, V. *Cell. Microbiol.* **2009**, *11*, 363–369; b) Kesarwani, M.; Hazan, R.; He, J.; Que, Y.; Apidianakis, Y.; Lesic, B.; Xiao, G.; Dekimpe, V.; Milot, S.; Déziel, E.; Lépine, F.; Rahme, L. G. *PLoS Pathog.* **2011**, *7*, e1002192.
- (7) Bjarnsholt, T.; Jensen, P. Ø.; Burmølle, M.; Hentzer, M.; Haagensen, J. A. J.; Hougen, H. P.; Calum, H.; Madsen, K. G.; Moser, C.; Molin, S.; Høiby, N.; Givskov, M. *Microbiology.* **2005**, *151*, 373–383.
- (8) Passador, L.; Cook, J. M.; Gambello, M. J.; Rust, L.; Iglewski, B. H. *Science.* **1993**, *260*, 1127–1130.
- (9) Ochsner, U. A.; Koch, A. K.; Fiechter, A.; Reiser, J. *J. Bacteriol.* **1994**, *176*, 2044–2054.
- (10) a) Pearson, J. P.; Gray, K. M.; Passador, L.; Tucker, K. D.; Eberhard, A.; Iglewski, B. H.; Greenberg, E. P. *Proc. Natl. Acad. Sci. U.S.A.* **1994**, *91*, 197–201; b) Ochsner, U. A.; Reiser, J. *Proc. Natl. Acad. Sci. U.S.A.* **1995**, *92*, 6424–6428.
- (11) Schauder, S.; Bassler, B. L. *Genes Dev.* **2001**, *15*, 1468–1480.
- (12) Pesci, E. C.; Milbank, J. B.; Pearson, J. P.; McKnight, S.; Kende, A. S.; Greenberg, E. P.; Iglewski, B. H. *Proc. Natl. Acad. Sci. U.S.A.* **1999**, *96*, 11229–11234.
- (13) Wade, D. S.; Calfee, M. W.; Rocha, E. R.; Ling, E. A.; Engstrom, E.; Coleman, J. P.; Pesci, E. C. *J. Bacteriol.* **2005**, *187*, 4372–4380.
- (14) Xiao, G.; Déziel, E.; He, J.; Lépine, F.; Lesic, B.; Castonguay, M.-H.; Milot, S.; Tampakaki, A. P.; Stachel, S. E.; Rahme, L. G. *Mol. Microbiol.* **2006**, *62*, 1689–1699.
- (15) Diggle, S. P.; Lumjiaktase, P.; Dipilato, F.; Winzer, K.; Kunakorn, M.; Barrett, D. A.; Chhabra, S. R.; Cámara, M.; Williams, P. *Chem. Biol. (Oxford, U. K.)* **2006**, *13*, 701–710.
- (16) Déziel, E.; Gopalan, S.; Tampakaki, A. P.; Lépine, F.; Padfield, K. E.; Saucier, M.; Xiao, G.; Rahme, L. G. *Mol. Microbiol.* **2005**, *55*, 998–1014.
- (17) Xiao, G.; He, J.; Rahme, L. G. *Microbiology.* **2006**, *152*, 1679–1686.
- (18) a) Déziel, E.; Lépine, F.; Milot, S.; He, J.; Mindrinos, M. N.; Tompkins, R. G.; Rahme, L. G. *Proc. Natl. Acad. Sci. U.S.A.* **2004**, *101*, 1339–1344; b) Dulcey, C. E.; Dekimpe, V.; Fauvelle, D.-A.; Milot, S.; Groleau, M.-C.; Doucet, N.; Rahme, L. G.; Lépine, F.; Déziel, E. *Chem. Biol. (Oxford, U. K.)* **2013**, *20*, 1481–1491.
- (19) Cao, H.; Krishnan, G.; Goumnerov, B.; Tsongalis, J.; Tompkins, R.; Rahme, L. G. *Proc. Natl. Acad. Sci. U.S.A.* **2001**, *98*, 14613–14618.
- (20) Gerdt, J. P.; Blackwell, H. E. *ACS Chem. Biol.* **2014**, *9*, 2291–2299.
- (21) Lu, C.; Kirsch, B.; Zimmer, C.; de Jong, J. C.; Henn, C.; Maurer, C. K.; Müsken, M.; Häussler, S.; Steinbach, A.; Hartmann, R. W. *Chem. Biol. (Oxford, U. K.)* **2012**, *19*, 381–390.
- (22) Lu, C.; Maurer, C. K.; Kirsch, B.; Steinbach, A.; Hartmann, R. W. *Angew. Chem., Int. Ed. Engl.* **2014**, *126*, 1127–1130.
- (23) Lu, C.; Kirsch, B.; Maurer, C. K.; Jong, J. C. de; Braunshausen, A.; Steinbach, A.; Hartmann, R. W. *Eur. J. Med. Chem.* **2014**, *79*, 173–183.
- (24) Ilangovan, A.; Fletcher, M.; Rampioni, G.; Pustelny, C.; Rumbaugh, K.; Heeb, S.; Cámara, M.; Truman, A.; Chhabra, S. R.; Emsley, J.; Williams, P. *PLoS Pathog.* **2013**, *9*, e1003508 EP -.

- (25) Starkey, M.; Lepine, F.; Maura, D.; Bandyopadhaya, A.; Lesic, B.; He, J.; Kitao, T.; Righi, V.; Milot, S.; Tzika, A.; Rahme, L. *PLoS Pathog.* **2014**, *10*, e1004321 EP -.
- (26) Zender, M.; Klein, T.; Henn, C.; Kirsch, B.; Maurer, C. K.; Kail, D.; Ritter, C.; Dolezal, O.; Steinbach, A.; Hartmann, R. W. *J. Med. Chem.* **2013**, *56*, 6761–6774.
- (27) Klein, T.; Henn, C.; Jong, J. C. de; Zimmer, C.; Kirsch, B.; Maurer, C. K.; Pistorius, D.; Müller, R.; Steinbach, A.; Hartmann, R. W. *ACS Chem. Biol.* **2012**, *7*, 1496–1501.
- (28) Ladbury, J. *Euro. Pharmaceut. Rev.* **2007**, 59–62.
- (29) Ladbury, J. E.; Klebe, G.; Freire, E. *Nat. Rev. Drug Discovery.* **2010**, *9*, 23–27.
- (30) Hopkins, A. L.; Groom, C. R.; Alex, A. *Drug Discovery Today.* **2004**, *9*, 430–431.
- (31) Adam, F. M.; Bish, G.; Calo, F.; Carr, C. L.; Castro, N.; Hay, D.; Hodgson, P. B.; Jones, P.; Knight, C. J.; Paradowski, M.; Parsons, G. C.; Proctor, K. J. W.; Pryde, D. C.; Rota, F.; Smith, M. C.; Smith, N.; Tran, T.-D.; Hitchin, J.; Dixon, R. *Org. Process Res. Dev.* **2011**, *15*, 788–796.
- (32) Maloney, K. M.; Nwakpuda, E.; Kuethe, J. T.; Yin, J. *J. Org. Chem.* **2009**, *74*, 5111–5114.
- (33) Liang, Y.; Xie, Y.-X.; Li, J.-H. *J. Org. Chem.* **2006**, *71*, 379–381.
- (34) Marion, N.; Navarro, O.; Mei, J.; Stevens, E. D.; Scott, N. M.; Nolan, S. P. *J. Am. Chem. Soc.* **2006**, *128*, 4101–4111.
- (35) Lu, Z.; Twieg, R. J. *Tetrahedron Lett.* **2005**, *46*, 2997–3001.
- (36) Macor, J. E.; Chenard, B. L.; Post, R. J. *J. Org. Chem.* **1994**, *59*, 7496–7498.
- (37) Hajduk, P. J.; Greer, J. *Nat. Rev. Drug Discovery.* **2007**, *6*, 211–219.
- (38) Cugini, C.; Calfee, M. W.; Farrow, J. M.; Morales, D. K.; Pesci, E. C.; Hogan, D. A. *Mol. Microbiol.* **2007**, *65*, 896–906.
- (39) Welch, M.; Hodgkinson, J. T.; Gross, J.; Spring, D. R.; Sams, T. *Biochemistry.* **2013**, *52*, 4433–4438.
- (40) Maddocks, S. E.; Oyston, P. C. F. *Microbiology.* **2008**, *154*, 3609–3623.
- (41) Karplus, M.; McCammon, J. A. *Nat. Struct. Biol.* **2002**, *9*, 646–652.
- (42) Khan, A. R.; Parrish, J. C.; Fraser, M. E.; Smith, W. W.; Bartlett, P. A.; James, M. N. *Biochemistry.* **1998**, *37*, 16839–16845.
- (43) Gallagher, L. A.; McKnight, S. L.; Kuznetsova, M. S.; Pesci, E. C.; Manoil, C. *J. Bacteriol.* **2002**, *184*, 6472–6480.
- (44) Lau, G. W.; Hassett, D. J.; Ran, H.; Kong, F. *Trends Mol. Med.* **2004**, *10*, 599–606.
- (45) Caldwell, C. C.; Chen, Y.; Goetzmann, H. S.; Hao, Y.; Borchers, M. T.; Hassett, D. J.; Young, L. R.; Mavrodi, D.; Thomashow, L.; Lau, G. W. *Am. J. Pathol.* **2009**, *175*, 2473–2488.
- (46) Storz, M. P.; Allegretta, G.; Kirsch, B.; Empting, M.; Hartmann, R. W. *Org. Biomol. Chem.* **2014**, *12*, 6094–6104.
- (47) Lépine, F.; Milot, S.; Déziel, E.; He, J.; Rahme, L. G. *J. Am. Soc. Mass Spectrom.* **2004**, *15*, 862–869.
- (48) Machan, Z. A.; Taylor, G. W.; Pitt, T. L.; Cole, P. J.; Wilson, R. *J. Antimicrob. Chemother.* **1992**, *30*, 615–623.
- (49) Hughes, D.; Andersson, D. I. *Nat. Rev. Genet.* **2015**, *16*, 459–471.
- (50) a) Allen, R. C.; Popat, R.; Diggle, S. P.; Brown, S. P. *Nat. Rev. Microbiol.* **2014**, *12*, 300–308; b) Ross-Gillespie, A.; Kümmerli, R. *Evolution, medicine, and public health.* **2014**, *2014*, 134–135.
- (51) Kabsch, W. *Acta Crystallogr., Sect. D: Biol. Crystallogr.* **2010**, *66*, 125–132.
- (52) Evans, P. R.; Murshudov, G. N. *Acta Crystallogr., Sect. D: Biol. Crystallogr.* **2013**, *69*, 1204–1214.
- (53) Winn, M. D.; Ballard, C. C.; Cowtan, K. D.; Dodson, E. J.; Emsley, P.; Evans, P. R.; Keegan, R. M.; Krissinel, E. B.; Leslie, A. G. W.; McCoy, A.; McNicholas, S. J.; Murshudov, G. N.; Pannu, N. S.; Potterton, E. A.; Powell, H. R.; Read, R. J.; Vagin, A.; Wilson, K. S. *Acta Crystallogr., Sect. D: Biol. Crystallogr.* **2011**, *67*, 235–242.

- (54) Strong, M.; Sawaya, M. R.; Wang, S.; Phillips, M.; Cascio, D.; Eisenberg, D. *Proc. Natl. Acad. Sci. U.S.A.* **2006**, *103*, 8060–8065.
- (55) McCoy, A. J.; Grosse-Kunstleve, R. W.; Adams, P. D.; Winn, M. D.; Storoni, L. C.; Read, R. J. *J. Appl. Crystallogr.* **2007**, *40*, 658–674.
- (56) Vagin, A. A.; Steiner, R. A.; Lebedev, A. A.; Potterton, L.; McNicholas, S.; Long, F.; Murshudov, G. N. *Acta Crystallogr., Sect. D: Biol. Crystallogr.* **2004**, *60*, 2184–2195.
- (57) Emsley, P.; Lohkamp, B.; Scott, W. G.; Cowtan, K. *Acta Crystallogr., Sect. D: Biol. Crystallogr.* **2010**, *66*, 486–501.
- (58) Afonine, P. V.; Grosse-Kunstleve, R. W.; Echols, N.; Headd, J. J.; Moriarty, N. W.; Mustyakimov, M.; Terwilliger, T. C.; Urzhumtsev, A.; Zwart, P. H.; Adams, P. D. *Acta Crystallogr., Sect. D: Biol. Crystallogr.* **2012**, *68*, 352–367.
- (59) Adams, P. D.; Afonine, P. V.; Bunkóczi, G.; Chen, V. B.; Davis, I. W.; Echols, N.; Headd, J. J.; Hung, L.-W.; Kapral, G. J.; Grosse-Kunstleve, R. W.; McCoy, A. J.; Moriarty, N. W.; Oeffner, R.; Read, R. J.; Richardson, D. C.; Richardson, J. S.; Terwilliger, T. C.; Zwart, P. H. *Acta Crystallogr., Sect. D: Biol. Crystallogr.* **2010**, *66*, 213–221.
- (60) Krieger, E.; Darden, T.; Nabuurs, S. B.; Finkelstein, A.; Vriend, G. *Proteins: Struct., Funct., Bioinf.* **2004**, *57*, 678–683.
- (61) Duan, Y.; Wu, C.; Chowdhury, S.; Lee, M. C.; Xiong, G.; Zhang, W.; Yang, R.; Cieplak, P.; Luo, R.; Lee, T.; Caldwell, J.; Wang, J.; Kollman, P. *J. Comput. Chem.* **2003**, *24*, 1999–2012.
- (62) Essar, D. W.; Eberly, L.; Hadero, A.; Crawford, I. P. *J. Bacteriol.* **1990**, *172*, 884–900.
- (63) Lépine, F.; Déziel, E.; Milot, S.; Rahme, L. G. *Biochim. Biophys. Acta, Gen. Subj.* **2003**, *1622*, 36–41.
- (64) Storz, M. P.; Maurer, C. K.; Zimmer, C.; Wagner, N.; Brengel, C.; Jong, J. C. de; Lucas, S.; Müsken, M.; Häussler, S.; Steinbach, A.; Hartmann, R. W. *J. Am. Chem. Soc.* **2012**, *134*, 16143–16146.

3.3 Chapter C:

Effects of Next Generation PqsR-targeting Anti-infectives against Biofilm and Virulence of *Pseudomonas aeruginosa*

The coworkers listed below made the following experimental contributions to this chapter:

Antonio G. G. de Mello Martins: Performed parts of the biofilm experiments

Christian Brengel: Performed parts of the biofilm experiments

Giuseppe Allegretta: Established and performed 2-AA assays

Lorenz Siebenbürger: Performed metabolic stability assays

Benjamin Kirsch: Planned *E. coli* reporter gene assays

Jens Eberhard: Developed MS methods for metabolic stability measurements

Stefanie Wagner: Performed lectin expression western blot analysis

Christine K. Maurer: Established and planned alkylquinolone and pyocyanin assays

Martin Empting: Performed modeling and docking studies

INTRODUCTION

“*It is time to close the book on infectious diseases, and declare the war against pestilence won*” – even if the origin of this statement cannot be precisely tracked down¹, it reflects the conventional wisdom² over decades in the 20th century. But this popular belief was quickly abandoned due to the alarming occurrence of multi- and pan-resistant microbial pathogens.³ This situation has even been worsened by shortening the research efforts in the field of antibacterial drug discovery.^{4,5} Nowadays, we are facing a lack of novel treatment options for many human pathogens which acquired resistance against nearly all available antibiotics.⁶ The development of compounds which reduce bacterial virulence without affecting viability has attracted increasing attention during the last years. These antivirulence drugs have the potential to overcome the burden of rapid development and spreading of resistance mechanisms and may help to regenerate the antimicrobial development pipeline.⁷

Inspired by this idea, we and others targeted the virulence of *Pseudomonas aeruginosa*, a Gram-negative opportunistic human pathogen, by interference with bacterial cell-to-cell communication.⁸ The release of virulence determinants is regulated mainly by a process called quorum sensing (QS).⁹ QS enables *P. aeruginosa* to coordinate gene expression collectively dependent on bacterial cell-density *via* the release and sensing of small diffusible molecules.⁹ *P. aeruginosa* employs the *las*^{10,11} and *rhl*^{12,13} QS systems which use acetyl homoserine lactones (AHLs) as signaling molecules, prevalent among Gram-negative bacteria. Furthermore, this

bacterium uses a rather unique system called *pqs*¹⁴ (*Pseudomonas* quinolone signal) applying alkylquinolones (AQs). The autoinducers 2-heptyl-3-hydroxy-4(1H)-quinolone (PQS) and its precursor 2-heptyl-4-quinolone (HHQ) activate the transcriptional regulator PqsR¹⁵ (*Pseudomonas* quinolone signaling receptor also referred to as MfR).^{16,17,18} The activated receptor regulates the expression of various genes involved in the production of virulence factors e.g. pyocyanin¹⁶, elastase, lectines etc.¹⁹ Additionally PqsR up-regulates the expression of the HHQ biosynthesis operon *pqsA-E* to form an autoinductive loop.^{20,21} Moreover, the *pqs* system is involved in the establishment of *P. aeruginosa* biofilms via multiple ways. Mutants lacking of a functional *pqs* system showed a reduced release of eDNA²² and expression of lectins A/B¹⁹. Both are integral parts for the *P. aeruginosa* biofilm architecture.^{22,23} *P. aeruginosa* strains which switched to a sessile biofilm lifestyle are the main cause of chronic persistent pneumonia found in cystic fibrosis patients.^{24,25} Bacteria growing in the biofilm mode adapt to intense antibiotic treatment and to the host immune response.²⁵ Taken together, the *pqs* system and its central regulator PqsR play a critical role during the acute and chronic infections.

Following a ligand-based approach, we were able to transform the native agonist HHQ into the potent antagonists showing a lack of activity due to metabolic conversion in *P. aeruginosa*.^{26,27} Further optimization led to the analog **1** which was able to fully protect *Galleria mellonella* larvae from a lethal *P. aeruginosa* infection providing the first *in vivo* proof of concept.²⁷ In a similar approach quinazolinone-based antagonists were developed and the first crystal structure of the ligand-binding domain (LBD) of PqsR was solved.²⁸ The potential of PqsR as drug target was further corroborated by the benzamido-benzimidazole antagonists **2** and **3**. These antagonists originated from a high throughput screening (HTS) campaign. **3** was demonstrated to be efficacious in mouse acute infection models as standalone treatment and as a pathoblocker-antibiotic combination therapy.²⁹ All discovered antagonist suffer from poor physicochemical properties. To address this issue, we initiated two fragment screening campaigns^{30,31} which led to chemically diverse ligands. The optimization of 2-amino-pyridine derivatives (**4**) resulted in nanomolar active antagonists as described in Chapter B.

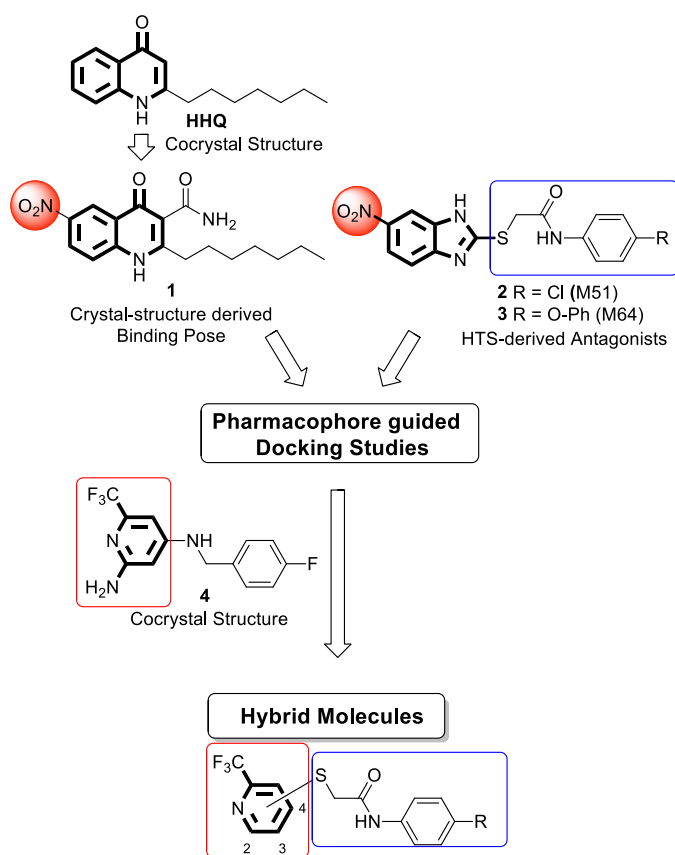


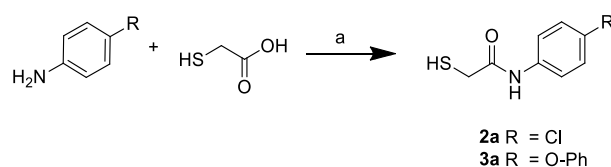
Figure 11: Published PqsR antagonists (1-4) and schematic representation of the applied medicinal chemistry strategy

This chapter deals with the nifty development of hybrid compounds by merging of the reported HTS hit **2** and the fragment-screening-derived antagonist **4**. We were able to generate a plausible binding-pose of **2** based on a pharmacophore-guided docking approach. An overlay with the crystal structure of **4** led to the synthesis of hybrid compounds consisting of a trifluoromethyl-pyridine headgroup derived from a fragment screening described in Chapter B and the thioglycolamide-aryl moieties of **2** and **3**, respectively. These hybrid compounds showed an improved physico-chemical profile while keeping high on-target and antivirulence activities. Furthermore, these compounds displayed specific effects on *P. aeruginosa* biofilms by abolishing the release of eDNA.

RESULTS AND DISCUSSION

Chemistry. Fragment hits **5** and **6** were obtained from commercial suppliers. The synthesis of the key precursors **2a** and **3a** is shown in Scheme 1. The particular anilines were condensed with thioglycolic acid in neat reaction at 130°C under an argon atmosphere.³² After cooling to RT the product was isolated in good yields by simple trituration with isopropanol and filtration.

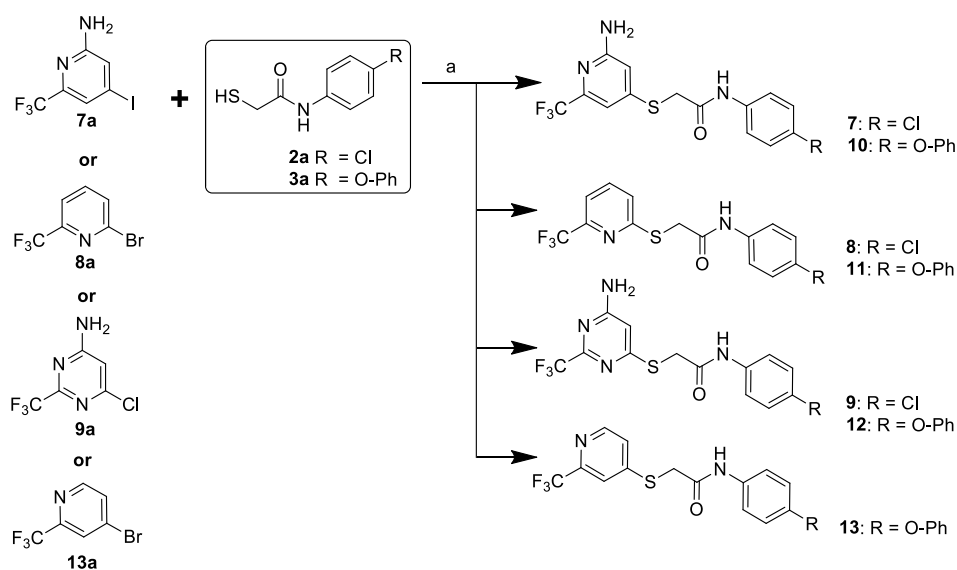
Scheme 1. Synthesis of Thioglycolamide Precursors^a



^aReagents and Conditions: a) pressure vial, neat, 130°C, Ar.

The heteroaryl halide **7a** was synthesized as described in Chapter B. Precursors **8a**, **9a** and **13a** were obtained from commercial suppliers. Hybrid compounds **7-12** were synthesized as outlined in Scheme 2. Heteroaryl halides **7a-9a**, **13a** were reacted with **2a** and **3a** in a classical S_NAr reaction using potassium carbonate as base to give the final products **7-13**.

Scheme 2. Synthesis of Hybrid Compounds



^aReagents and Conditions: a) K₂CO₃, DMF, -20°C to RT, Ar.

In-silico studies. Fragment-based lead discovery and HTS are often described as “mutually exclusive” strategies although there are complementary aspects of both approaches as well.³³ The discovery of benzamido-benzimidazole PqsR antagonists²⁹ (**2** and **3**) by a HTS screening inspired us to investigate on their binding mode (Figure 1) in order to combine these insights with structural information of the identified fragment hits. The nitro moiety was identified as obvious common feature in the quinolone class (**1**)²⁶ and in the benzamido-benzimidazole class (**2** and **3**)²⁹. Hence, we hypothesized that both antagonist classes overlap at this position in the LBD. The structure of the LBD in complex with the quinolone derivatives NHQ²⁸ (2-nonyl-4-quinolone) and HHQ were resolved. Based on these crystallographic results we derived a binding pose of the highly similar antagonist **1** (Figure 2A). Following our hypothesis, the nitro moiety and the adjacent aryl ring were defined as essential pharmacophore points. Subsequently, a pharmacophore-guided docking study with compound **2** was conducted. **2** was used due to lower number of rotatable bonds compared to **3** what facilitated a more accurate docking due to lower degrees of conformational freedom in the ligand.

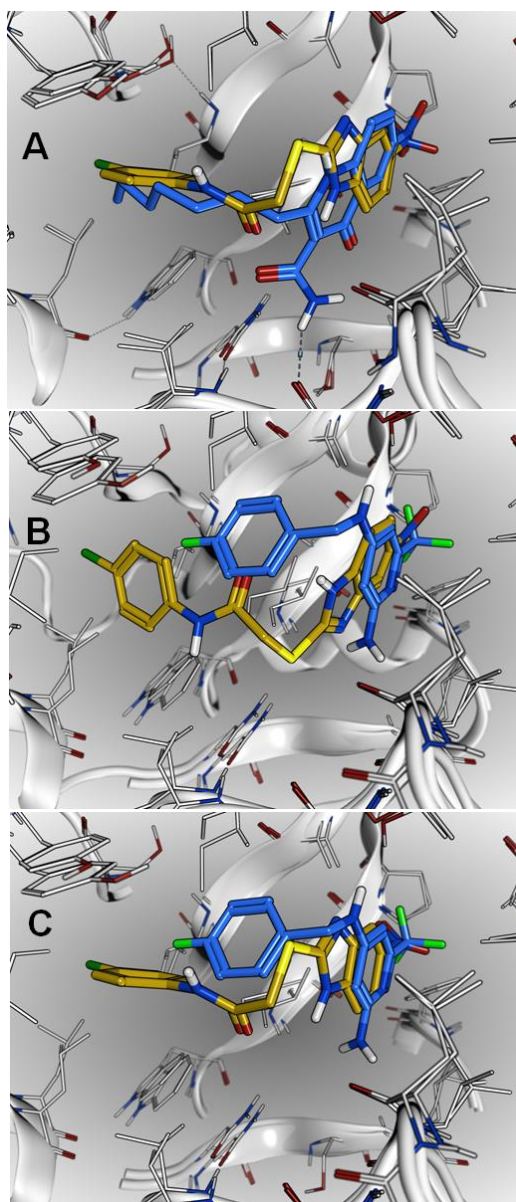


Figure 2: PqsR docking studies: **a)** overlay of modeled binding mode of **1** (blue) and highest scored docking pose for **2** (yellow) **b)** overlay of the crystal structure of **4** and highest ranked docking pose of **2** (yellow) **c)** alternative binding pose of **2** (yellow) superimposed with crystal structure of **4**

The thioglycol amide linker adopted an angled position in all generated docking poses which positioned the 4-chloro-phenyl ring in the alkyl sidechain pocket of HHQ. We superimposed these docking poses with the crystal structure of **4** (Figure 2B and 2C). The trifluoromethyl moiety of **4** is similarly oriented as the nitro group of **1** and **2**. This finding was in line with the SAR observed by Lu *et al.* where the nitro group was exchanged by trifluoromethyl without any change of the antagonistic activity.²⁶ To further validate our binding hypothesis, we used fragment competition studies. The amino-pyridine headgroup of **4** binds into the quinolone pocket (Figure 2B) and fragment **5** was used as a mimic thereof. According to our hypothesis the 5-nitro-benzimidazole heterocycle of **2** also occupies the same part of the pocket. In this case, fragment **6** was used.

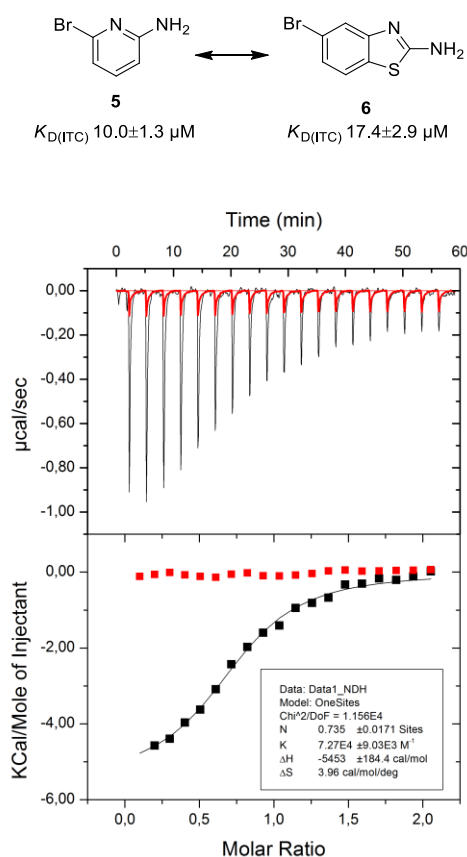
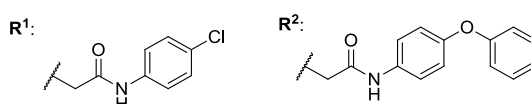


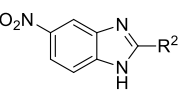
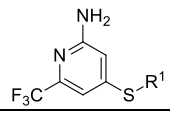
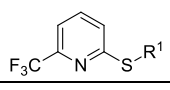
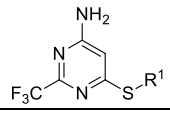
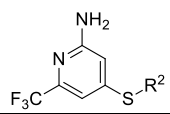
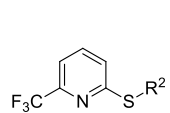
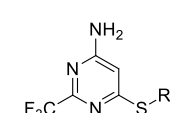
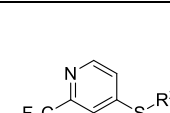
Figure 3: ITC competition experiments. Raw ITC data are shown on top and integrated normalized data on bottom. Titration of 150 μM PqsR with 1500 μM **6** (■, black curve); Titration of 150 μM PqsR with 1500 μM **6** in the presence of 1500 μM compound **5** (Δ, red curve).

According to isothermal titration calorimetry (ITC) competition experiments both fragments compete for binding to PqsR (Figure 3) what is indicated by the loss of heat release when **6** is titrated to PqsR in the presence of **5**. This finding clearly corroborates our binding model. Overall, the most striking difference between the particular docking poses of **2** was observed for the most flexible linker part. Comparing the poses depicted in Figure 2B and 2C, the position of the benzimidazole is shifted leading to altered linker geometry. These results promoted the positions 2-4 at the pyridine as possible attachment points for the thioglycolamide aryl moiety (Figure 1). In a parallel approach, the 4-position was discovered as vector for growing the trifluoromethyl pyridine headgroup (see Chapter B). Thus, this position was included and the fact that similar heteroaryl compounds were also reported as hits from the HTS campaign³⁴ encouraged us to pursue also the 2-position as possible attachment point. The 3-position, however, was lower ranked in priority due to the more difficult synthetic feasibility caused by the higher electron density in meta-position of the pyridine ring.

Hybrid antagonists. Compounds **7** and **8** were rapidly accessible via a nucleophilic substitution reaction in 2- and 4-position of the pyridine ring, respectively. At first, potential PqsR antagonists were evaluated in a heterologous *E. coli* reporter gene system. This system allows an undistorted analysis of agonistic or antagonistic properties without the penetration problems observed in *P. aeruginosa* and possible bacteria-mediated deactivation of test compounds.²⁷ Compounds displaying sufficient antagonistic properties were further analyzed for their effect on the virulence factor pyocyanin and the signaling molecule HHQ in *P. aeruginosa*. Moreover, the solubility of the compounds under assay conditions was determined. Subsequently, the ligand lipophilicity efficiency (LLE) was calculated which evaluates the potency normalized for the heavy atom count of a compound taking also lipophilicity into account.³⁵ Hybrid molecules **7** and **8** showed antagonistic activities in the nanomolar range and were able to translate these activities into inhibition of pyocyanin in the low micromolar range (Table 1). Additionally, both compounds were able to affect the levels of the signaling molecule HHQ and their superimposition suggested synthesizing compound **9**. The latter showed a comparable profile to **8** regarding antagonistic activity and pyocyanin inhibition but a significantly lowered clogD, which was also reflected in a slightly improved LLE.

Encouraged by these results and inspired by the SAR reported by Starkey *et al.*²⁹ we decided to exchange the chloro substituent for a phenoxy moiety (**10-12**). For all three headgroups an enhanced antagonistic activity was observed. There was a 22 fold (**7** vs. **10**) and 33 fold (**9** vs. **12**) boost in activity for the 4-position linked headgroups with amino function, whereas we measured a 2-fold increase (**8** vs. **11**) for the at the 2-position linked pyridine. These findings raised the question whether the presence of the NH₂ moiety or the positioning of thioglycolamide linker in 2- or 4-position of the pyridine nitrogen is pivotal for antagonistic activity. As an answer, the missing link **13** was synthesized. The latter showed a 2-fold improved antagonistic activity (**10** IC₅₀ = 0.019±0.001 μM vs. **13** IC₅₀ = 0.008±0.003 μM) leading to the conclusion that the amino group is an accessory feature to enhance the physicochemical properties but not fundamental for activity when combined with the R² tail. In contrary, the positioning of the pyridine nitrogen is more determining. The attachment of the linker in 4-position of the pyridine is clearly favored (**11** IC₅₀ = 0.086±0.05 μM vs. **13** IC₅₀ = 0.008±0.003 μM).

Table 1: Biological and physico-chemical properties of PqsR antagonists

Number	Structure	Antagonistic Activity IC ₅₀ [μM] ^a	Pyocyanin Inhibition IC ₅₀ [μM] ^b	HHQ Inhibition [μM] ^c	Solubility [μM] ^d	clogD pH 7.4 ^e	LLE (Astex) ^f
3 (M64)		0.005±0.001	0.12±0.01	0.22*	25	4.7	0.29
7		0.426±0.10	12±0.7	42±1 @ 50 μM	100	3.7	0.27
8		0.176±0.10	4.8±0.3	30±8 @ 50 μM	50	3.7	0.30
9		0.233±0.02	8.3± 4.6	40±2 @ 50 μM	100	3.0	0.33
10		0.019 ±0.001	0.276±0.02	0.52±0.05	25	4.4	0.28
11		0.086±0.05	0.822±0.30	44±3 @ 5 μM	12.5	4.5	0.24
12		0.007±0.004	0.384±0.13	2.29±0.1	50	3.0	0.36
13		0.008±0.003	0.339±0.02	0.54±0.05	12.5	4.3	0.30

^aevaluated in an *E. coli* reporter gene assay in the presence of 50 nM PQS; IC₅₀ represents the concentration of the half maximal antagonistic activity. ^bmeasured photometrically after extraction from PA14 cultures; IC₅₀ represents the concentration of 50% inhibition. ^cmeasured by UPLC-MS from PA14 cultures and referenced against DMSO control. ^ddetermined in PPGAS medium at 1% DMSO by visual inspection ^ecalculated using ACD/Percepta 2015. ^fligand lipophilicity efficiency³⁶ determined from antagonistic activity, heavy atom count and clogD. *measured once.

It was of major interest to quantify the effect of the top candidates **10** and **12** on the 2-aminoacetophenone (2-AA) in PA14 wt. 2-AA is a shunt product of the AHQ biosynthesis process³⁶ and promotes chronic infection phenotypes³⁷ as well as accumulation of persister cells³⁸ in *P. aeruginosa*. Compound **10** showed potent inhibition of 2-AA production ($IC_{50} = 1.2 \pm 0.2 \mu M$) whereas the effect of compound **12** leveled out at around 50% (Figure 4). Remarkably, both compounds showed comparable effects regarding pyocyanin inhibition (Figure 4) and antagonistic activity in the reporter gene assay (Table 1). A similar scenario was observed for the inhibition of HHQ production (**10** $IC_{50} = 0.54 \pm 0.05 \mu M$ vs. **12** $IC_{50} = 2.29 \pm 0.1 \mu M$). These data emphasizes that small changes (pyridine to pyrimidine) within a molecule can drastically influence the efficacy of the antagonists to inhibit the AHQ biosynthesis and virulence expression (pyocyanin).

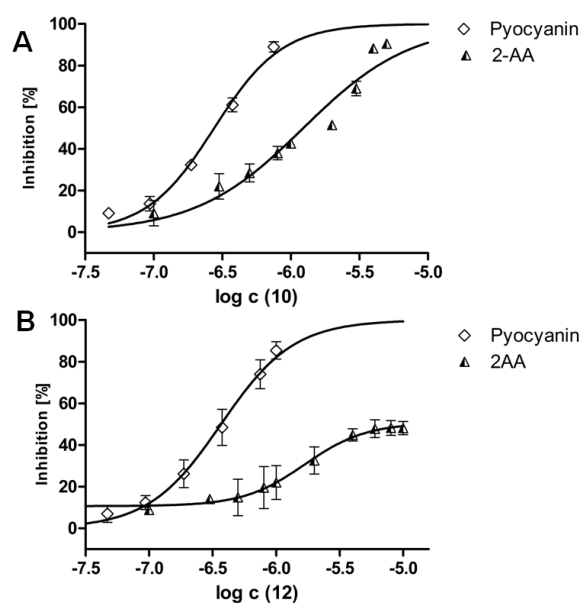


Figure 4: Dose-response curves for the inhibition of pyocyanin and 2-AA in PA14 wt for compound **10** (A, upper row) and **12** (B lower row). Given data represent the mean of at least two independent experiments with $n=3$. Non linear regression analysis (continuous black line) was applied to determine IC_{50} values using a four variables model with constrains (bottom = 0 and top = 100 % except for the effect of **12** on 2-AA) included in Graph Pad Prism (5.04).

Compounds containing an amino-pyridine and -pyrimidine scaffold are frequently reported as inhibitors of different kinases.^{39,40} Therefore, we analyzed selected compounds for potential cytotoxic effects on eukaryotic HEK293 cells (SI Table S1). None of the tested compounds affected cell viability except for compound **7** but only at a significantly higher concentration than the measured effect on pyocyanin. Additionally, the scaffolds were subjected to an *in silico* toxicology prediction⁴¹ using the Derek Nexus database. This screening displayed no alerts concerning the amino-pyridine and -pyrimidine headgroups.

Overall, compound **12** showed the best combination of nanomolar antagonistic activity, potent pyocyanin inhibition and remarkable physicochemical properties, which is reflected by a strikingly better LLE value compared to the benchmark compound **3**.

Effects on static biofilms and lecB expression in *P. aeruginosa*. Compound **12** was selected for further evaluation in a static biofilm assay. The bacteria growing in sessile biofilm phenotype are prevalently found in most chronic infections caused by *P. aeruginosa*.²⁵ Biofilms are bacterial communities embedded in a self-produced polymeric matrix attached to a surface.⁴² The structural components of this matrix are mainly polysaccharides, proteins and DNA.⁴³ The establishment of a biofilm is a complex regulatory process, which necessitates close coordination by the involved regulatory systems. The *pqs* QS system clearly affects *P. aeruginosa* biofilm formation¹⁹ regulatory mechanisms by triggering the release of eDNA²² and lectinA/B expression.²³ Besides its function as cell-connecting component during biofilm development,⁴⁴ eDNA protects sessile bacteria from host immune response and antibacterial treatment by the complexation of cationic peptides and xenobiotics.⁴⁵

LectinA/B are carbohydrate-binding proteins which play important roles for surface attachment and stability of *P. aeruginosa* biofilms.^{23,46} The effect of PqsR antagonists on *P. aeruginosa* biofilms was first reported by Ilangovan *et al.*²⁸ However, the doses employed for these experiments have not been reported. Hence, we sought to investigate the biofilm effects of our antagonist in more detail. PA14 static biofilms were grown in the presence of 5 μ M of the antagonist **12** for 24 h. We evaluated total biofilm volume (biomass) as well as the *pqs*-dependent biofilm component eDNA (Figure 4A). While the PqsR antagonist **12** displayed only minor effects on the whole biovolume, it completely inhibited the accumulation of eDNA. This observation is in line with our results for the *pqsR* negative mutant. Moreover, compounds **10** and **12** showed potent inhibition of lectinB in *P. aeruginosa* (Figure 4B). Notably, these experiments were performed in planktonic PAO1 cultures due to experimental feasibility and the specificity of the used antibody. Nonetheless, the results of these experiments clearly underline the specific antivirulence effects of these compounds.

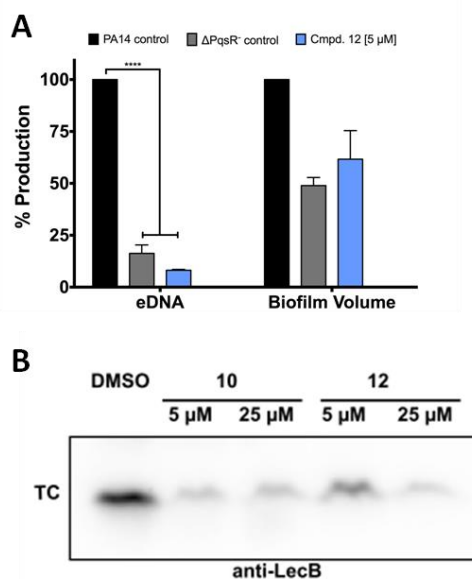


Figure 4. A) Effects of compound **12** on PA14 static biofilms. While only a low effect was observed on total biofilm volume, compound **12** was able to drastically reduce eDNA accumulation to levels comparable with the *pqsR* mutant strain. Error bars represent standard error of at least two independent experiments. **** = $p < 0.0001$. **B)** Western blot analysis of LecB expression in *P. aeruginosa* PAO1. Total cell (TC) fractions were analyzed by immunoblotting using anti-LecB serum. Cultures were grown for 24 h in absence or presence of compound **10** or **12** (5 μM or 25 μM).

CONCLUSION

Growing in a biofilm mode is the native form of bacterial lifestyle.⁴⁷ This lifestyle allows bacteria to colonize different niches and protects the single organism against severe external conditions.^{42,47} These insights altered the perspective on our bacterial opponent - from planktonic unicellular organisms to highly organized sessile communities. Nevertheless, learning, how these communities are organized, enables the development of alternative treatment strategies for the post antibiotic era.⁴⁸ In this study, we describe the development of improved lead compounds interfering with *P. aeruginosa* cell-to-cell communication with the aim to contribute to the development pipeline towards novel, innovative antimicrobials. Based on cocrystal structures and *in silico* methods, we developed a plausible binding-pose for the HTS hit **2**.²⁹ An overlay with the cocrystal-structure of in-house fragment derived antagonist **4** showed that both scaffolds partially overlap in the quinolone binding pocket of PqsR. This finding raised the idea to merge the trifluoro-pyridine headgroup with the benzamido-benzimidazole scaffold (**2** and **3**). This strategy resulted in the straightforward development of hybrid PqsR antagonists resulting in potent pyocyanin, HHQ and 2-AA inhibition in *P. aeruginosa* while keeping superior physicochemical properties. In doing so, the potentially problematic nitro moiety at the benzimidazole core was exchanged by a more drug-like trifluoromethyl group. Subsequently, these compounds were profiled for their effects on PA14 static biofilms. For some of the

described biofilm inhibiting compounds the exact mode of action is poorly understood or their effect might be mediated through a direct physicochemical interaction with the biofilm matrix.⁴⁹ In contrast, the effects of our PqsR antagonist were in accordance with the biofilm profile generated by a *pqsR* mutant strain: the overall biovolume was only slightly affected but the *pqs*-mediated release of eDNA was completely abolished. To what extent the reduction of eDNA and expression of lectinB affects the biofilm structure and permeability will be addressed in future experiments.

Taken together, in this approach we successfully combined the best features of two apparently mutual worlds – phenotypic HTS and fragment screening – in order to push the development of antivirulence agents against severe *P. aeruginosa* infections.

EXPERIMENTAL SECTION

In silico studies. The structure of the PqsR:1 complex was modelled based on a solved X-ray structure of HHQ (Chapter B) bound to its receptor. The original coordinates were loaded into Molecular Operating Environment (MOE 2014, Chemical Computing Group) and the additional carboxamide and nitro substituents were attached to the ligand using the “Builder” function. Then the resulting complex structure was energy minimized using the standard LigX parameters together with the AMBER10:EHT forcefield to yield the model of compound **1** in complex with PqsR. The structure of the PqsR:2 complex was generated through a pharmacophore-guided docking. To this end, a two-feature pharmacophore model comprising an aromatic cycle and an electron-withdrawing group, which were placed inside the quinolone pocket of PqsR. A solved X-ray structure of bound antagonist **4** was used as template (see Chapter B). Then, the built-in “induced-fit” docking protocol was applied using the described pharmacophore as placement constraint, AMBER10:EHT force field, and standard parameters. The two highest scoring docking poses of compound **2** were additionally energy minimized to yield the complex structures depicted in Figure 2.

Reporter Gene Assay in *E. coli*. The ability of the compounds to either stimulate or antagonize the PqsR-dependent transcription was analysed as previously described²⁶ using a β -galactosidase reporter gene assay in *E. coli*⁵⁰ expressing PqsR.

Pyocyanin Assay. Pyocyanin produced by *P. aeruginosa* PA14 was determined as reported previously²⁶ according to the method of Essar *et al.*⁵¹

Isothermal titration calorimetry ITC titrations were carried out as previously reported.^{30,31}

Determination of Extracellular HHQ and 2-AA Extracellular levels of HHQ from PA14 *pqsH* cultures were determined as previously reported^{27,52} according to the methods of Lépine *et al.*⁵³ For the quantification of 2-AA PA14 wt was used following the same protocol as for HHQ quantification whether a slightly modified sample work-up was performed. Briefly, 750 μ L of culture was diluted with the same volume of 1 μ M d_4 HHQ in acetonitrile, shaken for 5 min at 1,500 rpm, and centrifuged at 14,000 rpm for 10 min. Afterwards 1 mL of supernatant of each sample was transferred in a vial for analysis by HPLC-MS/MS. Calibration curve of 2-AA was prepared according to the same procedure using PA14 *pqsA* mutant as biomatrix.

Biofilm assay in PA14 For the determination of biofilm components in PA14 static biofilms, we followed reported procedures with a few modifications.^{22,54} Briefly, cultures of PA14 (or PA14*pqsR*) were grown in M63 medium in 96 well plates (Greiner, clear flat bottom) for 24 h at 37°C in the presence of test compound added as DMSO stock solution or DMSO as control to give 1% (v/v) final DMSO concentration. After washing the matured biofilm with PBS and water, biofilm components were stained either with crystal violet (0.1 mg/ml dissolved in water/ethanol 95/5 (v/v)) for the whole biomass or with propidium iodine solution (0.05 mg/ml dissolved in water). For quantification of the whole biomass absorbance was measured at 590 nm and for eDNA florescence at 620 nm using FLUOstar Omega (BMG Labtech). Given values represent the mean of at least two independent experiments with n=5. Differences in between treated and untreated samples were evaluated using a one way ANOVA followed by a two-sided Holm-Sidak's multiple comparison test using GraphPad Prism version 6.0f for Mac OS X, GraphPad Software. Differences were considered significant at a *p*-value < 0.05.

LectinB expression *P. aeruginosa* PAO1 cultures were grown in LB medium at 37 °C. Compounds were dissolved in DMSO. Compound **10** or **12** was added to 2.5 mL LB and the DMSO concentrations were adjusted to keep the same concentrations in all samples. Overnight cultures were used to inoculate fresh LB medium to an OD₆₀₀ of 0.02 and 2.5 mL of this bacterial culture was added to the 2.5 mL LB samples containing compound **10** or **12** or only DMSO. The final cultures had an starting OD₆₀₀ of 0.01 and final compound concentration of 5 μ M or 25 μ M. Bacterial cultures were incubated at 37 °C (200 rpm) for 24 h. Bacteria were harvested by centrifugation at 21380 rcf for 10 minutes. The supernatant was discarded and pellets were resuspended in SDS loading buffer (50 mM Tris-HCl pH 6.8, 10% (v/v) glycerol, 2% (v/v) SDS, 100 mM DTT, bromphenolblue) and denatured by heating (98 °C, 5 min). Total cell extracts were analyzed by 15% SDS–PAGE and Coomassie staining (SI Figure S3) or immune blotting. In each case, total cell extracts of approximately 2×10^8 bacteria were loaded per lane. For detection of LecB in total cells, proteins were transferred onto a nitrocellulose membrane (Amersham; GE Healthcare). After blocking the membrane (5% milk in PBST (137 mM NaCl, 2.7 mM KCl, 10 mM Na₂HPO₄, 1.8 mM KH₂PO₄ and 0.2% Tween)) immunodetection was carried out using rabbit antiserum against LecB (1:500 in 5% milk in PBST). Detection was

performed using the goat anti-rabbit secondary antibody conjugated to horseradish peroxidase (1:5000 in 5% milk in PBST; Dianova), before development with chemiluminescent substrate (100 mM Tris-HCl pH 8.5, 0.009% H₂O₂, 1.25 mM luminol, 225 μM coumaric acid) and detection with a Fusion imager (Vilber Lourmat).

Chemical and Analytical Methods. ¹H and ¹³C NMR spectra were recorded as indicated on a Bruker DRX-500 instrument or a Bruker Fourier 300 instrument. Chemical shifts are given in parts per million (ppm), and referenced against the residual solvent peak. Coupling constants (*J*) are given in hertz. Mass spectrometry and purity determination (LC/MS) was performed either on a SpectraSystems-MSQ LCMS system (Thermo Fisher Scientific) consisting of a pump, an autosampler, VWD detector or on Waters LCMS-System consisting of a 767 sample Manager, a 2545 binary gradient pump, a 2998 PDA detector and a 3100 electron spray mass spectrometer. All solvents were HPLC grade. The purity of tested final products was > 95%. Procedures were not optimized regarding yield. Microwave assisted synthesis was carried out in a Discover microwave synthesis system (CEM). Column chromatography was performed using the automated flash chromatography system Combiflash Rf+ (Teledyne Isco) equipped with RediSepRf silica columns. Final products were dried in high vacuum.

General Procedure A: *N*-phenyl-2-mercaptoacetamide precursors. Aniline (1 eq) was filled into a crimp vial (Biotage[®]). The vial was evacuated and backfilled with argon (3 times). 2-mercaptoacetic acid (1 eq) was added (neat reaction) and the vial flushed with argon (5 min). The reaction mixture was heated to 130°C in a metal block for 1.5 h. The mixture was allowed to cool to RT. The resulting solid was suspended in isopropanol and filtered. The resulting white cake was washed with IPA to give the titled product.

General Procedure B: Hybrid compounds. Heteroaryl halide (0.35 mmol) and K₂CO₃ (1.05 mmol) was suspended in DMF (1 ml) using a crimp vial (Biotage[®]). The vial was purged with argon. A solution of *N*-phenyl-2-mercaptoacetamide (0.38 mmol) in 1 ml DMF was added while cooling in an ice-bath. The mixture was again purged with argon. The reaction was aged at RT for 6 h. The mixture was poured into water and extracted with ethylacetate (3 times). The combined organics were washed with Na₂CO₃ saturated solution and brine. The organic extract was dried over Na₂SO₄, filtered and dried. Purification was done by automated flash chromatography or preparative HPLC.

2-((2-amino-6-(trifluoromethyl)pyridin-4-yl)thio)-*N*-(4-chlorophenyl)acetamide (7) was synthesized according to general procedure B from 4-iodo-6-(trifluoromethyl)pyridin-2-amine (100 mg, 0.347 mmol) and *N*-(4-chlorophenyl)-2-mercaptoacetamide (77 mg, 0.382 mmol). The crude product was purified by automated flash chromatography using a gradient of petroleum ether to pure ether. Further purification by prep HPLC afforded the titled product as white solid (24 mg, 0.066 mmol, 19 % yield). ¹H NMR (300 MHz, DMSO-*d*₆) δ ppm 3.99 (s, 2 H), 6.56 (s, 3

H), 6.89 (d, $J=1.3$ Hz, 1 H), 7.23 - 7.45 (m, 1 H), 7.52 - 7.68 (m, 2 H), 10.44 (s, 1 H); ^{13}C NMR (75 MHz, $\text{DMSO}-d_6$) δ ppm 35.12, 105.53 (q, $^3J(\text{C},\text{F})=2.2$ Hz, 1 C), 106.79, 125.21 (q, $^1J(\text{C},\text{F})=275.0$ Hz, 1 C), 120.77 (2 C), 127.19, 128.71 (2 C), 137.62, 145.00 (q, $^2J(\text{C},\text{F})=32.8$ Hz, 1 C), 149.43, 159.75, 166.06; MS (ESI +) m/z 362 (M+H) $^+$, 403 (M+ACN+H) $^+$.

N-(4-chlorophenyl)-2-((6-(trifluoromethyl)pyridin-2-yl)thio)acetamide (8) was synthesized according to general procedure B from 2-bromo-6-(trifluoromethyl)pyridine (226 mg, 1,000 mmol) and N-(4-chlorophenyl)-2-mercaptoacetamide (212 mg, 1.050 mmol). The mixture was stirred for 1 h at -78 °C and then at 0 °C for 1h. Purification was done by automated flash chromatography using a gradient of petroleum ether and ethylacetate. The crude product was titrated with DCM/pentane and filtered to give the titled product as a white solid (65 mg, 0.19 mmol, 18 % yield). ^1H NMR (500 MHz, $\text{DMSO}-d_6$) δ ppm 4.11 (s, 2 H), 7.30 - 7.39 (m, 2 H), 7.53 - 7.64 (m, 3 H), 7.70 (d, $J=7.9$ Hz, 1 H), 7.92 (t, $J=6.9$ Hz, 1 H), 10.40 (s, 1 H); ^{13}C NMR (126 MHz, $\text{DMSO}-d_6$) δ ppm 34.73, 116.59, 121.23 (q $^1J(\text{C},\text{F})=272.0$ Hz, 1 C), 120.66 (s, 2 C), 125.17, 126.86, 128.58 (s, 2 C), 137.92, 138.38, 146.10 (q, $^2J(\text{C},\text{F})=32.0$ Hz, 1 C), 159.57, 166.10; MS (ESI +) m/z not found.

2-((6-amino-2-(trifluoromethyl)pyrimidin-4-yl)thio)-N-(4-chlorophenyl)acetamide (9) was synthesized according to general procedure B from 6-chloro-2-(trifluoromethyl)pyrimidin-4-amine (100 mg, 0.51 mmol) and N-(4-chlorophenyl)-2-mercaptoacetamide (102 mg, 0.51 mmol). Purification was done by automated flash chromatography using a gradient petroleum ether and ethylacetate (9/1 to 1/1) to give the titled compound as light yellow solid (45 mg, 0.124 mmol, 24% yield). ^1H NMR (500 MHz, $\text{DMSO}-d_6$) δ ppm 4.03 (s, 2 H), 6.50 (s, 1 H), 7.27 - 7.42 (m, 2 H), 7.49 (br. s., 2 H), 7.53 - 7.67 (m, 2 H), 10.40 (s, 1 H); ^{13}C NMR (126 MHz, $\text{DMSO}-d_6$) δ ppm 34.22, 100.99, 119.42 (q, $^1J(\text{C},\text{F})=275.8$ Hz, 1 C), 120.73 (2 C), 127.00, 128.70 (2 C), 137.89, 154.52 (q, $^2J(\text{C},\text{F})=33.0$ Hz, 1 C), 163.27, 166.06, 166.62; MS(ESI+) m/z 363 (M+H) $^+$.

2-((2-amino-6-(trifluoromethyl)pyridin-4-yl)thio)-N-(4-phenoxyphenyl)acetamide (10) was synthesized according to general procedure B from 4-iodo-6-(trifluoromethyl)pyridin-2-amine (100 mg, 0.35 mmol) and 2-mercapto-N-(4-phenoxyphenyl)acetamide (99 mg, 0.38 mmol). Purification was done by automated flash chromatography using a gradient of petroleum ether and diethyl ether (1/1 to 2/8). Further purification by prep HPLC to give 2-((2-amino-6-(trifluoromethyl)pyridin-4-yl)thio)-N-(4-phenoxyphenyl)acetamide (20 mg, 0.05 mmol, 14 % yield) as white solid. ^1H NMR (300 MHz, $\text{CHLOROFORM}-d$) δ ppm 3.83 (s, 2 H), 4.76 (s, 2 H), 6.44 (d, $J=0.8$ Hz, 1 H), 6.91 (d, $J=1.4$ Hz, 1 H), 6.95 - 7.05 (m, 4 H), 7.07 - 7.14 (m, 1 H), 7.29 - 7.37 (m, 2 H), 7.39 - 7.47 (m, 2 H), 8.22 (s, 1 H); ^{13}C NMR (75 MHz, $\text{DMSO}-d_6$) δ ppm 35.08, 105.56 (q, $^1J(\text{C},\text{F})=3.0$ Hz, 1 C), 106.80, 117.93 (2 C), 119.43 (2 C), 121.61 (d, $^1J(\text{C},\text{F})=274.0$ Hz, 1 C), 120.95 (2 C), 123.03, 129.95 (2 C), 134.55, 145.03 (q, $^2J(\text{C},\text{F})=32.0$ Hz, 1 C), 149.55, 152.08, 157.22, 159.77, 165.71; MS(ESI+) m/z 420 (M+H) $^+$, 461 (M+ACN+H) $^+$.

N-(4-phenoxyphenyl)-2-((6-(trifluoromethyl)pyridin-2-yl)thio)acetamide (11) was synthesized according to general procedure B from 2-bromo-6-(trifluoromethyl)pyridine (100 mg, 0.44 mmol) and 2-mercapto-N-(4-phenoxyphenyl)acetamide (115 mg, 0.44 mmol) e mixture was poured into water solution and extracted using EA. Combined organics were washed with brine, dried (Na₂SO₄), filtered and concentrated. Purification was done by automated flash chromatography using a gradient of petroleum ether and ethylacetate (9/1 to pure ethylacetate) to give the titled product as off white solid (135 mg, 0.334 mmol, 75 % yield). ¹H NMR (500 MHz, DMSO-*d*₆) δ ppm 4.12 (s, 2 H), 6.88 - 7.03 (m, 4 H), 7.09 (t, J=7.4 Hz, 1 H), 7.31 - 7.41 (m, 2 H), 7.57 (d, J=8.8 Hz, 2 H), 7.60 (d, J=7.6 Hz, 1 H), 7.71 (d, J=8.2 Hz, 1 H), 7.92 (t, J=7.9 Hz, 1 H), 10.32 (s, 1 H); ¹³C NMR (126 MHz, DMSO-*d*₆) δ ppm 34.66, 116.58 (q, ¹J(C,F)=2.8 Hz, 1 C), 117.85 (2 C), 121.27 (q, ¹J(C,F)=274.9 Hz, 1 C), 119.37 (2 C), 120.85 (2 C), 122.95, 125.16, 129.92 (2 C), 134.83, 138.39, 146.10 (q, ²J(C,F)=33.9 Hz, 1 C), 151.79, 157.27, 159.70, 165.72; MS(ESI+) *m/z* 427 (M+Na)⁺.

2-((6-amino-2-(trifluoromethyl)pyrimidin-4-yl)thio)-N-(4-phenoxyphenyl)acetamide (12) was synthesized according to general procedure B from 6-chloro-2-(trifluoromethyl)pyrimidin-4-amine (200 mg, 1.012 mmol) and 2-mercapto-N-(4-phenoxyphenyl)acetamide (263 mg, 1.012 mmol). Purification was done by automated flash chromatography using a gradient of petroleum ether and ethylacetate (9/1 to pure ethylacetate) to give the titled product as white solid (45 mg, 0.107 mmol, 11 % yield). ¹H NMR (500 MHz, DMSO-*d*₆) δ ppm 4.03 (s, 2 H), 6.51 (s, 1 H), 6.89 - 7.04 (m, 4 H), 7.10 (t, J=7.4 Hz, 1 H), 7.30 - 7.40 (m, 2 H), 7.50 (br. s., 2 H), 7.55 - 7.62 (m, 2 H), 10.30 (s, 1 H); ¹³C NMR (126 MHz, DMSO-*d*₆) δ ppm 34.09, 100.91, 119.35 (q, ¹J(C,F)=275.8 Hz, 1 C), 117.86 (2 C), 119.40 (2 C), 120.87 (2 C), 122.97, 129.93 (2 C), 134.73, 151.87, 154.46 (q, ²J(C,F)=34.8 Hz, 1 C), 157.24, 163.24, 165.61, 166.71. MS(ESI+) *m/z* 421 (M+H)⁺.

N-(4-phenoxyphenyl)-2-((2-(trifluoromethyl)pyridin-4-yl)thio)acetamide (13) was synthesized according to general procedure B from 4-bromo-2-(trifluoromethyl)pyridine (200 mg, 0.885 mmol) and 2-mercapto-N-(4-phenoxyphenyl)acetamide (229 mg, 0.885 mmol). Purification was done by automated flash chromatography using a gradient of petroleum ether and ethylacetate (petroleum ether pure to 8/2) to give the titled product as white solid (210 mg, 0.519 mmol, 59% yield). ¹H NMR (500 MHz, DMSO-*d*₆) δ ppm 4.14 (s, 2 H), 6.90 - 7.04 (m, 4 H), 7.05 - 7.19 (m, 1 H), 7.30 - 7.42 (m, 2 H), 7.50 - 7.61 (m, 2 H), 7.66 (dd, J=5.4, 1.6 Hz, 1 H), 7.88 (d, J=1.6 Hz, 1 H), 8.56 (d, J=5.4 Hz, 1 H), 10.40 (s, 1 H); ¹³C NMR (126 MHz, DMSO-*d*₆) δ ppm 34.85, 117.26 (d, ³J(C,F)=2.7 Hz, 1 C), 117.96 (2 C), 121.49 (q, ¹J(C,F)=274.0 Hz, 1 C), 119.45 (2 C), 120.95 (2 C), 123.06, 123.49, 129.95 (2 C), 134.44, 146.37 (q, ²J(C,F)=33.0 Hz, 1 C), 149.47, 151.35, 152.14, 157.18, 165.59; MS(ESI+) *m/z* 405 (M+H)⁺.

REFERENCES

- (1) Spellberg, B.; Taylor-Blake, B. On the exoneration of Dr. William H. Stewart: debunking an urban legend. *Infect. Dis. Poverty*. **2013**, *2*, 3.
- (2) Pier, G. B. On the greatly exaggerated reports of the death of infectious diseases. *Clin. Infect. Dis.* **2008**, *47*, 1113–1114.
- (3) Alanis, A. J. Resistance to antibiotics: are we in the post-antibiotic era? *Arch. Med. Res.* **2005**, *36*, 697–705.
- (4) Boucher, H. W.; Talbot, G. H.; Bradley, J. S.; Edwards, J. E.; Gilbert, D.; Rice, L. B.; Scheld, M.; Spellberg, B.; Bartlett, J. Bad bugs, no drugs: no ESKAPE! An update from the Infectious Diseases Society of America. *Clin. Infect. Dis.* **2009**, *48*, 1–12.
- (5) Projan, S. J. Why is big Pharma getting out of antibacterial drug discovery? *Curr. Opin. Microbiol.* **2003**, *6*, 427–430.
- (6) Falagas, M. E.; Bliziotis, I. A. Pandrug-resistant Gram-negative bacteria: the dawn of the post-antibiotic era? *Int. J. Antimicrob. Agents*. **2007**, *29*, 630–636.
- (7) Clatworthy, A. E.; Pierson, E.; Hung, D. T. Targeting virulence: a new paradigm for antimicrobial therapy. *Nat. Chem. Biol.* **2007**, *3*, 541–548.
- (8) Rampioni, G.; Leoni, L.; Williams, P. The art of antibacterial warfare: Deception through interference with quorum sensing-mediated communication. *Bioorg. Chem.* **2014**, *55*, 60–68.
- (9) Schuster, M.; Peter Greenberg, E. A network of networks. *Int. J. Med. Microbiol.* **2006**, *296*, 73–81.
- (10) Gambello, M. J.; Iglewski, B. H. Cloning and characterization of the *Pseudomonas aeruginosa* lasR gene, a transcriptional activator of elastase expression. *J. Bacteriol.* **1991**, *173*, 3000–3009.
- (11) Passador, L.; Cook, J. M.; Gambello, M. J.; Rust, L.; Iglewski, B. H. Expression of *Pseudomonas aeruginosa* virulence genes requires cell-to-cell communication. *Science*. **1993**, *260*, 1127–1130.
- (12) Ochsner, U. A.; Koch, A. K.; Fiechter, A.; Reiser, J. Isolation and characterization of a regulatory gene affecting rhamnolipid biosurfactant synthesis in *Pseudomonas aeruginosa*. *J. Bacteriol.* **1994**, *176*, 2044–2054.
- (13) Ochsner, U. A.; Reiser, J. Autoinducer-mediated regulation of rhamnolipid biosurfactant synthesis in *Pseudomonas aeruginosa*. *Proc. Natl. Acad. Sci. U. S. A.* **1995**, *92*, 6424–6428.
- (14) Pesci, E. C.; Milbank, J. B. J.; Pearson, J. P.; McKnight, S.; Kende, A. S.; Greenberg, E. P.; Iglewski, B. H. Quinolone signaling in the cell-to-cell communication system of *Pseudomonas aeruginosa*. *Proc. Natl. Acad. Sci. U. S. A.* **1999**, *96*, 11229–11234.
- (15) Cao, H.; Krishnan, G.; Goumnerov, B.; Tsongalis, J.; Tompkins, R.; Rahme, L. G. A quorum sensing-associated virulence gene of *Pseudomonas aeruginosa* encodes a LysR-like transcription regulator with a unique self-regulatory mechanism. *Proc. Natl. Acad. Sci. U. S. A.* **2001**, *98*, 14613–14618.
- (16) Gallagher, L. A.; McKnight, S. L.; Kuznetsova, M. S.; Pesci, E. C.; Manoil, C. Functions Required for Extracellular Quinolone Signaling by *Pseudomonas aeruginosa*. *J. Bacteriol.* **2002**, *184*, 6472–6480.
- (17) Déziel, E.; Lépine, F.; Milot, S.; He, J.; Mindrinos, M. N.; Tompkins, R. G.; Rahme, L. G. Analysis of *Pseudomonas aeruginosa* 4-hydroxy-2-alkylquinolines (HAQs) reveals a role for 4-hydroxy-2-heptylquinoline in cell-to-cell communication. *Proc. Natl. Acad. Sci. U. S. A.* **2004**, *101*, 1339–1344.
- (18) Xiao, G.; Deziel, E.; He, J.; Lepine, F.; Lesic, B.; Castonguay, M.-H.; Milot, S.; Tampakaki, A. P.; Stachel, S. E.; Rahme, L. G. MvR, a key *Pseudomonas aeruginosa* pathogenicity LTTR-class regulatory protein, has dual ligands. *Mol. Microbiol.* **2006**, *62*, 1689–1699.
- (19) Diggle, S. P.; Winzer, K.; Chhabra, S. R.; Worrall, K. E.; Cámara, M.; Williams, P. The *Pseudomonas aeruginosa* quinolone signal molecule overcomes the cell density-dependency of the quorum sensing hierarchy, regulates rhl-dependent genes at the onset of stationary phase and can be produced in the absence of LasR. *Mol. Microbiol.* **2003**, *50*, 29–43.
- (20) Wade, D. S.; Calfee, M. W.; Rocha, E. R.; Ling, E. A.; Engstrom, E.; Coleman, J. P.; Pesci, E. C. Regulation of *Pseudomonas* Quinolone Signal Synthesis in *Pseudomonas aeruginosa*. *J. Bacteriol.* **2005**, *187*, 4372–4380.

- (21) Xiao, G.; He, J.; Rahme, L. G. Mutation analysis of the *Pseudomonas aeruginosa* *mvfR* and *pqsABCDE* gene promoters demonstrates complex quorum-sensing circuitry. *Microbiology*. **2006**, *152*, 1679–1686.
- (22) Allesen-Holm, M.; Barken, K. B.; Yang, L.; Klausen, M.; Webb, J. S.; Kjelleberg, S.; Molin, S.; Givskov, M.; Tolker-Nielsen, T. A characterization of DNA release in *Pseudomonas aeruginosa* cultures and biofilms. *Mol. Microbiol.* **2006**, *59*, 1114–1128.
- (23) Diggle, S. P.; Stacey, R. E.; Dodd, C.; Camara, M.; Williams, P.; Winzer, K. The galactophilic lectin, LecA, contributes to biofilm development in *Pseudomonas aeruginosa*. *Environ. Microbiol.* **2006**, *8*, 1095–1104.
- (24) Singh, P. K.; Schaefer, A. L.; Parsek, M. R.; Moninger, T. O.; Welsh, M. J.; Greenberg, E. P. Quorum-sensing signals indicate that cystic fibrosis lungs are infected with bacterial biofilms. *Nature*. **2000**, *407*, 762–764.
- (25) Høiby, N.; Ciofu, O.; Bjarnsholt, T. *Pseudomonas aeruginosa* biofilms in cystic fibrosis. *Future Microbiol.* **2010**, *5*, 1663–1674.
- (26) Lu, C.; Kirsch, B.; Zimmer, C.; Jong, J. C. de; Henn, C.; Maurer, C. K.; Musken, M.; Haussler, S.; Steinbach, A.; Hartmann, R. W. Discovery of antagonists of PqsR, a key player in 2-alkyl-4-quinolone-dependent quorum sensing in *Pseudomonas aeruginosa*. *Chem. Biol. (Oxford, U. K.)*. **2012**, *19*, 381–390.
- (27) Lu, C.; Maurer, C. K.; Kirsch, B.; Steinbach, A.; Hartmann, R. W. Overcoming the unexpected functional inversion of a PqsR antagonist in *Pseudomonas aeruginosa*: an in vivo potent antivirulence agent targeting pqs quorum sensing. *Angew. Chem., Int. Ed.* **2014**, *53*, 1109–1112.
- (28) Ilangovan, A.; Fletcher, M.; Rampioni, G.; Pustelny, C.; Rumbaugh, K.; Heeb, S.; Camara, M.; Truman, A.; Chhabra, S. R.; Emsley, J.; Williams, P. Structural basis for native agonist and synthetic inhibitor recognition by the *Pseudomonas aeruginosa* quorum sensing regulator PqsR (MvfR). *PLoS Pathog.* **2013**, *9*, e1003508.
- (29) Starkey, M.; Lepine, F.; Maura, D.; Bandyopadhyaya, A.; Lesic, B.; He, J.; Kitao, T.; Righi, V.; Milot, S.; Tzika, A.; Rahme, L. Identification of anti-virulence compounds that disrupt quorum-sensing regulated acute and persistent pathogenicity. *PLoS Pathog.* **2014**, *10*, e1004321.
- (30) Klein, T.; Henn, C.; Jong, J. C. de; Zimmer, C.; Kirsch, B.; Maurer, C. K.; Pistorius, D.; Müller, R.; Steinbach, A.; Hartmann, R. W. Identification of small-molecule antagonists of the *Pseudomonas aeruginosa* transcriptional regulator PqsR: biophysically guided hit discovery and optimization. *ACS Chem. Biol.* **2012**, *7*, 1496–1501.
- (31) Zender, M.; Klein, T.; Henn, C.; Kirsch, B.; Maurer, C. K.; Kail, D.; Ritter, C.; Dolezal, O.; Steinbach, A.; Hartmann, R. W. Discovery and biophysical characterization of 2-amino-oxadiazoles as novel antagonists of PqsR, an important regulator of *Pseudomonas aeruginosa* virulence. *J. Med. Chem.* **2013**, *56*, 6761–6774.
- (32) Shaitanov, P. V.; Lukashov S.S.; Turov O.V.; Yarmoluk S.M. Synthesis and structural study of N-substituted-1,7-dithia-4-azaspiro[4.4]nonan-3-one 7,7-dioxides. *Ukr. Bioorg. Acta.* **2007**, *2*, 56–61.
- (33) Barker, J.; Hestekamp, T.; Whittaker, M. Integrating HTS and fragment-based drug discovery. *Drug Discovery World.* **2008**, 69–75.
- (34) Rahme, L.; Lepine, F.; Starkey, M.; Lesic-Arsic, B. Antibiotic tolerance inhibitors. WO2012116010 A2.
- (35) Mortenson, P.; Murray, C. Assessing the lipophilicity of fragments and early hits. *J. Comput.-Aided Mol. Des.* **2011**, *25*, 663–667.
- (36) Drees, S. L.; Fetzner, S. PqsE of *Pseudomonas aeruginosa* Acts as Pathway-Specific Thioesterase in the Biosynthesis of Alkylquinolone Signaling Molecules. *Chem. Biol. (Oxford, U. K.)*. **2015**, *22*, 611–618.
- (37) Kesarwani, M.; Hazan, R.; He, J.; Que, Y.-A.; Que, Y.; Apidianakis, Y.; Lesic, B.; Xiao, G.; Dekimpe, V.; Milot, S.; Deziel, E.; Lépine, F.; Rahme, L. G. A quorum sensing regulated small volatile molecule reduces acute virulence and promotes chronic infection phenotypes. *PLoS Pathog.* **2011**, *7*, e1002192.
- (38) Que, Y.-A.; Hazan, R.; Strobel, B.; Maura, D.; He, J.; Kesarwani, M.; Panopoulos, P.; Tsurumi, A.; Giddey, M.; Wilhelmy, J.; Mindrinos, M. N.; Rahme, L. G. A quorum sensing small volatile molecule promotes antibiotic tolerance in bacteria. *PLoS one.* **2013**, *8*, e80140.

- (39) Hilton, S.; Naud, S.; Caldwell, J. J.; Boxall, K.; Burns, S.; Anderson, V. E.; Antoni, L.; Allen, C. E.; Pearl, L. H.; Oliver, A. W.; Wynne Aherne, G.; Garrett, M. D.; Collins, I. Identification and characterisation of 2-aminopyridine inhibitors of checkpoint kinase 2. *Bioorg. Med. Chem.* **2010**, *18*, 707–718.
- (40) Jain, R.; Mathur, M.; Lan, J.; Costales, A.; Atallah, G.; Ramurthy, S.; Subramanian, S.; Setti, L.; Feucht, P.; Warne, B.; Doyle, L.; Basham, S.; Jefferson, A. B.; Lindvall, M.; Appleton, B. A.; Shafer, C. M. Discovery of Potent and Selective RSK Inhibitors as Biological Probes. *J. Med. Chem.* **2015**, *58*, 6766–6783.
- (41) Muster, W.; Breidenbach, A.; Fischer, H.; Kirchner, S.; Müller, L.; Pähler, A. Computational toxicology in drug development. *Drug discovery today.* **2008**, *13*, 303–310.
- (42) Costerton, J. W. Bacterial Biofilms. *Science.* **1999**, *284*, 1318–1322.
- (43) Sutherland, I. The biofilm matrix – an immobilized but dynamic microbial environment. *Trends Microbiol.* **2001**, *9*, 222–227.
- (44) Whitchurch, C. B.; Tolker-Nielsen, T.; Ragas, P. C.; Mattick, J. S. Extracellular DNA required for bacterial biofilm formation. *Science.* **2002**, *295*, 1487.
- (45) Mulcahy, H.; Charron-Mazenod, L.; Lewenza, S. Extracellular DNA chelates cations and induces antibiotic resistance in *Pseudomonas aeruginosa* biofilms. *PLoS Pathog.* **2008**, *4*, e1000213.
- (46) Tielker, D. *Pseudomonas aeruginosa* lectin LecB is located in the outer membrane and is involved in biofilm formation. *Microbiology.* **2005**, *151*, 1313–1323.
- (47) Costerton, J. W.; Cheng, K. J.; Geesey, G. G.; Ladd, T. I.; Nickel, J. C.; Dasgupta, M.; Marrie, T. J. Bacterial biofilms in nature and disease. *Annu. Rev. Microbiol.* **1987**, *41*, 435–464.
- (48) Kostakioti, M.; Hadjifrangiskou, M.; Hultgren, S. J. Bacterial biofilms: development, dispersal, and therapeutic strategies in the dawn of the postantibiotic era. *Cold Spring Harbor Perspect. Med.* **2013**, *3*, a010306.
- (49) Worthington, R. J.; Richards, J. J.; Melander, C. Small molecule control of bacterial biofilms. *Org. Biomol. Chem.* **2012**, *10*, 7457–7474.
- (50) Cugini, C.; Calfee, M. W.; Farrow, J. M. 3.; Morales, D. K.; Pesci, E. C.; Hogan, D. A. Farnesol, a common sesquiterpene, inhibits PQS production in *Pseudomonas aeruginosa*. *Mol. Microbiol.* **2007**, *65*, 896–906.
- (51) Essar, D. W.; Eberly, L.; Hadero, A.; Crawford, I. P. Identification and characterization of genes for a second anthranilate synthase in *Pseudomonas aeruginosa*: interchangeability of the two anthranilate synthases and evolutionary implications. *J. Bacteriol.* **1990**, *172*, 884–900.
- (52) Storz, M. P.; Maurer, C. K.; Zimmer, C.; Wagner, N.; Brengel, C.; Jong, J. C. de; Lucas, S.; Müsken, M.; Häussler, S.; Steinbach, A.; Hartmann, R. W. Validation of PqsD as an anti-biofilm target in *Pseudomonas aeruginosa* by development of small-molecule inhibitors. *J. Am. Chem. Soc.* **2012**, *134*, 16143–16146.
- (53) Lepine, F.; Milot, S.; Deziel, E.; He, J.; Rahme, L. G. Electrospray/mass spectrometric identification and analysis of 4-hydroxy-2-alkylquinolines (HAQs) produced by *Pseudomonas aeruginosa*. *J. Am. Soc. Mass Spectrom.* **2004**, *15*, 862–869.
- (54) Frei, R.; Breitbach, A. S.; Blackwell, H. E. 2-Aminobenzimidazole derivatives strongly inhibit and disperse *Pseudomonas aeruginosa* biofilms. *Angew. Chem., Int. Ed.* **2012**, *51*, 5226–5229.

3.4 Chapter D:

Dissecting the multiple roles of PqsE in *Pseudomonas aeruginosa* virulence by discovery of small tool compounds

Michael Zender,[‡] Florian Witzgall,[‡] Steffen L. Drees, Elisabeth Weidel, Christine K. Maurer, Susanne Fetzner, Wulf Blankenfeldt, Martin Empting, and Rolf W. Hartmann

[‡]These authors contributed equally

Reprinted (adapted) with permission from *ACS Chem. Biol.*, **2016**, *11*, 1755–1763

Copyright (2016) American Chemical Society.

ABSTRACT

Pseudomonas aeruginosa uses quorum sensing (QS) as a cell-to-cell communication system to orchestrate the expression of virulence determinants. The biosynthesis of the important *Pseudomonas* quinolone signal (PQS) requires the *pqsABCDE* operon. Here, PqsE acts as a pathway-specific thioesterase, but it also contributes to the regulation of bacterial virulence via an unknown mechanism. In this manuscript, we report the discovery of PqsE inhibitors as tool compounds to gain further insights into its different functions. Differential scanning fluorimetry (DSF) was used to screen a fragment library and isothermal titration calorimetry (ITC) was employed as a secondary filter. As proven by X-ray crystallography, hit molecules bound to the active center inhibiting PqsE's thioesterase activity and in cell-based and *in vitro* assays. Notably, the ligands did not affect the levels of the PqsE-regulated virulence factor pyocyanin. These findings indicate that the regulatory function of PqsE is not linked to its thioesterase activity and must be encoded outside of the active center. This study highlights the potential of fragment-based screening for the discovery of tool compounds. This approach provided novel insight into complex biological systems, which could not be obtained by knockout studies.

INTRODUCTION

Pseudomonas aeruginosa is a Gram-negative opportunistically pathogenic bacterium that infects multiple host organisms.¹ It is extremely adaptable and thrives under manifold environmental conditions.² The pathogen is responsible for several chronic and acute infections especially in hospitalized and immunocompromised patients.³ Furthermore, *P. aeruginosa*-mediated pneumonia is the major cause of death in people suffering from cystic fibrosis.⁴ It is

more and more recognized that bacterial communities such as those of *P. aeruginosa* have the capability to coordinate their activities collectively. This process is called quorum sensing (QS) and relies on the release and uptake of small diffusible signaling molecules also referred to as autoinducers (AIs). The concentration of AIs increases as a function of bacterial cell-density. As soon as a certain threshold is reached, the expression of particular genes is altered. In *P. aeruginosa*, more than 6 % of the complete genome is regulated by QS networks.⁵ The QS-dependent regulon includes genes involved in production of virulence factors as well as in general metabolic processes, which accounts for the central role of QS during infection and adaptation processes.⁵ *P. aeruginosa* mainly uses three interconnected QS circuitries: The *las*⁶ and the *rhl*⁷ quorum sensing systems use acyl homoserine lactones (AHLs) as signaling molecules, which are a very common AI scaffold among Gram-negative bacteria. In addition, *P. aeruginosa* uses a rather unique system called *pqs*⁸ (Figure 1), which applies the alkylquinolones (AQs) PQS (the *Pseudomonas* Quinolone Signal) and HHQ (2-heptyl-4(1*H*)-quinolone) (Figure 2) as signaling molecules.

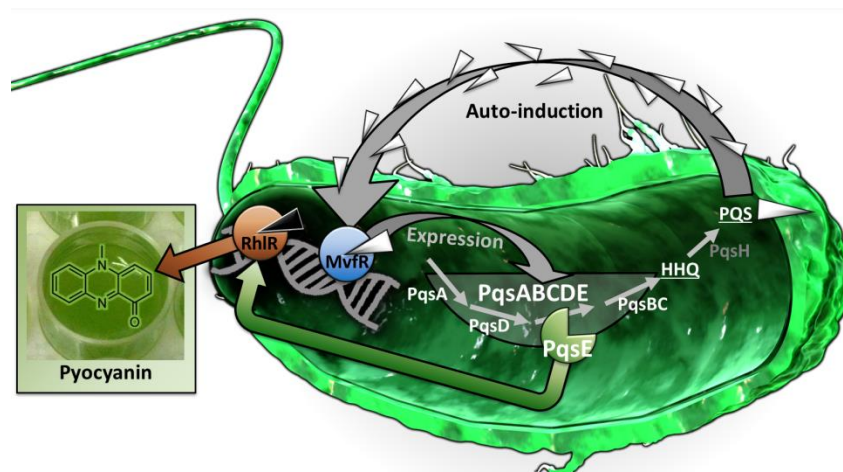


Figure 1. Schematic representation of the *pqs* system in *P. aeruginosa* emphasizing the impact of PqsE on virulence regulation. MvfR (PqsR; blue circle) is the transcriptional regulator which responds to the autoinducers of the *pqs* system (PQS and HHQ; white triangles). PqsA-E are signal molecule synthases (for details see Figure 2). RhlR (brown circle) is the transcriptional regulator which responds to the autoinducer of the *rhl* system (C4HSL; black triangle). Virulence regulation by RhlR (brown arrow) is modulated by PqsE (green arrow)

The biosynthesis of these quinolones (Figure 2) involves the expression of the *pqsABCDE* operon^{9,10} under the control of the signal receptor MvfR, often referred to as PqsR.¹¹ AQs originate from anthranilic acid, which is first converted to anthraniloyl-CoA by PqsA.¹² Anthraniloyl-CoA is then condensed with malonyl-CoA by PqsD to form 2-aminobenzoylacetyl-CoA (2-ABA-CoA).^{13,14} After hydrolysis by a thioesterase,¹⁵ the resulting 2-aminobenzoylacetate (2-ABA) is condensed with octanoyl-CoA by PqsBC to give HHQ,¹⁴ which undergoes hydroxylation catalyzed by PqsH to form PQS (Figure 2).¹⁶ Both alkylquinolones, HHQ and PQS, activate the receptor MvfR (PqsR) to upregulate their own biosynthesis via the *pqsABCDE* operon (autoinductive loop) and induce the production of several virulence factors.¹⁷

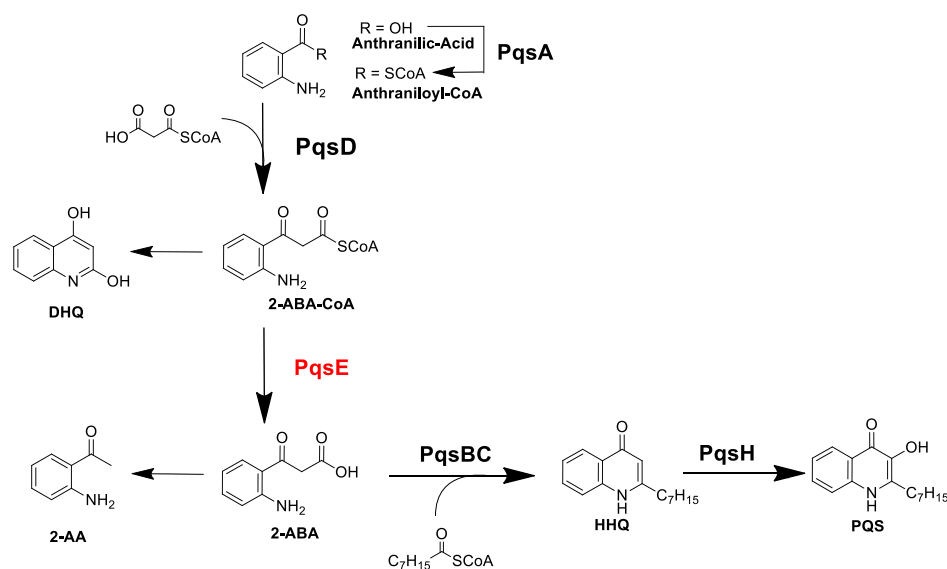


Figure 2. Biosynthesis of the signaling molecules HHQ and PQS

PqsE takes part in AQ biosynthesis by catalyzing the hydrolysis of 2-ABA-CoA to form 2-ABA. This function, however, can to some extent be bypassed by housekeeping thioesterases, such as TesB, making PqsE dispensable for AQ biosynthesis.¹⁵ Importantly, it was demonstrated that PqsE is crucial for full *P. aeruginosa* virulence and even activates *pqs*-controlled virulence in the absence of a functional *pqs* system. This implies a *pqs*-independent regulatory role.^{10,18–20} Some of PqsE's regulatory activities, for example the upregulation of the virulence factor pyocyanin, are mediated through the *rhl* system.^{18–20}

The crystal structure of PqsE shows a β -lactamase fold and a Fe(II)/Fe(III) center in the active site.²¹ An alanine scan identified key amino acids, which are required for the full production of pyocyanin.²² Taken together, despite many efforts, the exact biomolecular mechanism underlying the regulatory effect of PqsE remains elusive. However, due to its central role for *P. aeruginosa* virulence, PqsE might be an attractive future drug target. Hence, the discovery of specific tool compounds, which enable further insights into PqsE's functions is highly desirable.

To address this issue, a fragment screening using differential scanning fluorimetry (DSF) was conducted. This approach led to different carboxylic acid derivatives as top candidates (**1-3**; Figure 3). The hit molecules bound to the active center of PqsE and showed inhibition of the thioesterase activity in two different *in vitro* assays. The profiles of these compounds regarding Aqs and pyocyanin in *P. aeruginosa* (PAO1) highlight a new facet of the putative role of PqsE in virulence regulation beyond its thioesterase function.

RESULTS AND DISCUSSION

Fragment-Screening Approach. During a cell-free target-based drug discovery campaign, compounds with sufficient on-target activity have to be identified. In addition, good penetration through the bacterial cell envelope as well as evasion from efflux pumps have to be achieved.^{23,24} The physicochemical properties of most established antibiotics are strikingly different compared to compounds designed to hit eukaryotic targets.²⁵ It is believed, that this discrepancy contributed to the disillusioning outcomes of many high-throughput screening campaigns in antibiotic drug discovery when using chemical libraries optimized for human targets.²⁴ Fragment-based screening approaches are elegant tools to bypass these drawbacks.^{26,27} The screening of smaller libraries is sufficient to cover a large area of chemical space considering the possibility to grow, link, and merge fragments in subsequent optimization steps.²⁸

To identify PqsE ligands, a loose rule-of-three-compliant library sourced from Maybridge consisting of 500 fragments was screened by differential scanning fluorimetry (DSF). DSF is a spectroscopic technique that allows detection of a change in the protein melting temperature (ΔT_M) upon ligand binding.^{28,29} For a positive control, we employed anthranilic acid, which had previously been identified to be a ligand of PqsE by isothermal titration calorimetry (ITC)²¹ and shifted the melting temperature by 2.6 K (at 1 mM). It has to be mentioned that a sharp melting curve required the presence of Mn^{2+} in the buffer. The fragments were tested at a concentration of 500 μM . Compounds showing a positive shift form a stabilized protein-ligand complex, which is reported as beneficial for further crystallization experiments.³⁰ Hence, only fragments showing a $\Delta T_M \geq 1^\circ K$ were considered. In total, this setup led to 10 confirmed hits accounting for a 2% hit rate (Figure 3A). Fragments containing a carboxylic acid motif were found predominantly (5 out of 10; SI Table 1) which was in accordance with the fact that a benzoic acid-shaped ligand was observed in the crystal structure.²¹ Nevertheless, the presence of this motif alone seems not to be sufficient given that only 5 of 35 carboxylic acids within the library showed a pronounced positive shift in melting temperature. We ranked the carboxylic acid-containing hits according to their ΔT_M values and investigated top candidate **1** at different concentrations, which revealed a clear dose-dependency (Figure 3C). The other hit compounds were chemically diverse (SI, Table 1) and we decided to focus on the aforementioned carboxylic acid motif (**1-3**) as a privileged pharmacophore and on two additional unrelated scaffolds (**4, 5**).

Compounds **1-5** were subjected to hit validation using ITC analysis (Figure 3B, 3D) which is considered as the gold standard secondary screening tool.^{31,32} The binding of the three top carboxylic acid derivatives (**1-3**) to PqsE was confirmed by ITC. Compound **1** showed a surprisingly good affinity ($K_{D(ITC)} = 0.9 \pm 0.3 \mu M$) with respect to its fragment-like size. The binding was mostly enthalpy-driven, which accounts for specific non-covalent interactions between **1**

and PqsE.³³ A binding event was observed for screening hit **2**, but the heat release was too low to derive a defined K_D value under the tested conditions. Compound **3** showed a weaker affinity ($K_{D(\text{ITC})} = 19.6 \pm 3.7 \mu\text{M}$). The indole derivative **4** and phenoxazine **5** were not amenable to ITC analysis.

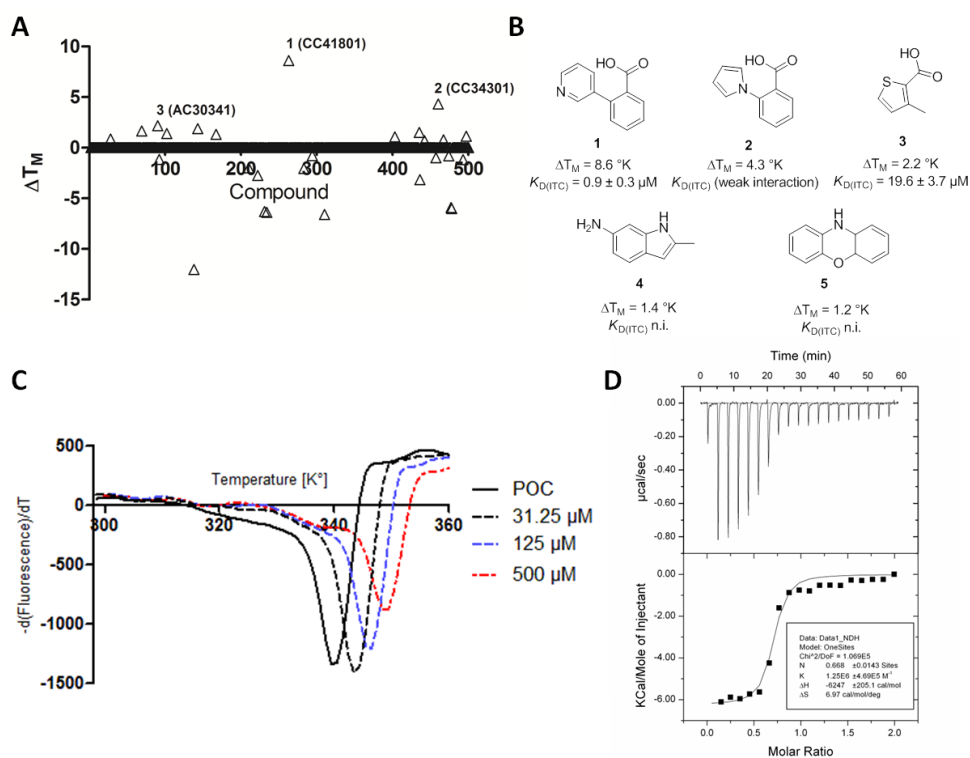


Figure 3. PqsE fragment screening workflow. **(A)** DSF screening of 500 fragments; single Δ represents the melting point shift in relation to DMSO control in $^{\circ}\text{K}$ **(B)** Structures of hit compounds showing highest ΔT_M (**1-3**) and chemically diverse hits **4** and **5** **(C)** Dose-dependent melting point shift for **1**; change of fluorescence while applying a temperature gradient shown as negative first derivative **(D)** representative ITC titration curve of **1** mM **1** against $100 \mu\text{M}$ H_6PqsE ; the recorded change of heat over time for 19 injections of ligand **1** (upper row); integrated heats (\blacksquare) against the molar ratio of the reaction and 1:1 binding-model fit (continuous black line; lower row).

X-ray crystallography. In a next step, we sought to gain insight into the exact binding modes of hit compounds **1-5** and to compare these with the structure of PqsE in complex with the reaction product 2-ABA.¹⁵ The short half-life ($< 40\text{s}$)¹⁵ of the PqsE substrate 2-ABA-CoA necessitated the use of the aforementioned hydrolysis product as a surrogate for crystallization experiments. To this end, crystals were soaked with the respective ligands. Only the carboxylic acid derivatives **1-3** yielded complex structures at resolutions of 1.77 to 2.16 \AA (Figure 4; Supplementary Table S2). Neither ITC (*vide supra*) nor crystallography indicated a specific binding of compound **4** and **5** what disqualified these compounds from further biological profiling. The three carboxylic acid derivatives **1-3** (Figure 4B-D) occupy the same site as the β -keto acid 2-ABA (Figure 4A), but their binding mode around the binuclear active center differs from that of 2-ABA. The

complexes containing fragments **1-3** exhibit a water molecule bridging the two metal atoms. Notably, in the 2-ABA-bound structure, this position is occupied by the carboxylic acid moiety of the ligand. Both 2-ABA and ligands **1-3** are stabilized by mainly hydrophobic interactions mediated by Y72, E182, L193, F195, F276, L277, H282 and S285. In addition, the 2-NH₂ group of 2-ABA forms a weak hydrogen bond with E182 (O-H distance: ~ 3.5 Å). Furthermore, the pyridine or pyrrole rings of compounds **1** and **2** undergo π - π -interactions with the side-chain of H71. For compound **3** an additional interaction between the sulfur of the thiophene group and the aromatic π -system of F195 is observed.

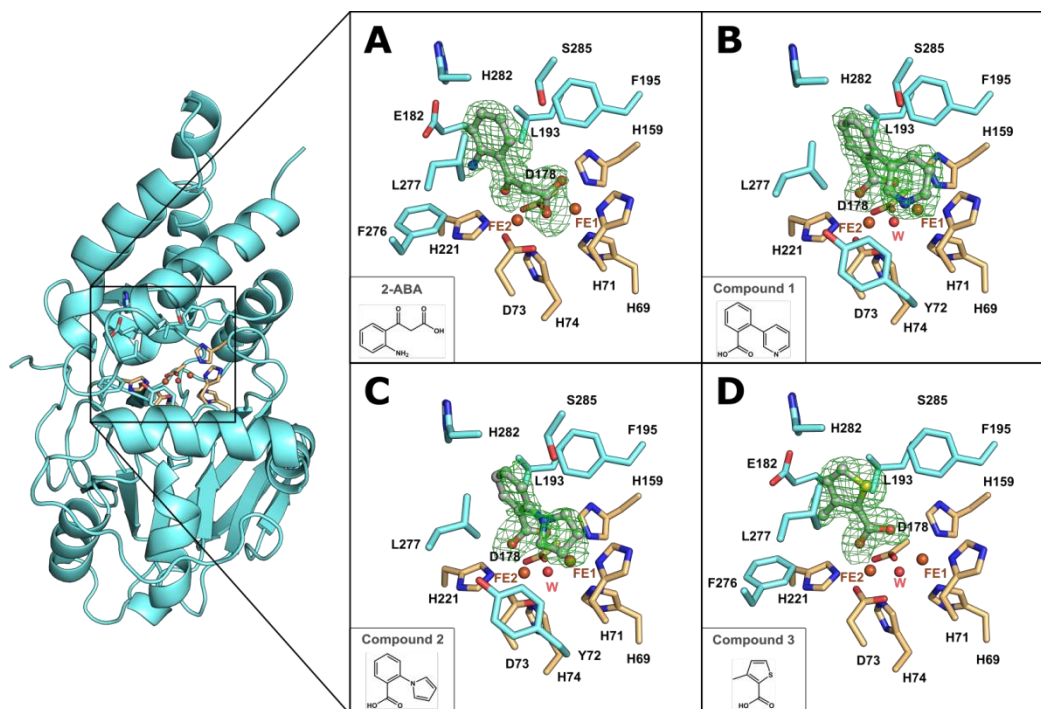


Figure 4. Crystal structures of PqsE in complex with 2-aminobenzoylacetate (**A**) and screening hits **1-3** (**B-D**). The compounds are depicted in a ball-and-stick representation and their chemical structures are shown in the left corner of each panel. The di-iron center (light orange) and the side-chains forming the binding pocket (blue) of each compound are indicated. Fo-Fc difference electron density maps (green) before incorporation of the ligand are contoured at 3.0 sigma.

In vitro evaluation. Because the crystal structures of PqsE in complex with ligands **1-3** revealed binding to the metal center in a similar position as 2-ABA, we investigated their inhibitory effect on the thioesterase activity of PqsE within AQ biosynthesis.¹⁵ The instability of PqsE's substrate (2-ABA-CoA), which has an estimated half-life of ≤ 40 s,¹⁵ necessitated the development of a combined PqsDE assay. 2-ABA-CoA was generated *in situ* by PqsD from anthraniloyl-CoA and malonyl-CoA. 2-ABA-CoA can then either be hydrolyzed to 2-ABA by PqsE or decomposes to DHQ in an uncatalyzed reaction (SI, Figure S1). Quantification of 2-ABA and DHQ was performed by LC-MS using a procedure that was optimized to prevent 2-ABA decomposition to DHQ or 2-AA (as tested using chemically synthesized 2-ABA, see Experimental Section). In the absence of inhibitor, the reaction yielded a 1:1 mixture of 2-ABA

and DHQ, whereas inhibition of PqsE by compounds **1**, **2**, and **3** led to a dose-dependent increase of DHQ and a corresponding decrease in 2-ABA concentrations (Figure 5A). At highest inhibitor concentrations (**1-3**), the DHQ:2-ABA ratio was shifted to about 9:1, which clearly showed that the spontaneous decomposition of 2-ABA-CoA to DHQ predominated over the PqsE-mediated hydrolysis to 2-ABA. Due to the complexity of the coupled reaction, the apparent inhibition is not linearly correlating to PqsE thioesterase inhibition (model described in the SI, Figure S1), impeding exact quantitative conclusions.

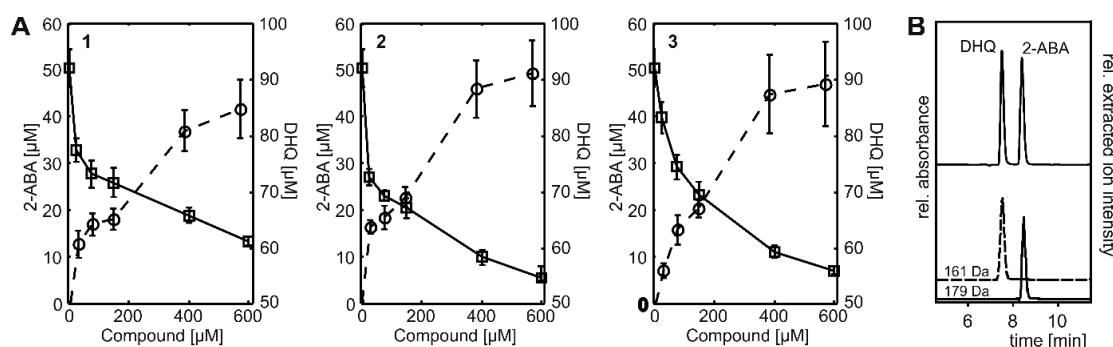


Figure 5. Coupled PqsDE assay. **(A)** effect of compounds **1**, **2** and **3** (from left to right) on 2-ABA concentration (depicted as \square) and DHQ concentration (depicted as \circ); inhibitor compound concentration shown on the x-axis. Data are from 2 independent experiments, each with 3 technical replicates. Error bars denote standard errors (SEM). **(B)** Exemplary LC-MS chromatogram illustrating the separation of DHQ (161 Da) and 2-ABA (179 Da); upper row: UV trace (322 nm) of mixture of reference compounds; lower row: extracted ion chromatograms (m/z bandwidth 0.3 Da).

To address this issue and to simplify the assay conditions, we used *S*-(4-nitrobenzoyl)mercaptoethane as an artificial PqsE substrate.²¹ According to the protocol of Yu *et al.*, the release of ethanethiol was followed photometrically using Ellman's reagent. Compounds **1-3** were able to inhibit this reaction showing IC_{50} values in the micromolar range (**1** $IC_{50} = 25 \pm 4 \mu M$; **2** $IC_{50} = 155 \pm 38 \mu M$; **3** $IC_{50} = 40 \pm 12 \mu M$). Taken together, the fragments identified by DSF showed inhibition of the isolated enzyme using an artificial substrate and were also active in a combined PqsDE assay reflecting a part of the natural AQ biosynthetic cascade.

In vivo characterization. Given that the hit compounds (**1-3**) inhibited the thioesterase activity of PqsE *in vitro*, we next asked if they are also active in *P. aeruginosa* and interrupt PqsE's role in virulence factor generation. To this end, we made use of the observation that a *pqsE* deletion mutant showed levels of HHQ comparable to those of wild-type *P. aeruginosa*,^{9,10} but strongly increased levels of DHQ.¹⁵ The biosynthesis of DHQ requires the enzymes PqsA and PqsD and DHQ emerges from spontaneous cyclisation of 2-ABA-CoA (Figure 2), whose concentration will be elevated in the absence of PqsE or when PqsE's thioesterase activity is inhibited.^{13,14,34} Consequently, compounds **1-3** were tested for their effect on HHQ and DHQ production in PAO1wt and PAO1*pqsE*. All three compounds (**1-3**) displayed a dose-dependent induction of DHQ formation in PAO1wt (Figure 6).

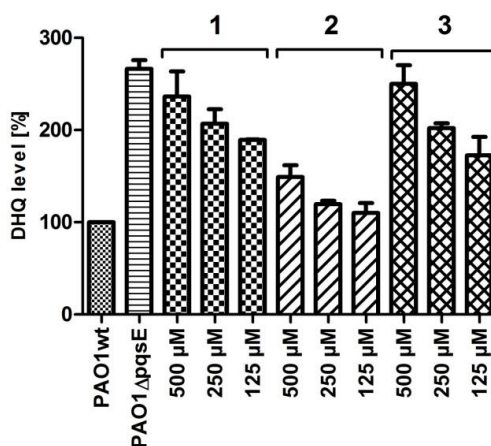


Figure 6. Effect of screening hits **1-3** on DHQ levels in PAO1. SD of the mean from at least two independent experiments with n=3.

Compounds **1** and **3** increased the DHQ levels almost up to the level found in the *pqsE* mutant strain. In contrast to compound **3**, **1** and **2** showed no additional inductive effect on DHQ production in the *pqsE* mutant, supporting an on-target mechanism of action in the living cell (SI, Figure S3). Moreover, no significant effect on HHQ levels (**1** and **2**) or only a low inhibition (**3**; SI, Figure S4) was found, which was in line with the results obtained for the *pqsE* mutant. Taken together, these findings clearly demonstrate that the PqsE thioesterase inhibitors (**1-3**) were able to permeate into *P. aeruginosa* and affect DHQ levels to a similar extent as deletion of the *pqsE* gene. Compounds (**1-3**) are therefore the first *in vivo* inhibitors of PqsE's thioesterase activity.

Knock-out studies clearly showed that production of the virulence factor pyocyanin, a blue redox-active phenazine pigment, depends on the presence of PqsE.^{10,18–20} Hence, hit compounds **1-3** were tested at 500 μM in PAO1 and the amount of pyocyanin was quantified photometrically after extraction. Notably, none of these PqsE thioesterase inhibitors had an inhibitory effect on pyocyanin production (Figure 7). This suggests that the regulatory function of PqsE is unrelated to its thioesterase activity.

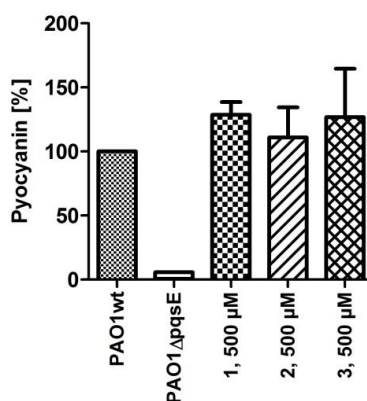


Figure 7. Effect of screening hits **1-3** on pyocyanin levels in PAO1. SD of the mean from three independent experiments with n=3

It has been shown that PqsE amplifies the induction of gene transcription by the QS regulator RhIR through an unknown mechanism, which leads to increased production of virulence factors (e.g. pyocyanin).^{18,20} To gain further insight, we sought to investigate the effect of our compounds on this PqsE-RhIR-mediated response. Farrow *et al.* described a heterologous *E. coli* reporter gene system to quantify the sensitizing effect of PqsE on C4-HSL-induced RhIR activity.¹⁸ We used this system to investigate whether the discovered PqsE ligands could attenuate this effect of PqsE. Compounds **1-3** were tested at 500 μ M in two *E. coli* strains: the first harboring an *rhIR-lacZ* reporter plasmid and a plasmid constitutively expressing PqsE; the second carrying the same *rhIR-lacZ* reporter and an empty plasmid vector. When comparing both reporter strains, the galactosidase activity in response to 10 μ M C4-HSL was enhanced 2.4-fold in the presence of PqsE. This ratio was not significantly altered upon addition of compounds **1-3** (Figure 8). It has to be noted that RhIR-mediated expression was marginally increased by our compounds regardless of the absence or presence of PqsE. Nevertheless, our data clearly show that the thioesterase inhibitors **1-3** do not interfere with the RhIR mediated regulatory function of PqsE, which is consistent with the unaffected pyocyanin levels observed in *P. aeruginosa*. This further supports the hypothesis of the PqsE regulatory function not being linked to its thioesterase activity.

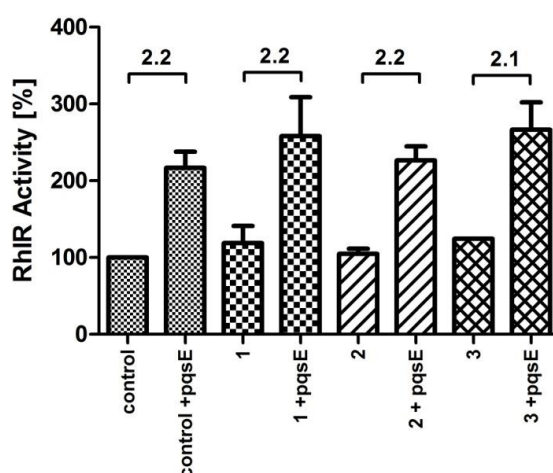


Figure 8. Effects of compounds **1-3** on the PqsE sensitizing effect on RhIR in *E. coli*. Bars represent RhIR-mediated β -galactosidase expression in percent (control =100%), in the presence of 500 μ M compound or DMSO as control. *E. coli* cultures harbour two plasmids: RhIR reporter gene plasmid and a plasmid for PqsE expression as indicated on the bars or the empty vector plasmid. RhIR was agonized with 10 μ M C4HSL. Numbers on the black lines over the bars represent the ratio of the sensitizing effect. SD of the mean from two independent experiments with n=4.

Conclusion

It has become more and more evident that *P. aeruginosa* colonies are not just an accumulation of unicellular organisms but rather highly organized communities. This behavior necessitates the use of fine-tuned regulatory mechanisms. In our study, we demonstrated the discovery of tool compounds, which shed light on the enigmatic role of PqsE within the complex QS regulatory systems of *P. aeruginosa*. A straightforward biophysical approach was initiated starting with a DSF screening of a fragment library, which led to various hits. Specific binding was proven for carboxylic acid derivatives **1-3** by ITC and protein crystallography. Moreover, the crystal structures revealed that all hit compounds bind to the catalytic center. The structure of PqsE in complex with its enzymatic product 2-ABA strongly indicated that all hits bind in competition to the native substrate 2-ABA-CoA. The identified PqsE ligands (**1-3**) inhibited the thioesterase activity of PqsE in two different *in vitro* assays. Applying these PqsE inhibitors to PAO1 cultures led to ambiguous results: On the one hand, an inductive effect on the DHQ levels similar to results of a *pqsE* mutant strain was observed. On the other hand, the production of virulence factor pyocyanin remained unaffected. These results are in accordance with the reported knock-out complementation studies showing that the effect of PqsE on pyocyanin does not depend on a functional *pqs* QS system.^{18,20} As virulence regulation is believed to be mainly mediated by RhIR, we evaluated the compounds in a combined PqsE-RhIR reporter gene assay. None of our thioesterase inhibitors influenced the RhIR-sensitizing effect of PqsE.

Based on these findings, we draw the conclusion that PqsE has two separate functions, the thioesterase enzymatic activity and the regulatory function, both working independently of each other. The use of small synthetic ligands allowed for the first time to distinguish between the two functions of PqsE. These results render the scenario quite unlikely that a so far not identified enzymatic activity of PqsE might be responsible for its regulatory function. The effect of PqsE on RhIR can be measured in a heterologous *E. coli* system in the absence of *Pseudomonas aeruginosa* QS specific components. Hence, we further hypothesize that this effect might arise rather from a protein-protein or protein-DNA/RNA interaction. Such interactions commonly occur on the protein surface, an area that was not affected upon binding of the PqsE ligands **1-3**, explaining the different results of these compounds regarding pyocyanin and AQs levels. However, this hypothesis remains to be corroborated. Due to its strong impact on *P. aeruginosa* virulence, PqsE remains a promising anti-virulence target. Future drug development should aim at the discovery of compounds that affect the regulatory role of PqsE. To this end, our thioesterase inhibitors might serve as valuable reference compounds or could even be used as molecular anchors for the design of larger compounds which address additional sites on the protein surface harboring the virulence-regulating function of PqsE.

Finally, the novel insight presented herein could not be gathered through knockout studies, which are routinely applied for target evaluation. Hence, we believe that fragment screening provides a rapid and facile method towards investigation of targets with elusive modes-of-action and should be considered as a reasonable complement to genetic target validation procedures.

EXPERIMENTAL PROCEDURES

Materials. PqsE was expressed heterologously in *E. coli*; a detailed protocol is given in the SI. PqsD and anthraniloyl-CoA were prepared as previously described.¹⁵ Malonyl-CoA was purchased from Sigma Aldrich. HPLC grade solvents were from Roth, Karlsruhe, Germany. Compounds **1-3** were initially sourced from the Maybridge fragment library as DMSO stocks and afterwards obtained from commercial suppliers: **1** (ChemPur GmbH), **2** (Maybridge) and **3** (ABCR GmbH). 2-ABA was synthesized as described previously,¹⁵ except that hydrogenation of the 2-nitrobenzoylacetate precursor was performed in 0.25 % ammonia solution at 25 psi for 30 min. The preparation yielded 2-ABA with approximately 95% purity (according to HPLC peak area).

Fragment screening by differential scanning fluorimetry. The used fragment library was obtained from Maybridge and stored as 10 mM DMSO solutions at 253°K. The DMSO fragments stocks were diluted (1:20) in freshly prepared DSF screening buffer (50 mM Tris-HCl, 150 mM NaCl, 2 mM MnCl₂, 10 % (v/v) glycerol, pH = 8.5) to give a final compound concentration of 500 μM at 5% (v/v) DMSO. The mastermix contained 4 μM H₆PqsE and 8-fold concentrated Sypro Orange (Sigma Aldrich). The mastermix was vigorously mixed by pipetting and shared into white opaque 96 well PCR plate FrameStar (GeneOn) using 2 or 3 wells per fragment. The loaded plate was sealed using PCR sealing foil and centrifuged at 1000 rpm for 1 min. Each plate contained a protein-only-control (POC) and 1000 μM anthranilic acid as positive control. The plate was heated in a StepOnePlus real-time PCR system (Applied Biosystems) with 1°K/min starting from 298°K to 368°K. The first derivations of obtained melting curves were analysed using the StepOne software and referenced against the POC. Fragments showing a shifted T_M were screened in a second experiment for validation. Fragment **1** was tested in dose-depend manner.

Isothermal Titration Calorimetry. ITC titrations were performed using a ITC₂₀₀ instrument (Microcal Inc., Malvern). DMSO stock solutions (20 mM) of fragments were diluted 1:20 (v/v) into ITC titration buffer (50 mM tricine, 2 mM MnCl₂, pH = 8.5) to give 1 mM final compound concentration at 5% (v/v) DMSO. Aliquots of the same buffer batch (stored at -253°K) were used as for protein storage to avoid buffer-mismatch. H₆PqsE was diluted in the same buffer to 100 μM and DMSO concentration was adjusted to 5% (v/v). Titrations were carried out at 298°K using 19 injections of 2 μL every 180s. Areas under the peaks were integrated. Baseline-peaks

at the end of a titration accounting for the heat of dilution and mixing were subtracted from the measurement. Data were fitted to a 1:1 binding model (MicroCal Origin 7 software).

Crystallization, Data Collection, Structure Solution, and Refinement. PqsE was crystallized in 0.1 M HEPES, 0.2 M MgCl₂ and 29-32 % (w/v) PEG400 at 293°K.²¹ The crystals were soaked with 0.5-10 mM 2-ABA or compounds **1-3** for 6-60 h and flash-cooled in liquid nitrogen. As the crystallization condition contained sufficient amounts of PEG400 no further cryoprotection was required. Diffraction data were collected at 100 K at beamline X06DA of the SLS synchrotron (Swiss Light Source, Paul Scherrer Insitutie, Villigen, Switzerland) for PqsE in complex with 2-ABA, compound **1** or compound **3** and at beamline BL14.2 of the BESSY II synchrotron (Berlin Electron Storage Ring Company for Synchrotron Radiation, Helmholtz Zentrum Berlin, Berlin, Germany) for PqsE in complex with compound **2**. Diffraction data were indexed and integrated with *XDS*³⁵ and scaled with *AIMLESS*.³⁶ Rigid-body refinement was performed with *REFMAC5*^{37,38} using the coordinates of the PDB entry 2Q0I.²¹ For model building *COOT*³⁹ was used and the structure was refined with *phenix.refine*⁴⁰ of the *PHENIX* software suite.⁴¹

Thioesterase Assay. The effect of compounds on the thioesterase activity of PqsE was measured using a procedure described by Yu et al. with slight modifications.²¹ The assay was carried out in 96 well plate (Nunc, clear, U-bottom) with an overall assay volume of 200 µL. The photometric measurements were performed on PHERAstar FS plate reader (BMG Labtech). H₆PqsE (2 µM) in assay buffer (50 mM Tricine, 2 mM MnCl₂, 2 mM Ellmanns reagent, 0.1 % (v/v) Tween80, pH = 8.5) was incubated for 10 min with different concentrations of test compound. Test compounds were added as DMSO stock solutions (5 µL, 1:40 dilution). Two controls were used: DMSO as reference control and a blank control without PqsE to monitor substrate hydrolysis. The enzymatic reaction was started by addition of the substrate S-(4-nitrobenzoyl)mercaptoethane (Matrix Scientific) dissolved in DMSO (5 µL; 500 µM final concentration) to give a final DMSO concentration of 5% (v/v). After vigorous mixing, the enzymatic reaction was followed photometrically at 412 nM using one measurement per minute over 15 min. Absorbance values were corrected for the blank controls and plotted over time. The derived slope (v_x) was used to calculate the residual enzyme activity (A_x) according to equation 1:

$$A_x = (v_x)/(v_0) \text{ (Equation 1)}$$

A_x corresponds to the enzyme activity, v_x measured slope of the enzymatic reaction in the presence of test compound; v_0 slope of the DMSO control. For the calculation of IC₅₀ values, A_x values were plotted against logarithmic inhibitor concentrations and fitted to the logistic model included in Origin 8.6 (Figure S2). The given values emerged from at least two independent experiments with n=4.

Coupled PqsDE assay. The thioesterase activity towards 2-ABA-CoA, the natural substrate of PqsE within the AQ biosynthesis pathway, was tested in a combined assay with PqsD. To this end, 0.5 μ M PqsD and 0.25 μ M PqsE were added to a mixture of 100 μ M anthraniloyl-CoA and 100 μ M malonyl-CoA in assay buffer (40 mM HEPES, pH 8.1, 40 mM NaCl and 2 mM MnCl₂). The total volume was 100 μ L. All components of the assay were supplemented with the respective inhibitor (in DMSO) prior to starting the reaction by mixing, thereby keeping the maximal DMSO concentration below 3% (v/v). Inhibitor concentrations were between 10 and 600 μ M. Reactions were stopped by adding 100 mM NH₄OH, 5 % isopropanol and subsequent freezing with liquid nitrogen. For analysis of the reaction products 2-ABA and DHQ, samples were thawed and centrifuged for 10 minutes at 20,000 \times g. Supernatants were analyzed by HPLC or HPLC-MS using a VWR LaChrom Elite HPLC system and a Thermo Dionex Ultimate 3000 UHPLC coupled to an amaZon speed ESI mass spectrometer (Bruker Daltonics), respectively. Separation was achieved using a Knauer Eurospher II C18H 150 \times 4 mm column and a chromatography program with 4 minutes isocratic flow at 5 % isopropanol/15 mM NH₄HCO₃ (pH 8.5) and a 15 minute gradient to 100 % acetonitrile at a flow of 0.6 mL/min. Concentrations were calculated from standards of authentic DHQ (Ferak, Berlin, Germany), 2-AA (Sigma-Aldrich, St. Louis, MO, USA) and 2-ABA, obtained by chemical synthesis.¹⁵ Runs with authentic 2-ABA verified its stability under the conditions used for HPLC and LC-MS. Data analysis and enzyme kinetic calculations were performed with Matlab R2015a optimization toolbox (Mathworks, Natick, MA, USA). Time dependent simulation of Michaelis-Menten kinetics was performed using the closed solution of Schnell and Medoza.⁴²

Quantification of HHQ and DHQ. In order to investigate the effects of PqsE ligands on the production of extracellular DHQ and HHQ, determination of these metabolites was performed according to a procedure modified from previously published methods.^{43,44} Briefly, cultures of *Pseudomonas aeruginosa* PAO1 or of its isogenic *pqsE* mutant as a reference were grown for 17 h in PPGAS medium⁴⁵ in the presence of inhibitors or DMSO as control. From each culture, DHQ and HHQ were worked-up in presence of 1 μ M of the internal standard 5,6,7,8-tetradeutero-2-heptyl-4(1H)-quinolone (HHQ-d4) by addition of methanol and by extraction with ethylacetate, respectively. UHPLC-MS/MS analysis was conducted as described by Storz *et al.*⁴³ monitoring the following ions (parent ion [m/z], product ion [m/z], scan time [s], scan width [m/z], collision energy [V], tube lens offset [V]): DHQ: 162, 89, 0.4, 0.02, 33, 52; HHQ: 244, 159, 0.5, 0.01, 30, 106; HHQ-d4: 248, 163, 0.1, 0.01, 32, 113. Xcalibur software was used for data acquisition and quantification using a calibration curve based on the peak area ratios of the respective analyte and the internal standard. Generally, triplicate samples were analyzed in at least two independent experiments. Values were given in percent of the DMSO control (PAO1wt control = 100%).

Pyocyanin assay. In order to assess the inhibitory potency of PqsE ligands towards the formation of virulence factor pyocyanin, we used a protocol adapted to previously reported procedures.^{46,47} In brief, cultures of *Pseudomonas aeruginosa* PAO1 incubated for 16 h with inhibitor or DMSO as control were extracted with chloroform and re-extracted with 0.2 M HCl. Pyocyanin was quantified by photometry and values were normalized by OD₆₀₀. All samples were analyzed at least in triplicate in three independent experiments except for PAO1

PqsE-RhIR reporter gene assay. To investigate the influence of the PqsE thioesterase inhibitors on the PqsE-mediated sensitizing effect on C4HSL/RhIR-dependent gene transcription, we performed an *E. coli*-based reporter gene assay according to the protocol by Farrow *et al.*¹⁸ with some modifications. Briefly, a two-plasmid system was used consisting of one plasmid including tacp-rhIR and a rhIA'-lacZ reporter gene fusion (pECP61.4) and a second plasmid, which was either the vector alone (pACYC184) or a plasmid harboring tacp-pqsE (pROSE04). Overnight cultures of *E. coli* DH5 α carrying the respective plasmid combinations were grown in supplemented A medium with the appropriate antibiotics and then diluted to an OD₆₀₀ of 0.2. After incubation of the subcultures at 310°K and 200 rpm to an OD₆₀₀ of 0.5, aliquots of 1 mL culture were transferred to a 96-deep-well plate containing dried C4-HSL and/or test compound in DMSO. The final assay concentrations were: 10 μ M C4-HSL, 500 μ M test compound, and 1% (v/v) DMSO. After 4 h of incubation at 310°K and 180 rpm, 300 μ L of the culture were transferred into a separate 96-deep-well plate for cell lysis. The lysis solution contained 800 μ L of chilled Z-buffer (40 mM NaH₂PO₄, 60 mM Na₂HPO₄, 10 mM KCl, 1 mM MgSO₄), 100 μ L of chloroform, and 50 μ L of 0.1% (m/v) sodium dodecyl sulfate. Cells were lysed by rigorous shaking for 30 s. The β -galactosidase activity was measured photometrically at OD₄₂₀ using PHERAstar Omega (BMG Labtech). Data are expressed as percent β -galactosidase induction of controls and represent mean values \pm the standard deviation of two independent experiments with n = 4. The given ratio was calculated by dividing the β -galactosidase activity in the presence of PqsE by the β -galactosidase activity in the absence of PqsE, respectively.

ASSOCIATED CONTENT

The X-ray structure reported herein have been deposited within the PDB with accession numbers: PDB: 5HIO, PqsE in complex with 2-aminobenzoylacetate (2-ABA); PDB: 5HIP PqsE in complex with 2-(pyridin-3-yl)benzoic acid (compound **1**); PDB: 5HIQ, PqsE in complex with 2-(1*H*-pyrrol-1-yl)benzoic acid (compound **2**); PDB: 5HIS, PqsE in complex with 3-methylthiophene-2-carboxylic acid (compound **3**).

REFERENCES

- (1) He, J., Baldini, R. L., Deziel, E., Saucier, M., Zhang, Q., Liberati, N. T., Lee, D., Urbach, J., Goodman, H. M., and Rahme, L. G. (2004). The broad host range pathogen *Pseudomonas aeruginosa* strain PA14 carries two pathogenicity islands harboring plant and animal virulence genes. *Proc. Natl. Acad. Sci. U.S.A.* 101, 2530–2535.
- (2) Stover, C. K., Pham, X. Q., Erwin, A. L., Mizoguchi, S. D., Warren, P., Hickey, M. J., Brinkman, F. S., Hufnagle, W. O., Kowalik, D. J., Lagrou, M., Garber, R. L., Goltry, L., Tolentino, E., Westbrook-Wadman, S., Yuan, Y., Brody, L. L., Coulter, S. N., Folger, K. R., Kas, A., Larbig, K., Lim, R., Smith, K., Spencer, D., Wong, G. K., Wu, Z., Paulsen, I. T., Reizer, J., Saier, M. H., Hancock, R. E., Lory, S., and Olson, M. V. (2000). Complete genome sequence of *Pseudomonas aeruginosa* PAO1, an opportunistic pathogen. *Nature* 406, 959–964.
- (3) Bodey, G. P., Bolivar, R., Fainstein, V., and Jadeja, L. (1983). Infections Caused by *Pseudomonas aeruginosa*. *Clin. Infect. Dis.* 5, 279–313.
- (4) Speert, D. P., Campbell, M. E., Henry, D. A., Milner, R., Taha, F., Gravelle, A., Davidson, A. G. F., Wong, L. T. K., and Mahenthiralingam, E. (2002). Epidemiology of *Pseudomonas aeruginosa* in Cystic Fibrosis in British Columbia, Canada. *Am. J. Respir. Crit. Care Med.* 166, 988–993.
- (5) Schuster, M., and Greenberg, E. P. (2006). A network of networks: quorum-sensing gene regulation in *Pseudomonas aeruginosa*. *Int. J. Med. Microbiol.* 296, 73–81.
- (6) Passador, L., Cook, J., Gambello, M., Rust, L., and Iglewski, B. (1993). Expression of *Pseudomonas aeruginosa* virulence genes requires cell-to-cell communication. *Science* 260, 1127–1130.
- (7) Ochsner, U. A., and Reiser, J. (1995). Autoinducer-mediated regulation of rhamnolipid biosurfactant synthesis in *Pseudomonas aeruginosa*. *Proc. Natl. Acad. Sci. U.S.A.* 92, 6424–6428.
- (8) Pesci, E. C., Milbank, J. B. J., Pearson, J. P., McKnight, S., Kende, A. S., Greenberg, E. P., and Iglewski, B. H. (1999). Quinolone signaling in the cell-to-cell communication system of *Pseudomonas aeruginosa*. *Proc. Natl. Acad. Sci. U.S.A.* 96, 11229–11234.
- (9) Déziel, E., Lépine, F., Milot, S., He, J., Mindrinos, M. N., Tompkins, R. G., and Rahme, L. G. (2004). Analysis of *Pseudomonas aeruginosa* 4-hydroxy-2-alkylquinolines (HAQs) reveals a role for 4-hydroxy-2-heptylquinoline in cell-to-cell communication. *Proc. Natl. Acad. Sci. U.S.A.* 101, 1339–1344.
- (10) Gallagher, L. A., McKnight, S. L., Kuznetsova, M. S., Pesci, E. C., and Manoil, C. (2002). Functions Required for Extracellular Quinolone Signaling by *Pseudomonas aeruginosa*. *J. Bacteriol.* 184, 6472–6480.
- (11) Wade, D. S., Calfee, M. W., Rocha, E. R., Ling, E. A., Engstrom, E., Coleman, J. P., and Pesci, E. C. (2005). Regulation of *Pseudomonas* quinolone signal synthesis in *Pseudomonas aeruginosa*. *J. Bacteriol.* 187, 4372–4380.
- (12) Coleman, J. P., Hudson, L. L., McKnight, S. L., Farrow, J. M., Calfee, M. W., Lindsey, C. A., and Pesci, E. C. (2008). *Pseudomonas aeruginosa* PqsA is an anthranilate-coenzyme A ligase. *J. Bacteriol.* 190, 1247–1255.
- (13) Zhang, Y.-M., Frank, M. W., Zhu, K., Mayasundari, A., and Rock, C. O. (2008). PqsD Is Responsible for the Synthesis of 2,4-Dihydroxyquinoline, an Extracellular Metabolite Produced by *Pseudomonas aeruginosa*. *J. Biol. Chem.* 283, 28788–28794.
- (14) Dulcey, C. E., Dekimpe, V., Fauvelle, D.-A., Milot, S., Groleau, M.-C., Doucet, N., Rahme, L. G., Lépine, F., and Déziel, E. (2013). The end of an old hypothesis: the *Pseudomonas* signaling molecules 4-hydroxy-2-alkylquinolines derive from fatty acids, not 3-ketofatty acids. *Chem. Biol.* 20, 1481–1491.
- (15) Drees, S. L., and Fetzner, S. (2015). PqsE of *Pseudomonas aeruginosa* Acts as Pathway-Specific Thioesterase in the Biosynthesis of Alkylquinolone Signaling Molecules. *Chem. Biol.* 22, 611–618.
- (16) Schertzer, J. W., Brown, S. A., and Whiteley, M. (2010). Oxygen levels rapidly modulate *Pseudomonas aeruginosa* social behaviours via substrate limitation of PqsH. *Mol. Microbiol.* 77, 1527–1538.
- (17) Xiao, G., Déziel, E., He, J., Lépine, F., Lesic, B., Castonguay, M.-H., Milot, S., Tampakaki, A. P., Stachel, S. E., and Rahme, L. G. (2006). MvfR, a key *Pseudomonas aeruginosa* pathogenicity LTTR-class regulatory protein, has dual ligands. *Mol. Microbiol.* 62, 1689–1699.

- (18) Farrow, J. M., Sund, Z. M., Ellison, M. L., Wade, D. S., Coleman, J. P., and Pesci, E. C. (2008). PqsE functions independently of PqsR-Pseudomonas quinolone signal and enhances the rhl quorum-sensing system. *J. Bacteriol.* 190, 7043–7051.
- (19) Rampioni, G., Pustelny, C., Fletcher, M. P., Wright, V. J., Bruce, M., Rumbaugh, K. P., Heeb, S., Cámara, M., and Williams, P. (2010). Transcriptomic analysis reveals a global alkyl-quinolone-independent regulatory role for PqsE in facilitating the environmental adaptation of *Pseudomonas aeruginosa* to plant and animal hosts. *Environ. Microbiol.* 12, 1659–1673.
- (20) Hazan, R., He, J., Xiao, G., Dekimpe, V., Apidianakis, Y., Lesic, B., Astrakas, C., Déziel, E., Lépine, F., and Rahme, L. G. (2010). Homeostatic interplay between bacterial cell-cell signaling and iron in virulence. *PLoS Pathog.* 6, e1000810.
- (21) Yu, S., Jensen, V., Seeliger, J., Feldmann, I., Weber, S., Schleicher, E., Häussler, S., and Blankenfeldt, W. (2009). Structure elucidation and preliminary assessment of hydrolase activity of PqsE, the *Pseudomonas* quinolone signal (PQS) response protein. *Biochemistry* 48, 10298–10307.
- (22) Folch, B., Déziel, E., and Doucet, N. (2013). Systematic mutational analysis of the putative hydrolase PqsE: toward a deeper molecular understanding of virulence acquisition in *Pseudomonas aeruginosa*. *PLoS ONE* 8, e73727.
- (23) Mills, S. D. (2006). When will the genomics investment pay off for antibacterial discovery? *Biochem. Pharmacol. (Amsterdam, Neth.)* 71, 1096–1102.
- (24) Payne, D. J., Gwynn, M. N., Holmes, D. J., and Pompliano, D. L. (2007). Drugs for bad bugs: confronting the challenges of antibacterial discovery. *Nat. Rev. Drug Discovery* 6, 29–40.
- (25) O'Shea, R., and Moser, H. E. (2008). Physicochemical properties of antibacterial compounds: implications for drug discovery. *J. Med. Chem.* 51, 2871–2878.
- (26) Waldrop, G. L. (2009). Smaller is better for antibiotic discovery. *ACS Chem. Biol.* 4, 397–399.
- (27) Zender, M., Klein, T., Henn, C., Kirsch, B., Maurer, C. K., Kail, D., Ritter, C., Dolezal, O., Steinbach, A., and Hartmann, R. W. (2013). Discovery and biophysical characterization of 2-amino-oxadiazoles as novel antagonists of PqsR, an important regulator of *Pseudomonas aeruginosa* virulence. *J. Med. Chem.* 56, 6761–6774.
- (28) Mashalidis, E. H., Śledź, P., Lang, S., and Abell, C. (2013). A three-stage biophysical screening cascade for fragment-based drug discovery. *Nat. Protoc.* 8, 2309–2324.
- (29) Niesen, F. H., Berglund, H., and Vedadi, M. (2007). The use of differential scanning fluorimetry to detect ligand interactions that promote protein stability. *Nat. Protoc.* 2, 2212–2221.
- (30) Vedadi, M., Niesen, F. H., Allali-Hassani, A., Fedorov, O. Y., Finerty, P. J., Wasney, G. A., Yeung, R., Arrowsmith, C., Ball, L. J., Berglund, H., Hui, R., Marsden, B. D., Nordlund, P., Sundstrom, M., Weigelt, J., and Edwards, A. M. (2006). Chemical screening methods to identify ligands that promote protein stability, protein crystallization, and structure determination. *Proc. Natl. Acad. Sci. U.S.A.* 103, 15835–15840.
- (31) Alessio Ciulli, C. A. (2008). Fragment-based approaches to enzyme inhibition Alessio Ciulli and Chris Abell. *Curr. Opin. Biotechnol.* 18, 489–496.
- (32) Storz, M. P., Brengel, C., Weidel, E., Hoffmann, M., Hollemeyer, K., Steinbach, A., Müller, R., Empting, M., and Hartmann, R. W. (2013). Biochemical and biophysical analysis of a chiral PqsD inhibitor revealing tight-binding behavior and enantiomers with contrary thermodynamic signatures. *ACS Chem. Biol.* 8, 2794–2801.
- (33) Ladbury, J. E., Klebe, G., and Freire, E. (2010). Adding calorimetric data to decision making in lead discovery: a hot tip. *Nat. Rev. Drug Discovery* 9, 23–27.
- (34) Lépine, F., Dekimpe, V., Lesic, B., Milot, S., Lesimple, A., Mamer, O. A., Rahme, L. G., and Déziel, E. (2007). PqsA is required for the biosynthesis of 2,4-dihydroxyquinoline (DHQ), a newly identified metabolite produced by *Pseudomonas aeruginosa* and *Burkholderia thailandensis*. *Biol. Chem.* 388.
- (35) Kabsch, W. (2010). XDS. *Acta Crystallogr., Sect. D: Biol. Crystallogr.* 66, 125–132.
- (36) Evans, P. R., and Murshudov, G. N. (2013). How good are my data and what is the resolution? *Acta Crystallogr., Sect. D: Biol. Crystallogr.* 69, 1204–1214.

- (37) Vagin, A. A., Steiner, R. A., Lebedev, A. A., Potterton, L., McNicholas, S., Long, F., and Murshudov, G. N. (2004). REFMAC5 dictionary: organization of prior chemical knowledge and guidelines for its use. *Acta Crystallogr., Sect. D: Biol. Crystallogr.* 60, 2184–2195.
- (38) Winn, M. D., Ballard, C. C., Cowtan, K. D., Dodson, E. J., Emsley, P., Evans, P. R., Keegan, R. M., Krissinel, E. B., Leslie, A. G. W., McCoy, A., McNicholas, S. J., Murshudov, G. N., Pannu, N. S., Potterton, E. A., Powell, H. R., Read, R. J., Vagin, A., and Wilson, K. S. (2011). Overview of the CCP4 suite and current developments. *Acta Crystallogr., Sect. D: Biol. Crystallogr.* 67, 235–242.
- (39) Emsley, P., Lohkamp, B., Scott, W. G., and Cowtan, K. (2010). Features and development of Coot. *Acta Crystallogr., Sect. D: Biol. Crystallogr.* 66, 486–501.
- (40) Afonine, P. V., Grosse-Kunstleve, R. W., Echols, N., Headd, J. J., Moriarty, N. W., Mustyakimov, M., Terwilliger, T. C., Urzhumtsev, A., Zwart, P. H., and Adams, P. D. (2012). Towards automated crystallographic structure refinement with phenix.refine. *Acta Crystallogr., Sect. D: Biol. Crystallogr.* 68, 352–367.
- (41) Adams, P. D., Afonine, P. V., Bunkóczi, G., Chen, V. B., Davis, I. W., Echols, N., Headd, J. J., Hung, L.-W., Kapral, G. J., Grosse-Kunstleve, R. W., McCoy, A. J., Moriarty, N. W., Oeffner, R., Read, R. J., Richardson, D. C., Richardson, J. S., Terwilliger, T. C., and Zwart, P. H. (2010). PHENIX: a comprehensive Python-based system for macromolecular structure solution. *Acta Crystallogr., Sect. D: Biol. Crystallogr.* 66, 213–221.
- (42) Schnell, S., and Mendoza, C. (1997). Closed Form Solution for Time-dependent Enzyme Kinetics. *J. Theor. Biol.* 187, 207–212.
- (43) Storz, M. P., Maurer, C. K., Zimmer, C., Wagner, N., Brengel, C., Jong, J. C. de, Lucas, S., Müsken, M., Häussler, S., Steinbach, A., and Hartmann, R. W. (2012). Validation of PqsD as an anti-biofilm target in *Pseudomonas aeruginosa* by development of small-molecule inhibitors. *J. Am. Chem. Soc.* 134, 16143–16146.
- (44) Lépine, F., Milot, S., Déziel, E., He, J., and Rahme, L. G. (2004). Electrospray/mass spectrometric identification and analysis of 4-hydroxy-2-alkylquinolines (HAQs) produced by *Pseudomonas aeruginosa*. *J. Am. Soc. Mass Spectrom.* 15, 862–869.
- (45) Zhang, Y., and Miller, R. M. (1992). Enhanced octadecane dispersion and biodegradation by a *Pseudomonas* rhamnolipid surfactant (biosurfactant). *Appl. Environ. Microbiol.* 58, 3276–3282.
- (46) Essar, D. W., Eberly, L., Hadero, A., and Crawford, I. P. (1990). Identification and characterization of genes for a second anthranilate synthase in *Pseudomonas aeruginosa*: interchangeability of the two anthranilate synthases and evolutionary implications. *J. Bacteriol.* 172, 884–900.
- (47) Klein, T., Henn, C., Jong, J. C. de, Zimmer, C., Kirsch, B., Maurer, C. K., Pistorius, D., Müller, R., Steinbach, A., and Hartmann, R. W. (2012). Identification of small-molecule antagonists of the *Pseudomonas aeruginosa* transcriptional regulator PqsR: biophysically guided hit discovery and optimization. *ACS Chem. Biol.* 7, 1496–1501.

4 Final Discussion

“Großes entsteht immer im Kleinen [big things come from small beginnings]”¹

The literal meaning of this advertising slogan aptly summarizes the overall strategy of fragment-based drug design – the structure of a small, weak but efficient binding fragment is gradually extended to generate a bigger lead molecule. The application of such an approach for the development of innovative antimicrobials against the virulence of *P. aeruginosa* was the major task of this study (see chapter 2). In more detail, fragment-based methods were utilized for two different intentions: for the development of compounds targeting the transcriptional regulator PqsR as outlined in the chapters 3.1 to 3.3 and the discovery of tool compounds to examine the different functions of PqsE as described in chapter 3.4.

Despite spending many resources and efforts, the application of HTS to antibiotic drug discovery was not able to replenish the antibiotic development pipeline. (Payne et al., 2007) Mochalkin *et al.* argued that these negative outcomes can be explained by the use of HTS libraries optimized for human drug targets. (Mochalkin et al., 2009) This hypothesis is corroborated by the fact that antibiotics cover a clearly different chemical space than other drugs. (Payne et al., 2007; O'Shea and Moser, 2008) Until nowadays, natural products have been a fruitful source for the discovery of antibiotics (Walsh, 2003) which is emphasized by the recent discoveries like the griselimycins (Kling et al., 2015) and teixobactin (Ling et al., 2015). However, the size and complexity of these structures hamper a straightforward lead optimization by chemical synthesis. (Mochalkin et al., 2009)

Especially in the context of antibacterial drug discovery, the screening of low molecular weight fragments can be an attractive alternative to overcome these drawbacks. (Waldrop, 2009) A relatively small fragment library efficiently covers a comparably wide chemical space (Leach et al., 2006) and these less complex structures are more likely to form suitable interactions with a target protein (Hann et al., 2001). Furthermore, the simplicity of such molecules facilitates synthetic accessibility and subsequent generation of drug-like molecules.

In the interest of convenience, the compound numbering in the following discussion is complemented by the addition of a capital letter referring to the corresponding chapter (e.g. compound **A2** refers to compound **2** shown in chapter **A**)

¹ slogan of the Saarland marketing campaign 2014 and matching English proverb

4.1 Development of PqsR Antagonists

Chapter A deals with the discovery of PqsR antagonist with a 2-amino-5-phenyl-1,3,4-oxadiazole scaffold. The thiadiazol **A5** was found in an SPR fragment screening and selected as starting point for further synthesis based on its high affinity and mixed agonistic/antagonistic properties in the *E. coli* reporter gene assay. Another highly similar hit **A9** containing an oxadiazole heterocycle was lower ranked according to its affinity but showed pure antagonistic activity. This finding gave a hint for the first fragment modifications. The outcome of this study is summarized in Figure 11. The combination of an oxadiazole heterocycle (Figure 12, Position A) with halogens like Cl and Br or halogen-isosters like CN and CF₃ in 3-position (Figure 12, Position B) led to antagonists showing potencies in the low micromolar range. Compound **A37** emerged from this activity-guided optimization approach as top candidate and showed antivirulence activities in *P. aeruginosa*. These results nicely demonstrate the value of the *E. coli* test system (Cugini et al., 2007) which allows the unbiased profiling of the functional properties even of weak interacting fragments. On the other hand, such a heterologous system does not provide any information whether a particular compound class can unfold its activity also in the target organism. A lack of activity in *P. aeruginosa* may have different reasons: Its cell envelop can be hardly permeable for xenobiotics (Nicas and Hancock, 1983). Furthermore, the presence of broad spectrum efflux pumps (Masuda et al., 2000) and enzymatic degradation as observed for the quinolone-derived PqsR antagonists (Lu et al., 2014) can result in an insufficient concentration at the target site. Therefore, the proof that a compound is active in *P. aeruginosa* should be provided as early as possible during the course of a project. This claim is confirmed by the fact that late-stage introduction of *in cellulo* activity by use of synthetic modifications is hardly to achieve as observed during the development of PqsD inhibitors. (Sahner et al., 2015)

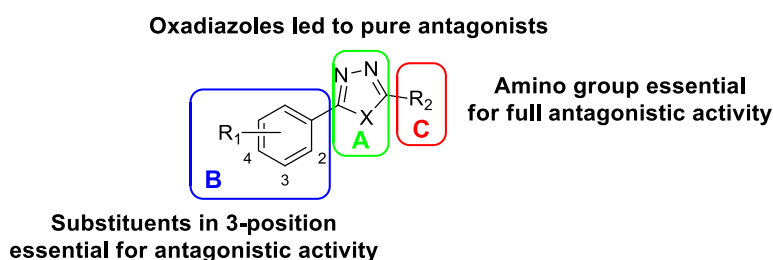


Figure 12: SAR obtained for the oxadiazole compound class

At this time, the crystal structure of the PqsR LBD was not published but the two amino acids F221 and Q194 were known to be located within the binding pocket. (Klein et al., 2012) Site-directed mutagenesis in combination with ITC analysis was applied to map the space covered by different fragments. This analysis revealed that carboxamide **A2** and oxadiazole **A37** share overlapping space in the pocket but adopted different binding modes. INPHARMA NMR

corroborated the competitive binding of both molecules but could not show which parts of both molecules overlaid. Notably, the application of such biophysical tools can be an attractive alternative in the absence of crystal structure in complex with a ligand. Such a strategy was successfully applied for the structure-based optimization of PqsD inhibitors. (Sahner et al., 2013) In case of PqsR, the structural knowledge about the LBD comprised only the above mentioned amino acids as potential partners for directed interactions. Hence, these efforts led to a rough idea about orientation of both compound classes but these insights did not translate into defined suggestions for further optimization. Moreover, the subsequently published crystal structure of PqsR in complex with NHQ (Introduction, Figure 9) revealed only hydrophobic protein-ligand interactions (Ilango et al., 2013) which might be hardly traceable in such an approach.

In the next step, structural modifications of the amino moiety (Figure 12, Position C) in combination with ITC analysis were carried out. Comparing the thermodynamic profiles of **A37** and **A47** suggested that the amino group does not form directed interactions with the receptor. Subsequent replacement or methylation (**A48-A53**) led to a complete loss of the antagonistic activity. These findings disqualified this moiety as handle for an enlargement of the scaffold.

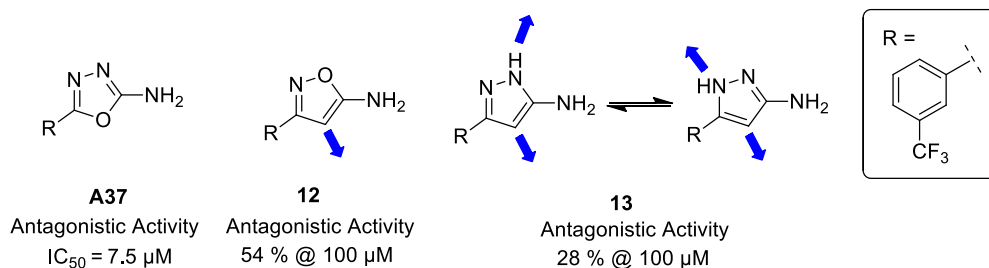


Figure 13: Bioisosteric replacement of the oxadiazole heterocycle (blue arrows represent potential growth vectors). Compounds **12** and **13** were obtained from commercial suppliers and antagonistic activities were measured in the *E. coli* reporter gene assay as described in chapter A.

During fragment optimization, it was not possible to identify a vector to extend the fragment structure. The constitution of the oxadiazole heterocycle does not allow the addition of further substituents. The bioisosteric replacement of the latter one for five-membered rings offering potential growth vectors (**12** and **13**, Figure 13) resulted in a drop of the antagonistic activity. Therefore, the further development of the 2-amino-oxadiazoles class was deprioritized in favor of an alternative scaffold as described in Chapter B.

Whereas the selection of **A5** was based on a combination of its functional properties and affinity, the 2-amino-pyridine **B3** was chosen due to its outstanding EE and LE values. The mainly lipophilic nature of the LBD of PqsR (Figure 9) makes the rational design of directed non-covalent interactions a difficult task. Hence, the enthalpic contribution as an indication of such interactions (Ladbury et al., 2010) was utilized as major selection criterion for hit nomination. The hit fragment **B3** showed a completely enthalpy-driven binding which is reflected in an

impressive EE of 1.17. This value indicates a good complementary shape between polar groups of the ligand and the receptor. (Ladbury et al., 2010) The potential of **B3** is also highlighted by its LE of 0.85 which significantly exceeded the minimum level (LE > 0.3) for a straightforward optimization (Hopkins et al., 2004). Moreover, the compact size of **B3** offers several positions for a fragment-growing approach.

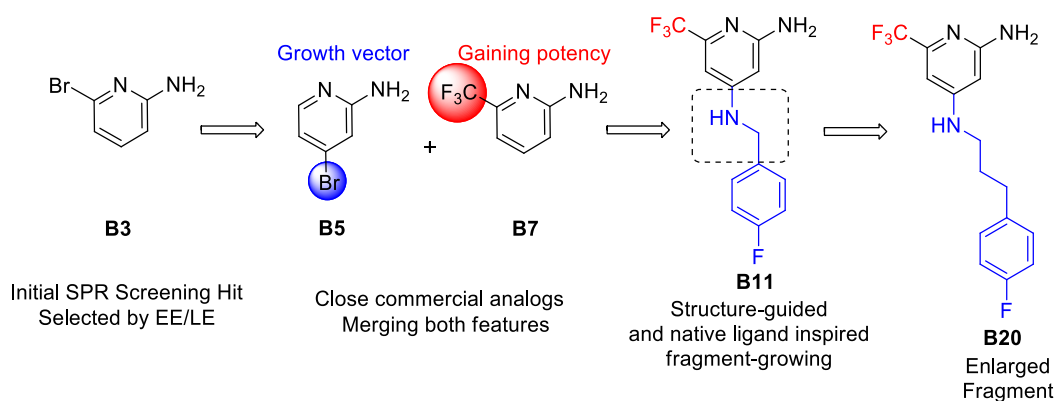


Figure 14: Fragment-growing strategy for 2-amino-pyridines

Due to the absence of structural information, close commercial analogs of **B3** were screened for their affinity to PqsR by ITC to establish a preliminary SAR. In doing so, compounds **B5** and **B7** were identified which guided further ligand design (Figure 14). **B5** promoted the 4-position of the pyridine ring as most promising growth vector and the exchange of Br for a CF₃ (**B7**) led to increased affinity and antagonistic activity. Furthermore, **B7** showed inhibition of pyocyanin, thereby, providing the first proof that the amino-pyridine scaffold is able to permeate into *P. aeruginosa*.

The next step aimed at the introduction of different moieties into the 4-position of **B7**. To accomplish this, the synthesis of intermediate **B4e** was pursued. The key step involved the introduction of the amino moiety into the 2-position of the pyridine ring. The reaction conditions were optimized up to 86:14 regioselectivity making **B4e** accessible in gram scale. The attachment of a flexible benzylamine moiety (**B11**, Figure 14) by a Buchwald-Hartwig cross coupling reaction led to boost in antagonistic activity and affinity.

The structure of the PqsR LBD in complex with **B11** could be solved (Figure 15). Additionally, the binding mode of antagonist **B11** was investigated by site-directed mutagenesis in combination with ITC (Figure 16). The crystal structure revealed that **B11** adopts an angled conformation in which the amino pyridine headgroup is located in the quinolone pocket and the 4-fluoro-phenyl moiety points into the alkyl chain pocket.

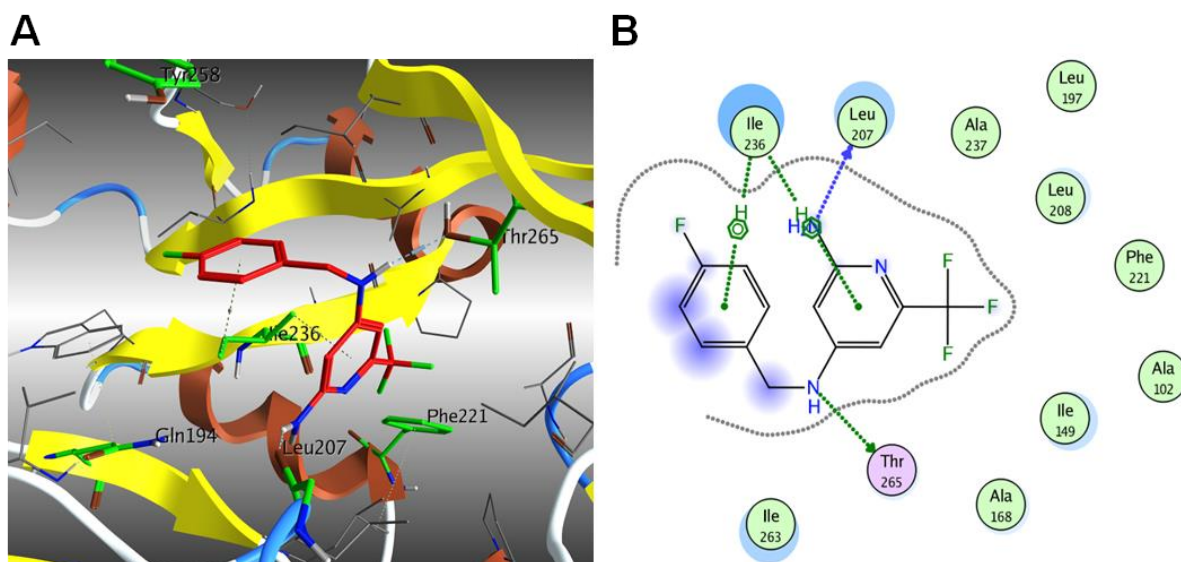


Figure 15: A) Crystal structure of PqsR LBD in complex with **B11** (ligand in red, key residues highlighted in green). B) 2-D summary of the observed ligand-receptor interactions

A comparison of the protein- ligand interactions observed in the crystal structure and the results obtained by ITC measurements illustrates the difficulty in the interpretation of thermodynamic data. A loss in the enthalpic contribution was observed when **B11** binds to PqsR_{F221A} (Figure 15C) indicating a strong interaction with this amino acid side chain. In contrary, the crystal structure revealed that F221 is more than 3.5 Å away from the ligand what is a strong argument against a direct interaction. This discrepancy might be due to the fact that the omission of this phenyl ring (phenylalanine to alanine mutation) has an impact on the overall protein conformation (Matthews, 1993) or allows the compound to adopt an alternative binding mode.

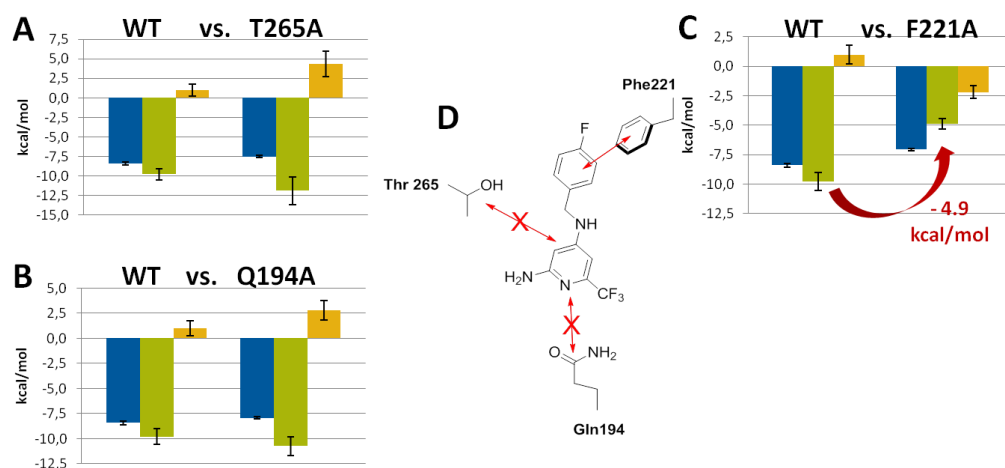


Figure 16: A-C) Thermodynamic profiles of **B11** binding to PqsR_{WT} compared to T265A, Q194A and F221A mutated PqsR, respectively (ΔG in blue, ΔH in green and $-T\Delta S$ in yellow). D) Schematic summary of the ITC-suggested interactions of **B11** with PqsR. Data derived from at least two independent experiments.

The *vice versa* scenario was observed for T265: The crystal structure clearly showed an H-bond interaction (Figure 14) whereas the enthalpy term was not significantly changed (Figure 15A). The observation that the formation of H-bond did not necessarily lead to a gain in enthalpy has been reported for different other protein-ligand pairs.(Connelly et al., 1994; Winquist et al., 2013) Moreover, Geschwinder *et al.* argued in a recent article that enthalpy and entropy are influenced by multiple factors e.g. solvation and conformational flexibility.(Geschwindner et al., 2015) These features are highly sensitive to even small changes on the ligand or the protein side what might mask the real contribution of a single protein-ligand interaction.(Geschwindner et al., 2015) These findings highlight that the use of thermodynamic data for the generation/validation of a hypothetical binding mode should be considered carefully.

By the use of structure-based methods, the structure of **B11** was step-by-step extended to point deeper into the alkyl chain pocket. This strategy afforded compound **B20** (Figure 13) as top candidate showing potent pyocyanin inhibition in *P. aeruginosa*. In this approach antagonistic activity was increased by the introduction of a flexible linker. Hondo *et al.* described a similar approach starting also from a highly efficient binding hit fragment (Hondo et al., 2013). This indicates that such a strategy might be applicable for a broader scope of target proteins.

Chapter C covers the development of hybrid PqsR antagonists by merging of fragment **B11** with the recently reported HTS hit **C2** (Starkey et al., 2014). The quinolone-derived antagonists **C1** (Lu et al., 2014) and **C2** share a nitro group as common structural feature. The position of the latter within the binding pocket was modeled based on a close HHQ analog. Subsequently, the binding mode of **C2** was investigated by a pharmacophore-guided docking study with the nitro group as an essential feature. A superimposition of the generated docking poses of **C2** and the crystal structure of **B11** (Figure 14) suggested to combine features of both scaffolds.

The introduction of thioglycolamide-aryl moieties at the 4-position of the amino-pyridine headgroup resulted in the most promising hybrid antagonists (Figure 16). The SAR derived from this small series of compounds is summarized in Figure 16. The exchange of a chlorine substituent for a phenoxy moiety led to tremendous increase in the antagonistic activity in *E. coli* as well as the anti-virulence activity in *P. aeruginosa* (e.g. **C7** vs. **C10**). This finding is in accordance with the SAR reported for the benzamido-benzimidazole scaffold (**C2**, **C3**). (Starkey et al., 2014)

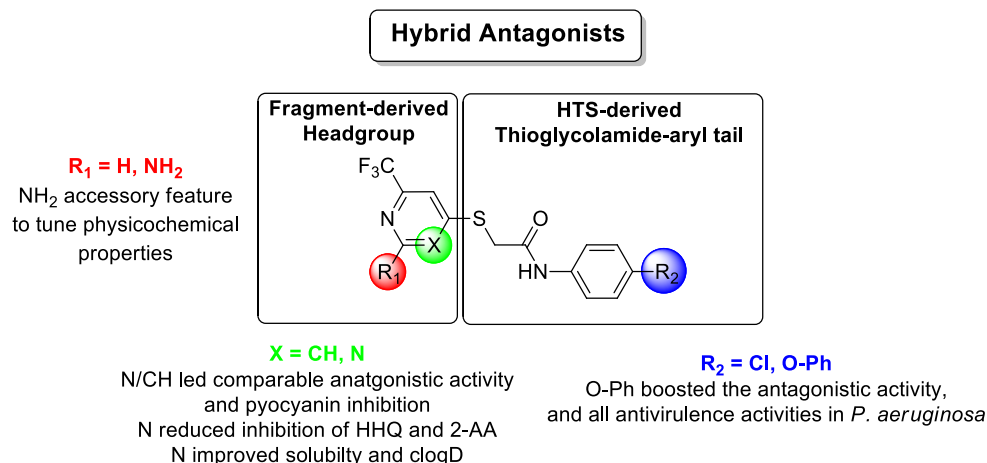


Figure 17: Overview of the SAR of hybrid PqsR antagonists.

The omission of the amino function at the pyridine head group resulted in a compound with a comparable anti-virulence profile; the antagonistic activity was even slightly enhanced (**C10** vs. **C13**). Given that during most fragment-growing approaches the initial protein-ligand interactions were retained (Hartshorn et al., 2005), this finding was not expected and might be due to the unconventional merging approach. Normally, the hit structure is extended gradually, whereas in this approach the large thioglycolamide-aryl moiety was added in a single step. As a consequence, the geometry of the linker might not be optimal what hinders the formation of an H-bond interaction as observed for **B11** (Figure 14). The exchange of a pyridine to a pyrimidine (**C10** to **C12**) led to ambiguous results: On the one hand, the antagonistic activity and pyocyanin inhibition were retained while improving the physico-chemical properties. On the other hand, the effect on HHQ and 2-AA was significantly lowered. Overall, the effects on virulence factor pyocyanin and HHQ levels differ regarding their response to the antagonization of PqsR depending on the compound used. But the finding that small synthetic modifications (as described above for **C10** to **C12**) influenced only the biosynthesis of HAQs without affecting pyocyanin levels implies that both parameters may be differently regulated by PqsR *via* a so far unknown mechanism. Another explanation would be that the particular compounds hit additional targets affecting pyocyanin or HHQ biosynthesis.

The antagonist **C12** showed reduction of eDNA in a *P. aeruginosa* static biofilm assay and inhibited the expression of lectinB. These effects are comparable to a *pqsR* negative strain. Furthermore, these compounds did not affect the viability of eukaryotic cells

In summary, the thiadiazole/oxadiazole (**A5/A9**) and the aminopyridine (**B3**) scaffold were selected out of the hits obtained in a SPR fragment screening. **A5** was transformed into a micromolar antagonist **A37** by small synthetic modifications. **B3** was developed into the potent nanomolar antagonist **B20**. This development process was initially guided by ITC and later on by the use of structure-based design methods. Additionally, **B3** was successfully combined with

moieties from an HTS hit (Starkey et al., 2014) leading to highly potent hybrid compounds **C10** and **C12**.

4.2 Discovery of PqsE Ligands

Chapter D describes the discovery and biological evaluation of synthetic PqsE ligands. At first, a library consisting of 500 fragments was screened using a thermal shift assay. This setup led to 10 initial hits. ITC was used as secondary screening tool and validated the binding of the carboxylic acid derivatives **D1-D3**. The crystal structures of **D1-D3** and enzymatic product **2-ABA** revealed that all these compounds form a complex with the iron center within the active site of PqsE and cover an overlapping space in this binding pocket. The discovered hits showed inhibition of the thioesterase enzymatic function of PqsE in two different *in vitro* assays. The profiling of these compounds in *P. aeruginosa* exhibited ambiguous results: On the one hand, the DHQ levels were elevated to a similar extent as measured in a *pqsE* negative strain proving that the hits were able to permeate into the bacterial cytoplasm. On the other hand, no effect on the major virulence factor pyocyanin was observed. The regulatory role of PqsE is at least partially mediated *via* the transcriptional regulator RhIR. (Farrow et al., 2008; Hazan et al., 2010) Farrow *et al.* showed that this sensitizing effect is also measurable in a heterologous *E. coli* reporter gene system. (Farrow et al., 2008) Hence, the compounds **D1-D3** were analyzed in this assay and showed no repression of this effect.

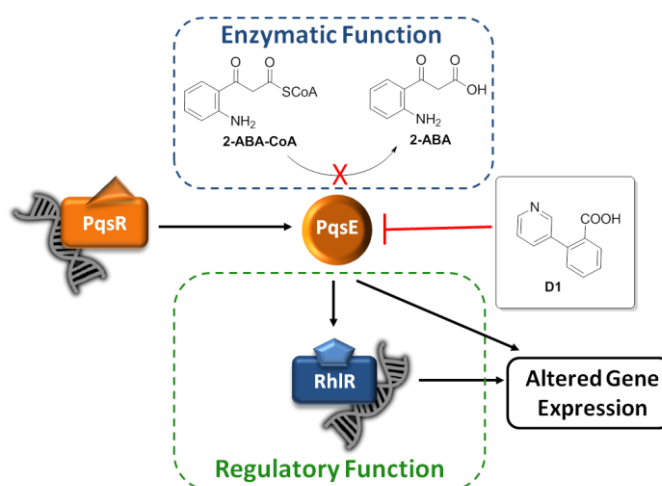


Figure 18: Schematic depiction of the different PqsE functions and the discovered screening hit **D1**.

Our results corroborate and extend the notion that PqsE has two functions which are working independently of each other (Figure 17). These insights classify PqsE as a member of the growing family of ‘moonlighting proteins’ – proteins performing multiple unrelated functions. (Huberts and van der Klei, 2010) Accordingly, the discovered compounds inhibited only the enzymatic activity but had no effect on the regulatory function. This is in line with knock-out complementation studies showing that PqsE unfolds its gene regulatory activity in

absence of a functional *pqs* system (Farrow et al., 2008). The obtained results allowed the hypothesis that the regulatory activity of PqsE is not linked to its enzymatic reaction taking place in the active center. Due to the fact that discovered compounds showed inhibition of the enzyme reaction *in vitro* and a similar DHQ/HHQ profile in *P. aeruginosa* as a *pqsE* negative strain, a not known enzymatic reaction should also be at least partially affected. A second argument for this hypothesis is the fact that the effect of PqsE on RhIR is also traceable in *E. coli* and, therefore, in the absence of the specific QS metabolome present in *P. aeruginosa*.(Farrow et al., 2008) Hence, it might be that the regulatory activity relies on a more general mechanism like a protein-protein or protein-DNA/RNA interaction. This assumption is further supported by the fact that an alanine scan identified amino acids at the protein surface leading to drastically reduced pyocyanin levels.(Folch et al., 2013) Notably, this study also found amino acids located in the active site which showed decreased pyocyanin production.(Folch et al., 2013) However, some of the latter are involved in the complexation of the double iron center. Mutations at this site might have a bigger impact on the overall protein structure than the ones at the protein surface.

This study contributes another important piece towards understanding complete 'PqsE puzzle'. In summary, by the use of fragment screening in combination with protein crystallography it was possible to discover tool compounds which allowed further insights into the different functions of PqsE. At this stage, it is not possible to conclusively evaluate the potential of PqsE as drug target. Moreover, it cannot be excluded that a fragment-growing approach would yield compounds providing additional features e.g. the interference with the gene regulatory activity

4.3 Outlook

The PqsR antagonists **B20** and **C10/C12** represent excellent candidates for further medicinal chemistry optimization. This optimization process should generate a lead compound suitable for the application in acute and chronic animal infection models. A proposal for the further optimization of the amino pyridine compound class is outlined in Figure 18. The linker (depicted in blue) and the tail part (depicted in red) of the scaffold should be prioritized. The crystal structure of **B20** suggested that fluorine at the tail part of the molecule could be replaced for more bulky substituents. This suggestion is corroborated by the SAR obtained for the hybrid antagonists. Here, the exchange of chlorine for phenoxy (compare **C7** vs. **C10**) boosted the antagonistic activity. Furthermore, the cocrystal structure of **B11/B20** showed that the flexibility of the linker allows the scaffold to adopt an angled conformation. In contrast, the hybrid antagonists **C10/C12** revealed that the linker part can at least partially be rigidified. Hence, the design strategy should aim at a reduction of flexibility while replacing the potentially instable amide bond. For this purpose, the amide moiety could be exchanged for different 5-membered aromatic ring systems either fused to phenyl ring or detached. During this optimization process, the head group (depicted in black) should be kept constant and chosen according to the synthetic feasibility. At a later stage, the influence of the amino group and the constitution of the heterocycle for the activity as well as for the physicochemical properties should be investigated.

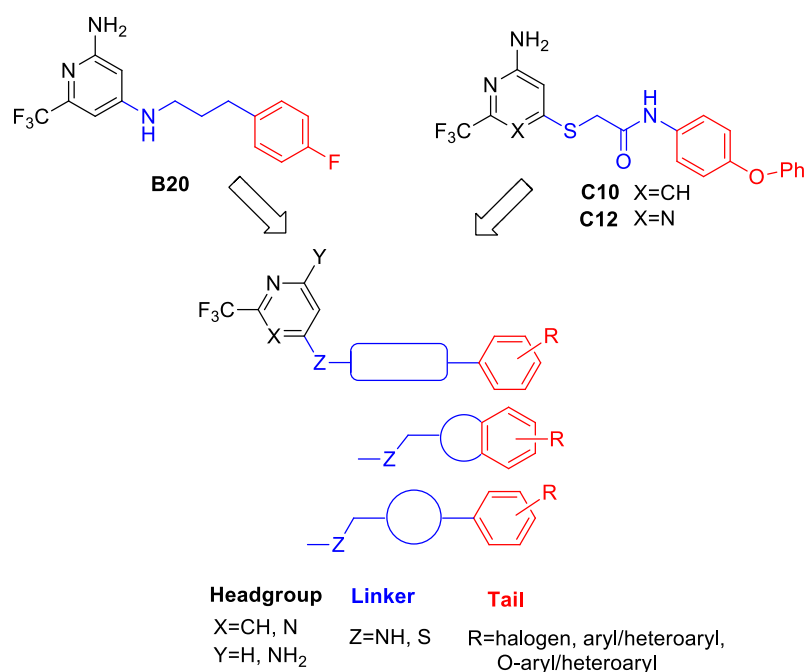


Figure 19: Proposal for further optimization of the amino pyridine scaffold

Different criteria should be considered during this lead generation process:

- The *E. coli* assay should be used as primary tool to derive a defined SAR of the compounds. This system resembles most closely the conditions in *P. aeruginosa* because it utilizes the native full-length PqsR protein in contrast to the truncated version used for ITC and SPR. Suitable compounds should possess an antagonistic activity below 50 nM.
- The anti-virulence activities regarding reduction of pyocyanin and AHQ levels in *P. aeruginosa* should be retained or even improved compared to **C10/C12**. The efficacy of the compounds should also be evaluated in different clinical isolates and under different medium conditions.
- Experiments should address the question which parameter is most relevant for the attenuation of virulent phenotypes – reduction of virulence factor pyocyanin or distinct AHQs. Especially, the influence of the antagonists on 2-AA and subsequent persister cell formation would be of further interest.
- Synthetic modifications should be evaluated by weighting the influence on the biological activities versus the change of the physicochemical properties. Thus, the LLE metric should be used routinely as guidepost during the optimization process.
- The lead nomination process should also encompass an *in vitro* pharmacokinetic and toxicological profiling like the assessment of the metabolic stability under different conditions and the cytotoxicity for relevant cell lines.
- An ideal lead compound should be applicable for oral administration, but also a local treatment in form of an ointment (for infected wound models) or a direct instillation into the lung could be an attractive alternative. In this context, modern drug delivery strategies like nanoparticles or liposomes should also be considered.

Besides the development of PqsR antagonists, the screening and biological evaluation of PqsE ligands was pursued. The structural information (**D1-D3**) gathered in this approach could be used for the structure-based design of inhibitors showing improved potencies. Whether a gain in potency would also lead to an effect on the virulence regulatory function of PqsE remains highly questionable. According to the assumption that a protein-protein or DNA-protein interaction is the underlying mechanism for this function, it would be of major interest to identify the regulatory 'hot-spot' at the protein surface. Therefore, the PqsE-RhIR reporter-gene assay in *E. coli* should be applied to screen for compounds inhibiting this sensitizing effect of PqsE on RhIR. Weak interacting fragments might not be detectable in such a setup. Thus, libraries containing larger molecules enriched with natural products might be the better source for such an approach. As an alternative, biomolecular NMR studies using PqsE/RhIR or PqsE/DNA could identify the interaction area of the particular binding partners. These findings could open the door for the structure-based design of PqsE-targeting anti-virulence agents.

5 References

- Adar YY, Ulitzur S. (1993) GroESL proteins facilitate binding of externally added inducer by LuxR protein-containing *E. coli* cells. *J. Biolumin. Chemilumin.* 8, 261-266.
- Alanis AJ. (2005) Resistance to Antibiotics: Are We in the Post-Antibiotic Era? *Arch. Med. Res.* 36, 697-705.
- Allegretta G, Weidel E, Empting M, Hartmann RW. (2015) Catechol-based substrates of chalcone synthase as a scaffold for novel inhibitors of PqsD. *Eur. J. Med. Chem.* 90, 351-359.
- Allen RC, Popat R, Diggle SP, Brown SP. (2014) Targeting virulence. Can we make evolution-proof drugs? *Nat. Rev. Microbiol.* 12, 300-308.
- Allesen-Holm M, Barken KB, Yang L, Klausen M, Webb JS, Kjelleberg S, Molin S, Givskov M, Tolker-Nielsen T. (2006) A characterization of DNA release in *Pseudomonas aeruginosa* cultures and biofilms. *Mol. Microbiol.* 59, 1114-1128.
- Amara N, Mashiach R, Amar D, Krief P, Spieser SAH, Bottomley MJ, Aharoni A, Meijler MM. (2009) Covalent inhibition of bacterial quorum sensing. *J. Am. Chem. Soc.* 131, 10610-10619.
- Anderson RD, Roddam LF, Bettiol S, Sanderson K, Reid DW. (2010) Biosignificance of bacterial cyanogenesis in the CF lung. *J. Cystic Fibrosis* 9, 158-164.
- Bejarano PA, Langeveld JP, Hudson BG, Noelken ME. (1989) Degradation of basement membranes by *Pseudomonas aeruginosa* elastase. *Infect. Immun.* 57, 3783-3787.
- Ben Jacob E, Becker I, Shapira Y, Levine H. (2004) Bacterial linguistic communication and social intelligence. *Trends Microbiol.* 12, 366-372.
- Bollag G, Tsai J, Zhang J, Zhang C, Ibrahim P, Nolop K, Hirth P. (2012) Vemurafenib: the first drug approved for BRAF-mutant cancer. *Nat. Rev. Drug Discovery* 11, 873-886.
- Boucher HW, Talbot GH, Bradley JS, Edwards JE, Gilbert D, Rice LB, Scheld M, Spellberg B, Bartlett J. (2009) Bad bugs, no drugs: no ESKAPE! An update from the Infectious Diseases Society of America. *Clin. Infect. Dis.* 48, 1-12.
- Bragonzi A, Worlitzsch D, Pier GB, Timpert P, Ulrich M, Hentzer M, Andersen JB, Givskov M, Conese M, Döring G. (2005) Nonmucoid *Pseudomonas aeruginosa* Expresses Alginate in the Lungs of Patients with Cystic Fibrosis and in a Mouse Model. *J. Infect. Dis.* 192, 410-419.
- Cao H, Krishnan G, Goumnerov B, Tsongalis J, Tompkins R, Rahme LG. (2001) A quorum sensing-associated virulence gene of *Pseudomonas aeruginosa* encodes a LysR-like transcription regulator with a unique self-regulatory mechanism. *Proc. Natl. Acad. Sci. U. S. A.* 98, 14613-14618.
- Centers for Disease Control and Prevention. (1999) Control of infectious diseases. *Morbidity and mortality weekly report* 48, 621-629.
- Chemani C, Imberty A, Bentzmann S de, Pierre M, Wimmerová M, Guery BP, Faure K. (2009) Role of LecA and LecB lectins in *Pseudomonas aeruginosa*-induced lung injury and effect of carbohydrate ligands. *Infect. Immun.* 77, 2065-2075.
- Cimpmperman P, Baranauskienė L, Jachimovičiūtė S, Jachno J, Torresan J, Michailoviene V, Matuliene J, Sereikaite J, Bumelis V, Matulis D. (2008) A quantitative model of thermal stabilization and destabilization of proteins by ligands. *Biophys. J.* 95, 3222-3231.
- Ciofu O, Mandsberg LF, Bjarnsholt T, Wassermann T, Høiby N. (2010) Genetic adaptation of *Pseudomonas aeruginosa* during chronic lung infection of patients with cystic fibrosis: strong and weak mutators with heterogeneous genetic backgrounds emerge in mucA and/or lasR mutants. *Microbiology* 156, 1108-1119.
- Ciulli A, Abell C. (2007) Fragment-based approaches to enzyme inhibition. *Curr. Opin. Biotechnol.* 18, 489-496.
- Clatworthy AE, Pierson E, Hung DT. (2007) Targeting virulence. A new paradigm for antimicrobial therapy. *Nat. Chem. Biol.* 3, 541-548.
- Coleman JP, Hudson LL, McKnight SL, Farrow JM3, Calfee MW, Lindsey CA, Pesci EC. (2008) *Pseudomonas aeruginosa* PqsA is an anthranilate-coenzyme A ligase. *J. Bacteriol.* 190, 1247-1255.

- Congreve M, Carr R, Murray C, Jhoti H. (2003) A 'Rule of Three' for fragment-based lead discovery? *Drug discovery today* 8, 876-877.
- Connelly PR, Aldape RA, Bruzzese FJ, Chambers SP, Fitzgibbon MJ, Fleming MA, Itoh S, Livingston DJ, Navia MA, Thomson JA. (1994) Enthalpy of hydrogen bond formation in a protein-ligand binding reaction. *Proc. Natl. Acad. Sci. U. S. A.* 91, 1964-1968.
- Cooper, M. and Mayr, L.M. (2011) Label-free technologies for drug discovery (Chichester: Wiley-Blackwell).
- Cooper MA. (2002) Optical biosensors in drug discovery. *Nat. Rev. Drug Discovery* 1, 515-528.
- Cornforth JW, James AT. (1956) Structure of a naturally occurring antagonist of dihydrostreptomycin. *Biochem. J.* 63, 124-130.
- Costerton JW, Stewart PS, Greenberg EP. (1999) Bacterial biofilms: a common cause of persistent infections. *Science* 284, 1318-1322.
- Cugini C, Calfee MW, Farrow JM, Morales DK, Pesci EC, Hogan DA. (2007) Farnesol, a common sesquiterpene, inhibits PQS production in *Pseudomonas aeruginosa*. *Mol. Microbiol.* 65, 896-906.
- Davies JC. (2002) *Pseudomonas aeruginosa* in cystic fibrosis. Pathogenesis and persistence. *Paediatr. Respir. Rev.* 3, 128-134.
- Dean M, White MB, Amos J, Gerrard B, Stewart C, Khaw K, Leppert M. (1990) Multiple mutations in highly conserved residues are found in mildly affected cystic fibrosis patients. *Cell* 61, 863-870.
- Dekimpe V, Déziel E. (2009) Revisiting the quorum-sensing hierarchy in *Pseudomonas aeruginosa*: the transcriptional regulator RhIR regulates LasR-specific factors. *Microbiology* 155, 712-723.
- Deziel E, Gopalan S, Tampakaki AP, Lepine F, Padfield KE, Saucier M, Xiao G, Rahme LG. (2005) The contribution of MvR to *Pseudomonas aeruginosa* pathogenesis and quorum sensing circuitry regulation: multiple quorum sensing-regulated genes are modulated without affecting lasRI, rhIRI or the production of N-acyl-L-homoserine lactones. *Mol. Microbiol.* 55, 998-1014.
- Dibdin GH, Assinder SJ, Nichols WW, Lambert PA. (1996) Mathematical model of β -lactam penetration into a biofilm of *Pseudomonas aeruginosa* while undergoing simultaneous inactivation by released β -lactamases. *J. Antimicrob. Chemother.* 38, 757-769.
- Diggle SP, Lumjiaktase P, Dipilato F, Winzer K, Kunakorn M, Barrett DA, Chhabra SR, Cámara M, Williams P. (2006a) Functional genetic analysis reveals a 2-Alkyl-4-quinolone signaling system in the human pathogen *Burkholderia pseudomallei* and related bacteria. *Chem. Biol. (Oxford, U. K.)* 13, 701-710.
- Diggle SP, Stacey RE, Dodd C, Camara M, Williams P, Winzer K. (2006b) The galactophilic lectin, LecA, contributes to biofilm development in *Pseudomonas aeruginosa*. *Environ. Microbiol.* 8, 1095-1104.
- Diggle SP, Winzer K, Chhabra SR, Worrall KE, Cámara M, Williams P. (2003) The *Pseudomonas aeruginosa* quinolone signal molecule overcomes the cell density-dependency of the quorum sensing hierarchy, regulates rhl-dependent genes at the onset of stationary phase and can be produced in the absence of LasR. *Mol. Microbiol.* 50, 29-43.
- Drees SL, Fetzner S. (2015) PqsE of *Pseudomonas aeruginosa* Acts as Pathway-Specific Thioesterase in the Biosynthesis of Alkylquinolone Signaling Molecules. *Chem. Biol. (Oxford, U. K.)* 22, 611-618.
- Dreser H. (1899) Pharmakologisches über Aspirin (Acetylsalicylsäure). *Pfluegers Arch. Gesamte Physiol. Menschen Tiere* 76, 306-318.
- Drews J. (2000) Drug discovery: a historical perspective. *Science* 287, 1960-1964.
- Dulcey CE, Dekimpe V, Fauvelle D, Milot S, Groleau M, Doucet N, Rahme LG, Lépine F, Déziel E. (2013) The end of an old hypothesis: the *Pseudomonas* signaling molecules 4-hydroxy-2-alkylquinolines derive from fatty acids, not 3-ketofatty acids. *Chem. Biol. (Oxford, U. K.)* 20, 1481-1491.
- Eberhard A, Burlingame AL, Eberhard C, Kenyon GL, Nealson KH, Oppenheimer NJ. (1981) Structural identification of autoinducer of *Photobacterium fischeri* luciferase. *Biochemistry* 20, 2444-2449.
- Ehrlich P (1909) Beiträge zur experimentellen Pathologie und Chemotherapie. Über moderne Chemotherapie (Leipzig: Akademische Verlagsgesellschaft m. b. H.).

- Emerson J, Rosenfeld M, McNamara S, Ramsey B, Gibson RL. (2002) *Pseudomonas aeruginosa* and other predictors of mortality and morbidity in young children with cystic fibrosis. *Pediatr. Pulmonol.* 34, 91-100.
- Engbrecht J, Silverman M. (1984) Identification of genes and gene products necessary for bacterial bioluminescence. *Proc. Natl. Acad. Sci. U. S. A.* 81, 4154-4158.
- Farrow JM, Sund ZM, Ellison ML, Wade DS, Coleman JP, Pesci EC. (2008) PqsE functions independently of PqsR-Pseudomonas quinolone signal and enhances the rhl quorum-sensing system. *J. Bacteriol.* 190, 7043-7051.
- Fink T, Bruggesser H, Reymond J. (2005) Virtual exploration of the small-molecule chemical universe below 160 Daltons. *Angew. Chem., Int. Ed. Engl.* 44.
- Fischbach MA, Walsh CT. (2009) Antibiotics for emerging pathogens. *Science* 325, 1089-1093.
- Fischer E. (1894) Einfluss der Configuration auf die Wirkung der Enzyme. *Ber. Dtsch. Chem. Ges.* 27, 2985-2993.
- Fleming A. (1929) On the antibacterial action of cultures of a penicillium, with special reference to their use in the isolation of *B. influenzae*. *Br. J. Exp. Pathol.* 10, 226-236.
- Folch B, Déziel E, Doucet N. (2013) Systematic mutational analysis of the putative hydrolase PqsE: toward a deeper molecular understanding of virulence acquisition in *Pseudomonas aeruginosa*. *PLoS one* 8, e73727.
- Foley BT, Moehring JM, Moehring TJ. (1995) Mutations in the Elongation Factor 2 Gene Which Confer Resistance to Diphtheria Toxin and Pseudomonas Exotoxin A. *J. Biol. Chem.* 270, 23218-23225.
- Franzetti F, Cernuschi M, Esposito R, Moroni M. (1992) Pseudomonas infections in patients with AIDS and AIDS-related complex. *J. Intern. Med.* 231, 437-443.
- Freire E. (2004) Isothermal titration calorimetry: controlling binding forces in lead optimization. *Drug Discovery Today: Technol.* 1, 295-299.
- Freyer MW, Lewis EA (2008) Isothermal Titration Calorimetry: Experimental Design, Data Analysis, and Probing Macromolecule/Ligand Binding and Kinetic Interactions. In *Biophysical Tools for Biologists, Volume One: In Vitro Techniques* (Elsevier), pp. 79–113.
- Gallagher LA, McKnight SL, Kuznetsova MS, Pesci EC, Manoil C. (2002) Functions Required for Extracellular Quinolone Signaling by *Pseudomonas aeruginosa*. *J. Bacteriol.* 184, 6472-6480.
- Gambello MJ, Iglewski BH. (1991) Cloning and characterization of the *Pseudomonas aeruginosa* lasR gene, a transcriptional activator of elastase expression. *J. Bacteriol.* 173, 3000-3009.
- Gaynes R, Edwards JR. (2005) Overview of nosocomial infections caused by gram-negative bacilli. *Clin. Infect. Dis.* 41, 848-854.
- Geschwindner S, Ulander J, Johansson P. (2015) Ligand Binding Thermodynamics in Drug Discovery: Still a Hot Tip? *J. Med. Chem.* 58, 6321-6335.
- Geske GD, Wezeman RJ, Siegel AP, Blackwell HE. (2005) Small molecule inhibitors of bacterial quorum sensing and biofilm formation. *J. Am. Chem. Soc.* 127, 12762-12763.
- Gordon CA, Hodges NA, Marriott C. (1988) Antibiotic interaction and diffusion through alginate and exopolysaccharide of cystic fibrosis-derived *Pseudomonas aeruginosa*. *J. Antimicrob. Chemother.* 22, 667-674.
- Hajduk PJ, Greer J. (2007) A decade of fragment-based drug design: strategic advances and lessons learned. *Nat. Rev. Drug Discovery* 6, 211-219.
- Hajduk PJ, Sheppard G, Nettesheim DG, Olejniczak ET, Shuker SB, Meadows RP, Steinman DH, Carrera GM, Marcotte PA, Severin J, Walter K, Smith H, Gubbins E, Simmer R, Holzman TF, Morgan DW, Davidsen SK, Summers JB, Fesik SW. (1997) Discovery of Potent Nonpeptide Inhibitors of Stromelysin Using SAR by NMR. *J. Am. Chem. Soc.* 119, 5818-5827.
- Hann MM, Leach AR, Harper G. (2001) Molecular Complexity and Its Impact on the Probability of Finding Leads for Drug Discovery. *J. Chem. Inf. Model.* 41, 856-864.
- Hartshorn MJ, Murray CW, Cleasby A, Frederickson M, Tickle IJ, Jhoti H. (2005) Fragment-based lead discovery using X-ray crystallography. *J. Med. Chem.* 48, 403-413.
- Harvey AL. (2008) Natural products in drug discovery. *Drug discovery today* 13, 894-901.

- Hays EE, Wells IC, Katzman PA, Cain CK, Jacobs FA, Thayer SA, Doisy EA, Gaby WL, Roberts EC, Muir RD, Carroll CJ, Jones LR, Wade NJ. (1945) Antibiotic substances produced by *Pseudomonas aeruginosa*. *J. Biol. Chem.* 159, 725-750.
- Hazan R, He J, Xiao G, Dekimpe V, Apidianakis Y, Lesic B, Astrakas C, Déziel E, Lépine F, Rahme LG. (2010) Homeostatic interplay between bacterial cell-cell signaling and iron in virulence. *PLoS Pathog.* 6, e1000810.
- Henderson, R., Orsenigo, L. and Pisano, G.P. (1999) The pharmaceutical industry and the revolution in molecular biology. From the book: Sources of industrial leadership Studies of seven industries (New York: Cambridge University Press).
- Hentzer M, Wu H, Andersen JB, Riedel K, Rasmussen TB, Bagge N, Kumar N, Schembri MA, Song Z, Kristoffersen P, Manefield M, Costerton JW, Molin S, Eberl L, Steinberg P, Kjelleberg S, Høiby N, Givskov M. (2003) Attenuation of *Pseudomonas aeruginosa* virulence by quorum sensing inhibitors. *EMBO J.* 22, 3803-3815.
- Hinsberger S, Jong JC de, Groh M, Hauptenthal J, Hartmann RW. (2014) Benzamidobenzoic acids as potent PqsD inhibitors for the treatment of *Pseudomonas aeruginosa* infections. *Eur. J. Med. Chem.* 76, 343-351.
- Hoffman LR, Kulasekara HD, Emerson J, Houston LS, Burns JL, Ramsey BW, Miller SI. (2009) *Pseudomonas aeruginosa* lasR mutants are associated with cystic fibrosis lung disease progression. *J. Cystic Fibrosis* 8, 66-70.
- Holdgate GA, Anderson M, Edfeldt F, Geschwindner S. (2010) Affinity-based, biophysical methods to detect and analyze ligand binding to recombinant proteins: matching high information content with high throughput. *J. Struct. Biol.* 172, 142-157.
- Homola J. (2003) Present and future of surface plasmon resonance biosensors. Analytical and Bioanalytical Chemistry. *Anal. Bioanal. Chem.* 377, 528-539.
- Hondo T, Warizaya M, Niimi T, Namatame I, Yamaguchi T, Nakanishi K, Hamajima T, Harada K, Sakashita H, Matsumoto Y, Orita M, Takeuchi M. (2013) 4-Hydroxypyridazin-3(2H)-one derivatives as novel D-amino acid oxidase inhibitors. *J. Med. Chem.* 56, 3582-3592.
- Hopkins AL, Groom CR. (2002) The druggable genome. *Nature reviews. Drug discovery* 1, 727-730.
- Hopkins AL, Groom CR, Alex A. (2004) Ligand efficiency: a useful metric for lead selection. *Curr. Top. Med. Chem.* 9, 430-431.
- Huberts D, van der Klei I. (2010) Moonlighting proteins: an intriguing mode of multitasking. *Biochimica et biophysica acta* 1803, 520-525.
- Hudson SA, McLean KJ, Surade S, Yang Y, Leys D, Ciulli A, Munro AW, Abell C. (2012) Application of Fragment Screening and Merging to the Discovery of Inhibitors of the *Mycobacterium tuberculosis* Cytochrome P450 CYP121. *Angew. Chem., Int. Ed. Engl.* 51, 9311-9316.
- Ilangovan A, Fletcher M, Rampioni G, Pustelny C, Rumbaugh K, Heeb S, Cámara M, Truman A, Chhabra SR, Emsley J, Williams P. (2013) Structural basis for native agonist and synthetic inhibitor recognition by the *Pseudomonas aeruginosa* quorum sensing regulator PqsR (MvfR). *PLoS Pathog.* 9, e1003508.
- Inglese J, Johnson RL, Simeonov A, Xia M, Zheng W, Austin CP, Auld DS. (2007) High-throughput screening assays for the identification of chemical probes. *Nat. Chem. Biol.* 3, 466-479.
- Ishida T, Ikeda T, Takiguchi N, Kuroda A, Ohtake H, Kato J. (2007) Inhibition of quorum sensing in *Pseudomonas aeruginosa* by N-acyl cyclopentylamides. *Appl. Environ. Microbiol.* 73, 3183-3188.
- Kaplan HB, Greenberg EP. (1985) Diffusion of autoinducer is involved in regulation of the *Vibrio fischeri* luminescence system. *J. Bacteriol.* 163, 1210-1214.
- Kesarwani M, Hazan R, He J, Que Y, Que Y, Apidianakis Y, Lesic B, Xiao G, Dekimpe V, Milot S, Déziel E, Lépine F, Rahme LG. (2011) A quorum sensing regulated small volatile molecule reduces acute virulence and promotes chronic infection phenotypes. *PLoS Pathog.* 7, e1002192.
- Keserü GM, Makara GM. (2009) The influence of lead discovery strategies on the properties of drug candidates. *Nat. Rev. Drug Discovery* 8, 203-212.
- Kim K, Kim YU, Koh BH, Hwang SS, Kim S, Lépine F, Cho Y, Lee GR. (2010) HHQ and PQS, two *Pseudomonas aeruginosa* quorum-sensing molecules, down-regulate the innate immune responses through the nuclear factor-kappaB pathway. *Immunology* 129, 578-588.

- Klebe G (2009) Wirkstoffdesign. Entwurf und Wirkung von Arzneistoffen (Heidelberg: Spektrum Akad. Verl.).
- Klein T, Henn C, Jong JC de, Zimmer C, Kirsch B, Maurer CK, Pistorius D, Müller R, Steinbach A, Hartmann RW. (2012) Identification of small-molecule antagonists of the *Pseudomonas aeruginosa* transcriptional regulator PqsR: biophysically guided hit discovery and optimization. *ACS Chem. Biol.* 7, 1496-1501.
- Kling A, Lukat P, Almeida DV, Bauer A, Fontaine E, Sordello S, Zaburanyi N, Herrmann J, Wenzel SC, König C, Ammerman NC, Barrio MB, Borchers K, Bordon-Pallier F, Brønstrup M, Courtemanche G, Gerlitz M, Geslin M, Hammann P, Heinz DW, Hoffmann H, Klieber S, Kohlmann M, Kurz M, Lair C, Matter H, Nuernberger E, Tyagi S, Fraisse L, Grosset JH, Lagrange S, Müller R. (2015) Antibiotics. Targeting DnaN for tuberculosis therapy using novel griselimycins. *Science (New York, N.Y.)* 348, 1106-1112.
- Koshland DE. (1958) Application of a Theory of Enzyme Specificity to Protein Synthesis*. *Proc. Natl. Acad. Sci. U. S. A.* 44, 98-104.
- Kubas H, Stark H. (2007) Medizinische Chemie von Histamin-H2-Rezeptorantagonisten: Klassische Wirkstoffentwicklung. *Pharm. Unserer Zeit* 36, 24-32.
- Ladbury JE, Klebe G, Freire E. (2010) Adding calorimetric data to decision making in lead discovery: a hot tip. *Nat. Rev. Drug Discovery* 9, 23-27.
- Lam J, Chan R, Lam K, Costerton JW. (1980) Production of mucoid microcolonies by *Pseudomonas aeruginosa* within infected lungs in cystic fibrosis. *Infect. Immun.* 28, 546-556.
- Latifi A, Foglino M, Tanaka K, Williams P, Lazdunski A. (1996) A hierarchical quorum-sensing cascade in *Pseudomonas aeruginosa* links the transcriptional activators LasR and RhIR (VsmR) to expression of the stationary-phase sigma factor RpoS. *Mol. Microbiol.* 21, 1137-1146.
- Lau GW, Hassett DJ, Ran H, Kong F. (2004) The role of pyocyanin in *Pseudomonas aeruginosa* infection. *Trends Mol. Med.* 10, 599-606.
- Leach AR, Hann MM, Burrows JN, Griffen EJ. (2006) Fragment screening. An introduction. *Mol. BioSyst.* 2, 429.
- Lee J, Wu J, Deng Y, Wang J, Wang C, Wang J, Chang C, Dong Y, Williams P, Zhang L. (2013) A cell-cell communication signal integrates quorum sensing and stress response. *Nat. Chem. Biol.* 9, 339-343.
- Lee J, Zhang L. (2015) The hierarchy quorum sensing network in *Pseudomonas aeruginosa*. *Protein Cell* 6, 26-41.
- Leeson PD, Springthorpe B. (2007) The influence of drug-like concepts on decision-making in medicinal chemistry. *Nat. Rev. Drug Discovery* 6, 881-890.
- Lepine F, Milot S, Deziel E, He J, Rahme LG. (2004) Electrospray/mass spectrometric identification and analysis of 4-hydroxy-2-alkylquinolines (HAQs) produced by *Pseudomonas aeruginosa*. *J. Am. Soc. Mass Spectrom.* 15, 862-869.
- Lesic B, Lépine F, Déziel E, Zhang J, Zhang Q, Padfield K, Castonguay M, Milot S, Stachel S, Tzika AA, Tompkins RG, Rahme LG. (2007) Inhibitors of pathogen intercellular signals as selective anti-infective compounds. *PLoS Pathog.* 3, 1229-1239.
- Lewis K. (2010) Persister cells. *Annu. Rev. Microbiol.* 64, 357-372.
- Ling LL, Schneider T, Peoples AJ, Spoering AL, Engels I, Conlon BP, Mueller A, Schäberle TF, Hughes DE, Epstein S, Jones M, Lazarides L, Steadman VA, Cohen DR, Felix CR, Fetterman KA, Millett WP, Nitti AG, Zullo AM, Chen C, Lewis K. (2015) A new antibiotic kills pathogens without detectable resistance. *Nature* 517, 455-459.
- Lipinski CA, Lombardo F, Dominy BW, Feeney PJ. (1997) Experimental and computational approaches to estimate solubility and permeability in drug discovery and development settings. *Adv. Drug Delivery Rev.* 23, 3-25.
- Liu Y, Wang Y, Walsh TR, Yi L, Zhang R, Spencer J, Doi Y, Tian G, Dong B, Huang X, Yu L, Gu D, Ren H, Chen X, Lv L, He D, Zhou H, Liang Z, Liu J, Shen J. (2015) Emergence of plasmid-mediated colistin resistance mechanism MCR-1 in animals and human beings in China: a microbiological and molecular biological study. *Lancet Infect. Dis.*, in press.
- Lo M, Aulabaugh A, Jin G, Cowling R, Bard J, Malamas M, Ellestad G. (2004) Evaluation of fluorescence-based thermal shift assays for hit identification in drug discovery. *Anal. Biochem.* 332, 153-159.

- Lu C, Kirsch B, Zimmer C, Jong JC de, Henn C, Maurer CK, Müsken M, Häussler S, Steinbach A, Hartmann RW. (2012) Discovery of antagonists of PqsR, a key player in 2-alkyl-4-quinolone-dependent quorum sensing in *Pseudomonas aeruginosa*. *Chem. Biol. (Oxford, U. K.)* 19, 381-390.
- Lu C, Maurer CK, Kirsch B, Steinbach A, Hartmann RW. (2014) Overcoming the Unexpected Functional Inversion of a PqsR Antagonist in *Pseudomonas aeruginosa*. An In Vivo Potent Antivirulence Agent Targeting pqs Quorum Sensing. *Angew. Chem., Int. Ed. Engl.* 126, 1127-1130.
- Lyczak JB, Cannon CL, Pier GB. (2000) Establishment of *Pseudomonas aeruginosa* infection. Lessons from a versatile opportunist¹*Address for correspondence: Channing Laboratory, 181 Longwood Avenue, Boston, MA 02115, USA. *Microbes Infect.* 2, 1051-1060.
- Maddocks SE, Oyston PCF. (2008) Structure and function of the LysR-type transcriptional regulator (LTTR) family proteins. *Microbiology* 154, 3609-3623.
- Malvern Instruments Ltd. (2015) Material relationships: Microcal ITC Systems. Understanding biomolecular interactions. <http://www.malvern.com/de/Assets/MRK2058.pdf>.
- Manefield M, Rasmussen TB, Henzter M, Andersen JB, Steinberg P, Kjelleberg S, Givskov M. (2002) Halogenated furanones inhibit quorum sensing through accelerated LuxR turnover. *Microbiology* 148, 1119-1127.
- Manny AJ, Kjelleberg S, Kumar N, Nys R de, Read RW, Steinberg P. (1997) Reinvestigation of the sulfuric acid-catalysed cyclisation of brominated 2-alkyllevulinic acids to 3-alkyl-5-methylene-2(5H)-furanones. *Tetrahedron* 53, 15813-15826.
- Masuda N, Sakagawa E, Ohya S, Gotoh N, Tsujimoto H, Nishino T. (2000) Substrate Specificities of MexAB-OprM, MexCD-OprJ, and MexXY-OprM Efflux Pumps in *Pseudomonas aeruginosa*. *Antimicrob. Agents Chemother.* 44, 3322-3327.
- Matthews BW. (1993) Structural and Genetic Analysis of Protein Stability. *Annu. Rev. Biochem.* 62, 139-160.
- Matulis D, Kranz JK, Salemme FR, Todd MJ. (2005) Thermodynamic Stability of Carbonic Anhydrase. Measurements of Binding Affinity and Stoichiometry Using ThermoFluor. *Biochemistry* 44, 5258-5266.
- Mochalkin I, Miller JR, Narasimhan L, Thanabal V, Erdman P, Cox PB, Prasad, J V N Vara, Lightle S, Huband MD, Stover CK. (2009) Discovery of antibacterial biotin carboxylase inhibitors by virtual screening and fragment-based approaches. *ACS Chem. Biol.* 4, 473-483.
- Mol, N.J.d. and Fischer, M.J. (2008) Chapter 5: Kinetic and Thermodynamic Analysis of Ligand–Receptor Interactions: SPR Applications in Drug Development. From the book: Handbook of Surface Plasmon Resonance (Cambridge: RSCPublishing).
- Mulcahy H, Charron-Mazenod L, Lewenza S. (2008) Extracellular DNA chelates cations and induces antibiotic resistance in *Pseudomonas aeruginosa* biofilms. *PLoS Pathog.* 4, e1000213.
- Murray CW, Rees DC. (2009) The rise of fragment-based drug discovery. *Nat. Chem.* 1, 187-192.
- Murray CW, Verdonk ML. (2002) The consequences of translational and rotational entropy lost by small molecules on binding to proteins. *J. Comput.-Aided Mol. Des.* 16, 741-753.
- Nealson KH, Hastings JW. (1979) Bacterial bioluminescence: its control and ecological significance. *Microbiol. Rev.* 43, 496-518.
- Nicas TI, Hancock RE. (1983) *Pseudomonas aeruginosa* outer membrane permeability: isolation of a porin protein F-deficient mutant. *J. Bacteriol.* 153, 281-285.
- Niesen FH, Berglund H, Vedadi M. (2007) The use of differential scanning fluorimetry to detect ligand interactions that promote protein stability. *Nat. Protoc.* 2, 2212-2221.
- Nys R de, Wright AD, König GM, Sticher O. (1993) New halogenated furanones from the marine alga *Delisea pulchra* (cf. *fimbriata*). *Tetrahedron* 49, 11213-11220.
- Ochsner UA, Koch AK, Fiechter A, Reiser J. (1994) Isolation and characterization of a regulatory gene affecting rhamnolipid biosurfactant synthesis in *Pseudomonas aeruginosa*. *J. Bacteriol.* 176, 2044-2054.
- Ochsner UA, Reiser J. (1995) Autoinducer-mediated regulation of rhamnolipid biosurfactant synthesis in *Pseudomonas aeruginosa*. *Proc. Natl. Acad. Sci. U. S. A.* 92, 6424-6428.
- O'Shea R, Moser HE. (2008) Physicochemical properties of antibacterial compounds: implications for drug discovery. *J. Med. Chem.* 51, 2871-2878.

- Ostroff RM, Vasil AI, Vasil ML. (1990) Molecular comparison of a nonhemolytic and a hemolytic phospholipase C from *Pseudomonas aeruginosa*. *J. Bacteriol.* 172, 5915-5923.
- Pantoliano MW, Petrella EC, Kwasnoski JD, Lobanov VS, Myslik J, Graf E, Carver T, Asel E, Springer BA, Lane P, Salemme FR. (2001) High-Density Miniaturized Thermal Shift Assays as a General Strategy for Drug Discovery. *J. Biomol. Screening* 6, 429-440.
- Passador L, Cook JM, Gambello MJ, Rust L, Iglewski BH. (1993) Expression of *Pseudomonas aeruginosa* virulence genes requires cell-to-cell communication. *Science* 260, 1127-1130.
- Payne DJ, Gwynn MN, Holmes DJ, Pompliano DL. (2007) Drugs for bad bugs: confronting the challenges of antibacterial discovery. *Nat. Rev. Drug Discovery* 6, 29-40.
- Pearson JP, Gray KM, Passador L, Tucker KD, Eberhard A, Iglewski BH, Greenberg EP. (1994) Structure of the autoinducer required for expression of *Pseudomonas aeruginosa* virulence genes. *Proc. Natl. Acad. Sci. U. S. A.* 91, 197-201.
- Pearson JP, Passador L, Iglewski BH, Greenberg EP. (1995) A second N-acylhomoserine lactone signal produced by *Pseudomonas aeruginosa*. *Proc. Natl. Acad. Sci. U. S. A.* 92, 1490-1494.
- Pesci EC, Milbank JB, Pearson JP, McKnight S, Kende AS, Greenberg EP, Iglewski BH. (1999) Quinolone signaling in the cell-to-cell communication system of *Pseudomonas aeruginosa*. *Proc. Natl. Acad. Sci. U. S. A.* 96, 11229-11234.
- Pesci EC, Pearson JP, Seed PC, Iglewski BH. (1997) Regulation of las and rhl quorum sensing in *Pseudomonas aeruginosa*. *J. Bacteriol.* 179, 3127-3132.
- Price DA, Blagg J, Jones L, Greene N, Wager T. (2009) Physicochemical drug properties associated with in vivo toxicological outcomes: a review. *Expert Opin. Drug Metab. Toxicol.* 5, 921-931.
- Projan SJ. (2003) Why is big Pharma getting out of antibacterial drug discovery? *Curr. Opin. Microbiol.* 6, 427-430.
- Proudfoot J, Nosjean O, Blanchard J, Wang J, Besson D, Crankshaw D, Gauglitz G, Hertzberg R, Homon C, Llewellyn L, Neubig R, Walker L, Villa P. (2011) Glossary of terms used in biomolecular screening (IUPAC Recommendations 2011). *Pure Appl. Chem.* 83.
- Pruitt BA, McManus AT. (1984) Opportunistic infections in severely burned patients. *Am. J. Med.* 76, 146-154.
- Que Y, Hazan R, Strobel B, Maura D, He J, Kesarwani M, Panopoulos P, Tsurumi A, Giddey M, Wilhelmy J, Mindrinos MN, Rahme LG. (2013) A quorum sensing small volatile molecule promotes antibiotic tolerance in bacteria. *PLoS one* 8, e80140.
- Rahme LG, Tan M, Le L, Wong SM, Tompkins RG, Calderwood SB, Ausubel FM. (1997) Use of model plant hosts to identify *Pseudomonas aeruginosa* virulence factors. *Proc. Natl. Acad. Sci. U. S. A.* 94, 13245-13250.
- Rampioni G, Pustelny C, Fletcher MP, Wright VJ, Bruce M, Rumbaugh KP, Heeb S, Cámara M, Williams P. (2010) Transcriptomic analysis reveals a global alkyl-quinolone-independent regulatory role for PqsE in facilitating the environmental adaptation of *Pseudomonas aeruginosa* to plant and animal hosts. *Environ. Microbiol.* 12, 1659-1673.
- Rasko DA, Sperandio V. (2010) Anti-virulence strategies to combat bacteria-mediated disease. *Nat. Rev. Drug Discovery* 9, 117-128.
- Riordan JR, Rommens JM, Kerem B, Alon N, Rozmahel R, Grzelczak Z, Zielenski J, Lok S, Plavsic N, Chou JL. (1989) Identification of the cystic fibrosis gene: cloning and characterization of complementary DNA. *Science (New York, N. Y.)* 245, 1066-1073.
- Sahner JH, Brengel C, Storz MP, Groh M, Plaza A, Müller R, Hartmann RW. (2013) Combining in silico and biophysical methods for the development of *Pseudomonas aeruginosa* quorum sensing inhibitors: an alternative approach for structure-based drug design. *J. Med. Chem.* 56, 8656-8664.
- Sahner JH, Empting M, Kamal A, Weidel E, Groh M, Börger C, Hartmann RW. (2015) Exploring the chemical space of ureidothiophene-2-carboxylic acids as inhibitors of the quorum sensing enzyme PqsD from *Pseudomonas aeruginosa*. *Eur. J. Med. Chem.* 96, 14-21.
- Sato H, Okinaga K, Saito H. (1988) Role of Pili in the Pathogenesis of *Pseudomonas aeruginosa* Burn Infection. *Microbiol. Immunol.* 32, 131-139.

- Schertzer JW, Brown SA, Whiteley M. (2010) Oxygen levels rapidly modulate *Pseudomonas aeruginosa* social behaviours via substrate limitation of PqsH. *Mol. Microbiol.* 77, 1527-1538.
- Schuffenhauer A, Ruedisser S, Marzinzik AL, Jahnke W, Blommers M, Selzer P, Jacoby E. (2005) Library design for fragment based screening. *Curr. Top. Med. Chem.* 5, 751-762.
- Schuster M, Greenberg EP. (2006) A network of networks: Quorum-sensing gene regulation in *Pseudomonas aeruginosa*. Quorum sensing in human pathogens. *Int. J. Med. Microbiol.* 296, 73-81.
- Shipe WD, Sharik SS, Barrow JC, McGaughey GB, Theberge CR, Uslaner JM, Yan Y, Renger JJ, Smith SM, Coleman PJ, Cox CD. (2015) Discovery and Optimization of a Series of Pyrimidine-Based Phosphodiesterase 10A (PDE10A) Inhibitors through Fragment Screening, Structure-Based Design, and Parallel Synthesis. *J. Med. Chem.* 58, 7888-7894.
- Silby MW, Winstanley C, Godfrey SAC, Levy SB, Jackson RW. (2011) *Pseudomonas* genomes: diverse and adaptable. *FEMS Microbiol. Rev.* 35, 652-680.
- Silvestre HL, Blundell TL, Abell C, Ciulli A. (2013) Integrated biophysical approach to fragment screening and validation for fragment-based lead discovery. *Proc. Natl. Acad. Sci. U. S. A.* 110, 12984-12989.
- Singh PK, Schaefer AL, Parsek MR, Moninger TO, Welsh MJ, Greenberg EP. (2000) Quorum-sensing signals indicate that cystic fibrosis lungs are infected with bacterial biofilms. *Nature* 407, 762-764.
- Smith EE, Buckley DG, Wu Z, Saenphimmachak C, Hoffman LR, D'Argenio DA, Miller SI, Ramsey BW, Speert DP, Moskowitz SM, Burns JL, Kaul R, Olson MV. (2006) Genetic adaptation by *Pseudomonas aeruginosa* to the airways of cystic fibrosis patients. *Proc. Natl. Acad. Sci. U. S. A.* 103, 8487-8492.
- Smith KM, Bu Y, Suga H. (2003) Induction and Inhibition of *Pseudomonas aeruginosa* Quorum Sensing by Synthetic Autoinducer Analogs. *Chem. Biol. (Oxford, U. K.)* 10, 81-89.
- Spellberg B, Taylor-Blake B. (2013) On the exoneration of Dr. William H. Stewart: debunking an urban legend. *Infect. Dis. Poverty* 2, 3.
- Starkey M, Lepine F, Maura D, Bandyopadhyaya A, Lesic B, He J, Kitao T, Righi V, Milot S, Tzika A, Rahme L. (2014) Identification of anti-virulence compounds that disrupt quorum-sensing regulated acute and persistent pathogenicity. *PLoS Pathog.* 10, e1004321.
- Stewart PS, William Costerton J. (2001) Antibiotic resistance of bacteria in biofilms. *Lancet* 358, 135-138.
- Storz MP, Maurer CK, Zimmer C, Wagner N, Brengel C, Jong JC de, Lucas S, Müsken M, Häussler S, Steinbach A, Hartmann RW. (2012) Validation of PqsD as an anti-biofilm target in *Pseudomonas aeruginosa* by development of small-molecule inhibitors. *J. Am. Chem. Soc.* 134, 16143-16146.
- Strebhardt K, Ullrich A. (2008) Paul Ehrlich's magic bullet concept: 100 years of progress. *Nat. Rev. Cancer* 8, 473-480.
- Sutherland I. (2001) The biofilm matrix – an immobilized but dynamic microbial environment. *Trends Microbiol.* 9, 222-227.
- Vedadi M, Niesen FH, Allali-Hassani A, Fedorov OY, Finerty PJ, Wasney GA, Yeung R, Arrowsmith C, Ball LJ, Berglund H, Hui R, Marsden BD, Nordlund P, Sundstrom M, Weigelt J, Edwards AM. (2006) Chemical screening methods to identify ligands that promote protein stability, protein crystallization, and structure determination. *Proc. Natl. Acad. Sci. U. S. A.* 103, 15835-15840.
- Wade DS, Calfee MW, Rocha ER, Ling EA, Engstrom E, Coleman JP, Pesci EC. (2005) Regulation of *Pseudomonas* quinolone signal synthesis in *Pseudomonas aeruginosa*. *J. Bacteriol.* 187, 4372-4380.
- Waldrop GL. (2009) Smaller is better for antibiotic discovery. *ACS Chem. Biol.* 4, 397-399.
- Walsh C. (2003) Where will new antibiotics come from? *Nat. Rev. Microbiol.* 1, 65-70.
- Walters MC, Roe F, Bugnicourt A, Franklin MJ, Stewart PS. (2003) Contributions of Antibiotic Penetration, Oxygen Limitation, and Low Metabolic Activity to Tolerance of *Pseudomonas aeruginosa* Biofilms to Ciprofloxacin and Tobramycin. *Antimicrob. Agents Chemother.* 47, 317-323.
- Waters CM, Bassler BL. (2005) Quorum sensing: cell-to-cell communication in bacteria. *Annu. Rev. Cell Dev. Biol.* 21, 319-346.
- Wermuth CG. (2006) Similarity in drugs: reflections on analogue design. *Drug discovery today* 11, 348-354.

- Winqvist J, Geschwindner S, Xue Y, Gustavsson L, Musil D, Deinum J, Danielson UH. (2013) Identification of structural-kinetic and structural-thermodynamic relationships for thrombin inhibitors. *Biochemistry* 52, 613-626.
- Xiao G, Deziel E, He J, Lepine F, Lesic B, Castonguay M, Milot S, Tampakaki AP, Stachel SE, Rahme LG. (2006) MvR, a key *Pseudomonas aeruginosa* pathogenicity LTTR-class regulatory protein, has dual ligands. *Mol. Microbiol.* 62, 1689-1699.
- Yu S, Jensen V, Seeliger J, Feldmann I, Weber S, Schleicher E, Häussler S, Blankenfeldt W. (2009) Structure elucidation and preliminary assessment of hydrolase activity of PqsE, the *Pseudomonas* quinolone signal (PQS) response protein. *Biochemistry* 48, 10298-10307.
- Zhang Y, Frank MW, Zhu K, Mayasundari A, Rock CO. (2008) PqsD is responsible for the synthesis of 2,4-dihydroxyquinoline, an extracellular metabolite produced by *Pseudomonas aeruginosa*. *J. Biol. Chem.* 283, 28788-28794.
- Zulianello L, Canard C, Köhler T, Caille D, Lacroix J, Meda P. (2006) Rhamnolipids are virulence factors that promote early infiltration of primary human airway epithelia by *Pseudomonas aeruginosa*. *Infect. Immun.* 74, 3134-3147.

6 Abbreviations

2-AA	2-amino-acetophenon
2-ABA	2-aminobenzoylacetate
2-ABA-CoA	2-aminobenzoylacetyl coenzyme A
AHL	<i>N</i> -acyl-homoserine lactone
AHQ	alkyl hydroxy quinolone
CDCI ₃	deuterated chloroform
CF	cystic fibrosis
CFTR	cystic fibrosis transmembrane conductance regulator
CoA	coenzyme A
DHQ	2,4-dihydroxyquinoline
DMSO	dimethyl sulfoxide
DNA	deoxyribonucleic acid
DSF	differential scanning fluorimetry
eDNA	extracellular DNA
EE	enthalpic efficiency
FBDD	fragment-based drug discovery
HAQ	4-hydroxy-2-akylquinolones
HHQ	2-heptyl-4(1 <i>H</i>)-quinolone
HQNO	2-heptyl-4-hydroxy quinoline- <i>N</i> -oxide
HTS	high throughput screening
IC ₅₀	half maximal inhibitory effect
INPHARMA	interligand NOE for pharmacophore mapping
IPA	isopropyl alcohol
ITC	isothermal titration calorimetry
K_A	association constant
K_D	dissociation constant
LBD	ligand binding domain
LE	ligand efficiency
LLE	ligand lipophilicity efficiency
LTTR	LysR-type transcriptional regulator
MS	mass spectroscopy
MvR	multiple virulence factor regulator
NHQ	2-nonyl-4-quinolone
NMR	nuclear magnetic resonance
NOE	nuclear Overhauser effect
PQS	<i>Pseudomonas</i> Quinolone Signal
PqsR	<i>Pseudomonas</i> quinolone signal receptor
QS	quorum sensing
RNA	ribonucleic acid
SAR	structure activity relationship
SPR	surface plasmon resonance
SPW	surface plasmon wave
TSA	thermal shift assay
UHPLC	ultra high performance liquid chromatography

7 Supplementary Material

7.1 Supplementary Material of Chapter A

Discovery and Biophysical Characterization of 2-Amino-Oxadiazoles as Novel Antagonists of PqsR, an Important Regulator of *Pseudomonas aeruginosa* Virulence

1) Surface-Plasmon-Resonance Screening

a) Protein Expression and Purification. *E. coli* BL21 (DE3) cells containing the pSUMO3_ck4_pqsR^{C87} plasmid were grown in 2x YT medium containing 50 µg mL⁻¹ kanamycin and incubated at 37 °C to an OD₆₀₀ of approximately 0.5 upon which the shaker temperature was gradually reduced to 16 °C. At an OD₆₀₀ of approximately 0.8 the protein expression was induced with 0.2 µM IPTG for 22 h at 16 °C. The cells were harvested by centrifugation (5000 xg, 10 min, 4 °C) and the cell pellet was resuspended in 100 mL His Trap binding buffer (20 mM sodium phosphate, pH 7.4, 500 mM NaCl, 20 mM imidazole, 2 mM MgCl₂, 10% glycerol (v/v)). To facilitate cellular lysis and to reduce suspension viscosity prior to cell crushing, lysozyme (Sigma) and Benzonase Nuclease (Novagen) were added to a final concentration of 0.025 mg/mL and 0.0025 units/mL, respectively. The bacterial suspension was subsequently passed three times through an EmulsiFlex-C5 cell crusher (Avestin; 15,000 psi at 4 °C). Cell debris were removed by centrifugation 20000 xg, 15 min, 4 °C) and the supernatant was filtered through a syringe filter (Millipore Millex SV-5µM). The clarified lysate was immediately applied to a two-step purification method (ÄKTExpress instrument, GE Healthcare). This method incorporated immobilized metal affinity chromatography (IMAC; HisTrap) and size exclusion chromatography column (HiLoad Superdex 200 16/60 Prep Grade). The captured H₆SUMO3-pqsR^{C87} protein was washed with HisTrap binding buffer (20 mM sodium phosphate pH 7.4, 500 mM NaCl, 20 mM imidazole, 10% glycerol (v/v)), and eluted with 250 mM imidazole. Eluted protein peak (total of 4 mL; A₂₈₀>50 mAU) was automatically collected and injected onto a HiLoad Superdex 200 16/60 Prep Grade column equilibrated in storage buffer (1x PBS, 10% glycerol (v/v)). The H₆SUMO-tagged protein were stored at -80 °C and used for biophysical studies.

b) Minimal biotinylation of H₆SUMO-PqsR^{C87}. Minimal biotinylation of the H₆SUMO-PqsR^{C87} was achieved by mixing 48 nmol of H₆SUMO-PqsR^{C87} (1 eq.) with 24 nmol of EZ-link sulfoNHS LC-LC-biotin (0.5 eq.; Thermofisher Scientific) that was freshly dissolved in water. Biotinylation reaction mixture was incubated on ice for 2 hours. To remove unreacted biotin reagent, the entire biotinylation mixture was subjected to size exclusion chromatography on a Superdex200 HR (10/300) column equilibrated in storage buffer (1x PBS, pH 7.4, 10% glycerol (v/v)). A protein peak containing biotinylated H₆SUMO-PqsR^{C87} protein was collected (66 µg/mL), stored at -80 °C and used for SPR studies.

c) Immobilization of Biotinylated H₆SUMO-PqsR^{C87}. The CM5 sensor chip and amine coupling kit were obtained from GE Healthcare. Streptavidin was simultaneously immobilized in all four channels of a CM5 sensor chip docked in a Biacore T100 instrument equilibrated with 1x HBS-P buffer (10 mM HEPES pH 7.4, 150 mM NaCl, 0.005% Tween-20). Immobilization was performed at 37 °C at a constant flow-rate of 10 µL/min using standard amide coupling chemistry.¹ Streptavidin was diluted in 10 mM sodium acetate buffer pH 4.5 to a final concentration of 100 µg/mL. This approach resulted in immobilization of 8800-10800 response units with minimal variation between the four channels on the same chip (SI, Table S1). Freshly immobilized surfaces were further conditioned with three consecutive 30 s injections of streptavidin surface conditioning solution consisting of 50 mM NaOH and 1 M NaCl. Minimally biotinylated H₆SUMO-PqsR^{C87} protein (66 µg/mL) was captured onto streptavidin chip surfaces at 20 °C in 1x HBS-P+ as instrument running buffer. H₆Sumo-PqsR^{C87} was gradually injected in

a single channel at a constant flow-rate of 2 $\mu\text{L}/\text{min}$ until SPR response increases were no longer observed. For negative protein target purposes, minimally biotinylated carbonic anhydrase isozyme II (CAII) from bovine erythrocytes was immobilized in one of the flow cells on each chip. Overall configurations of biotinylated proteins captured on each chip are summarized in Table S1.

Table S1: Configuration of biotinylated proteins captured on CM5 chips

Chip	Channel	Immobilized	RU (SA)	RU (bt proteins)	purpose
1	1	SA + D-biotin	9772	-	Screening 1 st half of fragment library + dosage experiments
	2	SA + bt-PqsR	9079	6309	
	3	SA + SrtA	9401	8573	
	4	SA + CAII	8795	7276	
2	1	SA + D-biotin	10777	-	Screening 2 nd half of fragment library + dosage experiments
	2	SA + bt-PqsR	10205	5467	
	3	SA + CAII	10442	7072	
	4	SA + bt-PqsR	10003	5712	

SA (Streptavidin; Sigma), CAII (Bovine Carbonic anhydrase II; Sigma), bt (biotinylated), PqsR ($\text{H}_6\text{SUMO-PqsR}^{\text{C87}}$), SrtA (sortase A enzyme from *Staphylococcus aerus*; prepared in house)

d) SUMO protease 2 cleavage of biotinylated $\text{H}_6\text{SUMO-PqsR}^{\text{C87}}$. H_6SUMO tag was cleaved from biotinylated $\text{H}_6\text{SUMO-PqsR}^{\text{C87}}$ using SUMO3 protease 2 according to manufacturer's instructions (LifeSensors). Briefly, a 200 μl (380 μg) sample of bt- $\text{H}_6\text{SUMO-PqsR}^{\text{C87}}$ in (1x PBS, pH 7.4, 10 % glycerol (v/v)) was mixed with 0.4 μl of 1 M DTT and 2 μl of SUMO3 protease 2 (7 units/ μl) and incubated at 30 $^\circ\text{C}$ for 2.5 hrs. The mixture was applied onto a 1 ml HisTrap FF column at 1 ml/min to remove the H_6SUMO tag and His-tagged SUMO3 protease 2. The flow-through protein (cleaved bt.-PqsRC87) was collected and concentrated down to approximately 50 ml using Nanosep Ultrafiltration concentrator (Pall, 3 kDa MW cut-off) and subjected to size exclusion chromatography at a constant flow-rate of 0.5 ml/min on a Superdex 75 5/150 column equilibrated in 1x PBS, 10 % (v/v) glycerol buffer. Collected cleaved bt-PqsR^{C87} protein (0.4 ml, ~20 $\mu\text{g}/\text{ml}$) was stored frozen in 100 μl aliquots at -80 C and used for competition experiments.

e) SPR Sensorgrams

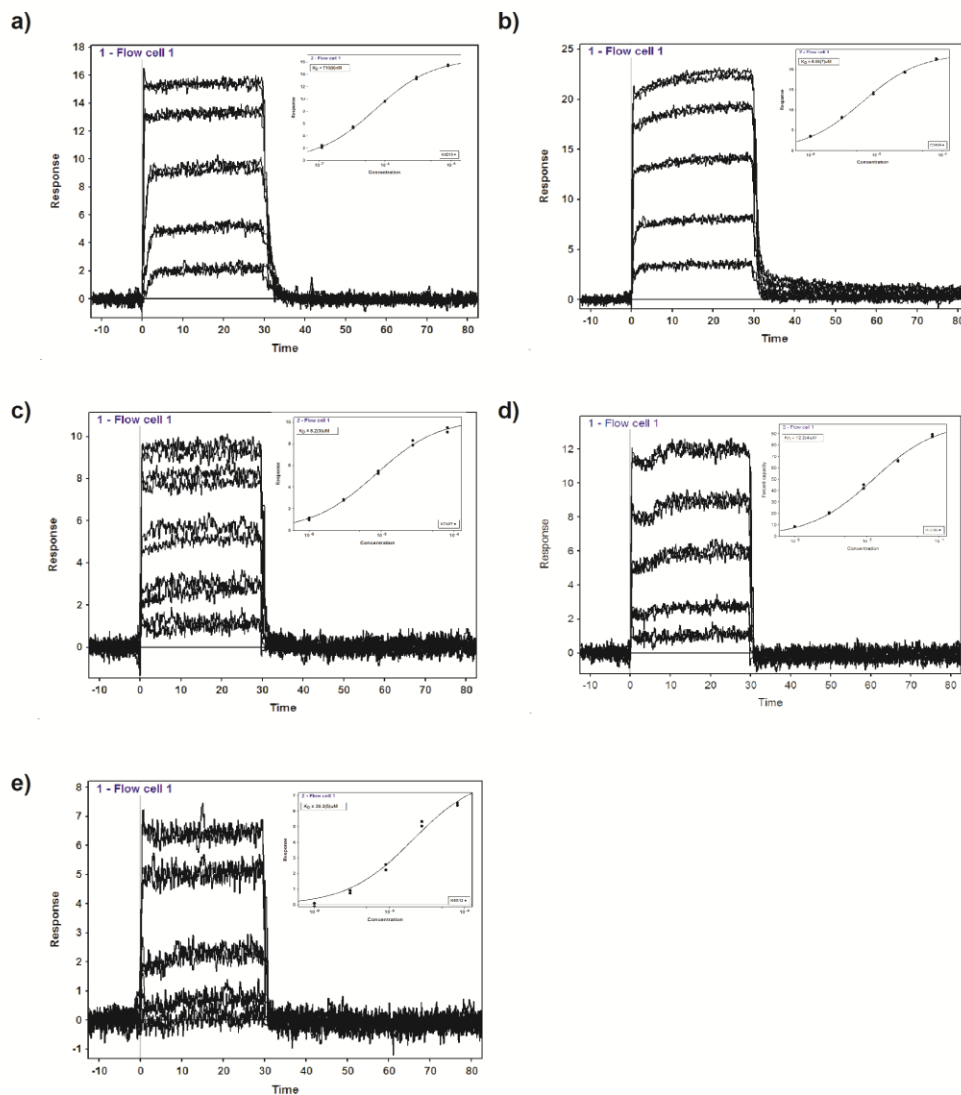


Figure S1: a – e) Binding affinities for hit compounds 4-8. SPR sensorgrams for fragment hits binding to H_6 SUMO-PqsR^{C87} analyzed in duplicate. Insets: fit of the binding responses at equilibrium (plotted against fragment concentration) to a simple 1:1 binding isotherm

f) SPR Competition Experiments

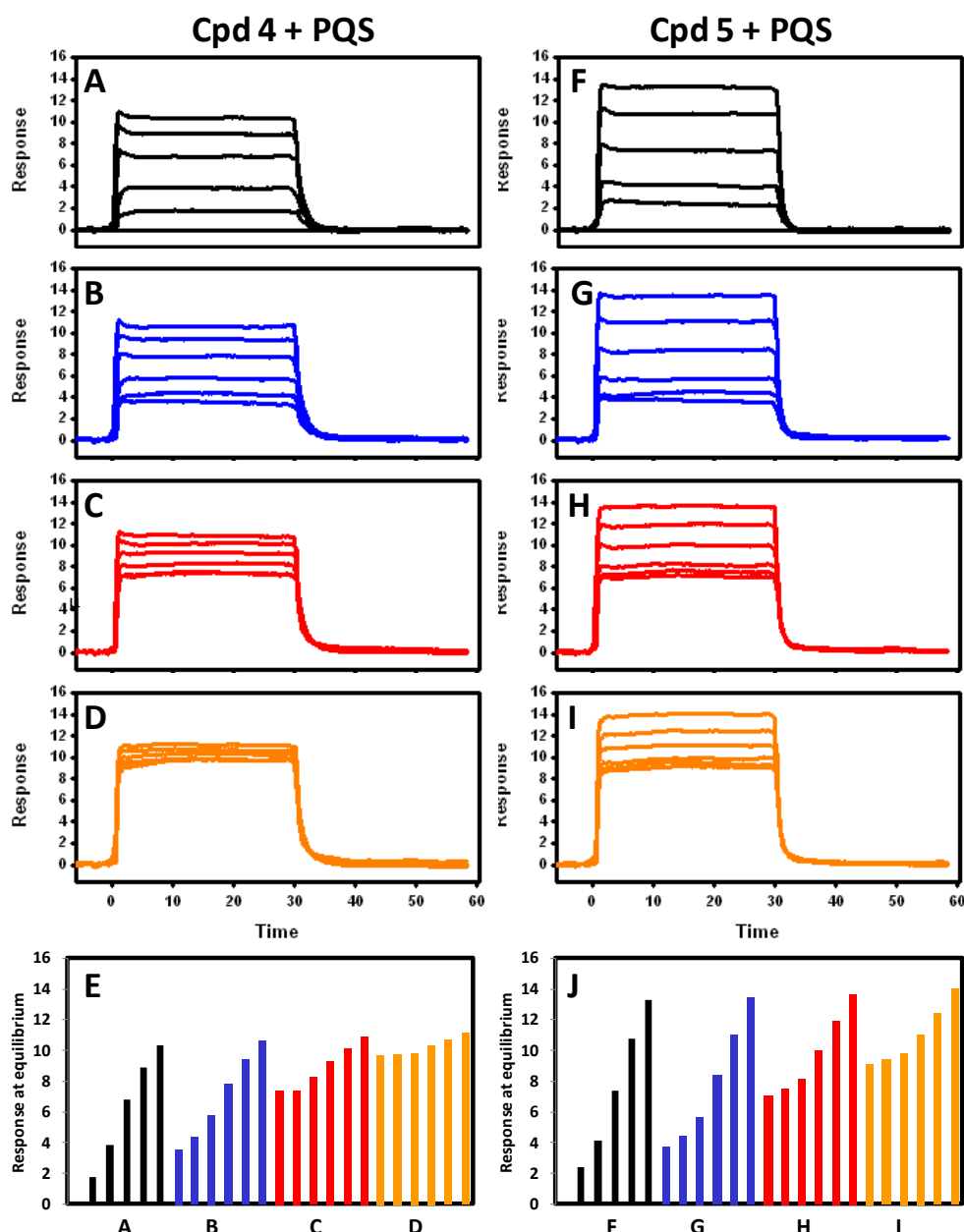


Figure S2: SPR Competition Experiments.

SPR sensorgrams obtained with mixtures consisting of PQS ligand and either **4** (left panels) or **5** (right panels) binding to immobilized pqsR^{C87} (2,600 RU). Compounds were diluted three-fold (**4** from 18 μ M and **5** from 81 μ M) and then mixed 1:1 with 4 different concentrations of PQS. Final injected concentration were: Compound **4** at 0 μ M (running buffer), 0.11 μ M, 0.33 μ M, 1 μ M, 3 μ M and 9 μ M all mixed with PQS at **a)** 0 μ M, **b)** 1 μ M, **c)** 3 μ M and **d)** 9 μ M; Compound **5** at 0 μ M (running buffer), 1 μ M, 3 μ M, 9 μ M, 27 μ M and 81 μ M all mixed with PQS at **f)** 0 μ M, **g)** 1 μ M, **h)** 3 μ M and **i)** 9 μ M. Bar charts of SPR responses taken at equilibrium for sensorgrams shown in A to D (**e**) and F to I (**j**).

g) Fragment Library

Fragments originate from the CSIRO compound collection consistent of approximately 50000 entities. The screening set is derived from two compound libraries which are described in detail in Table S2.

Table S2. Physicochemical Properties of Fragment Screening Set

Property	CSIRO heterocyclic chemistry diversity	CSIRO In silico diversity
Compounds	258	462
MW		
Min.–Max.	113–363	133–305
Mean	220	194
SD	49	35
cLogP		
Min.–Max.	-2.2–3.6	-2.2–5.1
Mean	0.79	0.84
SD	1.1	1.03
tPSA (Å²)		
Min.–Max.	24–137	13–117
Mean	65	51
SD	21	19
Rotatable bonds		
Min.–Max.	0–9	0–10
Mean	3.6	3.8
SD	1.8	2.1
HBA		
Min.–Max.	0–7	0–6
Mean	3.6	2.9
SD	1.5	1.2
HBD		
Min.–Max.	0–3	0–3
Mean	0.8	0.9
SD	0.7	0.7

2) Isothermal Titration Calorimetry

a) Protein Expression and Purification. Wild-type, Q194A mutant, and F221A mutant H₆SUMO-PqsR^{C87} were expressed in *E. coli* and purified using a single nickel affinity chromatography step. Briefly, *E. coli* BL21 (λDE3) cells containing the pSUMO3_ck4_pqsR^{C87}, the pSUMO3_ck4_Q194ApqsR^{C87} or the pSUMO3_ck4_F221ApqsR^{C87} plasmid² were grown in LB medium containing 50 μg mL⁻¹ kanamycin at 37 °C to an OD₆₀₀ of approximately 0.8 and over-expressed with 0.2 mM IPTG for 16 h at 16 °C. Protein purification was performed as described by Klein et al.²

b) Titration Procedure. ITC experiments were carried out using an ITC₂₀₀ instrument (Microcal Inc., GE Healthcare). Concentrations of ligand stock solutions in DMSO were determined by the weight of the compound. Final ligand concentrations were achieved by diluting 1:20 (v/v) in the experimental buffer resulting in a final DMSO concentration of 5% (v/v). Protein concentration was determined by measuring the absorbance at 280 nm using a theoretical molarity extinction coefficient of 22900 M⁻¹cm⁻¹. DMSO concentration in the protein solution was adjusted to 5% (v/v). ITC measurements were routinely performed at 25 °C in 20 mM Tris, pH 7.4, 150 mM NaCl, 10% glycerol (v/v), 5% DMSO (v/v) for the wild-type PqsR^{C87} and in 20 mM Tris, pH 7.8, 300 mM NaCl, 10% glycerol (v/v), 5% DMSO (v/v) for the Q194A and the F221A mutants, respectively. The titrations were performed on 43-190 μM H₆SUMO-PqsR^{C87}, H₆SUMO-Q194APqsR^{C87} or H₆SUMO-F221APqsR^{C87} in the 200 μL sample cell using 2-2.6 μL injections of 0.7-2.0 mM ligand solution every 180 s and a maximal syringe volume of 40 μL. To show competitive binding 43 μM H₆SUMO-PqsR^{C87} was incubated with 500 μM compound **2** for 30 min at 25 °C and a 500 μM solution of **37** was titrated subsequently into the preincubated mixture (19 injections of 2 μL). The *vice versa* experiment was performed accordingly. The data were collected and the area under each peak was integrated. To correct for heats of dilution and mixing the final base line consisting of small peaks of the same size at the end of the experiment was subtracted. The experimental data were fitted to a theoretical titration curve (one site binding model) using MicroCal Origin 7 software, with Δ*H* (enthalpy change in kcal/mol), *K_A* (association constant in M⁻¹), and *N* (number of binding sites) as adjustable parameters. Thermodynamic parameters were calculated from Eq. (1),

$$\Delta G = \Delta H - T\Delta S = RT\ln K_A = -RT\ln K_D \quad (1)$$

where Δ*G*, Δ*H*, and Δ*S* are the changes in free energy, enthalpy and entropy of binding, respectively, *T* is the absolute temperature, and *R* = 1.98 cal/mol/K. The LE for each compound was calculated from Eq. (2),

$$LE = -\Delta G/(\text{heavy atom count}) \quad (2)$$

where Δ*G* is the change in free energy and heavy atom count is the number of non-hydrogen atoms of the compound. For each ligand at least two independent experiments were performed (Figure S3).

c) ITC Titration Curves

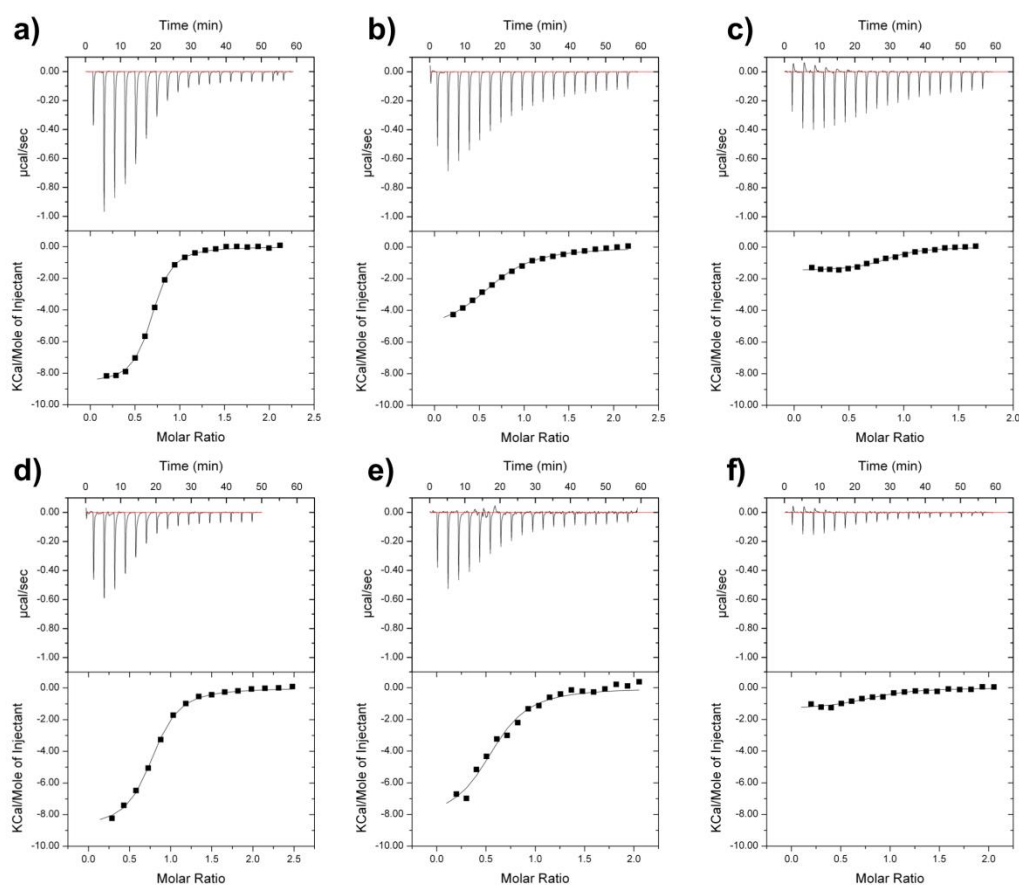


Figure S3: Representative ITC titrations

a) ITC titration of **4** (900 μM) against $\text{H}_6\text{SUMO-PqsR}^{\text{C87}}$ (86 μM). **b)** ITC titration of **4** (1 mM) against $\text{H}_6\text{SUMO-Q194APqsR}^{\text{C87}}$ (95 μM). **c)** ITC titration of **4** (1 mM) against $\text{H}_6\text{SUMO-F221APqsR}^{\text{C87}}$ (124 μM). **d)** ITC titration of **37** (500 μM) against $\text{H}_6\text{SUMO-PqsR}^{\text{C87}}$ (43 μM). **e)** ITC titration of **37** (500 μM) against $\text{H}_6\text{SUMO-Q194APqsR}^{\text{C87}}$ (50 μM). **f)** ITC titration of **37** (500 μM) against $\text{H}_6\text{SUMO-F221APqsR}^{\text{C87}}$ (50 μM). The recorded change in heat is shown in units of $\mu\text{cal/sec}$ as a function of time for successive injections of the ligand (upper row). Integrated heats (black squares) plotted against the molar ratio of the binding reaction. The continuous line represents the results of the non-linear least squares fitting of the data to a binding model (lower row).

d) Investigation of Competitive Binding by ITC

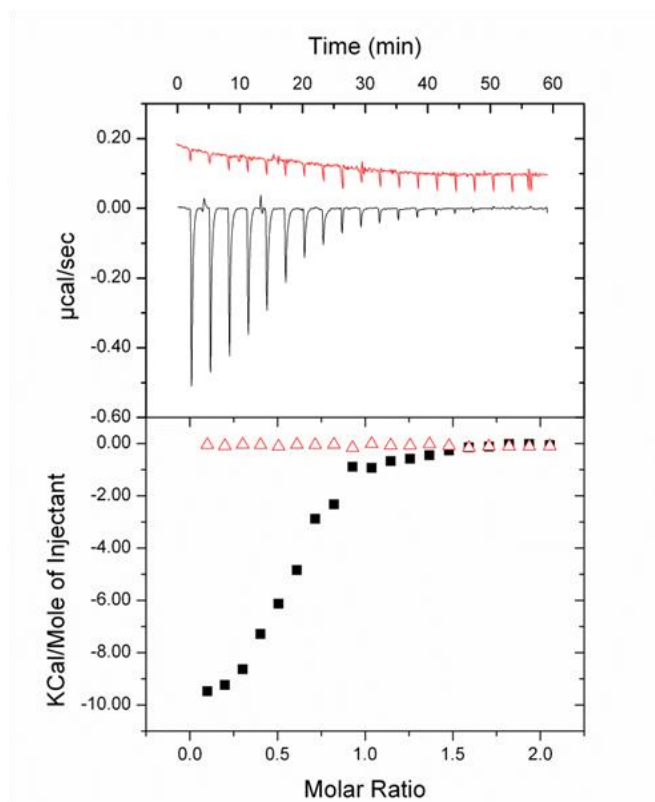


Figure S4: Competitive binding of **2** and **37** to PqsR. Raw ITC data (top) and integrated normalized data (bottom) for titrations of 50 μM PqsR with 500 μM **2** in the absence of **37** (\blacksquare , black curve) and in the presence of 500 μM compound **37** (\triangle , red curve).

3) Functional Evaluation of Compounds

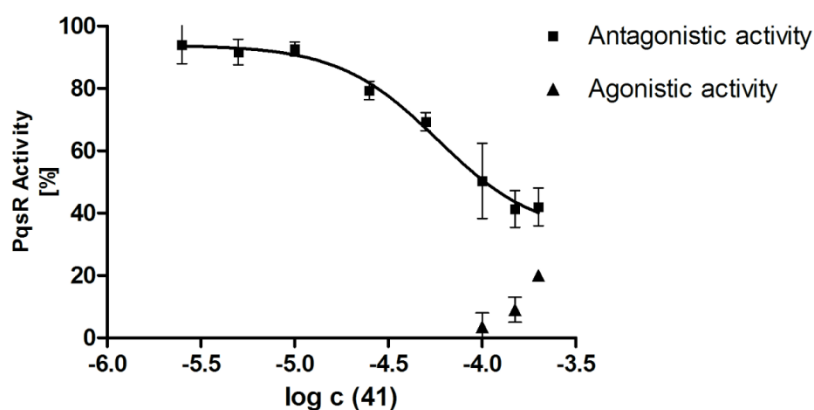


Figure S5: Dose response curve of **41** in *E. coli* reporter gene assay showing a partial antagonistic profile. Compound **41** was tested at 8 concentrations in competition to 50 nM PQS to determine the antagonistic activity and 3 different concentrations to show agonistic functionality. EC_{50} was 57.8 μ M; values obtained from 2 independent experiments with $n = 4$. Compound **41** tested up to maximum solubility under assay conditions (200 μ M). The log (inhibitor) vs. response model (Graph Pad Prism 5.04) was used to determine EC_{50} values.

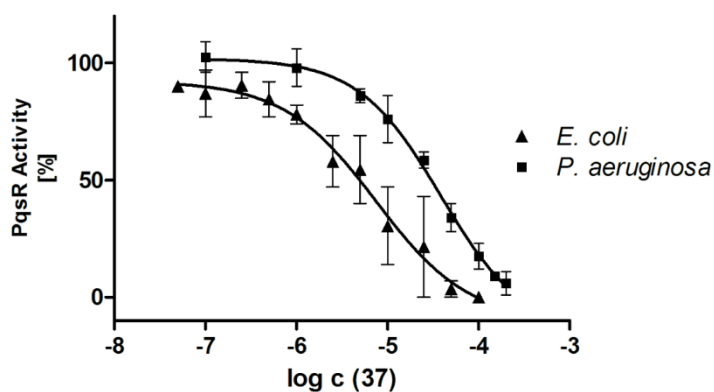


Figure S6: Dose response curve of **37** in *E. coli* and *P. aeruginosa*. Compound **37** was tested at 11 concentrations in *E. coli* (\blacktriangle) and 9 concentrations in *P. aeruginosa*. EC_{50} was 7.5 μ M in *E. coli* and 38.5 μ M in *P. aeruginosa*; values obtained from 2 independent experiments with $n = 4$. The log (inhibitor) vs. response model (Graph Pad Prism 5.04) was used to determine EC_{50} values.

4) Determination of Antibacterial Activity in *P. aeruginosa* PA14

Cultures of *P. aeruginosa* PA14 were inoculated with an overnight culture to obtain a starting $OD_{600} = 0.05$ and grown in three replicates in 100 ml Erlenmeyer flasks containing 10 ml LB medium at 37 °C, 200 rpm and a humidity of 75%. DMSO solutions of compound **37** were added to the cultures to a final DMSO concentration of 1%. Bacterial growth was measured as a function of OD_{600} using Spectronic Helios Epsilon spectrophotometer (Thermo Electron Corporation). *P. aeruginosa* PA14 cultures containing 1% DMSO were used as control.

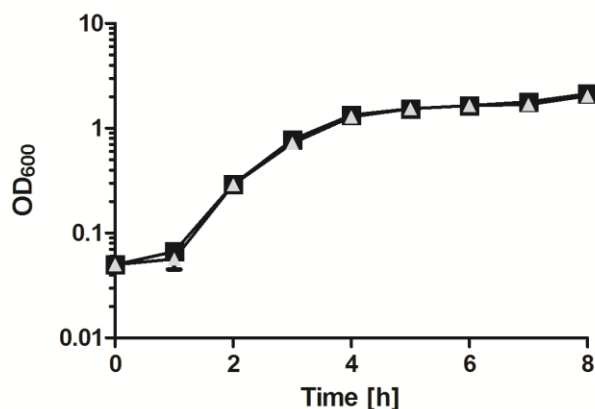


Figure S7. Growth Curves of *P. aeruginosa* PA14. Strains were grown in the absence (■) and presence of 250 μ M compound **37** (▲). Samples were taken at 0 h, 1 h, 2 h, 3 h, 4 h, 5 h, 6 h, 7 h and 8 h to measure OD_{600} . Mean value of one experiment with $n = 3$.

5) Synthesis and Characterization of Intermediates **23-30**, **43-46**

Benzoic acid derivatives **10-14** and benzoyl chloride derivatives **15-17**, **19**, **20** were obtained from commercial suppliers and used without further purification.

2-(3-Chlorobenzoyl)hydrazinecarbothioamide (23) was prepared according to General Procedure 3 starting from 3-chlorobenzoyl chloride (**15**, 2.73 g, 15.62 mmol) and hydrazinecarbothioamide (1.560 g, 17.12 mmol). The crude product was recrystallized from EtOH and obtained as yellow solid (3.724 g, 12.97 mmol, 83% yield). ^1H NMR (500 MHz, DMSO- d_6) δ ppm 7.52 (t, $J=7.9$ Hz, 1 H), 7.63 (dd, $J=7.6$, 0.9 Hz, 1 H), 7.71 (br. s., 1 H), 7.83 (d, $J=7.6$ Hz, 1 H), 7.90 (br. s., 1 H), 7.96 (s, 1 H), 9.36 (br. s., 1 H), 10.49 (s, 1 H); ^{13}C NMR (126 MHz, DMSO- d_6) δ ppm 126.55, 127.73, 130.19, 131.51, 132.96, 134.59, 164.60, 182.00; MS(ESI): m/z 229.84 (M+H) $^+$.

2-(3-Bromobenzoyl)hydrazinecarbothioamide (24) was prepared according to General Procedure 3 starting from 3-bromobenzoyl chloride (**16**, 1.25 g, 5.68 mmol) hydrazinecarbothioamide (1.56 g, 17.12 mmol) and obtained as white solid (1.55 g, 5.68 mmol, 100% yield). ^1H NMR (500 MHz, DMSO- d_6) δ ppm 7.45 (t, $J=7.88$ Hz, 1 H), 7.71 (br. s., 1 H), 7.77 (d, $J=8.20$ Hz, 1 H), 7.85 (d, $J=8.51$ Hz, 1 H), 7.90 (br. s., 1 H), 8.09 (s, 1 H), 9.35 (br. s., 1 H), 10.49 (br. s., 1 H); ^{13}C NMR (126 MHz, DMSO- d_6) δ ppm 121.4, 126.91, 130.43, 130.57, 134.39, 134.80, 164.53, 181.98; MS(ESI): m/z 273.71 (M+H) $^+$.

2-(3-(Trifluoromethyl)benzoyl)hydrazinecarbothioamide (25) was prepared according to General Procedure 3 starting from 3-(trifluoromethyl)benzoyl chloride (**17**, 10.00 g, 47.9 mmol) and hydrazinecarbothioamide (13.11 g, 144 mmol) and obtained as a white solid (10.6 g, 40.3 mmol, 84% yield). ^1H NMR (500 MHz, DMSO- d_6) δ ppm 7.69 - 7.80 (m, 2 H), 7.85 - 7.97 (m, 2 H), 8.16 (d, $J=7.9$ Hz, 1 H), 8.24 (s, 1 H), 9.39 (br. s., 1 H), 10.64 (br. s., 1 H); ^{13}C NMR (126 MHz, DMSO- d_6) δ ppm 123.93 (d, $^1J(\text{C},\text{F})=272.2$ Hz, 1 C), 124.58 (q, $^3J(\text{C},\text{F})=3.7$ Hz, 1 C), 128.23 (q, $^3J(\text{C},\text{F})=3.7$ Hz, 1 C), 128.94 (d, $^2J(\text{C},\text{F})=33.0$ Hz, 1 C), 129.50, 131.90, 133.52, 164.62, 182.00 MS(ESI): m/z 263.92 (M+H) $^+$.

2-(3-Cyanobenzoyl)hydrazinecarbothioamide (26) 3-Cyanobenzoic acid (**13**, 1.5 g, 10.2 mmol) was suspended in DCM (40 mL). Oxalyl chloride (1.5 mL, 17.14 mmol) and a catalytic amount of DMF were added. The solution was refluxed for 2 h. The mixture was concentrated under reduced pressure to obtain an orange oil (**18**). The oil was subsequently dissolved in dry THF (10 mL) and added portionwise to a suspension of hydrazinecarbothioamide (3.00 g, 32.9 mmol) in THF (30 mL). The resulting suspension was stirred over night at RT under nitrogen atmosphere. The suspension was quenched with water and alkalized using sat. NaHCO₃ solution. THF was removed under reduced pressure. The aqueous layer was extracted with ethyl acetate (2 times). A white solid dispersed between the layers. The aqueous layer was filtered to give a solid (S1). The combined ethyl acetate layers were washed with brine, dried over MgSO₄, filtered and concentrated to dryness to give a solid (S2). Both solids were recombined to obtain the expected product (1.14 g, 5.19 mmol, 51% yield). ¹H NMR (500 MHz, DMSO-*d*₆) δ ppm 7.71 (t, *J*=7.9 Hz, 1 H), 7.76 (br. s, 1 H), 7.95 (br. s, 1 H), 8.04 (d, *J*=7.6 Hz, 1 H), 8.17 (d, *J*=8.2 Hz, 1 H), 8.34 (s, 1 H), 9.41 (br. s, 1 H), 10.61 (br. s, 1 H); ¹³C NMR (126 MHz, DMSO-*d*₆) δ ppm 111.24, 118.25, 129.65, 131.64, 132.59, 133.67, 135.11, 164.22, 181.99; MS (ESI): *m/z* 220.99 (M+H)⁺.

2-(3-(Trifluoromethoxy)benzoyl)hydrazinecarbothioamide (27) was prepared according to General Procedure 3 starting from 3-(trifluoromethoxy)benzoyl chloride (**19**, 0.78 g, 3.48 mmol) and hydrazinecarbothioamide (950 mg, 10.43 mmol) and obtained as white solid (0.92 g, 3.34 mmol, 96% yield) ¹H NMR (500 MHz, DMSO-*d*₆) δ ppm 7.58 (d, *J*=8.8 Hz, 1 H), 7.63 (t, *J*=8.2 Hz, 1 H), 7.74 (br. s, 1 H), 7.85 (s, 1 H), 7.87 - 7.96 (m, 2 H), 9.38 (br. s, 1 H), 10.56 (br. s., 1 H); ¹³C NMR (126 MHz, DMSO-*d*₆) δ ppm 120.03 (q, ³*J*(C,F)=257.5 Hz, 1 C), 120.41, 124.21, 126.92, 130.38, 134.84, 148.09, 164.33, 181.96; MS (ESI): *m/z* 279.82 (M+H)⁺.

2-(3-Methoxybenzoyl)hydrazinecarbothioamide (28) was prepared according to General Procedure 3 starting from 3-methoxybenzoyl chloride (**21**, 0.55 g, 3.20 mmol) and hydrazinecarbothioamide (0.87 g, 9.61 mmol). The aqueous phase was filtered to obtain a mixture of product [*m/z* 225.99 (M+H)⁺] and an unknown side-product. The crude product was used in the next step without further purification.

2-(3-Methylbenzoyl)hydrazinecarbothioamide (29) was prepared according to General Procedure 3 starting from 3-methylbenzoyl chloride (**20**, 0.58 g, 3.79 mmol) and hydrazinecarbothioamide (1.04 g, 11.38 mmol) and obtained as a white solid (0.79 g, 3.79 mmol, 100 % yield). ¹H NMR (500 MHz, DMSO-*d*₆) δ ppm 2.36 (s, 3 H), 7.31 - 7.40 (m, 2 H), 7.58 (br. s, 1 H), 7.68 (d, *J*=7.3 Hz, 1 H), 7.73 (s, 1 H), 7.85 (br. s, 1 H), 9.31 (br. s, 1 H), 10.31 (br. s, 1 H); ¹³C NMR (126 MHz, DMSO-*d*₆) δ ppm 20.90, 124.94, 128.05, 128.39, 132.26, 132.48, 137.41, 165.97, 182.01; MS (ESI): *m/z* 209.96 (M+H)⁺.

3-(Tert-butyl)benzoylthiosemiamidecarbazine (30) 3-(Tert-butyl)benzoic acid (**14**, 1.10 g, 6.17 mmol) was suspended in DCM (20 mL). Oxalyl chloride (1.1 mL, 12.57 mmol) and a catalytic amount of DMF were added. The reaction mixture was refluxed for 2 h under a nitrogen atmosphere. The reaction mixture was concentrated under reduced pressure to give a yellow oil (**22**). The oil was dissolved in THF (10 mL) and slowly added to a suspension of hydrazinecarbothioamide (1.68 g, 18.43 mmol) in THF (30 mL) at 0 °C. The reaction mixture was allowed to warm to RT and was stirred for 24 h at ambient temperature. The reaction was quenched with water and alkalized using a saturated aqueous solution of NaHCO₃. THF was evaporated and a yellow solid precipitated. The suspension was sonicated and filtered. The resulting cake was washed with water and dried in a desiccator to afford the expected product (1.36 g, 5.41 mmol, 88% yield). ¹H NMR (500 MHz, DMSO-*d*₆) δ ppm 1.31 (s, 9 H), 7.39 (t, *J*=7.7 Hz, 1 H), 7.56 - 7.60 (m, 1 H), 7.63 (br. s, 1 H), 7.70 (dt, *J*=7.6, 1.4 Hz, 1 H), 7.84 (br. s, 1 H), 7.91 (t, *J*=1.7 Hz, 1 H), 9.32 (br. s, 1 H), 10.37 (s, 1 H); ¹³C NMR (126 MHz, DMSO-*d*₆) δ ppm 31.02 (3 C), 34.57, 124.62, 125.08, 127.93, 128.60, 132.21, 150.67, 166.13, 182.04; MS(ESI): *m/z* 252.20 (M+H)⁺

3-(Trifluoromethyl)benzohydrazide (43) A sealed reaction vial was charged with MeOH (100 mL) and triethylamine (10.0 ml, 71.9 mmol). 3-(Trifluoromethyl)benzoyl chloride (7.25 ml, 47.9 mmol) was added dropwise. The reaction was stirred overnight at RT. The solvent was evaporated and the crude product was diluted with water. The aqueous phase was extracted with ethyl acetate (3 times). The combined organic layers were concentrated to give a yellow oil. The resulting oil was filled into sealed reaction vessel. Water (40 mL) and hydrazine hydrate (5.0 mL, 126 mmol) were added. The reaction mixture consisting of two phases was heated for

5 h at 120 °C. The reaction was quenched by the addition of water. The resulting suspension was filtered to yield the expected product as colorless crystals (7.45 g, 36.5 mmol, 76% yield). ¹H NMR (500 MHz, DMSO-*d*₆) δ ppm 4.65 (br. s., 2 H), 7.70 (t, *J*=7.88 Hz, 1 H), 7.88 (d, *J*=7.88 Hz, 1 H), 8.13 (d, *J*=7.88 Hz, 1 H), 8.15 (s, 1 H), 10.05 (br. s., 1 H); ¹³C NMR (126 MHz, DMSO-*d*₆) δ ppm 123.93 (d, ¹*J*(C,F)=272.18 Hz, 1 C), 123.56 (q, ³*J*(C,F)=3.67 Hz, 1 C), 127.60 (q, ³*J*(C,F)=3.67 Hz, 1 C), 129.15 (q, *J*=32.1 Hz, 1 C), 129.6, 130.94, 134.16, 164.20; MS (ESI): *m/z* 205.06 (M+H)⁺.

Methyl-2-(3-(trifluoromethyl)benzoyl)hydrazinecarboxylate (44) 3-(Trifluoromethyl)benzohydrazide (**43**, 1.00 g, 4.90 mmol) was suspended in water and dioxane (15 mL each). NaHCO₃ (1.21 g, 14.4 mmol) was added. Methyl chloroformate (0.45 mL, 5.82 mmol) was added dropwise at 0 °C (ice bath). The reaction mixture was stirred at bath temperature for 1 h. It was then extracted twice with ethyl acetate and the combined organic fractions were washed with brine. The organic phase was dried over MgSO₄ and concentrated. Heptane was added and the solution concentrated to dryness to yield the expected product as a white solid (1.20 g, 4.58 mmol, 93% yield). ¹H NMR (500 MHz, DMSO-*d*₆) δ ppm 3.65 (s, 3 H), 7.77 (t, *J*=7.7 Hz, 1 H), 7.97 (d, *J*=7.9 Hz, 1 H), 8.17 (d, *J*=8.2 Hz, 1 H), 8.19 (s, 1 H), 9.34 (br. s., 1 H), 10.58 (br. s., 1 H); ¹³C NMR (126 MHz, DMSO-*d*₆) δ ppm 52.04, 123.83 (d, ¹*J*(C,F)=271.3 Hz, 1 C), 123.91, 128.50, 129.31 (q, ²*J*(C,F)=33.0 Hz, 1 C), 129.94, 131.46, 133.19, 156.75, 164.66; MS (ESI): *m/z* 262.06 (M+H)⁺.

N-(2,2,2-trifluoroacetyl)-3-(trifluoromethyl)benzohydrazide (45) 3-(Trifluoromethyl)benzohydrazide (**43**, 1.00 g, 4.90 mmol) and triethylamine (1.20 mL, 8.61 mmol) were dissolved in DCM (25 mL). Trifluoroacetic anhydride (0.80 mL, 5.66 mmol) was added slowly at 0 °C. The mixture was stirred at RT over night. After 22 h an additional amount of trifluoroacetic anhydride (0.10 mL, 0.708 mmol) was added. The reaction mixture was stirred for 2 h at RT. The mixture was poured into a saturated aqueous solution of NaHCO₃. The aqueous phase was extracted twice using DCM. The combined organic layers were washed with brine, dried over MgSO₄ and concentrated to afford a yellow oil. The oil was adsorbed on silica gel and purified by flash chromatography on silica gel using DCM:THF (95:5) to yield the product as a pale yellow solid (0.650 g, 2.16 mmol, 44% yield). ¹H NMR (500 MHz, DMSO-*d*₆) δ ppm 7.81 (t, *J*=7.6 Hz, 1 H), 8.02 (dd, *J*=7.9, 0.6 Hz, 1 H), 8.20 (d, *J*=8.2 Hz, 1 H), 8.21 (s, 1 H), 11.10 (s, 1 H), 11.76 (br. s., 1 H); ¹³C NMR (126 MHz, DMSO-*d*₆) δ ppm 115.79 (d, ¹*J*(C,F)=289.6 Hz, 1 C), 123.78 (d, ¹*J*(C,F)=271.3 Hz, 1 C), 123.98 (d, ³*J*(C,F)=4.6 Hz, 1 C), 128.94, 129.44 (q, ²*J*(C,F)=31.2 Hz, 1 C), 130.16, 131.61, 132.44, 155.83 (q, ²*J*(C,F)=37.6 Hz, 1 C), 163.84. MS (ESI): *m/z* (not detected)

Ethyl-5-(3-(trifluoromethyl)phenyl)-1,3,4-oxadiazole-2-carboxylate (46) 3-(Trifluoromethyl)benzohydrazide (**43**, 1.30 g, 6.37 mmol) was dissolved in DCM (50 mL) and triethylamine (4.00 mL, 28.7 mmol) was added. Ethyl oxalyl monochloride (1.20 g, 8.79 mmol) was added slowly at 0 °C. The mixture was stirred under nitrogen for 1.5 h at bath temperature. Tosyl chloride (1.82 g, 9.55 mmol) was added and the reaction was aged at RT for 12 h. The mixture was diluted with DCM, washed with NaHCO₃ (twice) and brine. The organic layer was dried over MgSO₄, filtered and concentrated under reduced pressure to yield a brown oil. The oil was adsorbed on silica gel and purified by flash chromatography with hexane/acetone (95:5) to obtain a colorless oil, which crystallized in the fridge (1.07 g, 3.74 mmol, 59% yield). ¹H NMR (500 MHz, CHLOROFORM-*d*) δ ppm 1.51 (t, *J*=6.9 Hz, 3 H), 4.59 (q, *J*=7.3 Hz, 2 H), 7.72 (t, *J*=7.9 Hz, 3 H), 7.88 (dd, *J*=7.9, 0.6 Hz, 6 H), 8.38 (d, *J*=7.9 Hz, 1 H), 8.45 (s, 1 H); ¹³C NMR (126 MHz, CHLOROFORM-*d*) δ ppm 14.08, 63.76, 123.32 (q, ¹*J*(C,F)=273.1 Hz, 1 C), 123.66, 124.52 (q, ³*J*(C,F)=3.7 Hz, 1 C), 129.32 (q, ³*J*(C,F)=3.7 Hz, 1 C), 130.00, 130.69, 132.06 (q, ²*J*(C,F)=33.9 Hz, 1 C), 154.19, 156.79, 165.19; HRMS: *m/z* calcd 287.0638 found 287.0649.

6) High Resolution Mass Spectroscopy

All measurements were performed on a Dionex Ultimate 3000 RSLC system using a Waters BEH C18, 50 x 2.1 mm, 1.7 μ m dp column. Separation of 1 μ L sample was achieved by a linear gradient with (A) H₂O + 0.1% FA to (B) ACN + 0.1% FA at a flow rate of 600 μ L/min and 45 °C. The gradient was initiated by a 1 min isocratic step at 5% B, followed by an increase to 95% B in 6 min to end up with a 1.5 min step at 95% B before reequilibration with initial conditions. UV spectra were recorded by a DAD in the range from 200 to 600 nm. The LC flow was split to 75 μ L/min before entering the maXis 4G hr-ToF mass spectrometer (Bruker Daltonics) using the standard ESI source. Mass spectra were acquired in centroid mode ranging from 50 – 1000 *m/z* at 2 Hz scan speed.

7) Purity of Final Compounds (LC/MS Determination)

Purity control was carried out using a SpectraSystems LC system (Thermo Fisher Scientific) consisting of a pump, an autosampler, and a VWD detector. Mass spectrometry was performed on an MSQ electro spray mass spectrometer (Thermo Fisher Scientific). The system was operated by the standard software Xcalibur. An RP-C18 NUCLEODUR 100-5 (125x3 mm) column (Macherey-Nagel GmbH) was used as stationary phase. All solvents were HPLC grade. For purity determination one of the following methods was used:

- 1) Mobile phase, A = water + 0.1% trifluoroacetic acid, B = acetonitrile + 0.1% trifluoroacetic acid; gradient, 0.0-15.0 min, 0-100% B, 15.0-20.0 min, 100% B; flow rate 0.8 mL/min; injection volume was 10 μ L
- 2) Mobile phase, A = water, B = acetonitrile; gradient, 0.0-15.0 min, 0-100% B, 15.0-20.0 min, 100% B; flow rate 0.8 mL/min; injection volume was 10 μ L

Low-resolution mass analysis was carried out at a spray voltage of 3800 V, a capillary temperature of 350 °C, and a source CID of 10 V. Spectra were acquired in positive mode from 100 to 1000 *m/z* at 254 nm for the UV trace.

Cmpd	t_R (min)	Method	UV purity	MS (ESI) m/z
5	7.09	1	98	252.88 (M+H+CH ₃ CN) ⁺
9	7.60	1	98	236.99 (M+H+CH ₃ CN) ⁺
31	8.12	1	96	252.82 (M+H+CH ₃ CN) ⁺
32	7.75	1	95	236.81 (M+H+CH ₃ CN) ⁺
33	6.47	1	98	252.89 (M+H+CH ₃ CN) ⁺
34	6.72	1	97	236.97 (M+H+CH ₃ CN) ⁺
35	5.97	1	99	203.09 (M+H+CH ₃ CN) ⁺
36	8.47	1	98	239.84 (M+H) ⁺
37	8.61	1	99	270.88 (M+H+CH ₃ CN) ⁺
38	6.27	1	99	227.94 (M+H+CH ₃ CN) ⁺
39	8.80	1	97	286.87 (M+H+CH ₃ CN) ⁺
40	6.96	1	99	192.02 (M+H) ⁺
41	7.18	1	95	176.06 (M+H) ⁺
42	9.75	1	96	259.09 (M+H+CH ₃ CN) ⁺
47	10.03	1	97	255.91 (M+H+CH ₃ CN) ⁺
48	10.49	1	99	270.00 (M+H+CH ₃ CN) ⁺
49	10.87	1	99	-
50	13.06	1	98	-
51	9.28	1	96	243.89 (M+H) ⁺
52	7.94	1	98	-
53	9.74	2	99	-

References

- (1) Johnsson, B.; Löfås, S.; Lindquist, G. Immobilization of proteins to a carboxymethyl-dextran-modified gold surface for biospecific interaction analysis in surface plasmon resonance sensors. *Anal. Biochem.* **1991**, *198*, 268–277.
- (2) Klein, T.; Henn, C.; Jong, J. C. de; Zimmer, C.; Kirsch, B.; Maurer, C. K.; Pistorius, D.; Müller, R.; Steinbach, A.; Hartmann, R. W. Identification of Small-Molecule Antagonists of the *Pseudomonas aeruginosa* Transcriptional Regulator PqsR: Biophysically Guided Hit Discovery and Optimization. *ACS Chem. Biol.* **2012**, *7*, 1496–1501.

7.2 Supplementary Material of Chapter B

1) Ligand Interaction Studies

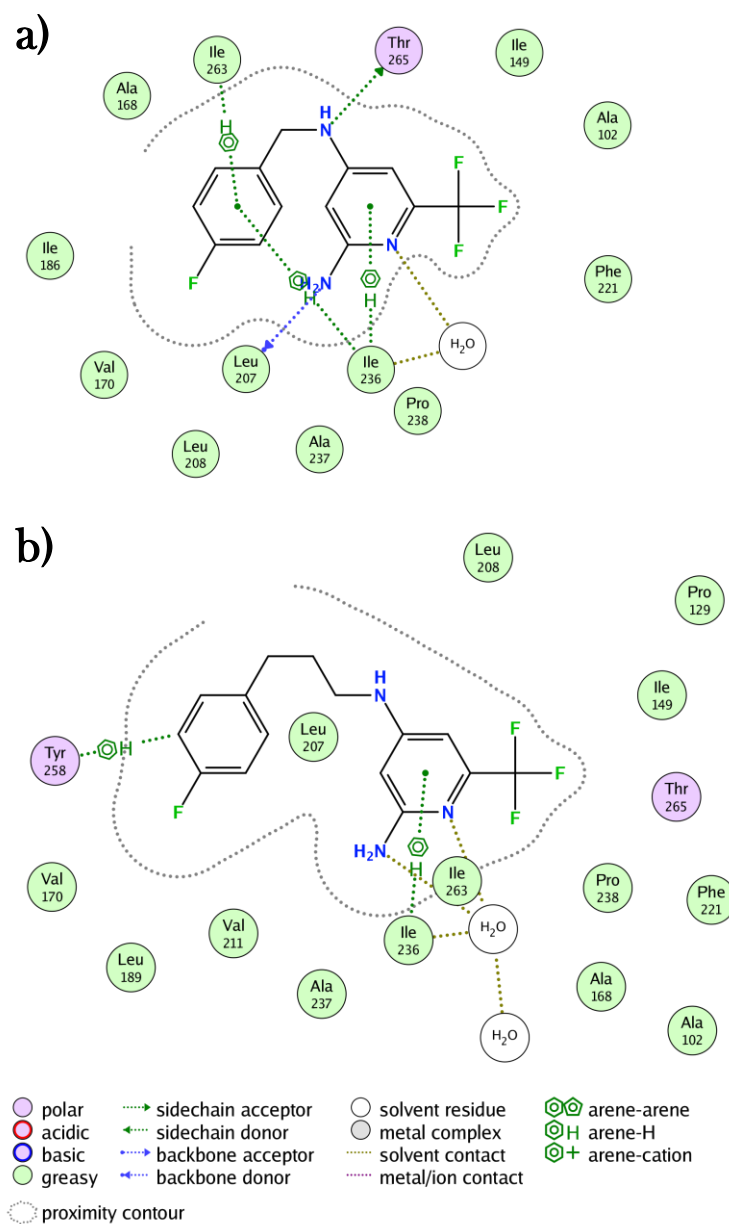


Figure S1: 2D schematic representation of compounds **11** (A) and **20** (B) in complex with PqsR_{c91}. Protein-ligand interactions after energy minimization using the “Quickprep” application included in the MOE software package were indicated as described in the legend.

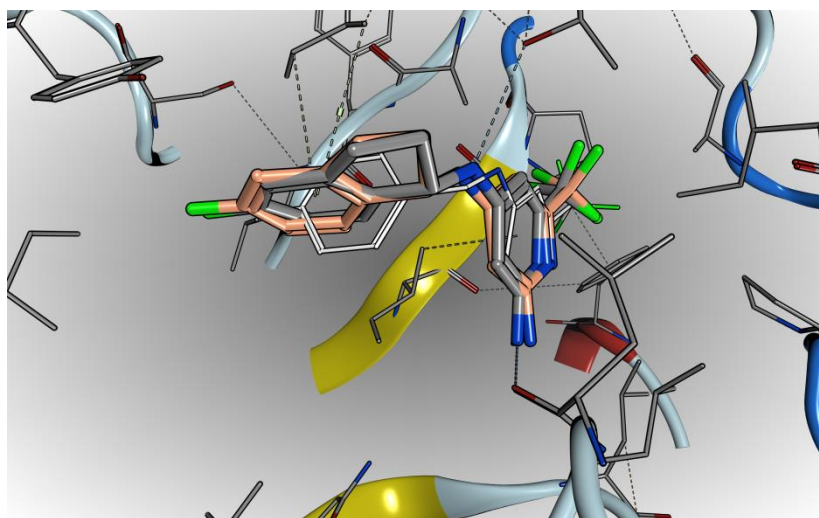


Figure S2: Modeled binding pose of compound **17**. Binding pose of **17** (before energy minimization with LigX rose fat line and after grey fat line) was modeled based on the crystal structure of PqsRc91 in complex with **11** (thin white line).

2) Isothermal Titration Calorimetry

a) Site-directed Mutagenesis PqsR_{T265A} mutant: The plasmid pSUMO3_ck4_T265ApqsR^{C87} was generated as previously described¹ using QuikChange Site-Directed Mutagenesis Kit (Stratagene) following the manufacturer's instructions. The following primer were used: forward 5' CGAACCGGGCGGCATCGACGCGAAGGTGTATTGC 3' and reverse 5' GCAATACACCTTCGCGTTCGATGCCGCCCGGTTTCG 3'. PCR condition to amplify the T265A gene: 16 cycles with 35s denaturation at 95 °C, 60 s annealing at 55 °C, and 13 min extension. The generated plasmid was transformed via electroporation into *E. coli* BL21

b) Expression and Purification of H₆SUMO-PqsR^{C87} H₆SUMO-PqsR^{C87} and T265A mutant H₆SUMO-PqsR^{C87} for ITC studies was expressed and purified as previously reported.^{1,2} Briefly, *E. coli* BL21 (λDE3) transfected with the pSUMO3_ck4_pqsR^{C87} or pSUMO3_ck4_T265ApqsR^{C87} plasmid² were grown in LB medium containing 50 μg mL⁻¹ kanamycin at 37 °C to an OD₆₀₀ of approximately 0.8 and expression was induced with 0.2 mM IPTG for 16 h at 16 °C. The protein was purified using nickel affinity chromatography in a one step gradient.

c) Titration Procedure. ITC titrations were performed as described before.^{1,2} Briefly, ITC experiments were carried out using an ITC₂₀₀ instrument (Microcal Inc., GE Healthcare). The titrations were performed on 50-150 μM H₆SUMO-PqsR^{C87} in the 200 μL sample cell using 19 injections of 2 μL ligand solution (0.5-1.5 mM) every 180 s. The data were collected and the area under each peak was integrated. To correct for heats of dilution and mixing the final base line consisting of small peaks of the same size at the end of the titration were subtracted. Ligand efficiency (LE) was calculated according to formula 1 and enthalpic efficiency (EE) was calculated according to formula 2:

$$LE = -\Delta G/(\text{heavy atom count}) \quad (1)$$

$$EE = -\Delta H/(\text{heavy atom count}) \quad (2)$$

ΔG is the change in free energy, ΔH is the enthalpic contribution and heavy atom count is the number of non-hydrogen atoms of the compound.

d) Thermodynamic profiles of **11** binding to PqsR_{wt} and PqsR_{T265A}

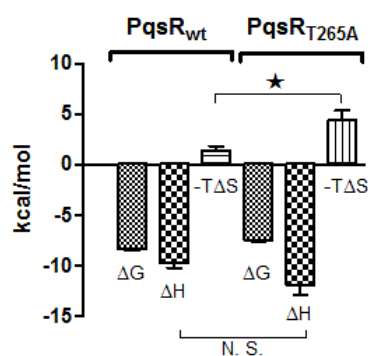


Figure S3: Comparison of the thermodynamic profiles of **11** binding to PqsR_{wt} (left part) and PqsR_{T265A} (right part). T-test of ΔH values (PqsR_{wt}/PqsR_{T265A}) showed no significant difference ($P > 0.05$). T-test of $-T\Delta S$ elucidated a significant difference ($P < 0.05$).

e) Representative ITC titration curves

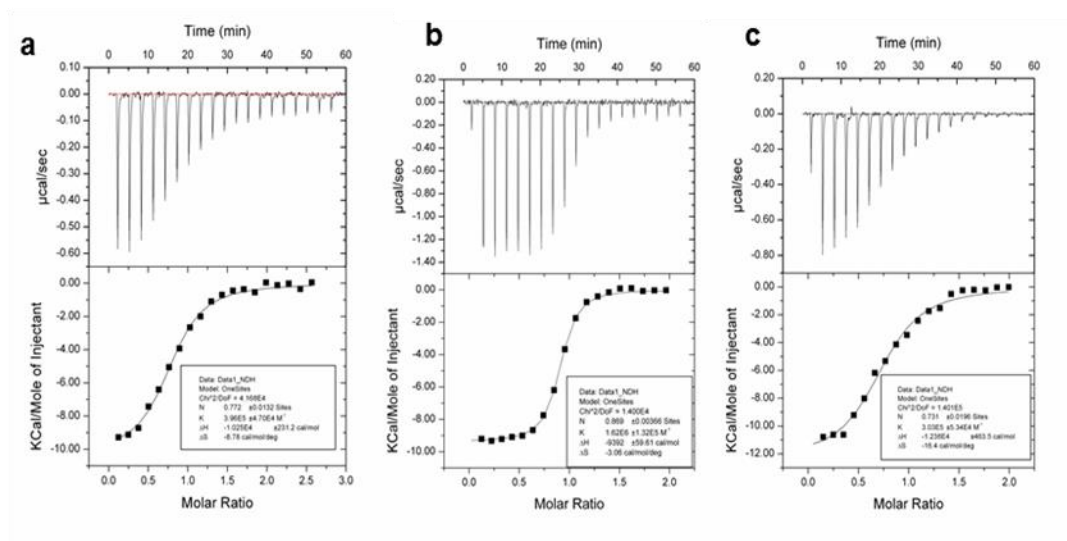


Figure S4: Representative ITC titrations against H_6 SUMO-PqsR^{C87} (50 μ M) **a**) **7** (500 μ M) **b**) **11** (500 μ M) **c**) (500 μ M) **c**) **20** (500 μ M). The upper row shows the heat change recorded over time in μ cal/sec for 19-injections of the ligand. The lower row shows the integrated heats (■) plotted against the molar ratio of the binding reaction. Data were fitted to a 1:1 binding model continuous black line. The continuous line represents the results of the non-linear least squares fitting of the

f) Thermodynamic profiles of selected compounds

Table S1: Thermodynamic evaluation of selected antagonists

Comp	K_D (ITC) [μ M]	ΔG [kcal mol ⁻¹]	ΔH [kcal mol ⁻¹]	$-T\Delta S$ [kcal mol ⁻¹]	EE ^a [kcal mol ⁻¹]	LE ^b [kcal mol ⁻¹]
9	7.5 \pm 0.1	-6.9 \pm 0.0	-3.7 \pm 0.6	-3.8 \pm 0.6	0.23	0.43
11	0.6 \pm 0.2	-8.4 \pm 0.2	-9.8 \pm 0.8	1.0 \pm 0.8	0.49	0.42
12	1.4 \pm 0.5	-8.1 \pm 0.3	-11.3 \pm 0.3	3.2 \pm 0.5	0.57	0.43
13	1.3 \pm 0.3	-8.0 \pm 0.1	-11.6 \pm 0.9	3.5 \pm 0.8	0.55	0.40
19	4.7 \pm 2.3	-7.4 \pm 0.3	-13.5 \pm 0.6	6.1 \pm 0.7	0.64	0.35
20	2.8 \pm 0.5	-7.6 \pm 0.1	-11.4 \pm 0.9	3.8 \pm 1.0	0.50	0.35
22	1.0 \pm 0.0	-8.2 \pm 0.2	-12.9 \pm 0.1	4.7 \pm 0.1	0.56	0.36

ITC titrations were performed at 298 K. Data represent mean \pm SD from at least two independent experiments; ^aEE = $-\Delta H/(\text{heavy atom count})$; ^bLE = $-\Delta G/(\text{heavy atom count})$

3) Protein Crystallography

a) Expression and Purification of PqsR₉₁₋₃₁₉. The ligand binding domain of PqsR comprising the residues 91-319 (PqsR₉₁₋₃₁₉) was expressed and purified as reported by Xu et al.⁴ with some modifications. The plasmid pOPIN-His6-SUMO-PqsR₉₁₋₃₁₉ was transformed into *E.coli* BL21-CodonPlus(DE3)-RIL cells and the protein expression was induced with 0.5 mM IPTG for 16 h at 20°C, when the culture reached an OD₆₀₀ of 2.5. After centrifugation, the cells were resuspended in buffer A (150 mM Na₂HPO₄/NaH₂PO₄, 300 mM NaCl, pH 8.0) supplemented with one EDTA-free protease inhibitor cocktail tablet (Roche Life Science). The cells were lysed with an Emulsiflex-C3 homogenizer (Avestin) in two cycles and the supernatant was applied onto a HisTrap HP column (GE Healthcare). His6-SUMO-PqsR₉₁₋₃₁₉ was eluted with a linear gradient of buffer B (150 mM Na₂HPO₄/NaH₂PO₄, 300 mM NaCl, 50-200 mM imidazole pH 8.0). After cleavage of the His6-SUMO tag by SUMO protease and a second nickel affinity chromatography, PqsR₉₁₋₃₁₉ was finally purified by size exclusion chromatography in 20 mM HEPES, 150 mM NaCl, 1 mM DTT, pH 8.0. The protein was concentrated to 33 mg/ml, flash-frozen in liquid nitrogen and stored at -80°C

Table S2: Crystallization conditions of PqsR91-319 in complex with HHQ/11/20

Protein - ligand complex	[Protein] (mM)	[Ligand] (mM)	Crystallization condition	Cryoprotectant
PqsR ₉₁₋₃₁₉ - HHQ	0.58	5	0.1 M Tris-HCl (pH 8.5), 50% (v/v) ethylene glycol, 0.2 M MgCl ₂ , 0.1 M CsCl	-
PqsR ₉₁₋₃₁₉ - 11	0.78	4	0.1 M MES (pH 5.7), 0.1 M NaH ₂ PO ₄ , 0.1 M K ₂ HPO ₄ , 2.4 M NaCl	20% (v/v) glycerol
PqsR ₉₁₋₃₁₉ - 20	0.39	2	0.085 M tri-sodium citrate (pH 5.6), 29.8% (v/v) 2-methyl-2-propanol, 15% (v/v) glycerol	-

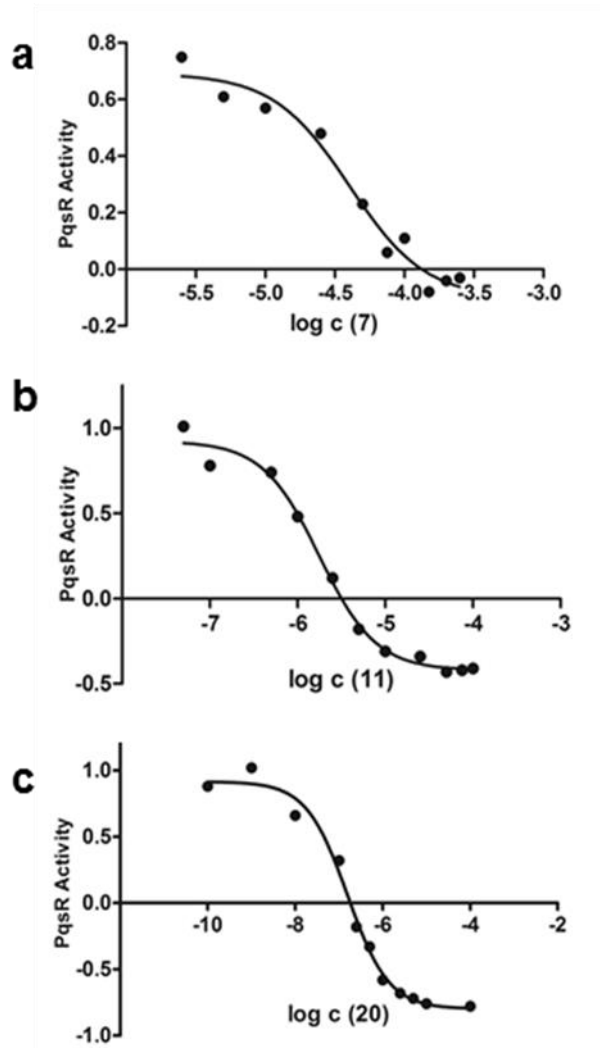
4) *E. coli* reporter-gene assay: dose-response curves

Figure S3: Antagonistic activity of different compounds measured in the *E. coli* reporter gene assay. Representative dose-response curves of **a)** compound **7** **b)** compound **11** and **c)** compound **20**. PqsR activity refers to the stimulation of PqsR induced by 50 nM PQS (= 1). Black dots (•) represent the PqsR activity measured in the presence of a single compound concentration. The continuous black line is the non-linear regression analysis to determine IC_{50} values using a log (inhibitor) vs. response model (Graph Pad Prism 5.04).

5) Effects on Pyocyanin in *P. aeruginosa*

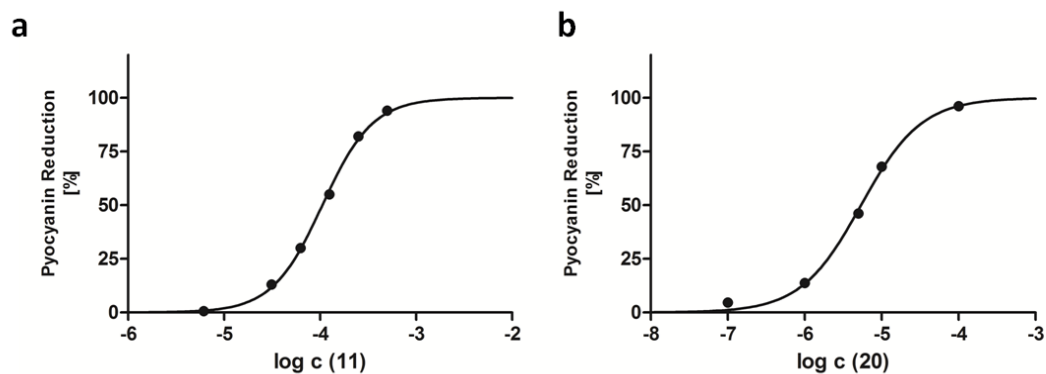
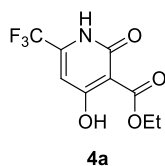


Figure S4: Inhibition of virulence factor pyocyanin was evaluated in the clinical isolate PA14. Representative dose-response curves **a)** compound **11** **b)** compound **20**. Black dots (•) represent the reduction of pyocyanin in presents of a given compound concentration relative to DMSO control (= 0 %). The continuous black line is the none-linear regression analysis to determine IC_{50} values using a log (inhibitor) vs. response model with constrains (bottom = 0; top = 100) (Graph Pad Prism 5.04).

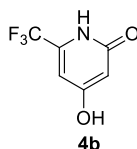
6) Synthesis and Characterization of Intermediates

a) Synthesis of intermediates 4a-4g

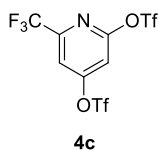


Ethyl-4-hydroxy-2-oxo-6-(trifluoromethyl)-1,2-dihydropyridine-3-carboxylate (4a)⁴ (E)-ethyl 3-amino-4,4,4-trifluorobut-2-enoate (20.1 ml, 137 mmol) and pyridine (13.5 ml, 166 mmol) were dissolved in dry DCM (200 ml). Ethyl-3-chloro-3-oxopropanoate (25.0 g, 166 mmol) was added slowly via syringe while cooling on a water bath. The reaction was stirred at ambient temperature for 4 days. The reaction mixture was diluted with DCM and quenched by addition of water. The aqueous layer was acidified by 2 M HCl. The organic layer was washed with NaHCO₃ saturated solution. Both aqueous layers were re-extracted with DCM. The combined organics were washed with brine, dried over MgSO₄, filtered and concentrated to yield a brown oil (41 g). Crude product was used in the next step.

The crude (28.2 g, 100 mmol) was dissolved in ethanol (100 ml). Potassium t-butoxide (22.35 g, 199 mmol) was added portionwise while keeping the temperature below 40°C. Afterwards the mixture was heated to 70°C for 2 h and stirred over night at RT. The reaction mixture was concentrated to give a brown solid. Saturated aqueous citric acid solution was added and the suspension stirred for 20 min. The suspension was filtered and the cake washed intensively with water. The resulting solid was dried at vacuum and 50°C to yield ethyl 4-hydroxy-2-oxo-6-(trifluoromethyl)-1,2-dihydropyridine-3-carboxylate as a white solid (12.6 g, 53.1 mmol, 53% yield). ¹H NMR (500 MHz, DMSO-*d*₆) δ ppm 1.25 (t, *J*=7.1 Hz, 3 H), 4.25 (q, *J*=6.9 Hz, 2 H), 6.80 (s, 1 H), 12.07 (br. s., 2 H); ¹³C NMR (126 MHz, DMSO-*d*₆) δ ppm 13.94, 60.94, 101.97 (q, *J*=2.7 Hz, 1 C), 105.88, 120.83 (q, *J*=274.9 Hz, 1 C), 162.25, 164.53, 164.56 (1 C missing).

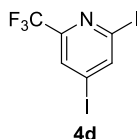


4-hydroxy-6-(trifluoromethyl)pyridin-2(1H)-one (4c)⁴ Ethyl-4-hydroxy-2-oxo-6-(trifluoromethyl)-1,2-dihydropyridine-3-carboxylate (24.9 g, 102.5 mmol) was added portionwise to a stirred solution of 6 M HCl (250 ml) at RT. The suspension was refluxed for 16 h. After cooling cooled to RT, the pH of the reaction mixture was adjusted to 4-6 using 10% aqueous ammonia solution. The suspension was filtered. The resulting cake was slurried in water and filtered again. The solid was dried at high vacuum to give 4-hydroxy-6-(trifluoromethyl)pyridin-2(1H)-one (16.97 g, 92.5 mmol, 90 % yield) as white solid. ¹H NMR (500 MHz, DMSO-*d*₆) δ ppm 6.02 (s, 1 H), 6.59 (s, 1 H); ¹³C NMR (126 MHz, DMSO-*d*₆) δ ppm 97.88, 103.17, 121.55 (q, *J*=274.9 Hz, 1 C), 144.23 (q, *J*=33.0 Hz, 1 C), 165.88, 169.20.

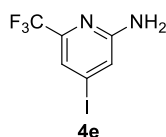


6-(trifluoromethyl)pyridine-2,4-diyl-bis(trifluoromethanesulfonate (4d)⁵ 4-hydroxy-6-(trifluoromethyl)pyridin-2(1H)-one (15.00 g, 84 mmol) was suspended in Acetonitrile (300 ml). Pyridine (14.9 ml, 184 mmol) was added while cooling the mixture on an ice bath. Triflic anhydride (31.1 ml, 184 mmol) was added while keeping the temperature below 10°C. An

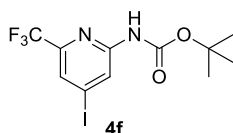
additional amount of triflic anhydride (10 ml, 59.2 mmol) was added and the reaction stirred over night. The mixture was poured into saturated Na_2CO_3 solution and extracted with EA. Combined organic extracts were washed with brine, dried (MgSO_4), filtered and concentrated. The crude was purified by column chromatography using PE:EA 95:5 to give 6-(trifluoromethyl)pyridine-2,4-diyl bis(trifluoromethanesulfonate) (12 g, 27.1 mmol, 32.3 % yield) a pale yellow solid ^1H NMR (500 MHz, CHLOROFORM-d) δ ppm 7.37 (d, $J=1.9$ Hz, 1 H), 7.70 (d, $J=1.9$ Hz, 1 H); ^{13}C NMR (126 MHz, CHLOROFORM-d) δ ppm 111.46, 114.25 (d, $J=2.7$ Hz, 1 C), 118.53 (q, $J=320.8$ Hz, 1 C), 118.55 (q, $J=320.8$ Hz, 1 C), 119.44 (q, $J=275.8$ Hz, 1 C), 149.70 (q, $J=38.5$ Hz, 1 C), 156.58, 159.31; MS (APCI-): m/z 460 ($\text{M}+\text{OH}$) $^-$.



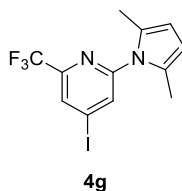
2,4-diiodo-6-(trifluoromethyl)pyridine (4d)⁵ 6-(trifluoromethyl)pyridine-2,4-diylbis(trifluoromethanesulfonate) (5.00 g, 11.28 mmol) was dissolved in dry acetonitrile (70 ml). KI (11.24 g, 67.7 mmol) was added. Triflic acid (1.50 ml, 16.9 mmol) was added slowly keeping the temperature below 30°C and the reaction was stirred at RT for 24 h under a nitrogen atmosphere. The mixture was quenched by addition of water and NaS_2SO_3 10% (m/V) solution was added dropwise until the brown color changed to light yellow. ACN was evaporated under reduced pressure and the resulting suspension filtered. The cake was washed intensively with water and dried at high vacuum to give 2,4-diiodo-6-(trifluoromethyl)pyridine (3.6 g, 9.03 mmol, 80 % yield) as pale yellow solid ^1H NMR (500 MHz, CHLOROFORM-d) δ ppm 7.98 (s, 1 H), 8.34 (s, 1 H); ^{13}C NMR (126 MHz, CHLOROFORM-d) δ ppm 106.43, 118.49 (q, $J=273.1$ Hz, 1 C), 117.69, 129.06 (d, $J=2.7$ Hz, 1 C), 145.83, 149.13 (q, $J=35.7$ Hz, 1 C); MS (ESI+): m/z 400 ($\text{M}+\text{H}$) $^+$.



4-iodo-6-(trifluoromethyl)pyridin-2-amine (4e). A crimp vial was charged with 2,4-diiodo-6-(trifluoromethyl)pyridine (1.00 g, 2.51 mmol) and DMSO (10 ml). The solution was purged with argon and stirred under an argon atmosphere. 1,10-phenanthroline (0.059 g, 0.251 mmol) and copper(I)oxide (0.018 g, 0.125 mmol) were dissolved in 1 ml DMSO (catalyst solution); this mixture was stirred 5 min at RT under an argon atmosphere. The catalyst solution was transferred to the reaction mixture while cooling on an ice-bath. $\text{NH}_3(\text{aq})$ (0.35 ml, 2.69 mmol) was slowly added and the reaction stirred at RT for 5 h. An additional amount of $\text{NH}_3(\text{aq})$ (0.35 ml, 2.69 mmol) was added. DMSO was evaporated under high vacuum at 40°C . The crude was quenched by addition of water and extracted with EA (3 times). The combined organics were washed with NH_4Cl saturated solution and brine, dried over MgSO_4 , filtered and concentrated. The crude product was purified by chromatography on silica gel (PE:EA 8:2) to give 4-iodo-6-(trifluoromethyl)pyridin-2-amine (390 mg, 1.35 mmol, 54% yield) as pale yellow solid. ^1H NMR (500 MHz, CHLOROFORM-d) δ ppm 4.93 (br. s., 2 H), 7.07 (d, $J=0.6$ Hz, 1 H), 7.32 (d, $J=0.9$ Hz, 1 H); ^{13}C NMR (126 MHz, CHLOROFORM-d) δ ppm 105.25, 119.54 (q, $J=274.0$ Hz, 1 C), 118.11 (q, $J=3.7$ Hz, 1 C), 119.40, 145.79 (q, $J=33.9$ Hz, 1 C), 157.60; MS (ESI+): m/z 289 ($\text{M}+\text{H}$) $^+$.

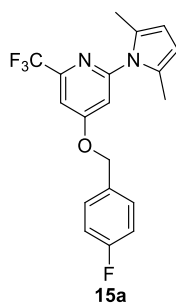


tert-butyl-4-iodo-6-(trifluoromethyl)pyridin-2-yl-carbamate (4f) 4-iodo-6-(trifluoromethyl)pyridin-2-amine (200 mg, 0.7 mmol), di-tert-butyl dicarbonate (167 mg, 0.76 mmol), triethylamine (0.10 ml, 0.76 mmol) and DMAP (5 mg, 0.04 mmol) were dissolved in t-butanol (2 ml). The mixture was stirred at 35°C over night. The mixture was quenched with brine and extracted with EA (3 times). The combined organic extracts were washed with brine, dried (MgSO₄), filtered and concentrated. The crude was purified by automated flash chromatography (Hex:EA 98:2 to 97:3) to give (4-iodo-6-(trifluoromethyl)pyridin-2-yl)carbamic acid (110 mg, 0.331 mmol, 48 % yield) as a white solid. ¹H NMR (300 MHz, CHLOROFORM-*d*) δ ppm 1.53 (s, 9 H), 7.32 (br. s., 1 H), 7.67 (d, *J*=1.1 Hz, 1 H), 8.62 (s, 1 H); ¹³C NMR (75 MHz, CHLOROFORM-*d*) δ ppm 28.14 (3 c), 82.15, 107.41, 120.24 (d, *J*=273.4 Hz, 1 C), 123.99, 146.53 (d, *J*=33.5 Hz, 1 C), 151.70, 152.09; MS (ESI+) *m/z* 389 (M+H)⁺, 333 (M+H-tButyl)⁺.



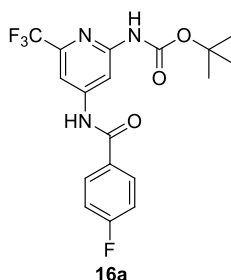
2-(2,5-dimethyl-1H-pyrrol-1-yl)-4-iodo-6-(trifluoromethyl)pyridine (4g)⁶ 4-iodo-6-(trifluoromethyl)pyridin-2-amine (0.50 g, 1.74 mmol) and hexane-2,5-dione (0.24 g, 2.08 mmol) were dissolved in toluol (40 ml). The reaction mixture was heated at reflux using a dean starck trap. The reaction mixture was quenched with Na₂CO₃ saturated solution and the aqueous phase was extracted with EA (3 times). The combined organics were washed with brine, dried and concentrated to give a brown oil. The crude product was purified by column chromatography using hexane:EA 90:10 to yield the 2-(2,5-dimethyl-1H-pyrrol-1-yl)-4-iodo-6-(trifluoromethyl)pyridine (0.55 g, 1.50 mmol, 87 % yield) as brown solid. ¹H NMR (300 MHz, CHLOROFORM-*d*) δ ppm 2.20 (s, 6 H), 5.93 (s, 2 H), 7.79 (s, 1 H), 7.99 (d, *J*=1.1 Hz, 1 H); MS (ESI+) *m/z* not found.

b) Synthesis of protected precursors 15a and 16a



2-(2,5-dimethyl-1H-pyrrol-1-yl)-4-((4-fluorobenzyl)oxy)-6-(trifluoromethyl)pyridine (15a) (4-fluorophenyl)methanol (517 mg, 4.10 mmol) was slowly added to a suspension of sodium hydride (197 mg, 4.92 mmol) in dry DMF (5 ml). The reaction mixture was heated at 70°C for 10 min and 2-(2,5-dimethyl-1H-pyrrol-1-yl)-4-iodo-6-(trifluoromethyl)pyridine (300 mg, 0.82 mmol) dissolved in dry DMF (1 ml) was added. The mixture was stirred at 50°C over night. The reaction mixture was poured into water and EA was added. After stirring for 10 min at RT, the aqueous layer was extracted with EA. The combined organic extracts were washed with NH₄Cl (2 times) and brine (2 times), dried (MgSO₄) and concentrated. The crude was purified by

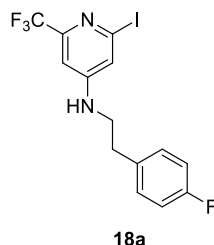
column chromatography (Step gradient 99:1 PE:EA to 95:5 PE:EA) to give 2-(2,5-dimethyl-1H-pyrrol-1-yl)-4-((4-fluorobenzyl)oxy)-6-(trifluoromethyl)-pyridine (80 mg, 0.220 mmol, 26.8 % yield) as yellow oil. ^1H NMR (300 MHz, CHLOROFORM-*d*) δ ppm 2.15 (s, 6 H), 5.17 (s, 2 H), 5.91 (s, 2 H), 6.87 (d, $J=2.0$ Hz, 1 H), 7.14 (m, 2 H), 7.27 (s, 1 H), 7.35-7.51 (m, 2 H); ^{13}C NMR (75 MHz, CHLOROFORM-*d*) δ ppm 13.32 (2c), 70.20, 106.92, 107.88, 109.79, 115.99 (d, $J=21.6$ Hz, 2 C), 121.01 (d, $J=274.9$ Hz, 1 C), 128.72, 129.50 (d, $J=8.2$ Hz, 2 C), 130.37 (d, $J=3.7$ Hz, 1 C), 148.88 (q, $J=34.3$ Hz, 1 C), 153.81, 162.94 (d, $J=250.3$ Hz, 1 C), 166.86; MS (ESI+) m/z 365 (M+H) $^+$.



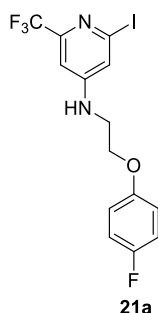
tert-butyl (4-(4-fluorobenzamido)-6-(trifluoromethyl)pyridin-2-yl)carbamate (16a) A crimp reaction vial was charged with tert-butyl-4-iodo-6-(trifluoromethyl)pyridin-2-yl-carbamate (75 mg, 0.19 mmol), 4-fluorobenzamide (81 mg, 0.580 mmol) and Cs_2CO_3 (189 mg, 0.58 mmol). Dioxane (6 ml) was added and the solution purged with argon. A solution of $\text{Pd}_2(\text{dba})_3$ (9 mg, 0.01 mmol) and xantphos (11 mg, 0.02 mmol) was slowly added and the mixture stirred at 50°C for 1 h. An additional amount of $\text{Pd}_2(\text{dba})_3$ (9 mg, 0.01 mmol) and xantphos (11 mg, 0.02 mmol) were and the temperature was increased to 80°C and stirred at this temperature for 3 h. The reaction mixture was quenched by addition of ether and filtered through cellite. The crude product was adsorbed to silica gel and purified by automated flash chromatography (Hex:EtOAc 100 to 80:20) to give tert-butyl (4-(4-fluorobenzamido)-6-(trifluoromethyl)pyridin-2-yl)carbamate (46 mg, 0.115 mmol, 59.6 % yield) as pale yellow oil. ^1H NMR (300 MHz, CHLOROFORM-*d*) δ ppm 1.54 (s, 9 H), 7.15 - 7.26 (m, 2 H), 7.84 - 8.05 (m, 2 H), 8.20 (s, 1 H), 8.27 (s, 1 H); MS (ESI+) m/z 400 (M+H) $^+$, 344 (M+H-t-butyl) $^+$.

c) Synthesis of intermediates 18a, 20a and 21a

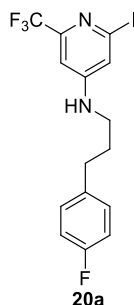
General Procedure for microwave assisted S_{NAr} reactions 2,4-diiodo-6-(trifluoromethyl)pyridine (0.9 mmol) was dissolved in dry ACN (2 ml). Hunig'sBase (1.8 mmol) and amine (1.0 mmol) were added using a MW vial (CEM[®]). The mixture was heated for 45 min at 120°C in the microwave. The mixture was poured into NH_4Cl saturated solution and extracted with EA (3 times). Combined organics were washed with brine, dried over Na_2SO_4 , filtered and concentrated. Regioisomeres and different sideproducts were separated by automated flash chromatography. The 4-substituted regioisomere was identified by 2D NOESY NMR.



N-(4-fluorophenethyl)-2-iodo-6-(trifluoromethyl)pyridin-4-amine was synthesized according to the general procedure from 2,4-diiodo-6-(trifluoromethyl)pyridine (500 mg, 1.25 mmol) and 2-(4-fluorophenyl)ethanamine (192 mg, 1.38 mmol). The crude product was purified by automated flash chromatography using a gradient (PE to PE:EA 75:25) to give N-(4-fluorophenethyl)-2-iodo-6-(trifluoromethyl)pyridin-4-amine (130 mg, 0.32 mmol, 25% yield) as yellow oil. ^1H NMR (500 MHz, $\text{CHLOROFORM-}d$) δ ppm 2.91 (t, $J=6.9$ Hz, 2 H), 3.44 (td, $J=6.8, 5.7$ Hz, 2 H), 4.42 (br. s., 1 H), 6.73 (d, $J=1.9$ Hz, 1 H), 6.96 (d, $J=2.2$ Hz, 1 H), 7.01 - 7.07 (m, 2 H), 7.14 - 7.19 (m, 2 H); MS (ESI+) m/z 411 ($\text{M}+\text{H}$)⁺.

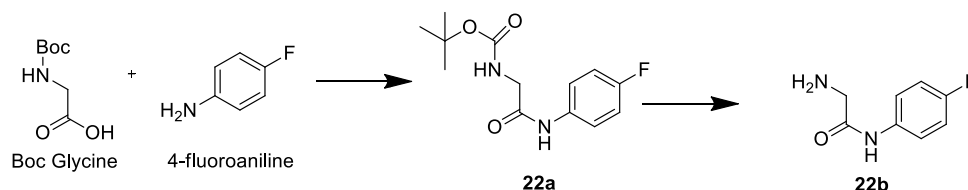


N-(2-(4-fluorophenoxy)ethyl)-2-iodo-6-(trifluoromethyl)pyridin-4-amine was synthesized according to the general procedure from (2,4-diiodo-6-(trifluoromethyl)pyridine (350 mg, 0.88 mmol) and 2-(4-fluorophenoxy)ethanamine (150 mg, 0.96 mmol). The crude product was purified by automated flash chromatography using a gradient (PE to PE:EA 55:45) to give N-(2-(4-fluorophenoxy)ethyl)-2-iodo-6-(trifluoromethyl)pyridin-4-amine (60 mg, 0.14 mmol, 16 % yield) as yellow oil. ^1H NMR (500 MHz, $\text{CHLOROFORM-}d$) δ ppm 3.58 (q, $J=5.4$ Hz, 2 H), 4.14 (t, $J=5.0$ Hz, 2 H), 4.88 (br. s., 1 H), 6.81 - 6.90 (m, 3 H), 6.96 - 7.05 (m, 2 H), 7.07 (d, $J=2.2$ Hz, 1 H); MS (ESI+) m/z 427 ($\text{M}+\text{H}$)⁺.



N-(3-(4-fluorophenyl)propyl)-2-iodo-6-(trifluoromethyl)pyridin-4-amine was synthesized according to Method B from 2,4-diiodo-6-(trifluoromethyl)pyridine (500 mg, 1.25 mmol) and 3-(4-fluorophenyl)propan-1-amine (211 mg, 1.38 mmol). The crude product was purified by automated flash chromatography using a gradient (PE to PE:EA 75:25) to give N-(3-(4-fluorophenyl)propyl)-2-iodo-6-(trifluoromethyl)pyridin-4-amine (140 mg, 0.33 mmol, 26 % yield) as yellow oil. $^1\text{H NMR}$ (500 MHz, $\text{CHLOROFORM-}d$) δ ppm 1.95 (quin, $J=7.4$ Hz, 2 H), 2.71 (t, $J=7.4$ Hz, 2 H), 3.17 (td, $J=7.1, 5.7$ Hz, 2 H), 4.40 (br. s., 1 H), 6.70 (d, $J=2.2$ Hz, 1 H), 6.91 (d, $J=2.2$ Hz, 1 H), 6.99 - 7.05 (m, 2 H), 7.11 - 7.17 (m, 2 H); MS (ESI+) m/z 425 (M+H) $^+$.

d) Synthesis of intermediates 22a and 22b



tert-butyl (2-((4-fluorophenyl)amino)-2-oxoethyl)carbamate (22a): BOC Glycine (1.65 g, 9.45 mmol), EDC HCl (3.45 g, 18 mmol) and DMAP (0.110 g, 0.90 mmol) were filled into a three necked flask and suspended in THF (Volume: 20 ml). Et₃N (3,76 ml, 27,0 mmol) and 4-fluoroaniline (1.00 g, 9.00 mmol) were added and the white suspension stirred under a nitrogen atmosphere for 8 h at RT. The mixture was poured into 10% citric acid and stirred for 10 min. The white precipitate was filtered off and the resulting cake washed 2 times with water. The white solid was dried at high vacuum over night. $^1\text{H NMR}$ (300 MHz, $\text{CHLOROFORM-}d$) δ ppm 1.49 (s, 9 H), 3.92 (d, $J=6.1$ Hz, 2 H), 5.19 (br. s., 1 H), 6.92 - 7.11 (m, 2 H), 7.35 - 7.55 (m, 2 H), 8.12 (br. s., 1 H); MS (ESI-) m/z 267 (M-H) $^-$.

2-amino-N-(4-fluorophenyl)acetamide (22b): tert-butyl(2-((4-fluorophenyl)amino)-2-oxo-ethyl)carbamate (1.60 g, 5.96 mmol) was suspended in DCM (20 ml). TFA (2.5 ml, 32.4 mmol) was added while cooling on an ice bath. The reaction was stirred at RT for 8 h. The mixture was poured into a NaHCO₃ saturated solution and extracted with EA (5 times). Combined organics were washed with brine, dried (MgSO₄), filtered and concentrated. The product was dried at high vacuum to give 2-amino-N-(4-fluorophenyl)acetamide (0.6 g, 3.57 mmol, 59.8 % yield) as yellow material. $^1\text{H NMR}$ (500 MHz, $\text{DMSO-}d_6$) δ ppm 3.31 (s, 2 H), 7.08 - 7.19 (m, 2 H), 7.59 - 7.70 (m, 2 H); $^{13}\text{C NMR}$ (126 MHz, $\text{DMSO-}d_6$) δ ppm 44.78, 115.07 (d, $J=22.9$ Hz, 2 C), 120.59 (d, $J=7.3$ Hz, 2 C), 135.01 (d, $J=2.8$ Hz, 1 C), 157.76 (d, $J=238.3$ Hz, 1 C), 171.06; MS (ESI+) m/z 169 (M+H) $^+$.

7) High Resolution Mass Spectroscopy

All measurements were performed on a Dionex Ultimate 3000 RSLC system using a Waters BEH C18, 50 x 2.1 mm, 1.7 μm dp column. Separation of 1 μL sample was achieved by a linear gradient with (A) H_2O + 0.1% FA to (B) ACN + 0.1% FA at a flow rate of 600 $\mu\text{L}/\text{min}$ and 45 $^\circ\text{C}$. The gradient was initiated by a 1 min isocratic step at 5% B, followed by an increase to 95% B in 6 min to end up with a 1.5 min step at 95% B before reequilibration with initial conditions. UV spectra were recorded by a DAD in the range from 200 to 600 nm. The LC flow was split to 75 $\mu\text{L}/\text{min}$ before entering the maXis 4G hr-ToF mass spectrometer (Bruker Daltonics) using the standard ESI source. Mass spectra were acquired in centroid mode ranging from 50 – 1000 m/z at 2 Hz scan speed.

8) Purity of Final Compounds (LC/MS Determination)

Purity control was carried out on two different systems:

SpectraSystems LC system (Thermo Fisher Scientific) consisting of a pump, an autosampler, and a VWD detector. Mass spectrometry was performed on an MSQ electro spray mass spectrometer (Thermo Fisher Scientific). The system was operated by the standard software Xcalibur. An RP-C18 NUCLEODUR 100-5 (125x3 mm) column (Macherey-Nagel GmbH) was used as stationary phase. All solvents were HPLC grade. For purity determination the following methods was used:

Mobil phase, A = water + 0.1% trifluoroacetic acid, B = acetonitrile + 0.1% trifluoroacetic acid; gradient, 0.0-15.0 min, 0-100% B, 15.0-20.0 min, 100% B; flow rate 0.8 mL/min.

LCMS-System (Waters) consisting of a 767 sample Manager, a 2545 binary gradient pump, a 2998 PDA detector and a 3100 electron spray mass spectrometer equipped with a C-18 column (Nucleodur 100-5 C18 ec 150 x 4.6 mm). For purity determination the following methods was used:

Mobil phase, A = water + 0.1% formic acid, B = acetonitrile + 0.1% formic acid; gradient, 0.0-13.0 min, 0-100% B; flow rate 1 mL/min

9) References

- (1) Klein, T.; Henn, C.; Jong, J. C. de; Zimmer, C.; Kirsch, B.; Maurer, C. K.; Pistorius, D.; Müller, R.; Steinbach, A.; Hartmann, R. W. Identification of small-molecule antagonists of the *Pseudomonas aeruginosa* transcriptional regulator PqsR: biophysically guided hit discovery and optimization. *ACS Chem. Biol.* **2012**, *7*, 1496–1501.
- (2) Zender, M.; Klein, T.; Henn, C.; Kirsch, B.; Maurer, C. K.; Kail, D.; Ritter, C.; Dolezal, O.; Steinbach, A.; Hartmann, R. W. Discovery and biophysical characterization of 2-amino-oxadiazoles as novel antagonists of PqsR, an important regulator of *Pseudomonas aeruginosa* virulence. *J. Med. Chem.* **2013**, *56*, 6761–6774.
- (3) Xu, N.; Yu, S.; Moniot, S.; Weyand, M.; Blankenfeldt, W. Crystallization and preliminary crystal structure analysis of the ligand-binding domain of PqsR (MfR), the *Pseudomonas* quinolone signal (PQS) responsive quorum-sensing transcription factor of *Pseudomonas aeruginosa*. *Acta Crystallogr. Sect. F Struct. Biol. Cryst. Commun.* **2012**, *68*, 1034–1039.
- (4) Adam, F. M.; Bish, G.; Calo, F.; Carr, C. L.; Castro, N.; Hay, D.; Hodgson, P. B.; Jones, P.; Knight, C. J.; Paradowski, M.; Parsons, G. C.; Proctor, K. J. W.; Pryde, D. C.; Rota, F.; Smith, M. C.; Smith, N.; Tran, T.-D.; Hitchin, J.; Dixon, R. Development of a Practical Synthesis of Toll-like Receptor Agonist PF-4171455. *Org. Process Res. Dev.* **2011**, *15*, 788–796.

- (5) Maloney, K. M.; Nwakpuda, E.; Kuethe, J. T.; Yin, J. One-pot iodination of hydroxypyridines. *J. Org. Chem.* **2009**, *74*, 5111–5114.
- (6) Macor, J. E.; Chenard, B. L.; Post, R. J. Use of 2,5-Dimethylpyrrole as an Amino-Protecting Group in an Efficient Synthesis of 5-Amino-3-[(N-methyl-pyrrolidin-2(R)-yl)methyl]indole. *J. Org. Chem.* **1994**, *59*, 7496–7498.

7.3 Supplementary Material of Chapter C

1) *E. coli* reporter-gene assay: dose-response curves

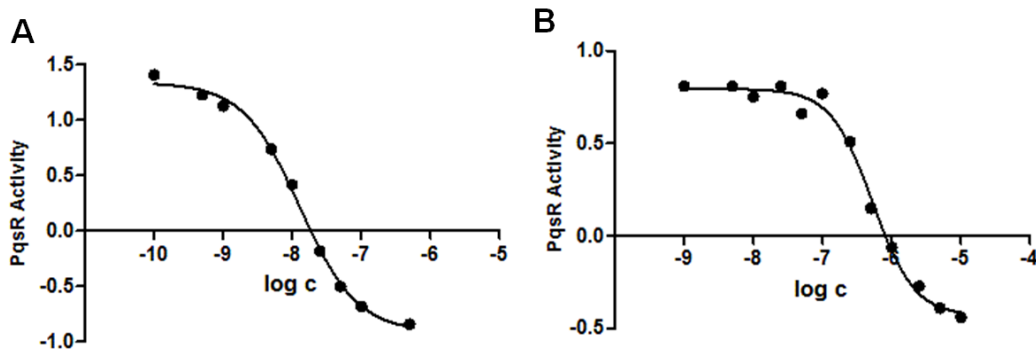


Figure S1: Antagonistic activity of different compounds measured in the *E. coli* reporter gene assay. Representative dose-response curves of **a)** compound **7** **b)** compound **12**. PqsR activity refers to the stimulation of PqsR induced by 50 nM PQS (= 1). Black dots (•) represent the PqsR activity measured in the presence of a single compound concentration. The continuous black line is the non-linear regression analysis to determine IC_{50} values using a log (inhibitor) vs. response model (Graph Pad Prism 5.04).

2) Effects on pyocyanin in *P. aeruginosa*

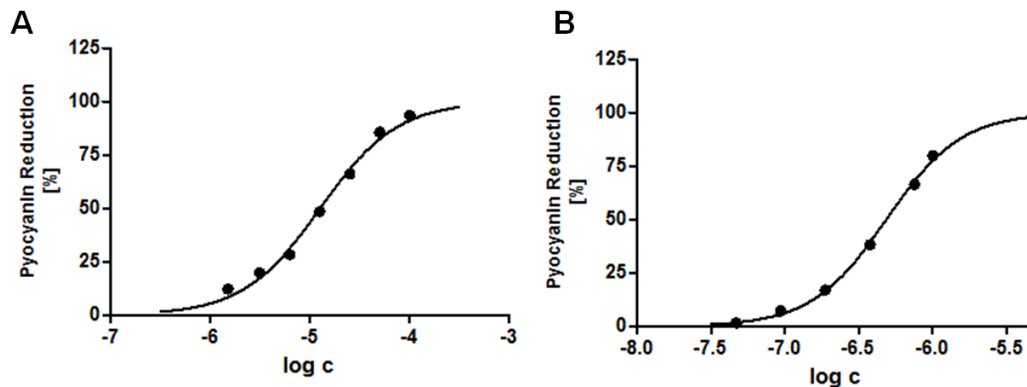


Figure S2: Inhibition of virulence factor pyocyanin was evaluated in the clinical isolate PA14. Representative dose-response curves **a)** compound **7** **b)** compound **12**. Black dots (•) represent the reduction of pyocyanin in presents of a given compound concentration relative to DMSO control (= 0 %). The continuous black line is the non-linear regression analysis to determine IC_{50} values using a log (inhibitor) vs. response model with constrains (bottom = 0; top = 100) (Graph Pad Prism 5.04).

3) UPLC-MS/MS quantification of extracellular 2-AA

The quantification of 2-AA was performed following a modified protocol of Kesarwani *et. al.*¹ The analysis was performed on an Accela-HPLC system (Thermo Scientific) coupled with a triple quadrupole mass spectrometer TQS Quantum Access Max (Thermo Scientific) using 5,6,7,8-tetradeutero-2-heptyl-4(1*H*)-quinolone (*d*₄-HHQ) as internal standard. An NUCLEODUR C₁₈ Pyramid column (2x125 mm, 3 μm; Macherey-Nagel) was used as stationary phase along with a mobile phase consisting of water + 0.1% formic acid (A) and methanol + 0.1% formic acid (B) at a flow rate of 0.7 ml/min. The following chromatographic conditions were applied: 0.0-0.5 isocratic 10% B, 0.5-2.0 linear gradient up to 100 % B, 2.0-3.0 isocratic 100% B, ending 3.0-4.5 initial conditions. The compounds were ionized using electrospray ionization in positive ion mode with the following parameters: spray voltage: 3500 V; vaporizer temperature: 370 °C; sheath gas pressure (nitrogen): 35 units; auxiliary gas pressure (nitrogen): 30 units; skimmer offset voltage: 0 V; capillary temperature: 270 °C. Selected reaction monitoring was used for detecting 2-AA (136.016→91.048 [quantitative], collision energy: 24 V, tube lens: 68 V; 136.016→117,998 [qualitative], collision energy: 13 V, tube lens: 68 V) and *d*₄-HHQ (248.081→162.965 [quantitative], collision energy: 32 V, tube lens: 100 V; 248.081→175.982 [qualitative], collision energy: 34 V, tube lens: 100 V) employing: scan width: 0.002 m/z; scan time: 0.100 s; peak width: 0.70.

4) Cytotoxicity assay

HEK 293 cells (2x10⁵ cells per well) were seeded in 24-well, flat-bottomed plates. Culturing of cells, incubations and OD measurements were performed as described previously with small modifications.² 24 h after seeding the cells the incubation was started by the addition of compounds in a final DMSO concentration of 1 % (v/v). The living cell mass was determined after 24, 48 and 72 h followed by the calculation of LD₅₀ values.

Table S1: Cytotoxicity of selected compounds^a

Number	Cytotoxicity
	HEK293 ^a LD ₅₀ [μM]
7	30
8	>50 ^b
10	> 25 ^b
12	> 50 ^b

^aviability of HEK293 cells was quantified in the presence of test compound after 72h using MTT.

^bno effect on cell viability at solubility maximum.

5) LectinB expression in *P. aeruginosa*

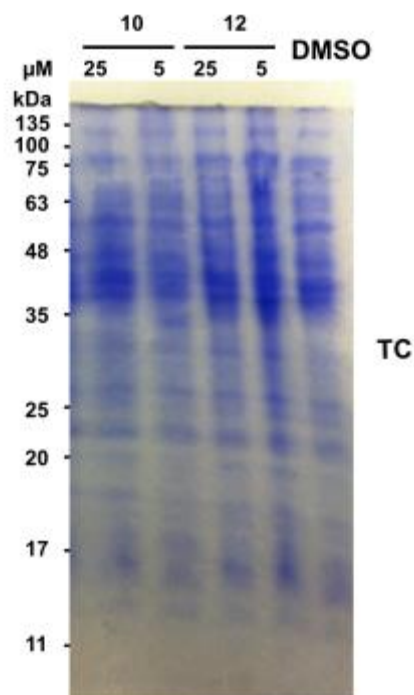


Figure S3: Expression of LecB in *P. aeruginosa* PAO1. Coomassie-stained 15% SDS-PAGE of total cell (TC) fractions of *P. aeruginosa* cultures grown for 24 h in absence or presence of compound **10** or **12** (5 μ M or 25 μ M).

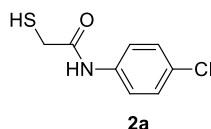
6) LLE Calculation (Ligand Lipophilicity Efficiency)

The ligand lipophilicity efficiency was calculated according to equation 1³

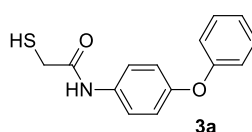
$$LLE = 0.11 + 1.4 * \frac{pIC_{50} - clogD}{NHA} \quad (1)$$

with pIC_{50} antagonistic activity measured in *E.coli*, calculated logD (ACD/Percepta 2015) and NHA (number of heavy atoms). This equation based on the ones suggested by Mortenson and Murray⁴ and Shultz⁵.

7) Synthesis of Intermediates



N-(4-chlorophenyl)-2-mercaptoacetamide (2a) was synthesized according to general procedure A⁶ from 4-chloroaniline (2.77 g, 21.71 mmol) and 2-mercaptoacetic acid (2.00 g, 21.7 mmol) and afford the expected product as pale yellow solid (2.99 g, 14.8 mmol, 68 % yield). ¹H NMR (300 MHz, CHLOROFORM-*d*) δ ppm 2.04 (t, *J*=9.2 Hz, 1 H), 3.41 (d, *J*=9.3 Hz, 2 H), 7.28 - 7.37 (m, 2 H), 7.40 - 7.60 (m, 2 H), 8.53 (br. s., 1 H); MS (ESI+) *m/z* 202 (M+H)⁺.



2-mercapto-N-(4-phenoxyphenyl)acetamide (3a) was synthesized from 4-phenoxyaniline (1.00 g, 5.40 mmol) and 2-mercaptoacetic acid (0,547 g, 5,94 mmol) to give the expected product as grey solid (1.1 g, 4.24 mmol, 79 % yield). ¹H NMR (300 MHz, CHLOROFORM-*d*) δ ppm 1.96 - 2.13 (m, 1 H), 3.42 (d, *J*=9.1 Hz, 2 H), 6.97 - 7.05 (m, 4 H), 7.06 - 7.15 (m, 1 H), 7.29 - 7.40 (m, 2 H), 7.44 - 7.59 (m, 2 H), 8.51 (br. s., 1 H); MS (ESI+) *m/z* 260 (M+H)⁺, 282 (M+Na)⁺.

8) References

- (1) Kesarwani, M.; Hazan, R.; He, J.; Que, Y.-A.; Que, Y.; Apidianakis, Y.; Lesic, B.; Xiao, G.; Dekimpe, V.; Milot, S.; Deziel, E.; Lépine, F.; Rahme, L. G. A quorum sensing regulated small volatile molecule reduces acute virulence and promotes chronic infection phenotypes. *PLoS pathogens*. **2011**, *7*, e1002192.
- (2) Haupenthal, J.; Baehr, C.; Zeuzem, S.; Piiper, A. RNase A-like enzymes in serum inhibit the anti-neoplastic activity of siRNA targeting polo-like kinase 1. *Int. J. Cancer*. **2007**, *121*, 206–210.
- (3) Thomann, A.; Zapp, J.; Hutter, M.; Empting, M.; Hartmann, R. W. Steering the azido-tetrazole equilibrium of 4-azidopyrimidines via substituent variation - implications for drug design and azide-alkyne cycloadditions. *Org. Biomol. Chem*. **2015**, *13*, 10620–10630.
- (4) Mortenson, P.; Murray, C. Assessing the lipophilicity of fragments and early hits. *J. Comput.-Aided Mol. Des*. **2011**, *25*, 663–667.
- (5) Shultz, M. D. Setting expectations in molecular optimizations: Strengths and limitations of commonly used composite parameters. *Bioorganic & medicinal chemistry letters*. **2013**, *23*, 5980–5991.
- (6) Shaitanov, P. V.; Lukashov S.S.; Turov O.V.; Yarmoluk S.M. Synthesis and structural study of N-substituted-1,7-dithia-4-azaspiro[4.4]nonan-3-one 7,7-dioxides. *Ukr. Bioorg. Acta*. **2007**, *2*, 56–61.

7.4 Supplementary Material of Chapter D

Dissecting the multiple roles of PqsE in *Pseudomonas aeruginosa* virulence by discovery of small tool compounds

1) Coupled PqsDE assay

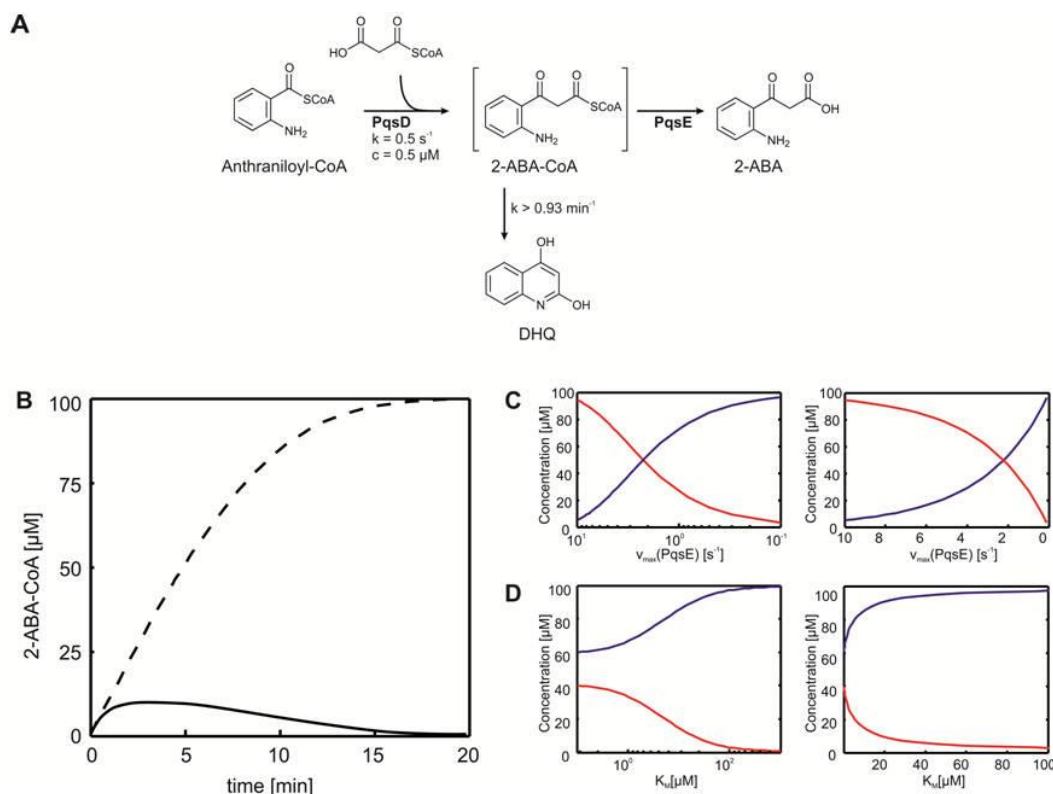


Figure S1. Simulation of the coupled reaction of PqsD and PqsE (**A**) Schematic representation of the enzymatic reaction with the known kinetic parameters (**B**) The total amount of 2-ABA-CoA released by PqsD over time under the given conditions (dashed line). Taking into account the intrinsic decomposition of 2-ABA-CoA (rate of at least 0.93 min^{-1} (Drees and Fetzner, 2015)), the concentration accessible for hydrolysis by PqsE is significantly lower (solid line). Models shown in B and C incorporate the PqsE reaction into the model shown in A. Calculations are based on the assumption that PqsD and PqsE reactions can be described by Michaelis-Menten kinetics and both enzymes possess similar apparent K_M or v_{\max} values. Blue lines are calculated DHQ, red lines are 2-ABA concentrations. **C** Given PqsD and PqsE possess similar K_M values, the simulation provides product concentrations as a function of $v_{\max}(\text{PqsE})$ (left: semi-logarithmic, right: linear plot; calculations conducted assuming a turnover number of 0.5 s^{-1} for PqsD and a K_M of $35 \text{ }\mu\text{M}$ for PqsD and PqsE). This model can be used to estimate the effect caused by an inhibitor that would act non-competitively on PqsE. **D** provides a model for competitive inhibition, in which K_M (PqsE) is affected as function of inhibitor concentration (left: semi-logarithmic, right: linear plot; calculations conducted assuming a turnover number of 0.5 s^{-1} for both PqsD and PqsE and a K_M of $35 \text{ }\mu\text{M}$ for PqsD). The model suggests that in the coupled reaction, competitive inhibitors are more potent than non-competitive inhibitors.

2) Thioesterase Assay

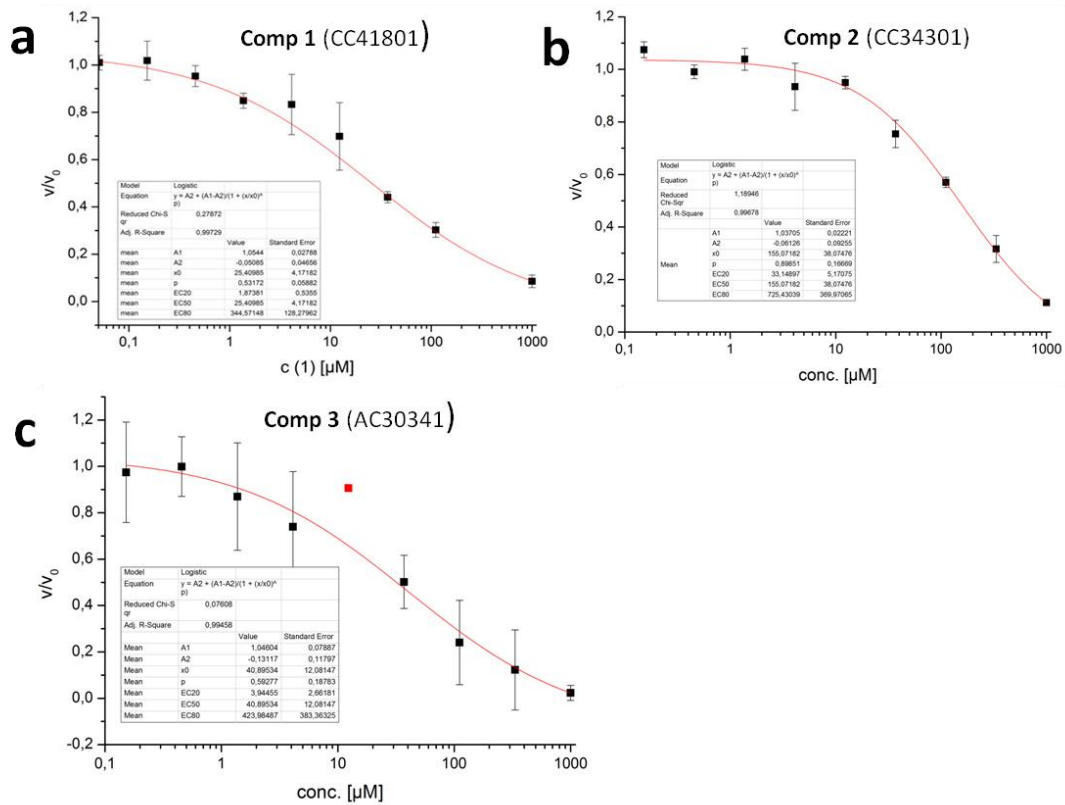


Figure S2. Dose-response curve for hit compounds 1-3. Black squares (■) represent the residual enzyme activity (v/v_0) in the presence of a given compound concentration. The continuous red line represents the non-linear regression analysis (logistic fit) used for IC_{50} determination. (a) compound 1 (b) compound 2 (c) compound 3. SD of at least two independent experiments with $n=3$.

3) Effects on alkylquinolones in *P. aeruginosa*

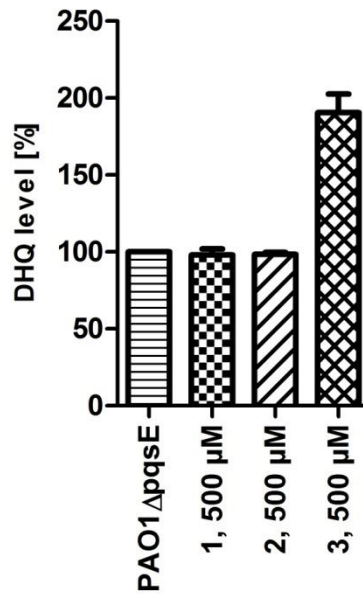


Figure S3. Effects of compounds 1-3 on DHQ levels in PAO1pqsE referenced for DMSO control (=100%). SD of at least two independent experiments with n=3.

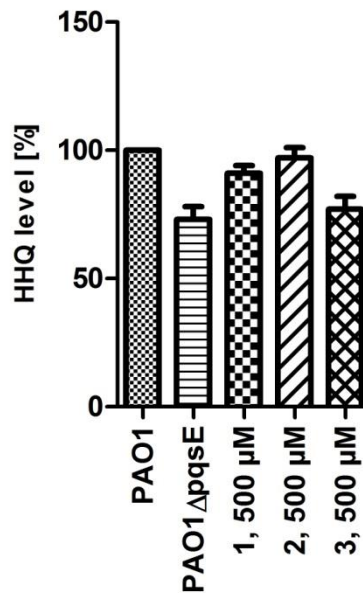
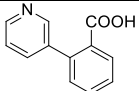
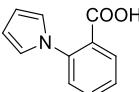
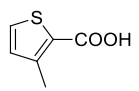
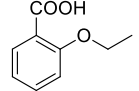
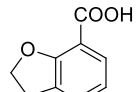
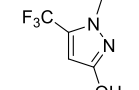
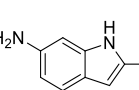
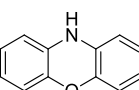
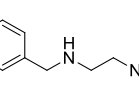
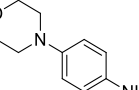


Figure S4. Effects of compounds 1-3 on the level of signalling molecule HHQ in PAO1 referenced for the DMSO control (=100%). SD of at least two independent experiments with n=3.

4) Differential Scanning Fluorimetry

Table S1. DSF derived screening hits

Category	Lib. Name	Structure	ΔT_{M1} [°K]	ΔT_{M2} [°K]	Mean [°K]
Carboxylic Acids	CC41801 (1)		8.57	8.66	8.62
	CC34301 (2)		4.82	3.83	4.33
	AC30341 (3)		2.10	2.26	2.18
	AC16433		2.01	1.28	1.65
	CC00901		1.75	0.88	1.32
Diverse	BTB09194		1.96	1.07	1.52
	AC34875 (4)		1.94	0.88	1.41
	AC13022 (5)		1.37	0.88	1.13
	SB01744		ambiguous	1.07	-
	BTB01373		ambiguous	1.88	-

5) Protein Crystallography

Table S2. Data Collection and Refinement Statistics

Sample	PqsE – 2-ABA	PqsE – comp 1	PqsE – comp 2	PqsE – comp 3
Data collection[#]				
Beamline ⁺	X06DA, SLS	X06DA, SLS	BL 14.1, BESSY II	X06DA, SLS
Wavelength (Å)	1.0000	0.9790	0.9184	1.0000
Resolution range (Å)	48.66-1.90 (1.94-1.90)	49.96-1.99 (2.04-1.99)	42.76-2.10 (2.16-2.10)	48.76-1.77 (1.81-1.77)
Space group	P3 ₂ 21	P3 ₂ 21	P3 ₂ 21	P3 ₂ 21
Cell dimensions				
a, b, c (Å)	61.1, 61.1, 146.0	61.3, 61.3, 147.0	60.9, 60.9, 146.2	61.1, 61.1, 146.3
α, β, γ (°)	90.0, 90.0, 120.0	90.0, 90.0, 120.0	90.0, 90.0, 120.0	90.0, 90.0, 120.0
Mosaicity (°) [§]	0.15	0.18	0.14	0.06
Total No. of measured reflections	496248 (30421)	439051 (32755)	212632 (17142)	308334 (16459)
unique reflections	25730 (1596)	22719 (1674)	19077 (1514)	31806 (1807)
Mean I/σ(I)	18.8 (2.0)	20.8 (2.0)	10.3 (2.0)	26.4 (2.0)
Multiplicity	19.3 (19.1)	19.3 (19.6)	11.1 (11.3)	9.7 (9.1)
Completeness (%)	100.0 (100.0)	100.0 (100.0)	100.0 (100.0)	100.0 (100.0)
R _{merge} (%) [†]	12.0 (185.3)	11.0 (169.0)	19.5 (137.6)	5.0 (114.0)
R _{p.i.m.} (%) [‡]	2.8 (43.5)	2.6 (39.1)	6.1 (43.0)	1.7 (39.9)
CC _{1/2} [*]	99.8 (68.8)	100.0 (69.2)	99.6 (42.5)	100.0 (67.8)
Solvent content (%)	46.8	47.5	46.4	46.9
Wilson B-factor (Å ²)	29.6	34.3	29.2	28.6
Refinement				
R _{work} (%)	16.4 (24.2)	16.2 (23.2)	19.3 (28.2)	16.2 (31.9)
R _{free} (%)	19.8 (30.1)	20.6 (26.5)	23.6 (30.4)	20.0 (34.2)
No. of non H-atoms				
Protein	2606	2585	2580	2325
Ligand/Ion	15	17	16	11
Water	195	185	158	145
R.m.s. deviations				
Bonds (Å)	0.018	0.018	0.011	0.018
Angles (°)	0.88	1.15	0.46	1.097
Average B factors (Å ²)				
Protein	37	42	37	36
Ligand/Ion	38	32	31	32
Water	41	47	40	37
Ramachandran plot (%)				
Favored regions	97.1	96.7	97.1	97.0
Outliers	0.0	0.0	0.3	0.3
MolProbity score [¶]	1.16	1.43	1.14	1.34
PDB code	5HIO	5HIP	5HIQ	5HIS

Footnotes of Table S2:

Values in parentheses refer to the highest resolution shell. The chemical structures of compounds **1-3** are depicted in Figure 2B.

Data set for each structure was collected from a single crystal.

+SLS: Swiss Light Source (Paul Scherrer Institute, Villigen, Switzerland). BESSY II: Berlin Electron Storage Ring Company for Synchrotron Radiation (Helmholtz-Zentrum Berlin, Berlin, Germany).

§ Values as reported by *AIMLESS*.(Evans and Murshudov, 2013)

† $R_{\text{merge}} = \frac{\sum_{\text{hkl}} \sum_i |I_i(\text{hkl}) - \langle I(\text{hkl}) \rangle|}{\sum_{\text{hkl}} \sum_i I_i(\text{hkl})}$, where $I_i(\text{hkl})$ is the intensity of the i th measurement of the reflection hkl and $\langle I(\text{hkl}) \rangle$ is the mean intensity of multiple observations of the reflection hkl .

‡ $R_{\text{p.i.m.}} = \frac{\sum_{\text{hkl}} [1 / (N - 1)]^{1/2} \sum_i |I_i(\text{hkl}) - \langle I(\text{hkl}) \rangle|}{\sum_{\text{hkl}} \sum_i I_i(\text{hkl})}$, where N is the multiplicity.(Weiss and Hilgenfeld, 1997; Weiss, 2001)

¥ $CC_{1/2}$: Correlation coefficient between the intensities of two random half data sets.(Karplus and Diederichs, 2012)

¶ *MolProbity* score: Quality criterion that includes the clashscore, the Ramachandran and rotamer statistics for the respective structure reported by *MolProbity*.(Chen et al., 2010)

6) Expression and Purification of PqsE

For Crystallization Studies. The DNA sequence encoding PqsE was amplified by PCR from genomic *Pseudomonas aeruginosa* PAO1 DNA and cloned into pET19m, which is a modified version of the pET19-b vector (Novagen) and produces the target protein with an *N*-terminal His₆ tag followed by a recognition sequence for TEV protease (MGHHHHHAENLYFQ↑GH; arrow indicates the TEV protease cleavage site). *E. coli* Rosetta 2(DE3) was transformed with the plasmid pET19m-*pqsE* and the cells were grown in Terrific Broth medium supplemented with 100 µg/ml ampicillin and 33 µg/ml chloramphenicol at 37°C. At OD₆₀₀ of 1.4 the expression of recombinant PqsE was induced with 1 mM IPTG for 3 h at 37°C. The cells were harvested by centrifugation at 6.800 g for 10 min at 10°C, resuspended in buffer A (50 mM Tris-HCl, 300 mM NaCl, pH 8.0) supplemented with 2 mM MgCl₂, 10 nM DNase I (Roche Life Science) and one protease inhibitor cocktail tablet (Roche Life Science) followed by cell disruption with an Emulsiflex-C3 homogenizer (Avestin) with two cycles. After removal of cellular debris by centrifugation the target protein was purified by Ni-NTA affinity chromatography with buffer B (50 mM Tris-HCl, 300 mM NaCl, 100 mM imidazole, pH 8.0) and the *N*-terminal His₆-tag was cleaved off with His₆-tagged TEV protease (1 mg protease per 25 mg His₆-TEV-PqsE) at 4°C for 16 h. During tag removal the buffer was exchanged to buffer C (20 mM Tris-HCl, 150 mM NaCl, pH 8.0) by dialysis. Untagged PqsE was separated from uncleaved PqsE and TEV protease by a second Ni-NTA affinity chromatography with buffer D (20 mM Tris-HCl, 150 mM NaCl, 50-200 mM imidazole). As a final purification step PqsE was loaded on a Superdex 75 26/60 size exclusion chromatography column (GE Healthcare) and eluted with buffer C. Afterwards, the protein was concentrated to ~34 mg/ml and stored at 4 °C for up to 6 months, as protein that was flash-frozen in liquid nitrogen and stored at - 80 °C only yielded poorly diffracting crystals.

For DSF Screening / ITC Experiments /Biological Assays. PqsE was expressed as reported by Yu *et al.* (Yu *et al.*, 2009) with slight modifications. *Escherichia coli* Rosetta(DE3)pLysS containing the plasmid pET28a-*pqsE* were grown in TB medium supplemented with 50 µg/mL kanamycin and 25 µg/mL chloramphenicol. Protein expression was induced using IPTG (0.6 mM) at OD₆₀₀ of 0.8 and the temperature was reduced to 20°C. For use in DSF screening, ITC studies and thioesterase assay, PqsE was purified by Ni-NTA affinity chromatography using binding buffer (50 mM Tris-HCl, 150 mM NaCl, 20 mM imidazole pH 8.0) and one step elution (50 mM Tris-HCl, 150 mM NaCl, 500 mM imidazole pH 8.0). For DSF screening and thioesterase assays H₆PqsE was buffer exchanged to (50 mM Tris-HCl, 150 mM NaCl, 10 % (v/v) glycerol, pH 8.5) and stored at -80°C. For ITC studies H₆PqsE was concentrated and buffer exchanged to (50 mM Tricine, 2 mM MnCl₂) and stored at -80°C.

7) Supplemental References

Chen, V.B., Arendall, W.B., Headd, J.J., Keedy, D.A., Immormino, R.M., Kapral, G.J., Murray, L.W., Richardson, J.S., and Richardson, D.C. (2010). MolProbity: all-atom structure validation for macromolecular crystallography. *Acta crystallographica. Section D, Biological crystallography* 66, 12-21.

Drees, S.L., and Fetzner, S. (2015). PqsE of *Pseudomonas aeruginosa* Acts as Pathway-Specific Thioesterase in the Biosynthesis of Alkylquinolone Signaling Molecules. *Chem. Biol.* 22, 611-618.

Evans, P.R., and Murshudov, G.N. (2013). How good are my data and what is the resolution? *Acta crystallographica. Section D, Biological crystallography* 69, 1204-1214.

Karplus, P.A., and Diederichs, K. (2012). Linking crystallographic model and data quality. *Science (New York, N.Y.)* 336, 1030-1033.

Weiss, M.S. (2001). Global indicators of X-ray data quality. *J Appl Crystallogr* 34, 130-135.

Weiss, M.S., and Hilgenfeld, R. (1997). On the use of the merging R factor as a quality indicator for X-ray data. *J Appl Crystallogr* 30, 203-205.

Yu, S., Jensen, V., Seeliger, J., Feldmann, I., Weber, S., Schleicher, E., Häussler, S., and Blankenfeldt, W. (2009). Structure elucidation and preliminary assessment of hydrolase activity of PqsE, the *Pseudomonas* quinolone signal (PQS) response protein. *Biochemistry* 48, 10298-10307.

8 Appendix

8.1 Curriculum Vitae

Persönliche Daten

Name Michael Georg Zender
Geburtstag/-ort: 05.09.1985 in Saarlouis

Schulbildung

1992 – 1996 Grundschule in Wadgassen-Differten
1996 – 2005 Staatliches Gymnasium am Stadtgarten in Saarlouis
Abschluss: Zeugnis der Reife im Frühjahr 2005

Zivildienst

09/2005 – 04/2006 St. Elisabeth Klinik Saarlouis
Krankenhausapotheke

Hochschulstudium

04/2006 – 04/2010 Universität des Saarlandes
Studiengang Pharmazie
03/2008 Erstes Staatsexamen
04/2010 Zweites Staatsexamen
06/2011 Drittes Staatsexamen
07/2011 Approbation zum Apotheker

Berufserfahrung

05/2010 – 10/2010 Forschungspraktikum betreut von Prof. Rolf W. Hartmann im
Novartis Institute of Biomedical Research Basel, Schweiz
Abschluss: Diplom Pharmazeut
11/2010 – 04/2011 Praxissemester in der Gangolf Apotheke Differten
08/2011 – 12/2015 Doktorarbeit bei Prof. Rolf W. Hartmann am
Helmholtz Institut für Pharmazeutische Forschung Saarland
Abteilung Wirkstoff Design und Optimierung

Auszeichnungen

03/2014 Posterpreis der Gesellschaft Deutscher Chemiker (GDCh)
Frontiers in Medicinal Chemistry Conference (FIMC), Tübingen
06/2010 Buchpreis der Deutschen Pharmazeutischen Gesellschaft
(DPhG) für exzellente Resultate im zweiten Staatsexamen
Pharmazie
03/2008 Erlassung der Studiengebühren aufgrund sehr guter Leistungen im
ersten Staatsexamen Pharmazie

8.2 Publications

- 1) Zender M, Witzgall F, Drees SL, Weidel E, Maurer CK, Fetzner S, Blankenfeldt W, Empting M, Hartmann RW. Dissecting the multiple roles of PqsE in *Pseudomonas aeruginosa* virulence by discovery of small tool compounds. *ACS Chem. Biol.*, **2016**, 11, 1755–1763
- 2) Wu SC, Li LS, Kopp N, Montero J, Chapuy B, Yoda A, Christie AL, Liu H, Christodoulou A, van Bodegom D, van der Zwet J, Layer JV, Tivey T, Lane AA, Ryan JA, Ng SY, DeAngelo DJ, Stone RM, Steensma D, Wadleigh M, Harris M, Mandon E, Ebel N, Andraos R, Romanet V, Dölemeyer A, Sterker D, Zender M, Rodig SJ, Murakami M, Hofmann F, Kuo F, Eck MJ, Silverman LB, Sallan SE, Letai A, Baffert F, Vangrevelinghe E, Radimerski T, Gaul C, Weinstock DM; Activity of the Type II JAK2 Inhibitor CHZ868 in B Cell Acute Lymphoblastic Leukemia. *Cancer Cell*, **2015**, 13;28: 29-41.
- 3) Meyer SC, Keller MD, Chiu S, Koppikar P, Guryanova OA, Rapaport F, Xu K, Manova K, Pankov D, O'Reilly RJ, Kleppe M, McKenney AS, Shih AH, Shank K, Ahn J, Papalexis E, Spitzer B, Socci N, Viale A, Mandon E, Ebel N, Andraos R, Rubert J, Dammassa E, Romanet V, Dölemeyer A, Zender M, Heinlein M, Rampal R, Weinberg RS, Hoffman R, Sellers WR, Hofmann F, Murakami M, Baffert F, Gaul C, Radimerski T, Levine RL; CHZ868, a Type II JAK2 Inhibitor, Reverses Type I JAK Inhibitor Persistence and Demonstrates Efficacy in Myeloproliferative Neoplasms. *Cancer Cell*, **2015**, 13, 28:15-28.
- 4) Zender M, Klein T, Henn C, Kirsch B, Maurer CK, Kail D, Ritter C, Dolezal O, Steinbach A, Hartmann, RW. Discovery and Biophysical Characterization of 2-Amino-oxadiazoles as Novel Antagonists of PqsR, an Important Regulator of *Pseudomonas aeruginosa* Virulence. *J. Med. Chem.*, **2013**, 56, 6761-6774.
- 5) Zimmer, C; Hafner, M; Zender, M; Ammann, D; Hartmann, RW; Vock, C; N-(Pyridin-3-yl)benzamides as selective inhibitors of human aldosterone synthase (CYP11B2). *Bioorg. Med. Chem. Lett.*, **2011**, 21, 186-190.

8.3 Oral Presentations

- 1) Zender M, Klein T, Henn C, Kirsch B, Maurer CK, Kail D, Ritter C, Dolezal O, Steinbach A, Hartmann, RW. Discovery and Biophysical Characterization of 2-Amino-Oxadiazoles as Novel Antagonists of PqsR, an Important Regulator of *Pseudomonas aeruginosa* Virulence. *3rd International Symposium of the SFB 630*, 2013, Wuerzburg, Germany.

8.4 Poster Presentations

- 1) Zender M, Kirsch B, Maurer CK, Empting M, Hartmann, RW. Development of Novel Antagonists of PqsR, an Important Regulator of *Pseudomonas aeruginosa* Virulence. *1st International Symposium on Quorum Sensing Inhibition*, 2015, Santiago de Compostela, Spain
- 2) Zender M, Klein T, Henn C, Kirsch B, Maurer CK, Kail D, Ritter C, Dolezal O, Steinbach A, Hartmann, RW. Discovery and Biophysical Characterization of 2-Amino-Oxadiazoles as Novel Antagonists of PqsR, an Important Regulator of *Pseudomonas aeruginosa* Virulence. *Fragment-based Lead Discovery Conference*, 2014, Basel, Switzerland.
- 3) Zender M, Klein T, Henn C, Kirsch B, Maurer CK, Kail D, Ritter C, Dolezal O, Steinbach A, Hartmann, RW. Discovery and Biophysical Characterization of 2-Amino-Oxadiazoles as Novel Antagonists of PqsR, an Important Regulator of *Pseudomonas aeruginosa* Virulence. *Frontiers in Medicinal Chemistry*, 2014, Tuebingen, Germany.
- 4) Zender M, Lu C, Klein T, Kirsch B, Maurer CK, Steinbach A, Hartmann RW. Development of Antagonists Targeting the Transcriptional Regulator PqsR, a Key Player in the *Pseudomonas aeruginosa* Quorum Sensing Machinery. *2nd International Conference on Antimicrobial Research ICAR*, 2012, Lisbon, Portugal.

9 Acknowledgments

An erster Stelle möchte ich mich bei Herrn Prof. Dr. Rolf W. Hartmann dafür bedanken, dass er mich mit diesem spannenden sowie herausfordernden Projekt betraut hat. Seine leidenschaftliche Bereitschaft zur wissenschaftlichen Diskussion hat wesentlich zum Gelingen dieser Arbeit beigetragen. Herzlichen Dank für das entgegengebrachte Vertrauen und die stete Unterstützung bei sämtlichen Problemen.

Mein besonderer Dank gilt auch Herrn Prof. Dr. Rolf Müller für die Übernahme des Koreferates und die konstruktiven Vorschläge in allen Thesis Committee Meetings.

Im Weiteren möchte ich bei allen Personen bedanken, die ebenfalls direkt oder indirekt zum Gelingen dieser Arbeit beigetragen haben:

Dr. Martin Empting und Dr. Anke Steinbach für die kompetente Leitung des PQS Projektes sowie die stete Bereitschaft zu wissenschaftlichen Diskussionen und die darüber hinaus gehende Unterstützung.

Dr. Dagmar Kail und Dr. Carsten Börger für die Hilfestellung bei synthetischen Problemen. Dr. Stefan Boetcher und Dr. Jens Eberhardt für ihr Mitwirken bei diversen LC-MS Messungen. Dr. Josef Zapp für die Messungen auch von unmöglichen NMR Proben.

Florian Witzgall und Prof. Dr. Wulf Blankenfeldt für die enge und gute Zusammenarbeit sowie das Lösen von so vielen wichtigen Kristallstrukturen.

Katrin Schmitt und May Sena Küffner für die Organisation des Sekretariats sowie Lothar Jager für die technische Unterstützung bei allen unlösbaren technischen Problemen.

Simone Amann, Jeannine Jung und Carina Scheid für gewissenhafte Durchführung von unzähligen biologischen Tests.

Allen ehemaligen und aktuellen Kollegen im Arbeitskreis Hartmann, die für eine stets gute und freundschaftliche Arbeitsatmosphäre gesorgt haben. Hier möchte ich mich insbesondere bei meinen Schreibtischnachbarn Christian „Coach“ Brengel, Andreas „Andy“ Thomann, Dr. Henning Sahrer und Andreas Kany bedanken, die die Bürozeit durch viel Humor zu einem Erlebnis gemacht haben. Außerdem sei den „Guten Leuten“ für die vielen Aktivitäten auch außerhalb der Arbeit gedankt. Vielen Dank an Stefan Boetcher für die super Organisation. Es war eine tolle Zeit!!!

Martina Fruth für Ihr offenes Ohr und die vielen freundschaftlichen Gespräche.

Dr. Christine Maurer als kompetente Begleiterin auf allen Irrungen und Wirrungen des Quorum Sensings Systems.

Dr. Matthias Groh und Alexander Kiefer für die vielen lustigen Stunden im Labor und bei diversen sportlichen und kulinarischen Aktivitäten.

Allen ehemaligen und aktuellen Mitbewohnern der WG für eine tolle und manchmal auch chaotische Zeit in Saarbrücken.

Meinen „OldDirtyBastards“ die ich schon so lange kenne und mit denen es trotzdem nie langweilig wird.

Meiner Eltern Stefan und Elke, die mir meine Ausbildung ermöglicht und die mich immer auf meinem Weg unterstützt haben. Dafür, dass Ihr mir vermittelt habt, wie wichtig es ist seine Träume zu verwirklichen.

Meiner Yvonne, die mich in allen Höhen und Tiefen immer ertragen hat und mir immer eine so verlässliche Stütze war und ist.